CRANFIELD UNIVERSITY

Aminu Ishaq Bukar

NUMERICAL STUDY OF COUPLING BETWEEN MULTIPHASE FLOW-INDUCED VIBRATIONS (MFIV) AND VORTEX-INDUCED VIBRATIONS (VIV) OF SLENDER FLEXIBLE PIPES.

School of Water, Energy, and Environment
Energy and Power

PhD
Academic Year: 2021 - 2022

Supervisor: Dr Patrick Verdin
August 2022

CRANFIELD UNIVERSITY

School of Water, Energy, and Environment
Energy and Power

PhD

Academic Year 2021 - 2022

Aminu Ishaq Bukar

NUMERICAL STUDY OF COUPLING BETWEEN MULTIPHASE FLOW-INDUCED VIBRATIONS (MFIV) AND VORTEX-INDUCED VIBRATIONS (VIV) OF SLENDER FLEXIBLE PIPES.

Supervisor: Dr Patrick Verdin

August 2022

This thesis is submitted in partial fulfilment of the requirements for the degree of PhD

ABSTRACT

The dynamic response of a riser subjected to external and internal flow-induced vibration is studied numerically through the coupling of a computational fluid dynamics (CFD) solver and a finite element (FE) solver. This thesis describes the vortex-induced vibration (VIV) of elastically mounted rigid cylinders, empty flexible risers and fluid conveying risers using three-dimensional (3D) numerical simulations. The dynamic characteristics of the riser, such as inline (IL) and crossflow (CF) displacements and vibrating frequencies, are provided and discussed. The effects of fluid flow, including velocity magnitude and profile, on the dynamic response are also investigated.

A 1 degree of freedom (1DOF) VIV of an elastic cylinder is studied first using 2D and 3D numerical models. The effects of mass and damping ratio on the amplitude of vibration of the cylinder over a reduced velocity range are analysed. Results show a good agreement with published experimental studies. It is demonstrated that increasing the mass and damping ratio reduces the maximum vibration amplitude of the cylinder.

A 3D numerical study is then carried out to investigate the effects of velocity magnitude, velocity profile, the elastic modulus of the riser, orientation, and aspect ratio. The study establishes that the IL displacement, CF vibration mode, and frequencies increase with the flow velocity, aspect ratio and reduction of elastic modulus.

In addition, the VIV of the riser transporting single-phase internal flow is presented. The numerical study describes the effects of internal flow velocity magnitude on the dynamic response of the riser. It is shown that the internal flow velocity magnitude affects the vibration mode of the riser.

Finally, the effects of internal air-water volume fractions on the dynamic response of a riser transporting a two-phase flow are examined in detail. The influence of gas fraction on a pipe with no external flow, on a jumper pipe with no external flow and on a fluid conveying pipe exposed to external flow is investigated. The

numerical results show that a variation of the air volume fraction slightly affects the dynamic characteristics of the riser.

Keywords:

Fluid-Structure Interaction (FSI); Computational Fluid Dynamics (CFD); Finite Element Method (FEM); Flow Induced Vibration (FIV); Vortex Induced Vibration (VIV); Flow Induced Vibration (FIV); Multiphase Flow Induced Vibration (MFIV)

ACKNOWLEDGEMENTS

All praise be to Allah for giving me the wisdom and strength to complete this PhD.

I want to express my gratitude to my supervisor Dr Patrick Verdin for his guidance and support during this PhD. He has always been available throughout the entire PhD journey, and I appreciate that.

I wish to thank Petroleum Technology Development Fund (PTDF) Nigeria for funding my PhD and financial support. I would also like to thank Ahmadu Bello University, Zaria for granting me a study fellowship.

My sincere gratitude to my wife Fatima and my son Abdullah for being with me through this journey.

I wish to acknowledge the moral support from my parents. AVM Isyaka Bukar and Hajia Hadiza Bukar. Also, I would like to appreciate my late uncle Engr Mustapha Bukar Madawakin Daura who believes in me and encouraged me to strive for excellence. I would also like to thank my uncle Engr Abdullahi Bukar, Sarkin kudun daura for the technical support and industrial advice during the PhD.

To my friends Dr Abdulhakim Shittu, Dr Dahiru Aminu, Dr Victor Etim, Lawal Hano, Auwal Dodo, Nafiu Babaji and others too many mentions. Your moral and friendly support throughout the PhD journey is highly appreciated.

TABLE OF CONTENTS

LIST OF FIGURES

LIST OF TABLES

LIST OF EQUATIONS

LIST OF ABBREVIATIONS

2-D	Two Dimension
3-D	Three Dimension
DOF	Degree of Freedom
CF	Cross Flow
IL	In line
CFD	Computational Fluid Dynamics
CSD	Computational Solid Dynamics
FVM	Finite Volume Method
FEM	Finite Element Method
VIV	Vortex Induced Vibration
FIV	Flow Induced Vibration
MFIV	Multiphase Flow Induced Vibration
FSI	Fluid Structure Interaction
RANS	Reynolds Average Navier Stokes
DNS	Direct Numerical Simulation
LES	Large Eddy Simulation
DES	Detached Eddy Simulation
SST	Shear Stress Transport
RMS	Root Mean Square
Max	Maximum
Min	Minimum

1 INTRODUCTION

The search for hydrocarbon has pushed drilling activities into ultra-deep-water zones in the oil and gas industry exposing offshore structures such as pipeline and rises to harsh environmental conditions. In offshore environment, environmental forces such as waves and current posed danger to offshore structures hence, affecting the stability and integrity of the structure. As oil and gas production moves deeper into the ocean, long pipe/risers are required to transport the oil and gas from the wellhead to the platform. Thereby making the design and installation of long pipe and riser in deep ocean capital intensive. Thus, extensive research and analysis is required to safely design and installed subsea pipeline in deep-water.

In most instances, the hydrocarbon from the well is a mixture of oil, gas, and water. A flow containing different phases, such as oil, gas and water, is referred to as multiphase flow while a flow containing single fluid is referred to as single phase flow. At the wellhead, the oil and gas mixture exit at high pressure and temperature, also, affecting the stability and integrity of the subsea jumper and pipe. In essence, the subsea jumpers and pipe are subjected to high internal fluid pressure due to the internal multiphase flow and external hydrodynamic pressure due to the external subsea currents and waves. Therefore, the combined effect of external and internal flow is a fluid structure interaction problem because the vibration of the body affects the fluid flow and vice versa.

When external flow past bluff bodies such as pipe and riser, vortices are shed behind the riser at a certain frequency called the vortex shedding frequency. These vortices induce an oscillatory motion onto the body. This phenomenon is referred to as Vortex-induced vibration (VIV). When the vortex shedding frequency approaches the natural frequency of the riser, the vortex shedding frequency ‘lock-in’ to the riser’s natural frequency, thereby causing significant vibration and subsequent failure of the structure (Williamson and Govardhan 2004).

When a multiphase fluid flows through the pipe/jumper, fluid forces acting on the pipe fluctuate due to the non-uniform distribution of the gas and liquid phases, thereby inducing oscillation on the pipe, referred to as multiphase flow-induced vibration (MFIV). When the induced vibration frequency coincides the pipe/jumper's natural frequency, a resonance occurs, resulting in high vibration amplitude and fatigue failure of the structure. The vibration caused by MFIV affects the integrity and stability of subsea structures. Therefore, it is pertinent for engineers to understand the mechanism of MFIV and how to prevent it (Miwa et al., 2015).

The coupling between VIV and MFIV is a fluid fluid-structure interaction (FSI) problem, where the vibration of the pipe affects the multiphase flow regime and vice versa. The combined effect VIV AND MFIV becomes a complex FSI problem. Therefore, understanding the physics of fluid flow and how it affects the dynamic response of the subsea riser will help engineers to be better informed and optimise their design thereby designing and installing more reliable structures. In addition, the understanding of the coupled mechanism will give insight into various method of how to mitigate the vibration.

There are several ways to analyse the dynamic response of flexible riser. The main methods include the experimental, analytical, and computational fluid dynamics (CFD) methods. Experimental studies are usually expensive and difficult to scale up, hence, much research has been devoted to developing numerical and analytical methods to predict the dynamic response of risers. Mostly, the finite elements are used to calculate structural response of the structure. While the hydrodynamic forces acting on the structures can be obtained through the CFD or analytical method. In CFD, the hydrodynamic forces acting on the riser are obtained by solving the Navier-Stokes (N-S) equations while in the analytical method, mathematical models are used to predict it. For example, a nonlinear oscillator model is used in the wake oscillator method. The analytical method can be completely empirical or semi empirical. In the semiempirical method, results obtained from experimental model are used in the model. Semiempirical method of predicting VIV can be further classified into the time-

domain and frequency domain prediction methods. Tools such as SHEAR7, VIVA and VIVANA are examples of the frequency domain methods because they operate in the frequency domain method, they require linear model to predict the VIV. The major advantages of these models are they are simple and fast, However, the model doesn't cater to non-linearities such as varying axial load. Also, the hydrodynamic forces coefficient in these models are mostly based on model test of rigid cylinder. In addition, the models neglect the in-line response of the riser. Therefore, simulations are limited to low range of Reynold number. To deal with the limitation of frequency domain models, a time domain models are developed which considers non-linear effects. However, the major disadvantage of this model is that it's difficult to have a single time domain model that can predict VIV under over a wide range of flow regimes. Example of time domain methods include the wake oscillator model where the lift forces are represented using the van der pol oscillators.

Compared to the CFD method, the analytical methods are computationally less expensive but does not capture the whole dynamics of the riser motion under all flow conditions. Also, the major disadvantage of the empirical method is that it focuses on the structural dynamics and neglects the flow field around the riser. Therefore, the CFD approach, which simulates the flow field around the riser by solving the Navier-Stokes (N-S) equations has become more popular.

Due to the large computational time required to perform CFD analysis, different CFD methods have developed that requires less time. For example, a meshless method called the Discrete Vortex Method (DVM) was developed to predict the VIV response of a riser. The DVM method computes the motion of the vorticity field to obtain the force acting on the cylinder rather than solving the full N-S equations. Therefore, it becomes faster. Another CFD method is the strip method, where multiple two-dimensional planes along the span of the riser are used to model the flow field around the riser and calculate the fluid force acting on the riser. This approach is cheaper than a full 3D CFD simulation, but the disadvantage of this approach is that it does not capture the three-dimensionality of the flow fields. Therefore, the response of the riser not accurately captured.

With the increase in computational power, the full CFD method have become more attractive in the past few decades. However, as the aspect ratio of the riser increases the cost of performing CFD analysis increases. Direct Numerical Simulation (DNS) CFD methods solve the full Navier-Stokes (N-S) equations, but this is a highly demanding (CPU and time) approach and not practical for most engineering applications. Therefore, different methods-based turbulence models have been developed to the solve the N-S equations. CFD methods can therefore be categorised based on the turbulence model used to solve the N-S equation. Large Eddy Simulations (LES) CFD method are less demanding than DNS. Only the large eddies are resolved in LES, this approach is therefore not as accurate as DNS, but is increasingly considered to solve engineering problems.

The Reynolds Averaged Navier-Stokes (RANS) methods required turbulence modelling as the Navier stoke equation is decomposed into mean and fluctuating component and averaged. Therefore, a turbulence model is required to close the equation. The turbulence model includes the Sparlart Allmaras, k-e model and k-w model. RANS-based models are computationally more efficient than DNS and LES, although limitations are present, depending on the RANS-based turbulence model considered. The RANS methods are still the most used CFD approaches for engineering applications as they are fast and accurate enough for most cases.

The CFD methods has been used over the years to solve wide range of fluid structure interaction (FSI) problem, such as those found in human heart in biomedical field and turbomachinery problem in the rotating engineering field.

The use of CFD to solve VIV of a riser which is a fluid interaction problem has been a subject of research over the years. Researchers such as Williamson and Govardhan (2008), Bearman (2011) and Derakhshandeh and Alam (2019) have conducted comprehensive reviews on experimental and numerical studies of an elastically mounted rigid cylinders undergoing VIV. However, elastically mounted rigid cylinder does not accurately represent the actual riser which are generally flexible and have a large length to diameter ratio. Nevertheless, their studies give insight into the physics of flexible riser undergoing VIV.

The prediction of VIV of flexible risers using CFD has been performed in recent times by authors such as Menter et al. (2006), Huang et al. (2011) and Wang and Xiao (2016). Other methods of predicting VIV of flexible risers have recieved reasonable attention. For example researchers such as Lehn (2003), Trim et al. (2005), Chaplin et al. (2005b), Song et al. (2011), and Huera-Huarte et al. (2014) explored the dynamic response of flexible riser using the experimental method while, authors such as Facchinetti et al. (2004), Srinil (2011), Zanganeh and Srinil (2016) and Gao et al. (2019a, 2019b, 2019c) developed mathematical to predict VIV response of risers.

Most risers usually transport multiphase fluids from the seabed to the platform, the effects of the internal flow on the dynamic response of the riser cannot be ignored. The Internal fluid flow can either be single phase or multiphase flow. When a multiphase fluid flows through the pipe/jumper, fluid forces acting on the pipe fluctuate due to the non-uniform distribution of the gas and liquid phases, thereby inducing oscillation on the pipe, referred to as multiphase flow-induced vibration (MFIV). When the induced vibration frequency coincides with the pipe/jumper's natural frequency, a resonance occurs, resulting in high vibration amplitude and fatigue failure of the structure. The vibration caused by MFIV affects the integrity and stability of subsea structures. Therefore, it is pertinent for engineers to understand the mechanism of MFIV and how to prevent it (Miwa et al., 2015). MFIV is a fluid fluid-structure interaction (FSI) problem where the vibration of the pipe affects the multiphase flow regime and vice versa. One of the leading causes of high fluid force fluctuation is the rate of the fluid and the type of flow pattern formed by the multiphase fluid.

Many studies have been performed on two phase flow and how this type of flow affects the dynamic response of a pipeline carrying multiphase fluids. Wang et al. (2018), Zhu et al. (2021b) and Ma et al. (2020, 2021) used experimental method to analysed the MFIV of a riser transporting multiphase. While researchers such as An and Su (2015), Gu et al. (2016) Ma et al. (2017), and Li et al. (2020) studied the dynamic response of a flexible pipe transporting slug flow using mathematical models. Likewise, the improved computing capacity of high-performance

computers has made it possible to simulate the vibration characteristics of a pipe transporting a multiphase flow. Li et al. (2016), Jia (2012, 2013) and Onuoha et al. (2018) examine the effect of a gas fraction on the MFIV of a pipe transporting a multiphase flow. At the wellhead, curve-shaped pipes called jumpers are used to connect the wellhead and the subsea manifold and pipeline. The jumpers are subjected to high internal pressure and external current. Therefore, the dynamics of curved pipes, such as the riser, can be more complex than the straight pipe (Kim and Srinil 2018).

Most of these studies have, however, focused on the effects of external VIV on risers and neglect the effects of the internal flow. Most work has thus been devoted to either VIV based on external flows surrounding the risers, or to internal flow-induced vibrations in pipes due to multiphase flows (multiphase Flow-induced vibrations, MFIV), but not for both phenomena acting simultaneously.

Performing CFD analysis of a pipeline under the effect of MFIV and VIV is resource intensive. Thus, limited research has been conducted to analysed this phenomenon using the CFD method. Therefore, in this study, the combined effect of external and internal flow is analysed. As the internal fluid flows through the pipe, it induced vibration. The magnitude of the vibration can be influence by the fluid properties and the structural properties of the pipe. Fluid properties such as speed, types of flow (single phase or multiphase) can affect the dynamic response of the pipe. Also, the solid properties such as the aspect ratio, diameter, elastic modulus, and orientation of the pipe can affect the magnitude of the dynamic response.

A complete understanding of how these two sources of vibration (MFIV and VIV) affect the structural integrity of risers and pipes is required. There is currently a lack of clear methodology in the literature regarding ways of investigating the combined effects of these two sources of vibration. The Energy Institute (EI) has generated guidelines for Avoidance of Vibration Induced Fatigue Failure (AVIFF). However, these guidelines do not provide a framework for the direct estimation of vibration levels, stress levels, or fatigue life (Pontaza, 2014). To address this gap, a more detailed investigation based on numerical simulation is performed in

this PhD work. The combined effect of internal MFIV and external VIV on the structural integrity of a subsea riser is thus investigated numerically. A full-scale three-dimensional (3D) FSI analysis of the dynamic response of a riser under internal multiphase flow and external VIV is performed. The system coupling in ANSYS software is used to link the flow solver ANSYS FLUENT through computational fluid dynamics (CFD) and the structure solver ANSYS Mechanical through computational structural dynamics (CSD). The system coupling provides an interface between CFD and CSD for exchanging information during an FSI simulation.

1.1 Aim and Objectives

This PhD aims to numerically investigate the combined effect of internal MFIV and external VIV on the dynamic response of a subsea riser.

Objectives

The main objectives of the study are:

- To carry out a comprehensive literature review on MFIV, external VIV and the coupled FSI between them.
- To numerically investigate the effect of VIV on a rigid and flexible riser using CFD.
- To numerically investigate the structural behaviour of a fluid conveying riser subjected to the combined effect of FIV and VIV.
- To numerically investigate the dynamic behaviour of a riser subjected to the combined effect of MFIV and VIV.

1.2 Thesis outline

The thesis is structured in a paper format, each distinct paper represented as chapters. In each paper, literature review, numerical method, problem description, results and discussion, and conclusion are presented as sub-sections. At the end of the thesis, an overall conclusion is presented that summarise the overall findings obtained from each paper. The introduction, aim and objectives of the overall study are presented in chapter 1.

Chapter 2 presents 2D and 3D numerical simulations of an elastically mounted cylinder undergoing flow VIV in the crossflow (CF) direction. The effect of mass ratio and damping on the maximum CF displacement under varying reduced velocities are presented and discussed.

Chapter 3 describes the effects of velocity profile, velocity magnitude, riser aspect ratio, elastic modulus and orientation on the dynamic response of a flexible riser with no internal fluid passing through it. The dynamic characteristics such as the inline (IL) displacement, CF displacement, vibrating frequencies and orbital trajectories are compared and examined based on the varying parameters.

Chapter 4 deals with the effect of different internal and external velocities on the IL displacement, CF displacement, vibrating frequencies, and orbital trajectories of a flexible horizontal and vertical riser subjected to the combined impact of different internal and external velocities.

Chapter 5 presents the effects of a two-phase internal flow on the VIV response of a flexible horizontal and jumper pipe transporting multiphase flow without external velocity. This chapter also describes results in a horizontal pipe transporting multiphase flow exposed to an external flow velocity. The IL displacement, CF displacement, vibrating frequencies, and orbital trajectory of the riser under different internal flow conditions and constant external velocity are examined.

Finally, Chapter 6 provides the overall conclusions of this study. Results obtained in the four papers are summarised to answer the research aim and objectives. Figure 1-1 shows a flowchart demonstrating the different analysis carried out and the parameters varied to achieve the aim and objectives of the thesis. In addition, the flowchart shows how the thesis chapters and research objectives are linked sequentially.

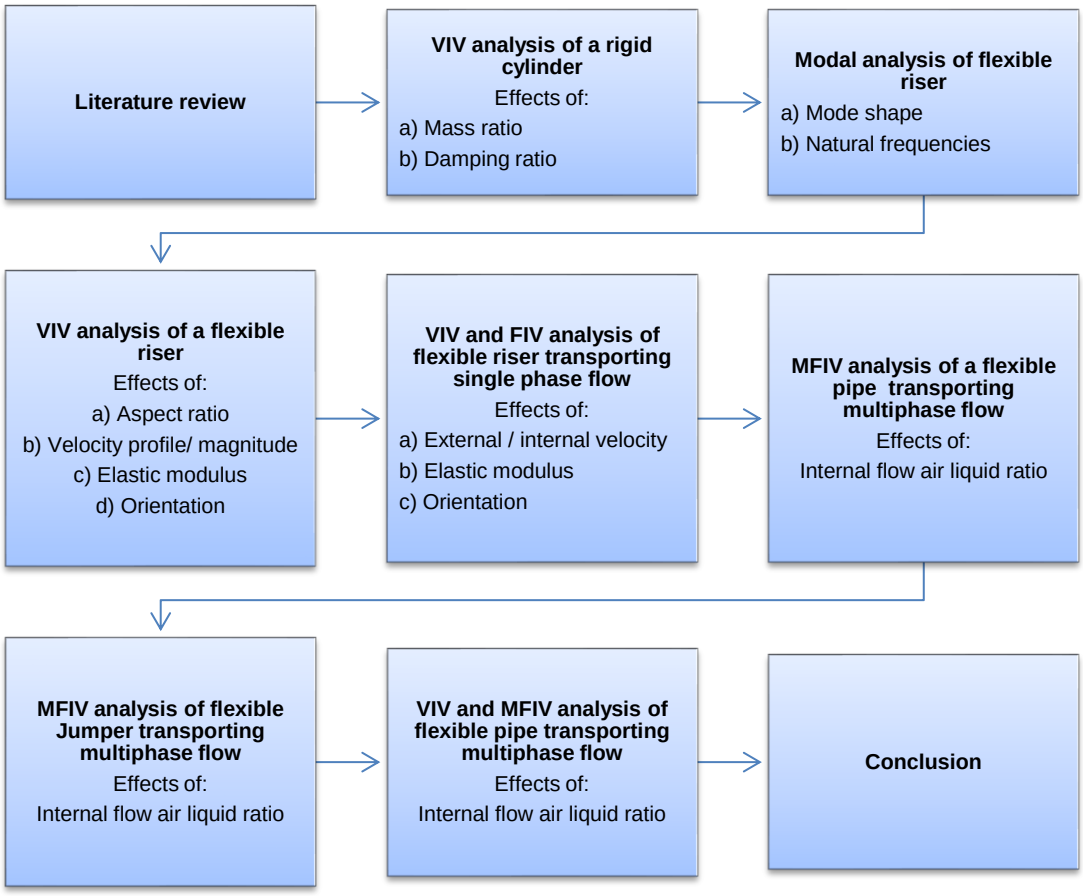

Figure 1-1 Flowchart illustration of the thesis outline and how the research objectives are related linked to each other.

Chapter 2

2 VIV OF A RIGID CYLINDER

ABSTRACT

The effect of mass (m*) and damping (ζ) ratio on the vortex induced vibration (VIV) of an elastically mounted cylinder free to vibrate in the crossflow (CF) direction is numerically investigated using the 2D and 3D methods. The Vibration amplitude is investigated over a reduced velocity (Ur) range of 2 to 12. The results obtained from this study agree with the previous numerical and experimental results. The results show that increasing the mass and damping ratio reduced the vibration amplitude.

2.1 Introduction

In the oil and gas industry, drilling activities have moved into deep waters. Therefore, subsea structures such as pipelines and risers are subjected to harsh environmental conditions. When fluid flows past a riser, vortices are shed in its wake, thereby inducing oscillation forces onto it. This phenomenon is referred to as vortex-induced vibration (VIV). When the vortex shedding frequency of the vortices coincides with the natural frequency of the riser, ‘lock-in’ or resonance occurs, causing a large vibration amplitude and eventual failure of the structure. Therefore, understanding the physic of VIV and how to prevent it is essential in designing offshore risers.

Different methods such as experimental, analytical, and computational fluid dynamic (CFD) methods have been used by many researchers to understand the physics of VIV. Comprehensive reviews on VIV can be found in Gabbai and Benaroya (2005), Williamson and Govardhan (2004, 2008), and Bearman (2011). When studying the VIV of a riser, the study of flow past a stationary cylinder gives insight into vortex formation before moving to the complex examination of the oscillating cylinder. Many researchers have investigated the VIV of a stationary cylinder using experimental and numerical methods, see studies by Qu et al. (2013), Jiang et al. (2016), Ye and Wan (2017), and Zheng and Wang (2018).

Not surprisingly, the dynamics of an oscillating cylinder is more complicated than for a stationary one, as it involves interaction between fluid and structural components. There are two different types of cylinder motion. One is for the cylinder to oscillate at a predetermined frequency (forced oscillation), and the second is for the cylinder to oscillate due to the force of the moving fluid (free oscillation).

Several studies have covered the flow characteristics of a rigid cylinder under forced oscillation using experimental and numerical methods. For example, researchers such as Jeon and Gharib (2001) used the experimental method, while Placzek et al. (2009) used the numerical method to investigate the VIV of a rigid cylinder under forced oscillation. However, most risers are under free oscillation, where the vibration of the cylinder is determined by the hydrodynamic forces acting on the cylinder.

In the past decades, extensive research has been conducted to investigate the VIV of an elastically mounted cylinder using experimental and numerical methods. The variation of vibration amplitude against the reduced velocities (Ur) are examined in most VIV study. The vibration amplitude is classified into three branches (initial, upper, and lower branches) depending on the reduced velocity. The initial and lower branches are observed at low and high reduced velocities. While the upper branch is associated with reduced velocity where lock-in occurs.

Feng (1968) conducted an experiment on a cylinder with a high mass damping ratio and observed only two branches, i.e., the initial and the lower branches. Subsequently, Khalak and Williamson (1996, 1997a, 1997b) conducted an experiment using a low-mass damping cylinder. They found out that the amplitude increases, and the vibration amplitude under varying reduced velocities depicts three distinct branches (initial upper and lower branches). Khalak and Williamson (1999) further showed that the response amplitude was mainly influenced by the mass damping parameter ($m^*\xi$), while the synchronization range was influenced by the mass ratio (m^*). Govardhan and Williamson (2000) utilised particle image velocimetry (PIV) to examine the 1DOF VIV of a cylinder with varying mass ratios. They found out that for high mass

damping, two branches of amplitude were present, while for low mass damping, three branches of response, namely the initial, upper, and lower branches, were present. Govardhan and Williamson (2002, 2004) further showed that the lower branch disappears below the critical mass ratio, and the upper branch continues indefinitely. Wang et al. (2017) also used digital PIV to examine the 1DOF VIV of an elastically mounted rigid cylinder with a low mass damping ratio.

Apart from experimental studies, many studies were conducted using numerical methods. There are different types of numerical methods, including analytical methods which are based on a mathematical model to predict the VIV, and CFD methods that solve the Navier-Stokes (N-S) equations to simulate the fluid flow and forces acting on a cylinder. One numerical technique is Direct Numerical Simulation (DNS), in which the full Navier-Stokes equations are solved without approximation. This makes the method expensive and time-consuming and usually only applicable for research, not for engineering applications. Nevertheless, researchers such as Newman and Karniadakis (1997), Lucor et al. (2005), Dong et al. (2006), and Gsell et al. (2019) used DNS to simulate the flow past an oscillating cylinder. Their simulations captured the upper branch of the vibration amplitude.

Rather than DNS, Reynolds Average Navier-Stokes (RANS)-based models are used for both research and industrial applications as such models run faster than DNS, and provide relatively good accuracy, depending on the complexity of the problem. Willden and Graham (2006) examined the 1DOF VIV of a circular cylinder with a low mass ratio over an extensive range of reduced velocities. Their results captured all three branches of the vibration amplitude under varying reduced velocities. Placzek et al. (2009) used a 2D RANS code to study the VIV of a cylinder with a low mass ratio and low Reynolds number (*Re*). Their numerical code predicted the vibration amplitude in the upper branch. Guilmineau and Queutey (2004) and Pan et al. (2007) used the shear stress transport (SST) k-ω RANS turbulence model to simulate the 1DOF VIV of a cylinder with a low mass ratio. However, the upper branch was not captured in their study. Nguyen and Nguyen (2016) used a Detached Eddy Simulation (DES) model to analyse

the VIV of a stationary and 1DOF cylinder at a high Reynold number and low mass ratio. Their results agreed with the experimental results of Hover et al. (1997). Khan and Ibrahim (2019) and Chang and Lua (2020) used the (SST) k-ω turbulence model to examine the flow around a cylinder free to vibrate in the CF direction.

Zhao and Cheng (2014) used a numerical method to simulate the effects of aspect ratio on the 1DOF VIV of a 3D cylinder. They established that a 3D flow could be reasonably represented if the aspect ratio exceeds 5. Lee et al. (2014) applied a Delayed Detached Eddy Simulation (DDES) model to examine the effect of the cylinder length on the flow characteristics of a stationary and free oscillating cylinder at *Re*=5,000. They suggested that large aspect ratios are preferred for the VIV calculations. Saltara et al. (2011) used DES to perform 3D simulations of 1DOF VIV of an elastically mounted cylinder with an aspect ratio of 5. Matin Nikoo et al. (2019) used the 3D SST k-ω model to simulate 1DOF VIV of an elastically mounted rigid cylinder with an aspect ratio of 8 at Reynolds numbers between 2,000 and 12,000. Their results agreed with previous numerical and experimental results.

This study investigates the effects of mass ratio, damping ratio and Reynolds number on the CF vibration amplitude of an elastically mounted cylinder. 2D and 3D computational methods are used to simulate the VIV. The results are compared with experimental and numerical studies extracted from the literature for validation. This chapter is organised as follows. First, the description of the problem is elaborated in Section 2.2. Then the numerical method utilised to perform the simulation is described in Section 2.3. Next, the variation of the CF displacement of the cylinder to its reduced velocity is investigated in Section 2.4. Finally, the conclusions and recommendations for further study are provided in Section 2.5.

2.2 Problem description

Two-dimensional (2D) and three-dimensional (3D) simulations are carried out to investigate the VIV dynamics of flow past a one degree of freedom (1DOF) cylinder free to vibrate in the CF direction. The dynamics of the oscillating cylinder is more complicated than stationary because it involves interaction between fluid and structural components. Therefore, studying elastically mounted cylinders will help better understand the fluid-structure interaction of flexible risers. The effect of mas ratio (2, 2.4, 10 and 11) and damping ratio on the vibration amplitude of the cylinder are investigated.

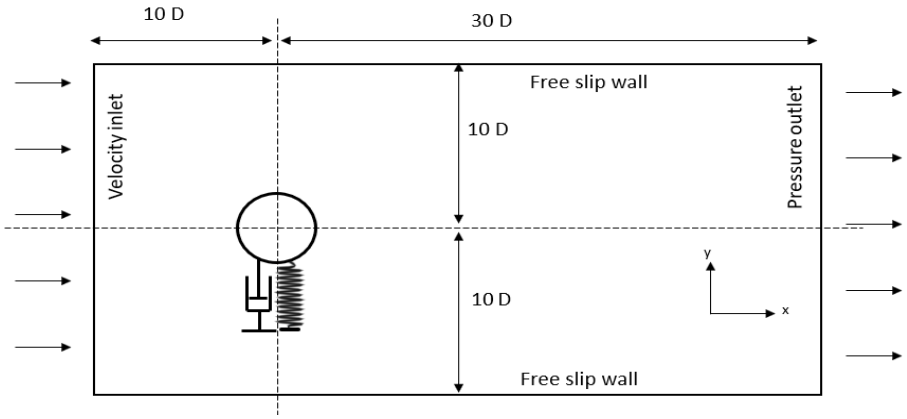

Figure 2-1 2D computational domain

2.3 Numerical method

2.3.1 Fluid domain

Figure 2-1 shows the computational domain in two-dimensional (2D) form. The rectangular domain has a length of 40D and a width of 20D. The cylinder is located 10D and 30D far from the inlet and outlet boundaries. The top and bottom boundaries are located 10D from the centre of the cylinder. Figure 2-2 shows the 3D computational domain of the cylinder. The origin of the Cartesian coordinate system is located at the centre of the bottom end of the cylinder. The domain has a length of 40D, a width of 20D, and a height of 5D, which corresponds to the length of the cylinder. For both 2D and 3D simulations, a velocity inlet type

boundary condition was considered at the inlet of the domain. This inlet flow velocity was assumed to be uniform. A pressure outlet type boundary condition was considered at the outlet section of the domain. Symmetry (free slip) boundary conditions were applied at the top and bottom boundaries for the 2D analysis. Likewise, symmetry boundary conditions were applied to the two-transverse and two spanwise boundaries in the 3D analysis. A symmetric condition implies that the velocity component perpendicular to the boundary is zero. A no-slip boundary condition was applied on the cylinder surface, which means that the fluid velocity is the same as the vibration velocity of the cylinder.

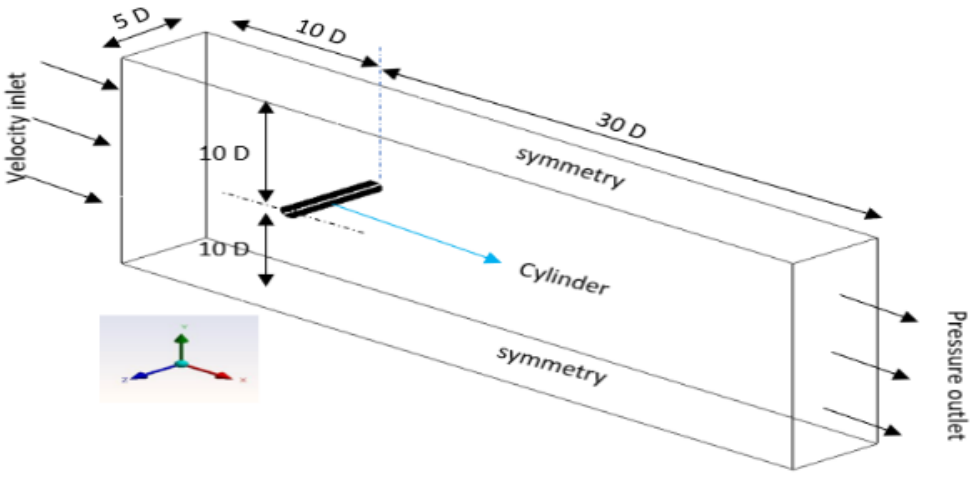

Figure 2-2 3D computational domain

2.3.2 Flow equations

The ANSYS FLUENT 2019 R2 flow solver was used to solve the governing equations describing the flow field around the cylinder. The flow field was considered transient and incompressible. The Reynolds Average Navier Stoke (RANS) method is used in this study to solve the mass and momentum equation.

$$\frac{\partial \bar{u}_i}{\partial x_i} = 0 \qquad (2\text{-}1)$$

$$\frac{\partial(\rho\bar{u}_i)}{\partial t} + \frac{\partial\left(\rho\bar{u}_i\bar{u}_j\right)}{\partial x_j} = -\frac{\partial\bar{p}}{\partial x_i} + + \frac{\partial}{\partial x_j}\left(2\mu\,\bar{S}_{ij} - \rho\,\overline{u'_\iota\,u'_J}\right) \quad (2\text{-}2)$$

Where x_i and x_i are the cartesian coordinate in the *i* and j direction, while $\bar{u}_i$ and $\bar{u}_j$ represent the time-averaged velocity in the *i* and j direction. $\bar{p}$ is the pressure, t is the time, ρ is the fluid density, μ is the dynamic viscosity, δ_{ij} is the Kronecker function, and u' is the velocity fluctuation component. In addition, $\bar{S}_{ij}$ in equation (2-2) is the mean rate of the strain tensor, obtained by equation (2-3).

$$\bar{S}_{ij} = \frac{1}{2}\left(\frac{\partial\bar{u}_i}{\partial x_j} + \frac{\partial\bar{u}_j}{\partial x_i}\right) \quad (2\text{-}3)$$

And, $\rho\,\overline{u'_\iota\,u'_J}$ in equation **(2-2)** is the Reynolds-stress tensor, which represents the small-scale fluctuation of the fluid velocity defined through equation (2-4).

$$-\overline{\rho u'_\iota\,u'_J} = 2\mu_t\bar{s}_{ij} - \frac{2}{3}k_t\rho\delta_{ij} \quad (2\text{-}4)$$

where μ_t is the turbulent viscosity, $k_t = \frac{1}{2}\overline{u'_i u'_i}$ is the turbulent kinetic energy. The k-ω two-equation formulation from Wilcox (1993) is commonly used, where one equation solves the transport of the turbulent kinetic energy k, and the other one solves the specific dissipation rate ω. The Shear Stress Transport (SST) model, developed by Menter (1994), is a variant of the k-ω model. This model switches automatically from a k-ω definition near the walls to a k-ε definition in the bulk flow, which makes this model efficient in the sublayer near the walls, and far away from the walls (Loyseau, Verdin and Brown, 2018). The SST k-ω turbulence model was used to compute the Reynolds stresses in this study.

A pressure-based segregated algorithm called the Semi-Implicit Method for Pressure Linked Equations (SIMPLE) algorithm was selected as the pressure-velocity coupling. In addition, a second-order upwind scheme was used to discretise the pressure and momentum equations, while a first-order upwind scheme was used for both k and ω. A first-order implicit transient formulation was selected to solve the time-dependent nature of VIV. A Squares Cell-Based scheme was applied for the gradient in spatial discretisation. Finally, a 10^{-3}

convergence criterion and a time-step of 0.002s were considered for all simulations, see, section 2.3.6 for timestep size dependency study.

2.3.3 Structural equation

The VIV of an elastically mounted cylinder vibrating with one degree of freedom (1DOF) can be modelled as a mass-spring-damper system which is described in the non-dimensional form in equations (2-5) and (2-6). The equation of motion of each cylinder is solved using the improved fourth order Runge-Kutta method, which is manually written into a User-Defined Functions (UDF) and run during the numerical simulation (Zhao et al. ,2014)

$$m\frac{\partial^2 X}{\partial t^2} + c\frac{\partial X}{\partial t} + kx = F_D \tag{2-5}$$

$$m\frac{\partial^2 Y}{\partial t^2} + c\frac{\partial Y}{\partial t} + kx = F_L \tag{2-6}$$

where m, c, and k are the mass, damping, and stiffness of the system, respectively, F_D and F_L are the drag and lift forces. The equation can be written in dimensionless (Zhao et al. ,2014) form as:

$$\ddot{X} + \frac{4\pi\zeta}{U_r}\dot{X} + \left(\frac{2\pi}{U_r}\right)^2 X = \frac{C_D}{2m^*} \tag{2-7}$$

$$\ddot{Y} + \frac{4\pi\zeta}{U_r}\dot{Y} + \left(\frac{2\pi}{U_r}\right)^2 Y = \frac{C_L}{2m^*} \tag{2-8}$$

Where $m^* = \frac{4\mathrm{m}}{\rho L\pi D^2}$ is the mass ratio, $U_r = \frac{U}{f_n D}$ is the reduced velocity, $\zeta = \frac{c}{2\sqrt{km}}$ structural damping ratio, $C_D = \frac{1}{2}F_D\rho U^2 DL$ and $C_L = \frac{1}{2}F_L\rho U^2 D$L depict drag and lift coefficient. Also, m*, ζ, U_r, F_D and F_L represent the mass ratio, damping ratio, reduced velocity, drag, and lift forces, respectively. Also, L, D and f_n are the length, diameter and the natural frequency of the cylinder. For 2D simulation, the length of the cylinder is assumed to be unity, while for 3D simulation, the length

takes a value greater than 1. X, $\dot{X}$ and $\ddot{X}$ represent the dimensionless in-line (IL) displacement, velocity, and acceleration of the cylinders, respectively, while Y, $\dot{Y}$ and $\ddot{Y}$ denote the same quantities associated with the CF motion.

2.3.4 Fluid-structure interaction

At each computational time-step, the hydrodynamic forces (drag and Lift forces) acting on the cylinder are obtained from the N-S equations, which are then substituted into equations (2-5) and (2-6) to calculate the cylinder motion via a user-defined function (UDF). The new position of the cylinder is then communicated to the fluid solver via the UDF before the next step. This process continues until convergence is reached.

The movement of the mesh during cylinder oscillation is enabled by the dynamic mesh method in ANSYS FLUENT. This study uses the smoothing and re-mesh dynamic mesh to update the mesh during oscillation to avoid potential negative volume errors. As the cylinder vibrates, the mesh moves according to the diffusion equation (2-9).

$$\nabla.(\gamma\nabla\vec{u}) = 0 \tag{2-9}$$

where $\vec{u}$ represents the velocity of mesh displacement, and γ which represents the diffusion coefficient.

2.3.5 Mesh

ANSYS meshing 2019R2 is used to mesh the 2D and 3D fluid domains. For 2D analysis, a structured grid was created using the mapped face meshing and edge sizing in ANSYS, as shown in Figure 2-3. The edge sizing enables the user to control the number division on edges. The 3D domain is divided into multiple blocks, as shown in Figure 2-4. It can be observed from Figure 2-4 that the mesh near the cylinder is finer, while away from the cylinder, a coarse mesh is generated. Accurate simulation results are achieved when the first cell height next to the cylinder was 0.0014D in order to obtain a y+ value around one and ensure compliance with the requirements of the turbulence model selected for this work.

The y+ value is a non-dimensional distance at the wall, the function of the wall shear stress, fluid density and viscosity.

$$y^+ = \frac{y u_\tau}{\nu} \tag{2-19}$$

Where y is the distance at the wall of the first cell, ν is the kinematic viscosity of the fluid, and u_τ is the friction velocity defined as:

$$u_\tau = \sqrt{\frac{\tau_w}{\rho}} \tag{2-20}$$

with ρ the density of the fluid, and τ_w the wall shear stress.

The mesh sensitivity study was carried out using three different mesh sizes to assess the influence of mesh size on the vibration amplitude of the 2D and 3D cylinder and ensure that the results are not affected by the mesh size. The mesh independency results for 2D and 3D cylinder are presented in Table 2-1 and Table 2-2. Nc refers to the number of elements around the circumference of the cylinder, while Nz refers to the number of elements along the span of the 3D cylinder. For the 2D vibrating cylinder, the CF response amplitudes of the cylinder at a reduced velocity (Ur) =5 were investigated. It can be seen in Table 2-1 that the maximum amplitude of vibration of mesh 2 and 3 are similar. Therefore, considering the computational resources, mesh 3 with a total element of 53 600 was chosen for all the 2D VIV simulations.

Table 2-1 Mesh independency Study of 1DOF VIV 2D cylinder (Re=500, Ur=5)

Simulation	Number of cells	Coefficient of drag	Y/D
Mesh 1	37,200	1.216	0.82
Mesh 2	47,200	1.217	0.80
Mesh 3	53, 600	1.232	0.81

Table 2-2 Mesh study of 3D cylinder VIV at Ur=5

	Nc	Nz	Number of cells	Cd	Y/D
Mesh 1	120	50	486,000	1.30	0.76
Mesh 2	160	50	624,000	1.32	0.79
Mesh 3	200	50	822,000	1.35	0.80

For the 3D vibrating cylinder, the CF response amplitudes of the cylinder at Ur=5 were used to perform a Mesh dependency study. It can be seen from **Table 2-2** that mesh 2 and 3 show similar results. Therefore, Mesh 2, with a total element of 624,00 elements, was chosen for 3D VIV analysis.

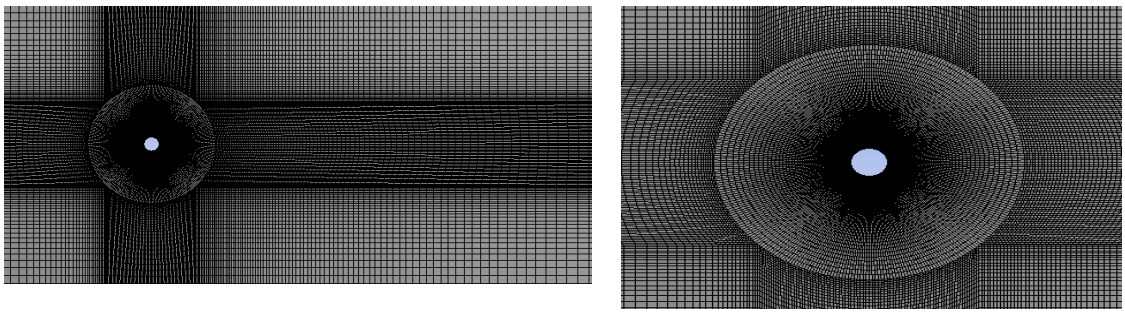

(a) **(b)**

Figure 2-3 (a) 2D computational mesh (b) close up mesh

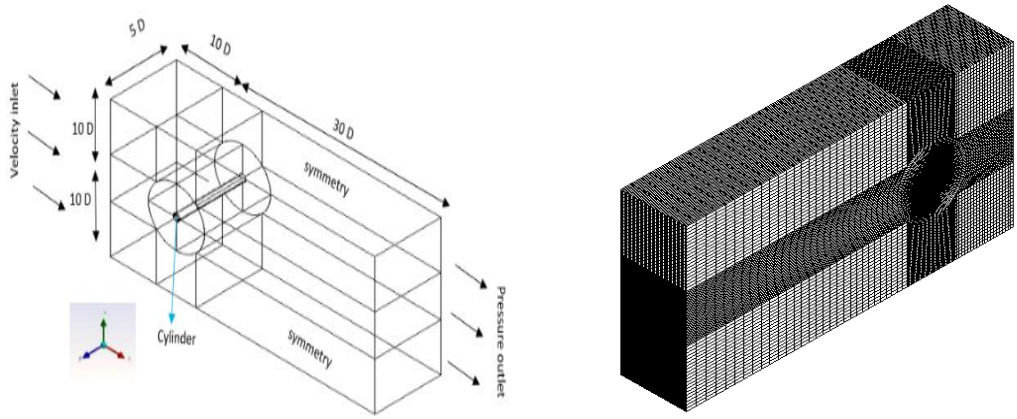

(a) **(b)**

Figure 2-4 3D multiblock computational domain (b) 3D computational mesh

2.3.6 Time step study

Time step study was performed against the drag coefficient (Cd) and crossflow vibration (Y/D) vibration. Three different time step sizes were used for both the 2D and 3D simulation as shown in Table 2-3 and Table 2-4 respectively. It can be seen from the results that as the time step reduces the Cd reduces slightly. Generally, the time required to perform a simulation is proportional to the timesteps size, hence an optimal timestep size must be chosen. From Table 2-3 and Table 2-4, it can be seen that for both 2D and 3D simulations, the difference between the Cd and Y/D value of time step 2 and 3 are small. Therefore, the time step size 0.002 seconds was used for all the simulation.

All the simulations were carried out on Cranfield university High performance computer (HPC), DELTA. The HPC is made up of two Intel E5 2620 v4 CPU, a user is allowed up to 128 cores in multiple of 16 cores and a total of 250GB of shared memory. The 2D simulation takes 8 hours using the 16 cores to achieve 10 seconds of simulation while the 3D simulation takes 20 hours to achieve 10 seconds of simulation using the 16 cores.

Table 2-3 Time step study of 2D cylinder under VIV at Ur=5

Simulation	Time(s)	Cd	Y/D
Time 1	0.005	1.216	0.823
Time 2	0.002	1.217	0.814
Time 3	0.001	1.232	0.832

Table 2-4 Time step study of 3D cylinder under VIV at Ur=5

Time step	Time(s)	Cd	Y/D
Time 1	0.005	1.331	0.769
Time 2	0.002	1.349	0.794
Time 3	0.001	1.344	0.801

2.4 Result and Discussion

This section analyses the 1DOF VIV of an elastically mounted rigid cylinder in two-dimension (2D) and three-dimension (3D). The simulations are conducted for a Reynold number range of 4000 to 24000, which corresponds to reduced velocity (Ur) 2-12. The non-dimensional vibrational amplitudes (Ay/D) are plotted against reduced velocity.

It can be seen from Figure 2-5 (a) that the present 2D numerical result of cylinder an elastically mounted cylinder with m*=2.4 and m ζ =0.0013 followed a similar trend as the experimental results of Khalak and Williamson (1996). The present numerical simulation captures the three response branches, i.e., the initial, upper and lower branches. However, the present 2D simulation recorded a lower maximum amplitude of 0.81 than the experimental result of 0.97.

Figure 2-5 (b) depicts the VIV of two cylinders with different mass ratios (2.4 and 11) but similar mass damping parameters (m*ζ) of 0.013. It can be observed from Figure 2-5 (b) that, as the mass ratio increases, the response amplitude decreases, and the range of reduced velocity where synchronisation occurs reduces. For example, at Ur=5, when the mass ratio increases from 2.4 to 11, the maximum amplitude reduces from 0.81 to 0.74. In addition, the effect of decreasing mass ratio was depicted in Figure 2-5 (C).it can be seen from the result that the variation of the vibration amplitude to decreasing mass ratio is nonlinear. As stated in Govardhan and Williamson (2004), below a certain critical mass ratio, the lower branch of the response disappears, and the upper branch continues to infinite reduced velocity. The 2D analysis does not capture the three-dimensionalities of the vortex shedding and may affect the response amplitude of the system; therefore, 3D simulation has been carried out at different mass ratios.

Figure 2-5 (d) and (e) shows the comparison of the 3D numerical result of a cylinder with m*=2 and 2.4 with the numerical results of Matin Nikoo et al. (2019) and Zhao et al. (2014). The graphs show that the result agrees well with the previous numerical result. In addition, it can also be seen from Figure 2-5 (d) and (e) that for m* 2 and 2.4, the 3D numerical simulation captures the three response

branches for the two-mass ratio considered. Furthermore, the effect of the two mass ratios and damping is shown in Figure 2-5 (f). The graph shows that both the damping parameter and mass ratio affect the VIV of an elastically mounted cylinder.

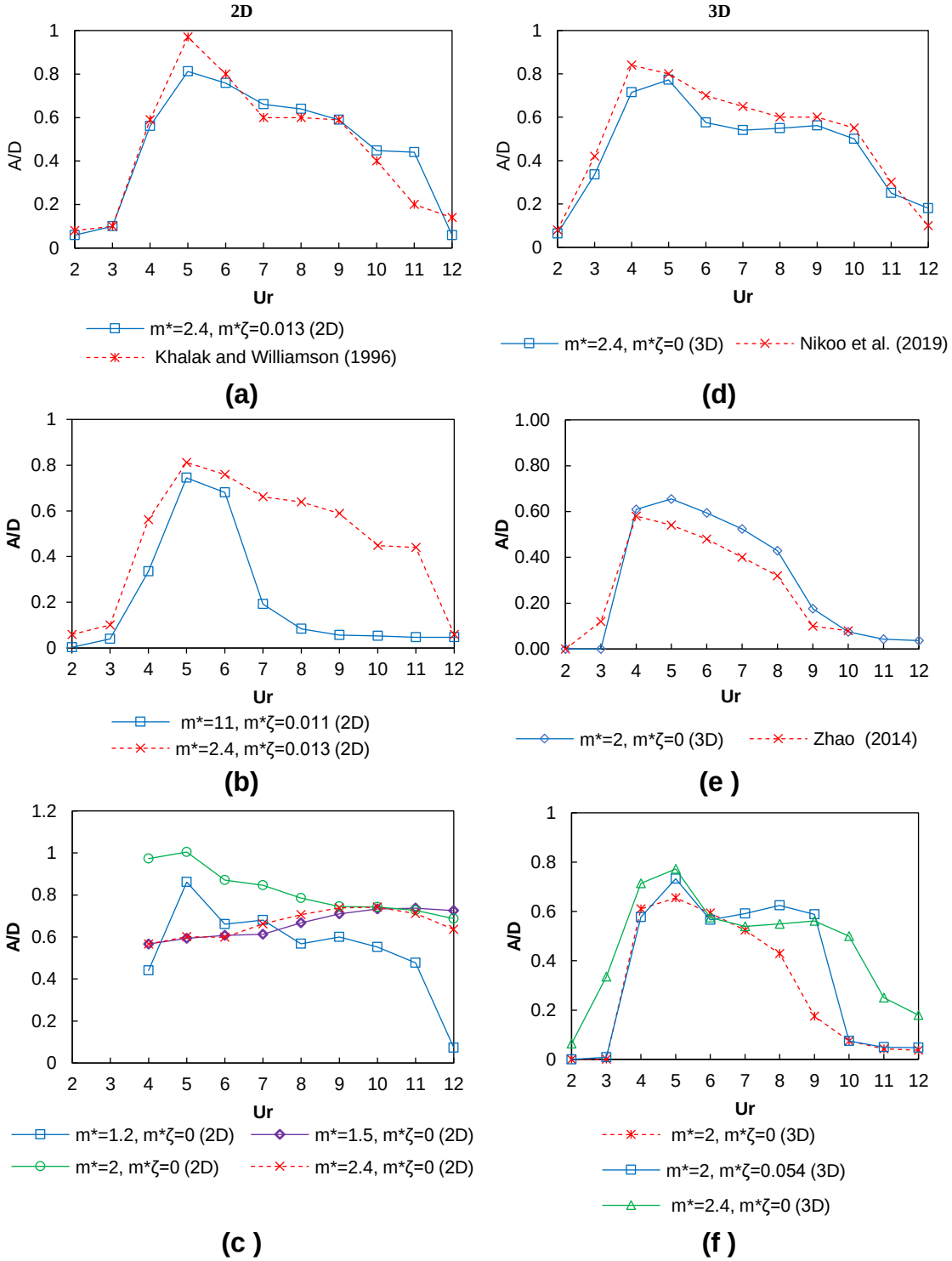

Figure 2-5 Variations of vibration amplitude of a 2D and 3D cylinder with reduced velocity(Ur) :(a) m*= 2, m* ζ =0 (; (b) 2D m*= 2, m* ζ =0, (c) 2D variation of m*and ζ ; (d) 3D m*= 2.4, m* ζ =0; (e) 3D m*= 2, m* ζ =0, (f) 3D variation of m* and ζ.

2.5 Conclusion

In this study, 2D and 3D numerical simulations have been performed to examine the effect of mass and damping ratios on an elastically mounted cylinder vibrating in the CF direction. The SST k-w model was used to solve the fluid flow governing equation. In addition, the vibration amplitude of the cylinder over a reduced velocities (Ur) range of 2-12 is examined and compared with the previous experimental and numerical results. As a result, the following conclusion can be drawn.

(1) The 2D and 3D analysis agree well with the previous experimental and numerical results.

(2) The three branches associated with low mass ratio cylinder are observed for both the 2D and 3D analysis.

(3) The vibration amplitude of the cylinder decreases with the increase in the mass ratio and damping ratio.

(4) The synchronous region reduces when the mass ratio reduces as the mass ratio increases.

Chapter 3

3 VIV OF A FLEXIBLE RISER

ABSTRACT

A series of 3D numerical simulations were conducted to investigate the effect of two different aspect ratios (300 and 482), velocity flow profile (uniform and sheared), velocity magnitude (0.42 and 0.84m/s), elastic modulus (102.5 and 1.025GPa), and orientation (horizontal and vertical) on the dynamic response of riser. The maximum Inline (IL) displacement, the Root Mean Square (RMS) of crossflow (CF) displacement, orbital trajectory, and vibrating frequency of the riser under different conditions are examined and compared. The results showed that the IL displacement and CF dominant vibration mode increased with increased flow velocity and aspect ratio (L/D). Similarly, the vibration mode increased with the reduction of elastic modulus.

3.1 Introduction

Risers are essential to transport hydrocarbon from the seabed to platforms safely. Vortex induced vibration (VIV) of risers has been studied using different methods such as experimental, analytical, and computational fluid dynamic (CFD) methods. Comprehensive reviews can be found in Wu et al.(2012) and Wang et al. (2020).

When fluid flows past a flexible riser, it deforms due to the hydrodynamic forces acting on it, thereby altering the fluid flow around it and the vortex shedding frequency of the fluid forces acting on it. The VIV of a flexible riser has been studied in the past few decades to understand the VIV response of such a flexible riser under different flow and structural conditions. Most studies on the VIV response of the riser are primarily experimental and analytical. As experimental studies are usually expensive, much research has been devoted to developing analytical models to predict the riser's dynamic response. Note that very little research has been based on the 3D numerical method to analyse the dynamic response of the riser due to high CPU and simulation time constraints. With the

increase in computational power, numerical methods, including 3D simulations, have become more attractive in the past few decades.

Lehn (2003) conducted an experiment to investigate the VIV of a bare and strake flexible riser with an aspect ratio of 482, exposed to a uniform and linearly sheared current. They observed that the vibration frequency increased with the current speed. Chaplin et al. (2005b) conducted an experiment to study the VIV response of a riser with an aspect ratio of 468 subjected to a stepped current. They found that the riser vibrates up to the eight vibration mode in the CF direction. Trim et al. (2005) performed an experiment to examine the VIV response of a bare and strake riser with an aspect ratio of 1400 subjected to a uniform and linearly sheared flow. They established that the bare riser's response differed from that of a strake riser. Lee and Allen (2010) conducted an experiment to analyse the effect of top tension on the dynamic response of a flexible cylinder subjected to a uniform flow. Their result showed that the top tension and structural stiffness significantly affect the riser's vibration frequencies and mode shape.

When the aspect ratio of the riser is low, Huera-Huarte and Bearman (2009a, 2009b) experimentally showed that the first-order mode was the dominant vibration mode. Huera-Huarte et al. (2014) observed that the dominant mode increases as the aspect ratio increases. Xu et al. (2009) conducted an experiment using a digital particle image velocimetry (DPIV) technique to evaluate the dynamic response of a flexible riser with an aspect ratio of 181. Xu et al. (2018) utilised the towing tank to examine the VIV of a flexible cylinder with an aspect ratio of 195.5. Their results agreed well with previous experimental results. Song et al. (2011) experimentally investigated the dynamic response of a long riser with an aspect ratio of 1750 and under a uniform flow. They observed the occurrence of multimodal vibrations in the CF direction. Song et al. (2016a, 2016b) obtained the hydrodynamic forces acting on a flexible riser subjected to a uniform and sheared flow from the measured strain obtained from a model experiment. They observed the presence of VIV increases the drag coefficient along the riser. Seyed-Aghazadeh et al. (2019) used a high-speed camera to predict the dynamic response of a flexible riser. They observed the transition from low to the high

mode when the flow velocity increased. Gedikli and Dahl (2017) investigated the spanwise motion of a cylinder subjected to a uniform flow using high-speed cameras. They observed the cylinder's vibration mode transition when the flow speed increased or decreased. Zhu et al. (2016) also used high-speed imaging technology to study the VIV of a curved flexible pipe exposed to external shear flows. They observed a multi-mode response and varying vibration frequencies under different flow velocities and locations along the pipe. Furthermore, Vandiver et al. (2009) conducted a field testing experiment in the ocean to investigate the dynamic response of a long flexible riser with an aspect ratio reaching up to 4200. They observed that the riser motion followed the regular 'figure eight', and the travelling wave was the dominant wave during VIV.

The major drawback of experimental testing is the high run cost and difficulty scaling up the model. Therefore, analytical and numerical methods are usually used to study the VIV of a riser with a high aspect ratio. Numerical methods can be classified into the time-domain and frequency domain methods. The time domain approach can be further divided into Computational Fluid Dynamics (CFD), wake oscillator, and force-decomposition models. In CFD, the hydrodynamic forces acting on the riser are obtained by solving the Navier-Stokes (N-S) equations.

In contrast, the hydrodynamic forces are obtained through a nonlinear oscillator model in the wake oscillator method. Those numerical approaches are cheaper than experiments and can also analyse large-scale risers. Therefore, numerical approaches are widely applied to study the VIV of long flexible risers.

Researchers such as Facchinetti et al. (2004), Mathelin and De Langre (2005), Violette et al. (2007), Xu et al. (2008), Ge et al. (2009) and Doan and Nishi (2015) used the wake oscillator model to predict the response of flexible riser. Srinil (2011) developed a model capable of predicting CF responses of variable-tension vertical risers placed in linearly sheared currents. Zanganeh and Srinil (2016) developed a semi-empirical model that considered the influence of the cylinder axial dynamics and mean drag on the VIV. They found that the mean inline and axial displacement increased with the uniform flow velocity. Gao et al. (2018)

developed a novel wake oscillator model that considered the influence of the Reynolds number to predict the vibration amplitudes and response frequencies of rigid and long flexible cylinders. Their results agreed well with previous studies. Recently, Gao et al. (2019a, 2019b, 2019c) used the wake oscillator model to investigate the effects of incoming velocity profile, aspect ratio and boundary conditions of a long flexible cylinder. They showed that the influence of the boundary conditions is more pronounced when the cylinder has a small aspect ratio. Also, the cylinder has mono-frequency and multi-frequency characteristics under uniform and linear shear flow, respectively.

Compared to the CFD method, the wake oscillator model is computationally less expensive but does not capture the whole dynamics of the riser motion under all flow conditions. The major disadvantage of the empirical method is that it focuses on the structural dynamics and neglects the flow field around the riser. Therefore, the CFD approach, which simulates the flow field around the riser by solving the Navier-Stokes equations, has been explored by many researchers.

To reduce the computational time of any full 3D numerical simulation, a meshless method called the Discrete Vortex Method (DVM) was developed to predict the VIV response of a cylinder. The DVM method computes the motion of the vorticity field to obtain the force acting on the cylinder. The DVM method is faster than a complete CFD approach, as the full N-S equations are not solved.

Meneghini et al. (2004) and Yamamoto et al. (2004) analysed the VIV of a riser exposed to a uniform and sheared flow using the 2D DVM approach. The hydrodynamic forces acting on the riser were calculated using DVM, while the dynamic response was calculated using the Finite Element Method (FEM), based on the Euler-Bernoulli beam equation. Their result showed that as the velocity increased, the dominant mode of the riser increased.

Sun et al. (2012) and Lin and Wang (2019) numerically investigated the VIV of a flexible riser using the strip-wise discrete vortex method (SDVM). They established that as the velocity increased, the mode shape increased, and their results compared well with the experimental investigation of Lehn (2003) and Chaplin et al. (2005a).

Another CFD method is the strip method, where multiple two-dimensional planes along the span of the riser are used to model the flow field around the riser and calculate the fluid force acting on the riser. This approach is cheaper than a full 3D CFD simulation, but the disadvantage of this approach is that it does not capture the three-dimensionality of the flow fields.

Willden and Graham (2004) used a 2D strip method called VIVIC to numerically study the effect of mass ratio on the dynamic response of long flexible vertical pipe with an aspect ratio of 1544 exposed to a uniform flow. The result showed that the vibration mode increased with increasing mass ratio. Bao et al. (2019) analysed the VIV of a flexible cylinder using the 3D thick strip model. The result showed that under a uniform velocity of 0.2m/s, the first mode dominated the vibration of the riser in the CF direction.

In addition, Duan et al. (2016, 2017, 2018) used the open-source CFD flow solver OpenFOAM to develop an in-house solver called the VIV-FOAM-SJTU. This flow solver is based on the strip theory CFD model, while the dynamic response is computed using 3D FEM. Duan et al. (2016) found out that the dominant mode decreased with the increase of top tension. Duan et al. (2017) established that the dominant mode increased with the aspect ratio. Duan et al. (2018) finally showed that the dominant mode increased with the increase of velocity and decreased with the increase of top tension. Fu et al. (2016, 2017) explored the impact of the cylinder mass and linear sheared rate on the dynamic response of the riser. They found that the dominant mode increased with increasing mass ratio shear rates. Deng et al. (2020) also extended the 2D strip plane to 3D and compared the results against the benchmark experiment of Lehn (2003) and Chaplin (2005). The result showed that the dominant mode increased with an increase in velocity and decreased with an increase in top tension.

As mentioned previously, the 2D strip method does not capture the three-dimensionality of the flow fields. Therefore, the response of the cylinder cannot be captured accurately. Therefore, a full 3D CFD simulation which solves the flow field around the riser has been used over time with the general increase in computing power. Direct Numerical Simulation (DNS) can be used to solve the

Navier-Stokes (N-S) equations of the flow, but this is a highly demanding (CPU and time) approach and not practical for most engineering applications.

DNS-based studies have however been reported. For instance, Newman and Karniadakis (1997) used DNS to investigate the VIV response of a flexible cylinder with an aspect ratio of 12.6 and 45 under a uniform flow. They found that the wake transition occurs at low *Re*. Evangelinos et al. (2000) and Lucor et al. (2001) also used DNS to analyse the VIV response of short and long flexible cylinders subjected to uniform and sheared flow. Lucor et al. (2001) observed a lower mode of vibration when the flow was linearly sheared, while higher modes were recorded when the flow had an exponential sheared profile. Bourguet et al. (2011a, 2011b, 2011c, 2013a, 2013b) studied the dynamic response of a cylinder with an aspect ratio of 200 under linear and exponential sheared flow.

Large Eddy Simulations (LES) are less demanding than DNS. Only the large eddies are resolved, this approach is therefore not as accurate as DNS, but is increasingly considered to solve engineering problems. However, Reynolds Averaged Navier-Stokes (RANS) methods are still the most commonly used approaches for engineering applications as they are fast and accurate enough for most cases. RANS-based models are computationally more efficient than DNS and LES, although limitations are present, depending on the RANS-based turbulence model considered.

More numerical studies are reported in the literature. For instance, Xie et al. (2011) used a finite volume CFD solver and an FEA solver-based Euler-Bernoulli beam theory to investigate the dynamic response of a flexible cylinder with an aspect ratio of 12. Stabile et al. (2018) developed a reduced-order model which coupled the FEM with CFD to investigate the VIV of a flexible riser. Holmes et al. (2006) used a finite element CFD solver to examine the VIV response of a plain and strake riser with an aspect ratio of L/D =1400 under a uniform velocity of 0.4m/s and 0.8 m/s. Their results showed that at low velocity, the solver under-predicted the vibration of the bare riser. In contrast, at intermediate current velocity, the vibration was over-predicted, which the authors attributed to the mesh size used in the study. Constantinides et al. (2007) performed a 3D

numerical simulation using the AcuSolve solver to investigate the dynamic response of riser with aspect ratios of 1407 and 4137. Their simulations were validated against the experimental result of Trim et al. (2005) and Vandiver et al. (2006). Constantinides and Oakley (2008a, 2008b) further simulated the VIV response of long bare and strake cylinders with aspect ratios of 4196 and 1407. Their results agreed with the experimental results from Jhingran and Vandiver (2007). Jaiman et al. (2009) then used AcuSolve and Abaqus to examine the dynamic response of flexible risers with aspect ratios of 50 and 1,407 under a uniform flow of 1.2 and 2 m/s. They observed that the mass ratio influenced the stability of the solver.

Numerical solvers like the Finite Analytic Navier-Stokes (FANS) code have also been used to model the fluid flow around a large flexible riser. For example, Huang et al. (2007) used the FANS code to investigate the VIV responses of a long riser (L/D=1400) under shear flows. They found that the vibration mode increased when the maximum velocity under the sheared velocity profile increased. Subsequently, Huang et al. (2011) investigate the effect of aspect ratio and top tension on the VIV response of a riser subjected to a uniform flow. Again, they found that the vibration mode increases when the velocity and aspect ratio increase. Recently, Menter et al. (2006) studied the dynamic response of a riser using the ANSYS MFX solver. They verified the accuracy of the ANSYS software in simulating fluid-structure problems. Chen and Kim (2010) performed a 3D numerical simulation using this solver to investigate the VIV response of a single and multi-assembled vertical flexible riser subjected to an external uniform and sheared flow. Wang et al. (2012, 2013, 2017) also used the ANSYS MFX solver to investigate the dynamic response of a long flexible exposed to a uniform and sheared flow. Subsequently, Wang and Xiao (2016) performed a 3D numerical simulation using ANSYS MFX to numerically investigate a flexible vertical riser's dynamic response under a uniform and sheared flow. Their results agreed with the experimental results of Lehn (2003). Wang et al. (2019a, 2019b, 2018) used the ANSYS system coupling to examine the effect of velocity, water depth and composite material on the vortex-induced vibration. The ANSYS system coupling provides an interface between CFD and CSD for exchanging information during

FSI simulations. It appears important to note that the study of a flexible riser with a large aspect ratio using 3D numerical simulations is still limited. Therefore, a full-scale 3D FSI analysis of the dynamic response of a riser was investigated in the present research using the ANSYS software (fluid and structural solvers along with the system coupling). This study provides a significant opportunity to advance the understanding of VIV response, instantaneous shape, oscillation modes, response amplitudes and frequencies of the flexible riser. To fully understand the dynamics of the flexible riser, firstly, the VIV of an elastic-mounted rigid cylinder was simulated using 2D and 3D methods. These numerical tests provided preliminary predictions. Secondly, 3D FSI simulations were performed on flexible risers. The riser displacement, vibration modes and frequencies were investigated. Finally, the effects of velocity profile, velocity magnitude, risers' orientation, aspect ratio and elastic modulus were studied in detail.

This chapter is organised as follows. First, the numerical method utilised to perform the VIV simulations are explained in section 3.2. Then, Section 3.3 provides a description of the problem, including the definition of the fluid and structure properties. Next, section 3.3.6 examines the riser's inline (IL) and crossflow (CF) displacements, vibrating frequencies, and orbital trajectory under different external flow conditions. Finally, the conclusions and recommendations for further study are provided in Section 3.5.

3.2 Problem description

The effect of velocity magnitude, velocity profile, riser's aspect ratio, elastic modulus, and orientation of the riser on the VIV characteristic such as the mode shape, vibrating frequencies, orbital trajectories, IL and CF displacement were investigated. Figure 3-2 (a) and (b) show the schematic of the horizontal and vertical risers. Note that the risers considered were free to vibrate in the IL and CF directions, and the two ends of the risers were fixed. Those risers were subjected to two velocity profiles: a uniform flow and a linearly sheared flow. In addition, the vertical riser was subjected to a uniform and linearly sheared velocity profile, while the horizontal riser was subjected to a uniform profile only. The velocity profiles applied for this work were chosen to cover offshore fields' typical

current velocity range (Chen, 2006). Therefore, four different velocities consisting of two uniform velocities (0.42m/s and 0.84m/s) and two linearly sheared flows with maximum velocities (Vmax) of 0.42m/s and 0.84m/s were considered. Table 3-1 presents the fluid properties, including density, kinematic viscosity coefficient, and fluid flow velocity. The riser considered here has an outer diameter (D) of 20mm, and a thickness (t) of 0.45mm. The length of the riser varied from 6m to 9.6m, corresponding to an aspect ratio of 300 and 481.5, respectively. The riser wall has a density (ρ) of 7850 kg/m^3 and a poison ratio (v) of 0.3. Furthermore, two Elastic moduli, E=102.5 GPa and 1.025 GPa, were considered to study the riser's elastic modulus effect on the VIV. Table 3-2 presents the summary of the physical and structural properties of the riser. In total, 16 cases were simulated, as summarised in Table 3-3.

Table 3-1 fluid properties for VIV analysis

Properties	Values	SI Units
Density of fluid (ρ_f)	1000	kg/m^3
Dynamic viscosity (μ)	0.001	Pa-s
Velocity (U_1, U_2)	0.42; 0.84	m/s

Table 3-2 Properties of flexible riser for VIV analysis

Properties	Values	SI Units
Outer diameter (D_o)	20	mm
Thickness (t)	0.45	mm
Length (L)	6; 9.63	m
Aspect ratio (L/D)	300; 482	
Density of riser (ρ_s)	7850	kg/m^3
Elastic Modulus (E_1, E_2)	102.5; 1.025	GPa
Poison ratio (v)	0.3	

Table 3-3 Cases for flexible riser VIV analysis

case	Orientation	L/D	Elastic modulus (GPa)	U(m/s)	Velocity profile
1	Horizontal	300	102.5	0.42	Uniform
2	Horizontal	300	102.5	0.84	Uniform
3	Vertical	300	102.5	0.42	Uniform
4	Vertical	300	102.5	0.84	Uniform
5	Vertical	300	102.5	0.42	Sheared
6	Vertical	300	102.5	0.84	Sheared
7	Horizontal	482	102.5	0.42	Uniform
8	Horizontal	482	102.5	0.84	Uniform
9	Vertical	482	102.5	0.42	Uniform
10	Vertical	482	102.5	0.84	Uniform
11	Vertica	482	102.5	0.42	Sheared
12	Vertical	482	102.5	0.84	Sheared
13	Horizontal	300	1.025	0.42	Uniform
14	Horizontal	300	1.025	0.84	Uniform
15	Horizontal	482	1.025	0.42	Uniform
16	Horizontal	482	1.025	0.84	Uniform

3.3 Numerical method

ANSYS Fluent and ANSYS Mechanical were used to simulate the flow field and the dynamic response of the riser, and the ANSYS system coupling was used for the coupling and data transfer during the FSI process. The VIV simulations of the flexible riser were performed on the Cranfield HPC system. A time step of 0.005s was applied for the numerical work, and it took approximately 50 hours to achieve a 5s VIV simulation using multiple 32 cores of the Cranfield University HPC system. Figure 3-1 shows a snapshot of how the fluid solver (FLUENT) and the structural solver (Transient structural) were connected via the system coupling module in ANSYS Workbench.

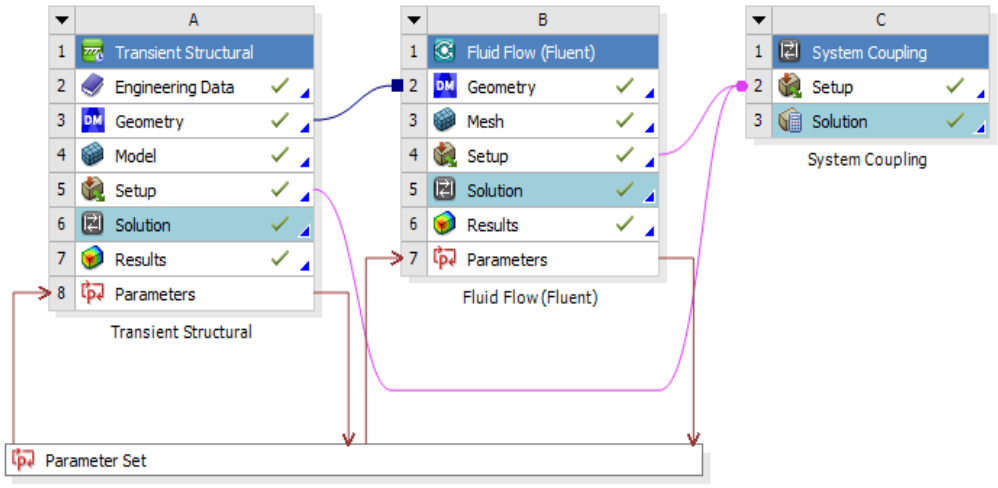

Figure 3-1 Snapshot of system coupling set up for ANSYS two-way FSI coupling

3.3.1 Fluid domain

The dimensions of the fluid domain affect the wake vortices and displacement of the riser. Therefore, a suitable domain is chosen based on simulations reported by Wang and Xiao (2016). Schematics of the horizontal and vertical riser fluid domains are shown in Figure 3-2 (a) and (b). The domain dimensions are normalised with the riser's outer diameter D. This fluid domain has a length of 40D and a width of 20D. The height of the domain is based on the riser's aspect ratios, i.e. 300 and 482. The riser is located 10D and 30D far from the inlet and outlet boundaries, respectively. A velocity inlet type boundary condition was considered at the inlet of the domain. This inlet flow velocity was assumed to be either uniform or sheared, as presented in Figure 3-3. The sheared flow velocity profile used is similar to that of Wang and Xiao (2016) which is described as:

$$V_{profile} = (1 - 0.86(y/L))\, V_{max} \tag{3-1}$$

where V_{max} is the maximum velocity, L the length of the riser and y the elevation of the riser.

A pressure outlet type boundary condition was considered at the outlet section of the domain. Symmetry (free slip) boundary conditions were applied at the two-

transverse and two spanwise boundaries. A symmetric condition implies that the velocity component perpendicular to the boundary is zero ($\partial u/\partial y = 0; v = 0$). A no-slip boundary condition was applied on the riser surface, which means that the fluid velocity is the same as the vibration velocity of the riser. In addition, the riser surface serves as the fluid-structure interaction surface, i.e., the data transfer surface between the fluid and structural solvers**.**

The Fluent flow solver was used to solve the governing equations describing the flow field around the riser. This flow field was considered transient and incompressible. The following equations of mass and momentum were solved when running the flow simulations.

$$\frac{\partial \bar{u}_i}{\partial x_i} = 0 \tag{3-2}$$

$$\frac{\partial(\rho\bar{u}_i)}{\partial t} + \frac{\partial\left(\rho\bar{u}_i\bar{u}_j\right)}{\partial x_j} = -\frac{\partial \bar{p}}{\partial x_i} + + \frac{\partial}{\partial x_j}\left(2\mu\overline{S_{ij}} - \rho\overline{u'_i u'_j}\right) \tag{3-3}$$

where μ is the dynamic viscosity, ρ the fluid density, t the time, x_i and x_j the position vectors of the fluid unit (*i, j* ∈ [1, 2, 3]). In addition, $\bar{u}$ and $\bar{p}$ represent the time averaged velocity and pressure, respectively, while $\bar{S}_{ij}$ is the mean rate of the strain tensor, obtained by Equation (3-4). Finally, $\overline{\rho\, u'_i u'_j}$ in Equation (3-3) is the Reynolds-stress tensor, which represents the small-scale fluctuation of the fluid velocity defined through Equation (3-5).

$$\bar{S}_{ij} = \frac{1}{2}\left(\frac{\partial \bar{u}_i}{\partial x_j} + \frac{\partial \bar{u}_j}{\partial x_i}\right) \tag{3-4}$$

$$\tau_{ij} = -\overline{\rho u'_i u'_j} = 2\mu_t \bar{S}_{ij} - \frac{2}{3}k_t\delta_{ij} \tag{3-5}$$

where μ_t is the turbulent viscosity, $k = \frac{1}{2}\overline{u'_i u'_i}$ is the turbulent kinetic energy, δ_{ij} is the Kronecker function, and τ_{ij} is the viscous stress tensor.

The (SST) k-ω turbulence model was used to compute the Reynolds stresses in this study. The k-ω two-equation formulation was formulated by Wilcox (1988, 1991, 1993). Wilcox (1988) is commonly used, where one equation solves the transport of the turbulent kinetic energy *k*, and the other one solves the specific dissipation rate ω. The Shear Stress Transport (SST), developed by Menter, (1994), is a variant of the k-ω model. This model switches automatically from a k-ω definition near the walls to the k-ε definition in the bulk flow, which makes this model efficient in the sublayer near the walls, and far away from the walls (Loyseau, Verdin and Brown, 2018).

A pressure-based segregated algorithm called the Semi-Implicit Method for Pressure Linked Equations (SIMPLE) algorithm was selected as the pressure-velocity coupling. In addition, a second-order upwind scheme was used to discretise the pressure and momentum equations, while a first-order upwind scheme was used for both k and ω. A first-order implicit transient formulation was selected to solve the time-dependent nature of VIV. A Squares Cell-Based scheme was used for the gradient in spatial discretisation. Finally, a convergence criterion of 10^{-3} was considered for all simulations.

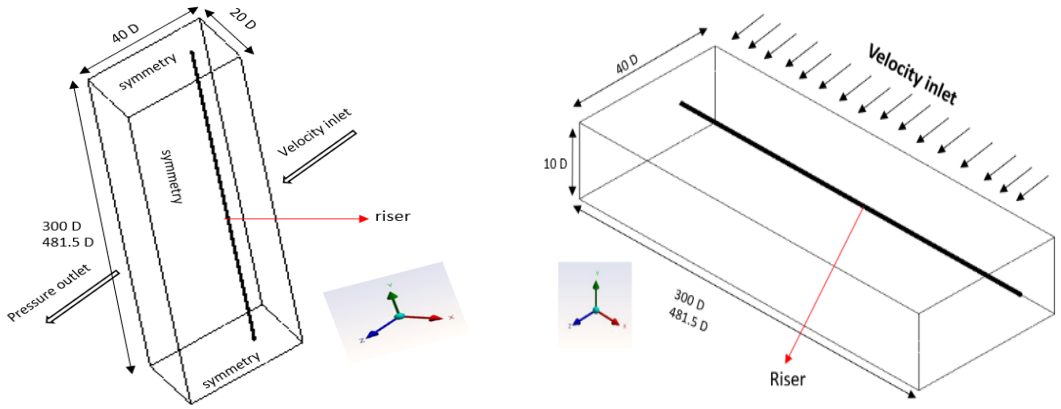

Figure 3-2 computational domain of (a) vertical riser and (b) horizontal riser

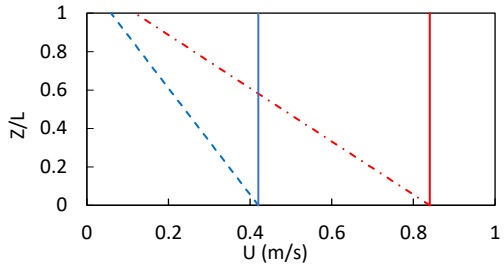

Figure 3-3 uniforms and linearly sheared inlet velocity profile

3.3.2 Solid domain

The riser geometry and the structural properties such as the density, Poisson's ratio, and young modulus of elasticity are listed in Table 3-2. The top and bottom end of the riser are defined as fixed supports, and the riser is free to vibrate in the IL and CF directions. The outer surface of the riser served as a fluid-solid interface where hydrodynamic forces obtained from the fluid solver were applied. The Finite element method (FEM)-based ANSYS Mechanical module in ANSYS 2019 R2, was used to solve the vibration response of the flexible riser, this flexible riser being modelled as beams, and the cylinders' vibrations satisfying the Euler-Bernoulli beam theory. Therefore, the motion of the non-tensioned Euler Bernoulli beam of flexible cylinders can be described as:

$$m\frac{\partial^2 x}{\partial t^2} + c\frac{\partial x}{\partial t} + \frac{\partial^2}{\partial z^2}\left[EI\ \frac{\partial^2 x}{\partial z^2}\right] = F_x \tag{3-6}$$

$$m\frac{\partial^2 y}{\partial t^2} + c\frac{\partial y}{\partial t} + \frac{\partial^2}{\partial z^2}\left[EI\ \frac{\partial^2 y}{\partial z^2}\right] = F_y \tag{3-7}$$

where E represents the elastic modulus, *I* the moment of inertia, m is the mass per unit length, c is the structural damping, z is the undeflected cylinder axial coordinate, x and y are the IL and transverse displacements, and finally F_x and F_y are the hydrodynamic forces in the IL and CF directions, respectively.

The FEM was used to discretise the riser into *n* elements. For each element, the governing equation was written as Equations (3-8) and (3-9)

$$m\ddot{X} + c\dot{X} + kx = F_x \tag{3-8}$$

$$m\ddot{Y} + c\dot{Y} + kY = F_y \tag{3-9}$$

where k is the stiffness of the structural element. Hence, the mass-spring-damping (MCK) equations of the whole system can be expressed as Equations (3-10) and (3-11).

$$M\{\ddot{X}\} + C\{\dot{X}\} + K\{X\} = \{F_X\} \tag{3-10}$$

$$M\{\ddot{Y}\} + C\{\dot{Y}\} + K\{Y\} = \{F_Y\} \tag{3-11}$$

where M , C , and K are the mass, damping and stiffness matrixes of the system, respectively. F_X and F_Y are hydrodynamic force vectors in the IL and CF directions, respectively, and a dot denotes a differentiation with respect to time. K is the equivalent stiffness matrix which is converted from the bending stiffness EI.

During the simulation, hydrodynamic forces (drag and lift forces) were exerted onto the riser. The hydrodynamic forces were obtained from the flow solver, which were then substituted into the mass spring damper, Equations (3-10) and (3-11), to determine the riser motion via ANSYS mechanical. The hydrodynamic forces are described through Equations ((3-12) and (3-13).

$$F_D = \frac{1}{2} C_D \rho U^2 D \tag{3-12}$$

$$F_L = \frac{1}{2} C_L \rho U^2 D \tag{3-13}$$

where F_D is the drag force, F_L the Lift force, C_D the drag coefficient and C_L the lift coefficient. Also, U is the velocity and D is the cylinder diameter.

3.3.3 Fluid structure interaction

As mentioned previously, the fluid flow around the riser is solved with ANSYS Fluent, and the dynamic response is solved with ANSYS Mechanical. The two solvers are connected via the ANSYS system-coupling to solve the fluid-structure interaction problem. Hydrodynamic forces acting on the riser are obtained first from the fluid solver and transferred to the structural solver as external forces. The structural solver then determines the riser's dynamic response. At this stage, the fluid mesh is deformed and updated. This process is repeated until convergence of the mechanical solver is reached.

The ANSYS system coupling provides a platform where data are transferred between solvers, thereby controlling whether the simulation is one-way or two-way coupling. When the data transfer is only from the fluid solver to the structural solver, the process is referred to as one-way FSI. A one-way coupling approach is thus not recommended for large deformations. However, when data is transferred from both the fluid and structural solvers, the process is referred to as two-way FSI (the fluid flow induces a deformation of the structure, which in turn affects the fluid flow). Two types of two-way coupling methods exist: monolithic and partitioned iterative. The flow and structural equations are solved using one solver in the monolithic method. Therefore, this method becomes mathematically challenging. In the partitioned iterative method, however, the fluid flow and structural response are solved using two separate solvers, making the calculations easier. The ANSYS system coupling uses a partitioned iterative implicit two-way coupling method. A time step size of 0.005s and a coupling limit of 5 iterations were considered with an implicit scheme. These values, established through trial and error, enhanced the stability of the solution. To ensure that a fully mapped load transfer is achieved between the fluid and the structural part, the FSI surfaces created in the fluid and structural domain are discretised with similar mesh elements.

The mesh deforms when the riser vibrates, the coupling process being activated. A dynamic mesh methodology enables fluid and solid meshes to move to a new position during the two-way FSI simulation. There are two types of dynamic mesh methods: moving and overset mesh. In the moving mesh method, the mesh moves as the riser deforms. This method is used in the current study. The overset mesh considered that the mesh is fixed, and the body moves inside it.

Smoothing and remeshing dynamic mesh methods are used in this work, to estimate the mesh's movement and deformation. When considering the smoothing method, the number of nodes and their connectivity remain constant with the motion of the zones, thereby avoiding negative volume errors. As the riser vibrates, the mesh moves according to the Laplace Equation (3-14).

$$\nabla.(\gamma\nabla\vec{u}) = 0 \tag{3-14}$$

where $\vec{u}$ represents the velocity of mesh displacement, and γ represents the diffusion coefficient.

The mesh continues to deform and update its new position throughout the simulation until a stable simulation is achieved over time. A time step of 0.005s was used to perform all the simulations.

3.3.4 Mesh

A 3D FSI calculation can be computationally intensive, depending on the mesh size in the fluid and solid domains. Therefore, a mesh sensitivity study was performed using three mesh sizes to determine the optimum mesh size and ensure that the numerical results are independent of the mesh density. ANSYS meshing was used to generate the meshes of the fluid and solid domains for the horizontal and vertical risers configurations. The computational domain was divided into multiple blocks, as shown in Figure 3-4 .

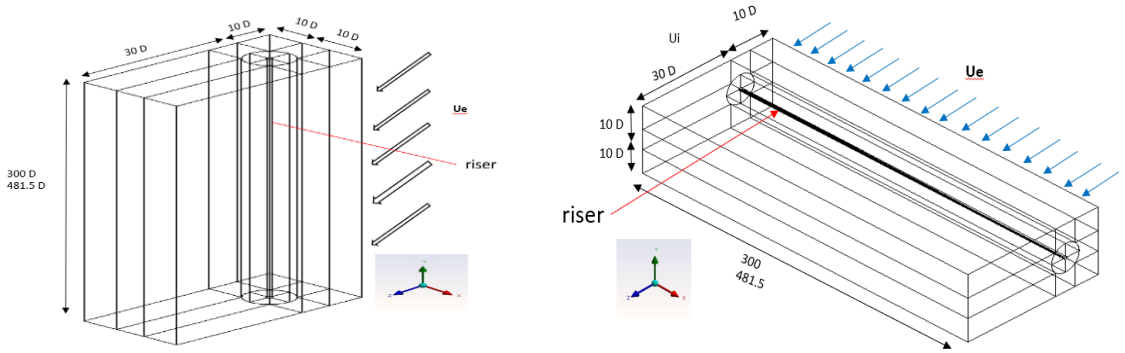

(a) **(b)**

Figure 3-4 Computational domain of (a)Vertical and (b) Horizontal risers divided into block

The multiblock concept controls the mesh size so that a fine mesh can be created near the riser to capture flow separation while a coarse mesh is generated far away from it, as shown in Figure 3-5 . The distance of the first cell next to the riser was 0.001D to obtain a y+ value less than 1 and ensure compliance with the requirements of the turbulence model selected for this work, the (SST) k-ω model, and ensure that the mesh at the wall is suitable for the wall treatment considered. The y+ value is a non-dimensional distance at the wall, function of the wall shear stress, fluid density and fluid viscosity.

$$y^+ = \frac{y u_\tau}{\nu} \tag{3-19}$$

where y is the distance at the wall of the first cell, ν is the kinematic viscosity of the fluid, and u_τ is the friction velocity, defined as:

$$u_\tau = \sqrt{\frac{\tau_w}{\rho}} \tag{3-20}$$

with ρ the density of the fluid, and τ_w the wall shear stress.

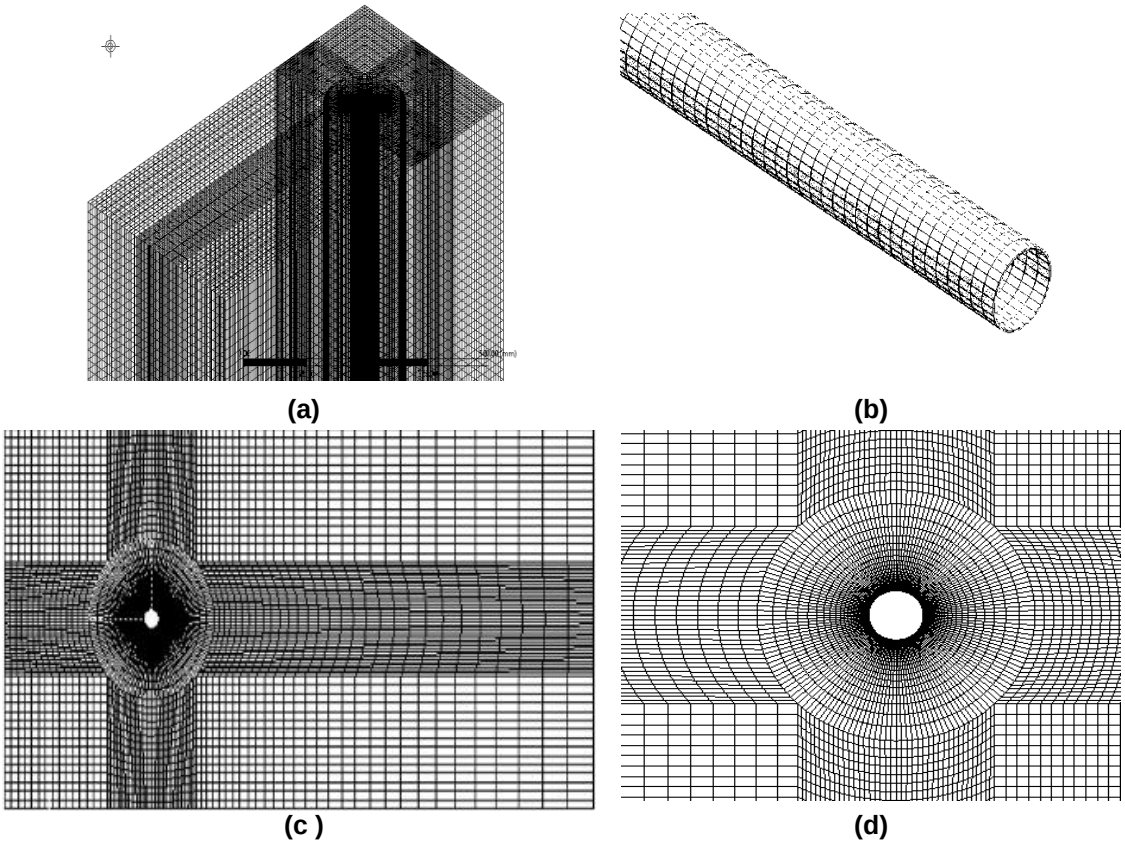

Figure 3-5 Computational (a) fluid domain meh (b) solid domain mesh (c) 2D mesh (d) close-up view of 2D mesh

Figure 3-5 (b) shows the solid mesh of the riser. The riser's inner and outer circumferential edges were divided into 60 equal divisions. The span of the riser was discretised into 500 elements. The solid meshing strategy adopted here is similar to the work of Wang and Xiao (2016).

For the fluid domain, the number of cells along the pipe span (Nz), and circumference (Nc) are adjusted to obtain an optimum mesh. As can be seen from Table 3-4, the drag coefficient Cd and maximum IL displacement are measured based on three different mesh size. It can be seen that increasing the number of cells of from mesh 2 to mesh 3 does not lead to any significant changes in those two parameters. Therefore, Mesh 2 is selected for all the numerical work.

Table 3-4 Mesh dependency study of s vertical riser with L/D=482 at U =0.84m/s

	CFD mesh			FEA mesh				
Mesh	Nz	Nc	Total	Nz	Nc	Total	Cd	IL
Mesh 1	30	160	369,600	250	30	7500	0.99	5.92
Mesh 2	50	160	656,000	250	30	7500	1.00	6.62
Mesh 3	100	160	1,312,000	250	30	7500	1.00	6.52
Mesh 4	100	160	1,920,000	250	30	7500	1.00	6.69

3.3.5 Time step study

The maximum IL displacement of three different time step sizes using the mesh 2 are tabulated in Table 3-5. It can be seen that the difference between the IL displacement of time steps 1 and 2 is significant. However, for times step 2 and 3 the difference is small. Therefore, timestep size of 0.005s is selected for the numerical simulations in the present study.

Table 3-5 Time study of a vertical riser with L/D=482 atUe=0.84

Time step	Time(s)	IL
1	0.05	6.12
2	0.02	6.60
3	0.005	6.62

The FSI simulations were carried out on Cranfield university High performance computer (HPC), DELTA. The HPC is made up of two Intel E5 2620 v4 (Broadwell) CPU, a user is allowed up to 128 cores in multiple of 16 cores and a total of 250GB of shared memory. In this research, for the 3D simulation of the flexible riser, it takes 50 hours with 32 cores to obtain 5 seconds of simulation. A sinusoidal vibration of the midpoint of the riser is achieved at 5 seconds. In addition, the simulation takes 50GB of space for each 5 seconds. One of the major challenges faced during simulation is the inability to restart the simulation at a given time when the simulation fails while running on the HPC. This has caused much delay in the simulation. In addition, the Cranfield HPC system

followed a queuing system before a simulation can start. Sometimes, the queueing time can be over 3 days.

3.3.6 Validation

The present horizontal riser with aspect ratio of 482, exhibits the second mode of vibration in the CF direction when exposed to uniform flow of 0.42m/s, which is in agreement to the experimental study of Lehn (2003) and the numerical study of Wang and Xiao (2016). Similarly, for a vertical riser under similar condition, it can be observed that the present simulation under predict the dominant vibration mode at Ue=0.42m/s. While Lehn (2003) and Wang and Xiao, 2016 observed a dominant second mode in the CF direction, in this study, a multimodal mode is observed comprising mode 1 and mode 2, with mode 1 being dominant for vertical riser. The discrepancies can be attributed to the tension applied in the riser in the experimental study of Lehn (2003) while tension is omitted in the present study. Tension is neglected in this study because it affects the stability of the simulation. The horizontal riser is tensioned due to its weight compared to the vertical riser.

3.4 Results and discussion

In order to investigate the VIV of a flexible pipe exposed to external current, simulations were carried out for two different aspect ratios (300 and 482), elastic moduli (102.5GPa and 1.025GPa), orientations (horizontal and vertical), velocity profiles (uniform and sheared) and velocity magnitude (0.42 and 0.84m/s). The effects of aspect ratio, elastic modulus, orientation, velocity profile and velocity magnitude on the IL and CF displacements, vibrating frequencies, and orbital trajectories were thus investigated. At least two flow and structural parameter combinations were varied or held constant in this analysis.

3.4.1 Modal analysis

The natural frequencies (f_n) and mode shape of the riser were obtained by performing a modal analysis using the ANSYS modal 2019 R2 feature. The modal analysis was performed for both aspect ratios of 300 and 482, and both orientations of the riser. The natural frequency of the horizontal and vertical risers was found to be similar. Table 3-6 and Figure 3-6 show the riser's natural frequency and mode shape.

Table 3-6 Natural frequency (f_n) of the riser with E= 102.5GPa

Mode	Frequency (Hz)	
	L/D=300	L/D482
1	2.47	0.96
2	6.81	2.64
3	13.35	5.18

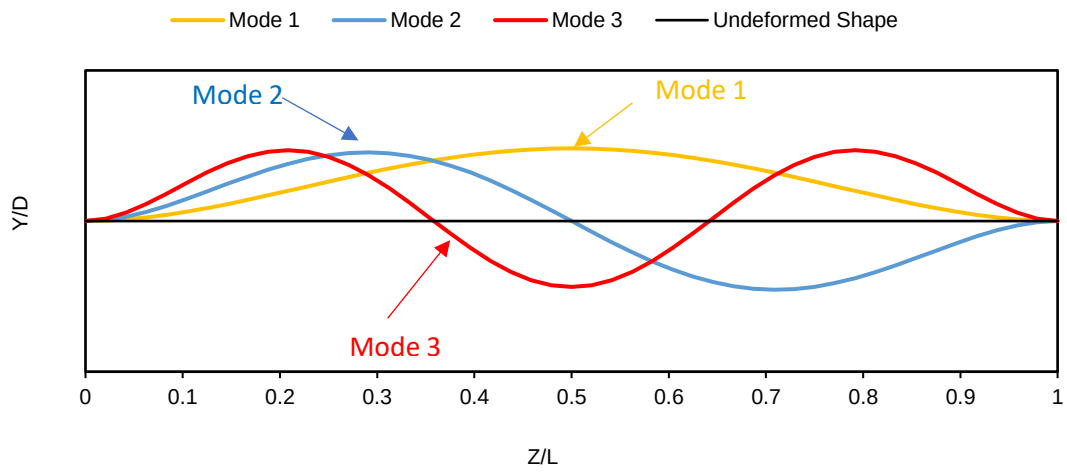

Figure 3-6 Vibration mode shape of a horizontal and vertical riser with E=102.5GPa for L/D=300 and 482.

3.4.2 VIV of a flexible riser with L/D =300

3.4.2.1 Inline displacement

Figure 3-7 (a-c) depicts the maximum IL displacement of the horizontal and vertical risers subjected to an external velocity, Ue=0.42 and 0.84m/s. The solid and dashed lines represent the results for 0.42m/s and 0.84m/s, respectively. When the riser is subjected to an external flow, it deflects in the IL and CF directions until it reaches an equilibrium position (Chen, 2006). For example, it can be seen from Figure 3-7 (a) that for a horizontal riser, the maximum IL displacement under a uniform flow of 0.42 and 0.84m/s reached 1.48 and 2.20, respectively. Similarly, for the vertical riser under a uniform velocity of 0.42m/s and 0.84m/s, the maximum IL displacement was 1.97 and 3.64, as shown in Figure 3-7 (b). In addition, under sheared flow conditions, the maximum IL displacement of the vertical riser was 0.39 and 1.05 when subjected to shear flow with maximum velocities of 0.42 and 0.84m/s, respectively, see Figure 3-7 (c). Thus, the results here showed that the maximum IL deflection increased as the velocity increased under a uniform and linear shear flow.

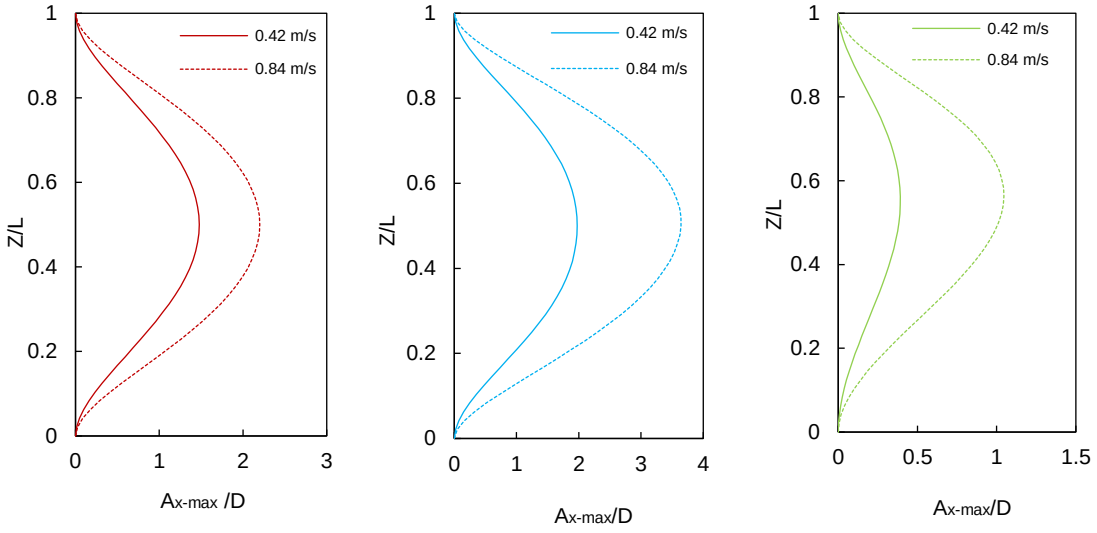

Figure 3-7 Comparison of maximum IL displacement of a riser with E = 102.5GPa and L/D= 300: (a) Horizontal and (b) vertical orientation subjected to uniform flow, and (c) vertical orientation subjected to sheared flow.

This can be explained by the fact that the drag force is proportional to the square of the current speed (Huang et al., 2011). It can also be seen in Figure 3-7 (a) and (b) that under uniform flow, the IL displacements occur at the riser's middle section irrespective of the velocity value and orientation. This shows that the IL displacement is symmetrical about the riser's elevation. However, under sheared flow conditions, the IL displacements of the vertical riser occur at around Z/L= 0.56 and 0.54 along the riser span, see Figure 3-7 (c). Therefore, the IL displacement is asymmetric about the elevation for all maximum sheared velocities considered.

3.4.2.2 Crossflow displacement

The root-mean-square (RMS) was used to evaluate the CF displacement along the span of the flexible riser since, at higher velocities, the CF displacements become more irregular. Figure 3-8 (a-c) thus shows this CF RMS displacement of the horizontal and vertical risers under uniform and sheared flows of 0.42m/s and 0.84m/s. The solid and dashed lines represent the CF vibration for 0.42m/s and 0.84m/s, respectively.

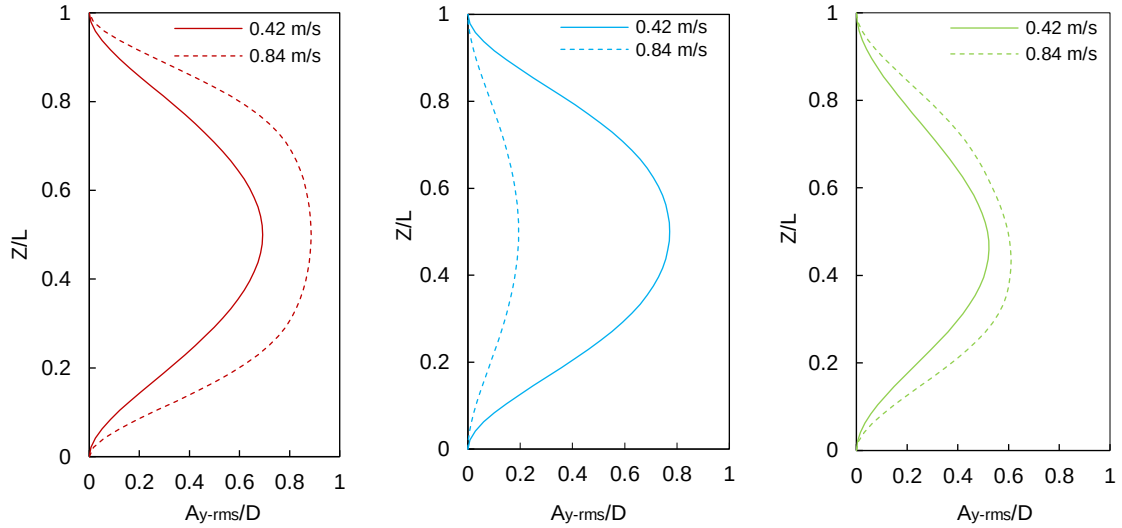

Figure 3-8 Comparison of CF RMS displacement of a riser with E = 102.5GPa and L/D= 300: (a) Horizontal and (b) vertical orientation subjected to uniform flow (c) vertical orientation subjected to sheared flow.

It can be seen from Figure 3-8 that the first vibration mode is the dominant mode, irrespective of the velocity magnitude, velocity profile and orientation. Under a uniform flow, the maximum CF RMS displacement occurs when Ue=0.42m/s for the horizontal riser, while for the vertical riser, the maximum CF RMS displacement occurs when Ue=0.84m/s. In addition, it can be seen from Figure 3-8 (b) and (c) that the maximum CF RMS displacements under the linearly sheared currents are lower than under a uniform flow when Ue=0.42m/s. The CF RMS displacement also appears symmetrical about the z-axis for all velocities under the uniform flow, as shown in Figure 3-8 (a) and (b). In contrast, the RMS displacements are asymmetrical about the z-axis under the linearly sheared currents. Figure 3-9 (a-c) shows the instantaneous non-dimensional response envelope of a vertical and a horizontal riser under a uniform flow and a shear flow. At an aspect ratio of 300, a single mode (Mode 1) is the dominant mode, irrespective of the velocity magnitude, velocity profile and orientation of the riser.

3.4.2.3 Vibrating frequencies and Orbital Trajectories

The time histories, response frequencies and orbital trajectories of the horizontal and vertical risers under a uniform linearly sheared flow are shown in Figure 3-10 , Figure 3-11 and Figure 3-12 , respectively. The first column represents the time histories of CF displacement, the second column represents the CF vibration response frequency, and the third column represents the orbital trajectory of the midsection of the riser. From the time histories, it can be seen that both risers under different flow and orientations reached harmonic vibration after 2 seconds. A Fast Fourier transform (FFT) analysis was conducted for the CF vibration to determine the riser's vibration frequency. VIV occurs when the natural frequency of the riser is close to the vortex shedding frequency, and the IL frequency of the riser is almost twice the CF frequency. The natural frequency of the riser was obtained by performing a modal analysis in ANSYS MECHANICAL see Table 3-6. For the horizontal riser under a uniform flow, it could be established from Figure 3-10 (b) that when Ue increased from 0.42m/s to 0.84m/s, the dominant frequency in CF oscillations increased from 3.32Hz to 4.49Hz, respectively.

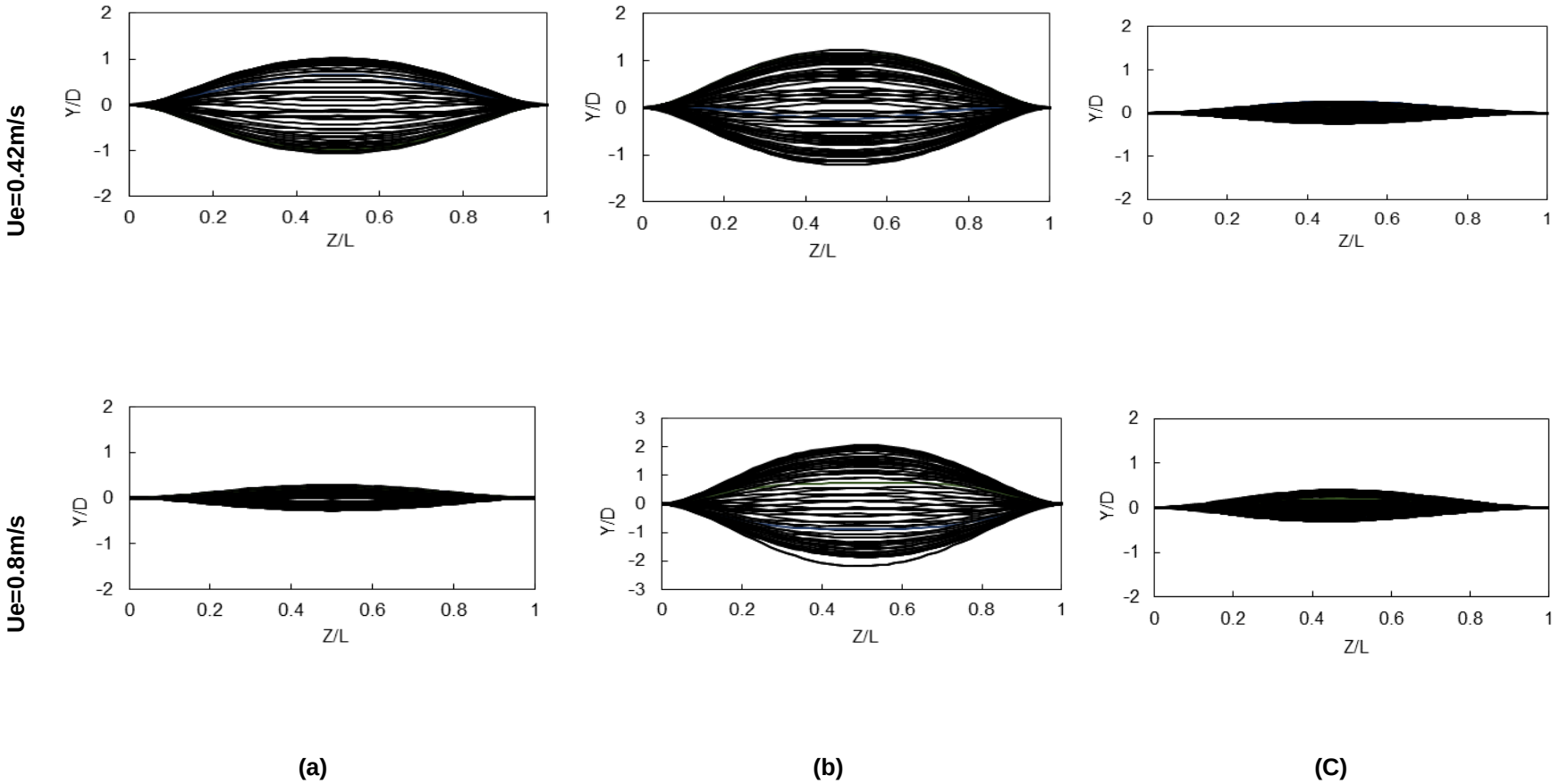

Figure 3-9 Comparison of CF response envelopes of a riser with a constant elastic modulus of 102.5GPa and aspect ratio of 300: (a) Horizontal orientation and uniform flow, (b) vertical orientation under uniform flow, and (c) vertical orientation under sheared flow.

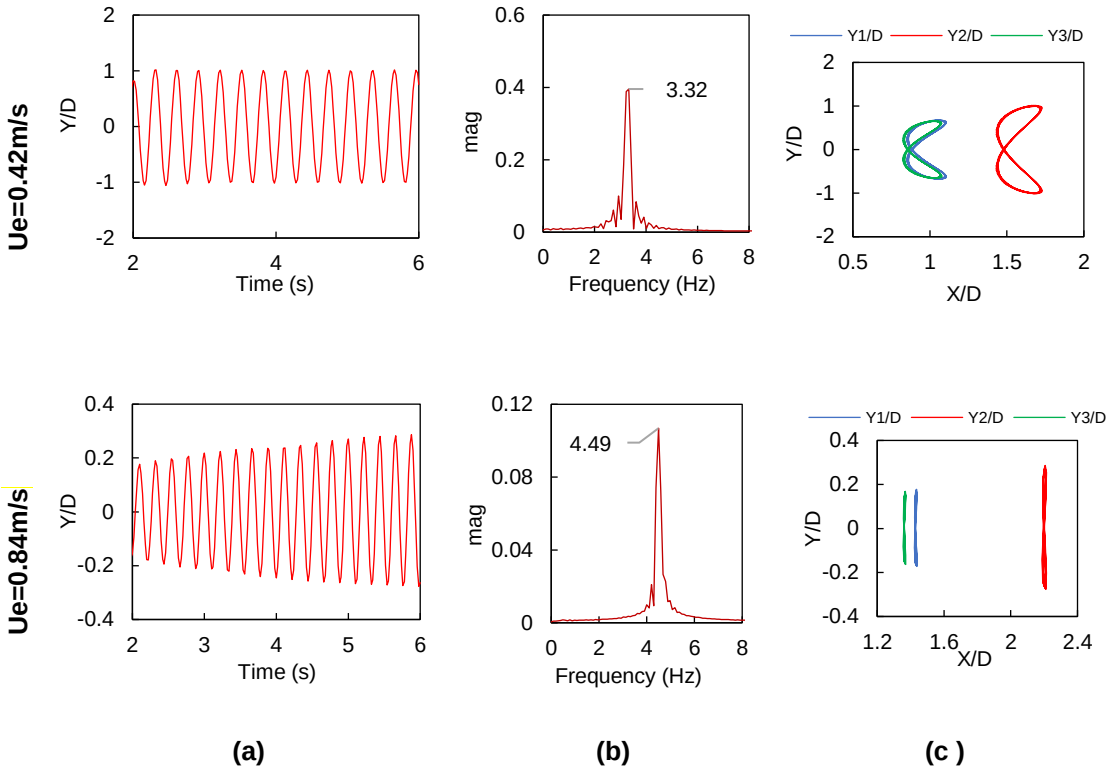

Figure 3-10 Comparison of (a) time histories, (b) Vibrating frequencies and (c) orbital trajectories, and of a horizontal riser with E= 102.5GPa and L/D = 300 subjected to a uniform velocity of Ue=0.42m/s (first row) and 0.84m/s(second row).

On the other hand, for the vertical riser under uniform flow conditions, it can be seen from Figure 3-11 (b) that when Ue increased from 0.42m/s to 0.84m/s, the dominant frequency in CF oscillation increased from 3.13Hz to 4.59Hz, respectively. Therefore, increasing the velocity increased the CF frequencies of the riser, this agrees with conclusions from Wang and Xiao (2016). Similarly, for a vertical riser under sheared flow conditions, when the maximum sheared velocity (Vmax) increased from 0.42m/s to 0.84m/s, the CF frequencies increased from 1.56Hz and to 2.25Hz, respectively, as shown in Figure 3-12 (b). Compared to the results of a vertical riser under uniform flow, the CF vibrating frequencies under sheared flow velocity profile are lower than those under uniform flow. Again, this is identical to conclusions from Wang and Xiao (2016).

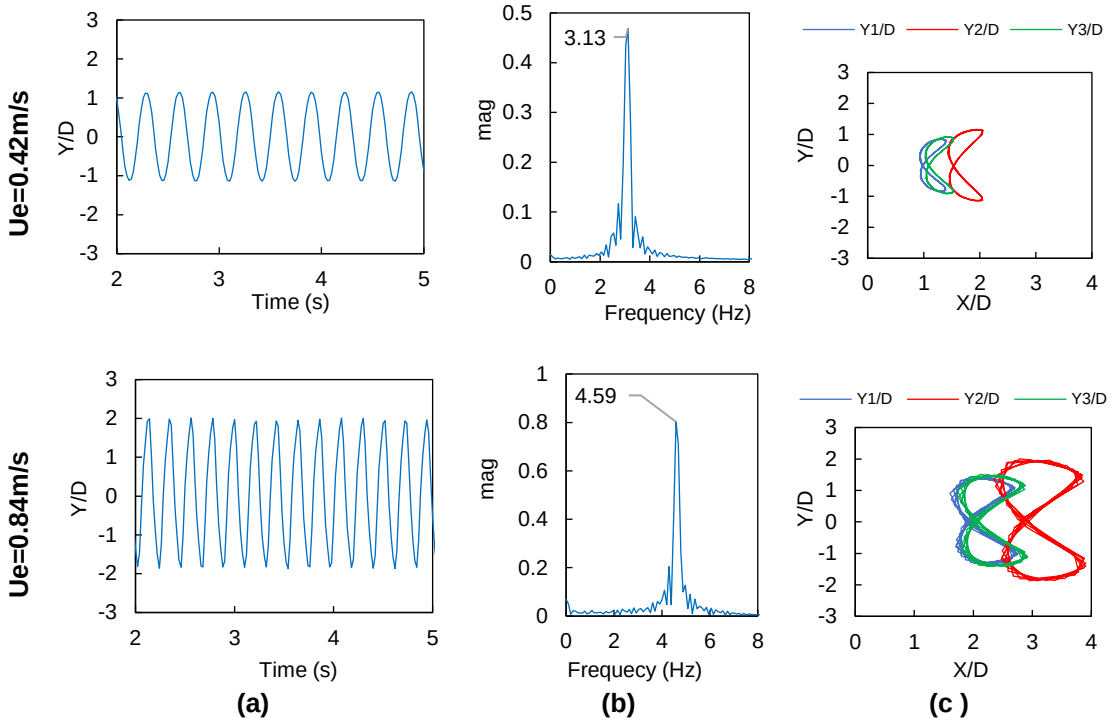

Figure 3-11 Comparison of (a) time histories, (b) Vibrating frequencies and (c) orbital trajectories, and of a vertical riser with E=102.5GPa and L/D= 300 subjected to a uniform velocity, Ue=0.42m/s (first row) and 0.84m/s(second row).

The orbital trajectories of the riser at three distinct points (Z/L= 0.25, 0.5, 0.75) along the riser were also investigated. Figure 3-11 (c) and Figure 3-12 (c) depict these orbital trajectories of the horizontal and vertical risers under a uniform and linearly sheared current. The horizontal axis represents the IL displacement, and the vertical axis represents the CF displacement. The orbital trajectory of the horizontal configuration at all the three locations under uniform velocities of 0.42m/s and 0.84m/s are shown in Figure 3-10 (c). It can be seen that when Ue=0.42m/s, a figure-eight orbit pattern is obtained. However, when the velocity increases to 0.84m/s, the orbital trajectory shrinks in the IL direction, showing a slight vibration in the IL direction. The orbital trajectories at the three points along the horizontal riser are similar in shape but differ in magnitude, with the magnitude at the mid-section larger than at the other locations.

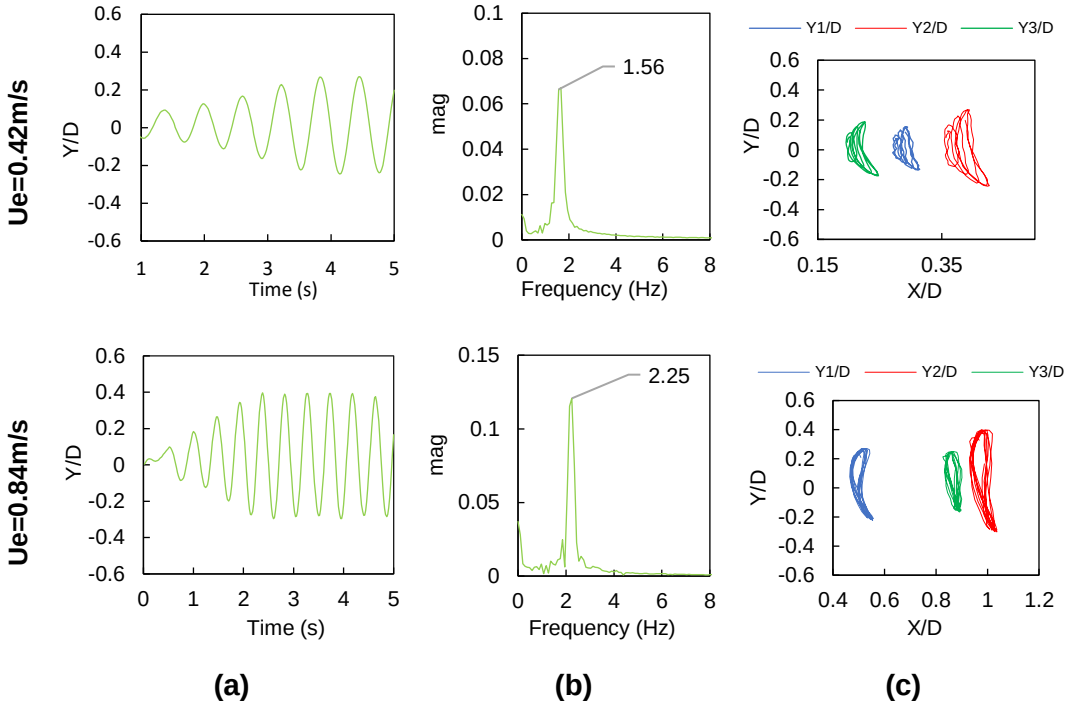

Figure 3-12 Comparison of (a) time histories, (b) vibrating frequencies and (c) orbital trajectories, and of a vertical riser with E = 102.5GPa and L/D = 300 subjected to sheared flow with maximum velocities of 0.42m/s (First row) and 0.84m/s (second row).

For the vertical riser under uniform flow, it can be seen in Figure 3-11 (c) that the trajectory at the three different points follows a 'figure 8' pattern regardless of the velocity. But the order of magnitude of the trajectory differs from point to point, with the highest order occurring at the midsection (Z/L =0.5) and smaller trajectories occurring at the top and bottom sections (Z/L =0.3 or 0.7). The 'figure 8' shape indicates the occurrence of dual resonance where the IL Vibration frequencies are approximatively twice the CF vibration. For a vertical riser under sheared flow conditions, it can be seen in Figure 3-12 (c) that at Ue=0.42m/s, the trajectory takes a squeezed C-shape. However, when the maximum velocity increases to Ue=0.84m/s, the trajectory shape resembles a tear-drop shape that is squeezed close to the bottom. From the results, for a riser with an aspect ratio (L/D) of 300, one can say that the velocity and orientation of the riser affect its orbital trajectory.

3.4.3 VIV of flexible riser with L/D =482

3.4.3.1 Inline displacement

When the aspect ratio increases to 482, It can be seen from Figure 3-13 (a) that for the horizontal riser under uniform flow velocities of 0.42m/s and 0.84m/s, the maximum IL displacement increases to 3.89 and 6.03, respectively. For the vertical riser configuration, Figure 3-13 (b) shows that under uniform flow velocities of 0.42 and 0.84m/s, the maximum IL displacement increases to 5.04 and 6.62, respectively. Similarly, under sheared flow conditions, Figure 3-13 (c) shows that the maximum IL displacement reached 2.76 and 4.92 when Ue=0.42 and 0.84m/s. Thus, compared with the results of L/D=300, the maximum RMS displacements of the riser increase with an increase in aspect ratio and velocity. It can also be noted that the maximum IL displacement of the riser under uniform flow velocity is higher than in the linearly sheared flow.

In addition, it can be seen that the maximum displacement of the riser under uniform flow is symmetrical about the elevation, where the maximum displacement is observed around the mid-section of the riser.

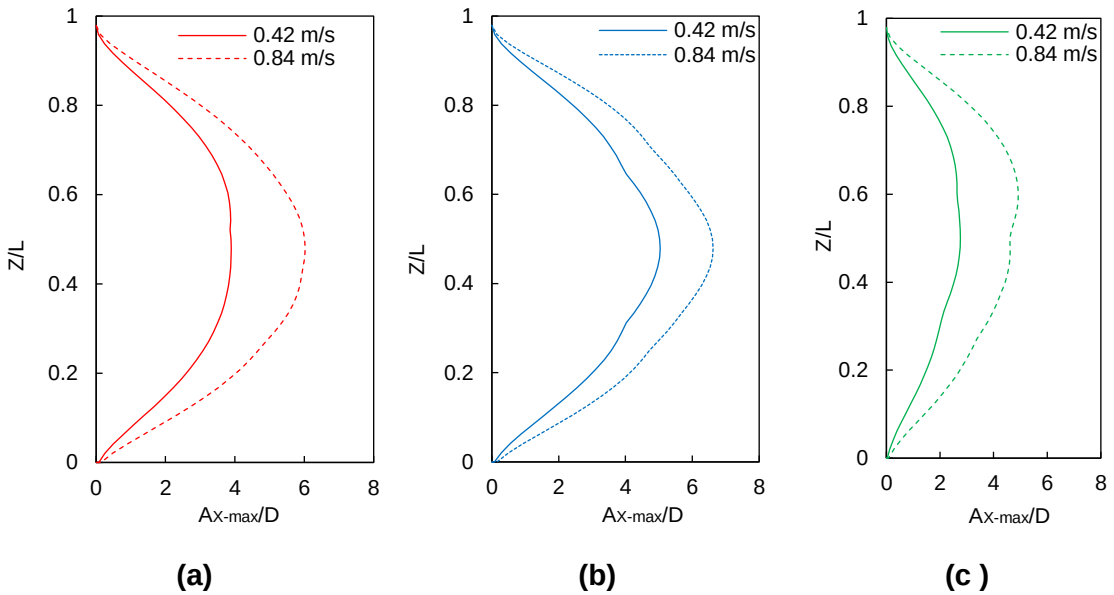

Figure 3-13 Comparison of Maximum IL displacement of a riser with E= 102.5GPa and L/D = 482: (a) Horizontal and (b) vertical orientation subjected to uniform flow and (c) vertical orientation subjected to sheared flow.

In contrast, the maximum displacement under sheared flow conditions is a-symmetrical because the maximum displacement occurs at a slightly higher position.

3.4.3.2 Crossflow displacement

The vibrating mode and dynamic response of the riser were investigated when the aspect ratio was increased to 482. Figure 3-14 (a-c) shows the CF RMS displacement of the horizontal and vertical risers with an aspect ratio of 482 under uniform and sheared flows. For the horizontal riser configuration, under uniform flow velocities of 0.42m/s and 0.84m/s, it can be seen from Figure 3-14 (a) that the second mode is dominant, irrespective of the velocity. Similarly, for the vertical riser under a uniform velocity, it can be seen from Figure 3-15 (b) that the CF vibrational mode of the riser when Ue=0.42m/s is multimodal, with Mode 1 being the dominant mode. As the uniform velocity increases to 0.84m/s, the dominant vibration mode increases to the 3rd mode.

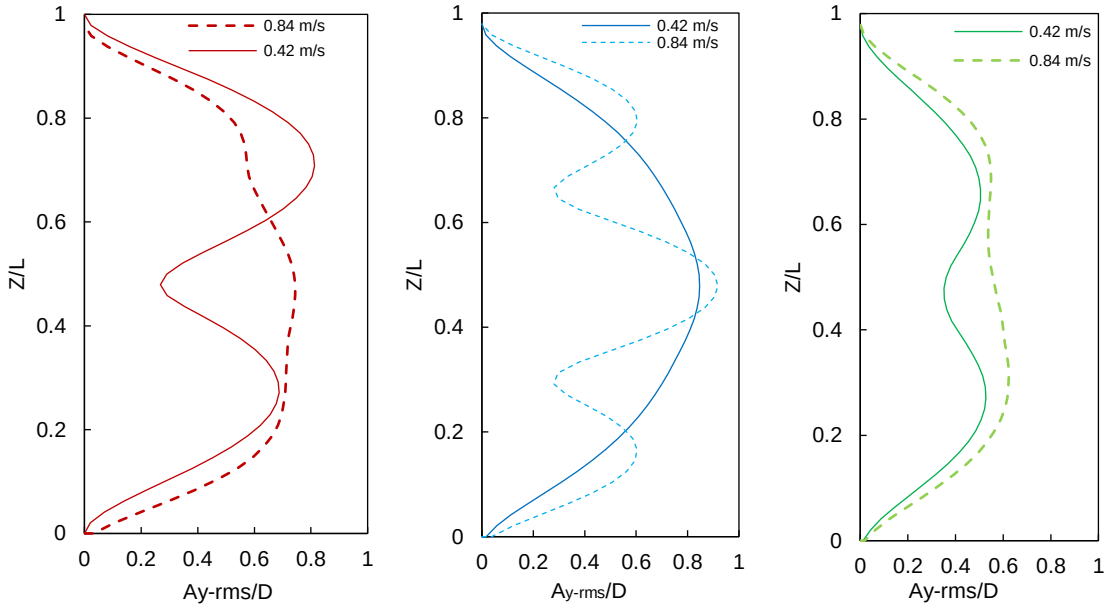

Figure 3-14 Comparison of CF RMS displacement of a riser with E= 102.5GPa and L/D = 482: (a) Horizontal and (b) vertical orientation subjected to uniform flow (c) vertical orientation subjected to sheared flow.

In addition, for the vertical riser under linearly sheared conditions, it can be seen from Figure 3-15 (c) that when the maximum velocity is Ue=0.42m/s, the second mode is dominant. However, as the maximum velocity increases to 0.84m/s, the vibration becomes multimodal, with Mode 1 being the dominant mode. The result obtained for L/D =482 contrast with the results obtained with L/D=300, where the first mode is the dominant mode. Thus, one can conclude that the mode shape of the riser is affected by the aspect ratio of the riser. The instantaneous response of a flexible riser can provide more information on the multimodal vibration occurring in some instances. Figure 3-15 shows the instantaneous response of a flexible riser with an aspect ratio of 482 under uniform and sheared flow conditions. The first and second columns show instantaneous CF displacements envelopes of a horizontal and vertical riser under a uniform flow. The third column represents the envelope of a vertical riser subjected to a sheared flow.

For the horizontal riser under a uniform flow, the CF vibration is dominated by a single mode (Mode 2) for all the velocities considered. For the vertical riser subjected to a uniform flow Ue=0.42m/s, a multimodal vibration is observed where the riser mode is transitioning from Mode 2 to Mode 1, with the first mode eventually dominating the vibration. As the velocity increases to 0.84m/s, a single mode (Mode 3) becomes the dominant mode. For a vertical riser under sheared flow, it can be observed that the second-order mode is dominant when Ue=0.42m/s. As the velocity increases to 0.84m/s, a multimodal vibration can be seen, comprising the first and second modes of vibration, with the Mode 1 being the dominant one, see Figure 3-15 (c).

3.4.3.3 Vibrating frequency and orbital trajectory

The aspect ratio of the riser was increased to 482, and the vibration frequencies at all velocities increased slightly under uniform and sheared conditions. Figure 3-16 -18 show the time histories of CF vibration, vibration response frequencies and orbital trajectories of a riser with different velocity magnitudes and velocity profiles. In the CF response frequency graph, the dashed line represents the natural frequency of the riser. The graphs show that the CF vibration’s time histories are non-periodic with varying amplitudes. For the horizontal riser under

uniform flow, it can be observed from Figure 3-16 (b) that when Ue increased from 0.42m/s to 0.84m/s, the CF frequency increased from 3.13Hz to 6.25Hz. Similarly, for the vertical riser under uniform flow conditions, Figure 3-17 (b) shows that when Ue increased from 0.42m/s to 0.84m/s, the dominant frequency in CF oscillation increased from 3.32Hz to 64Hz, respectively.

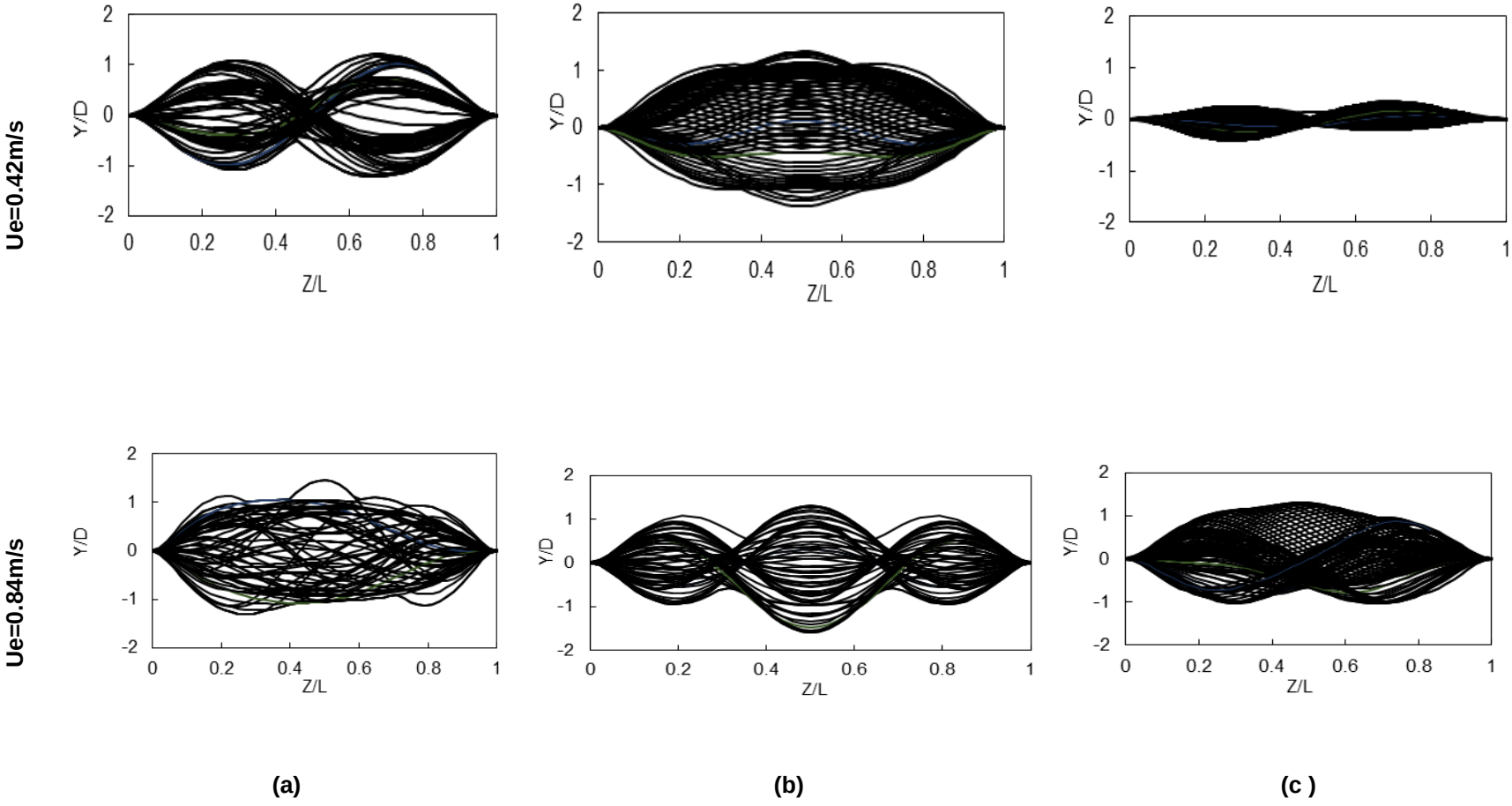

Figure 3-15 Comparison of CF response envelopes of a riser with L/D=482: (a) Horizontal orientation and uniform flow, (b) vertical orientation under uniform flow, and (c) vertical orientation under sheared flow

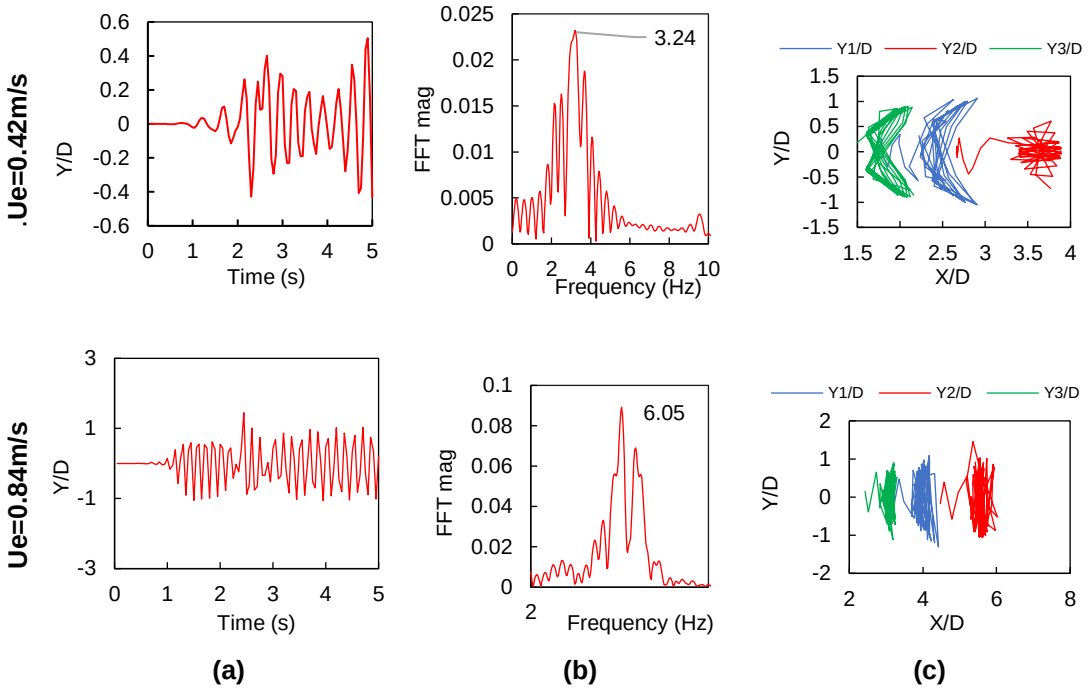

Figure 3-16 Comparison of (a) time histories, (b) Vibrating frequencies and (c) orbital trajectories, and of a horizontal riser with E= 102.5GPa and L/D = 482 subjected to a uniform velocity of Ue=0.42m/s (first row) and 0.84m/s(second row).

In addition, for the vertical riser under sheared flow conditions, when the velocity increases from 0.42m/s to 0.84m/s, it can be seen from Figure 3-18 that the CF oscillating frequencies increase from 2.7Hz to 4.8Hz, respectively, this is similar to results from Wang and Xiao, (2016). The CF frequencies spectra for both uniform and sheared currents are dominated by one strong frequency and accompanied by a weak frequency. This contrasts with the rigid cylinder, where a single-mode dominant is more likely to occur in a uniform current than in a sheared current. This may be due to the IL and CF response of the riser affecting each other. The orbital trajectories at the three selected spanwise locations along the axis direction of the riser (Z/L=0.3, 0.5, 0.7) at Ue=0.42m/s and 0.84 m/s under uniform and linearly sheared currents are plotted in Figure 3-16 -18 (c). For the horizontal riser under uniform velocities of 0.42 and 0.84m/s, a crescent trajectory shape is observed at the midsection of the riser, irrespective of the velocity, as shown in Figure 3-16 (c).

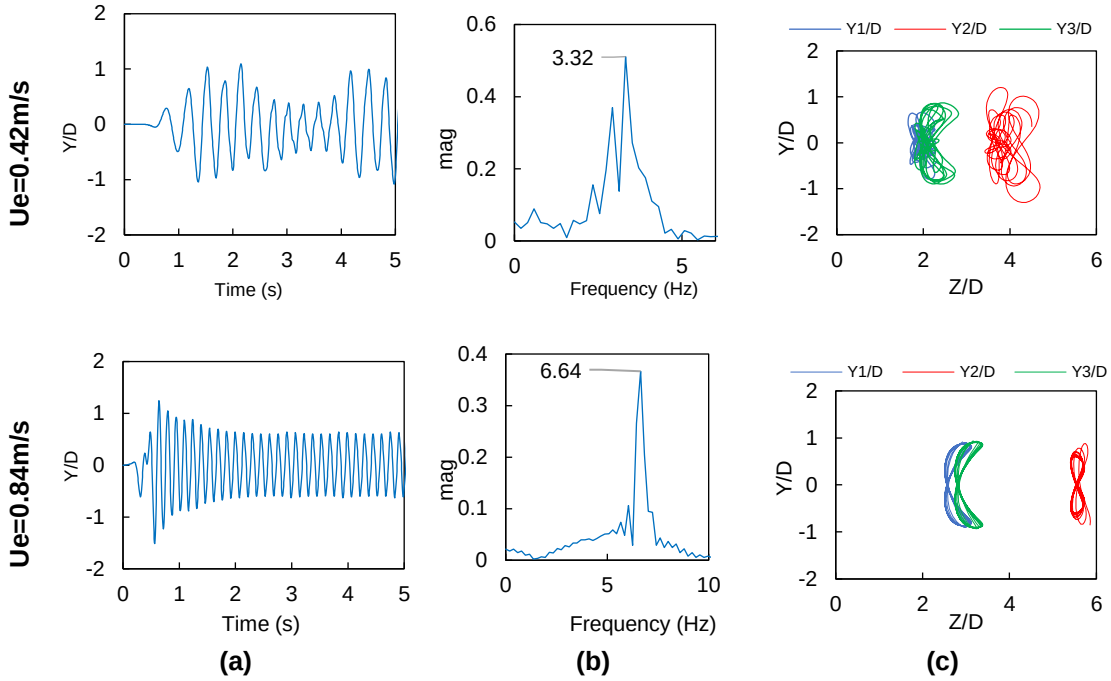

Figure 3-17 Comparison of (a) time histories, (b) Vibrating frequencies and (c) orbital trajectories, and of a vertical riser with E= 102.5GPa and L/D = 482 subjected to a uniform velocity of Ue=0.42m/s (first row) and 0.84m/s(second row).

For Ue=0.42m/s, an irregular shape is observed at the top and bottom sections of the riser. Similarly, it can be observed from Figure 3-17 (c) that under a uniform velocity of 0.42m/s, the vertical riser's orbital trajectory appears unstable and irregular. However, as the velocity increases to 0.84m/s, the orbital trajectories become regular and depict a ‘figure C’ shape. Figure 3-18 (c) shows the orbital trajectories at different locations along a vertical riser under sheared flow conditions. When the maximum sheared velocity is 0.42m/s, the orbital trajectories depict a ‘figure 8’ shape. This indicates a dual resonance, where the frequency of the IL response is approximately twice that of the CF response. As the maximum sheared velocity increases to 0.84m/s, the trajectory of the riser shows a crescent shape pattern. One exciting feature of the orbital trajectory at Ue=0.84m/s is that the lobe of the crescent shape is facing opposite directions at Z/L=0.25 and 0.75.

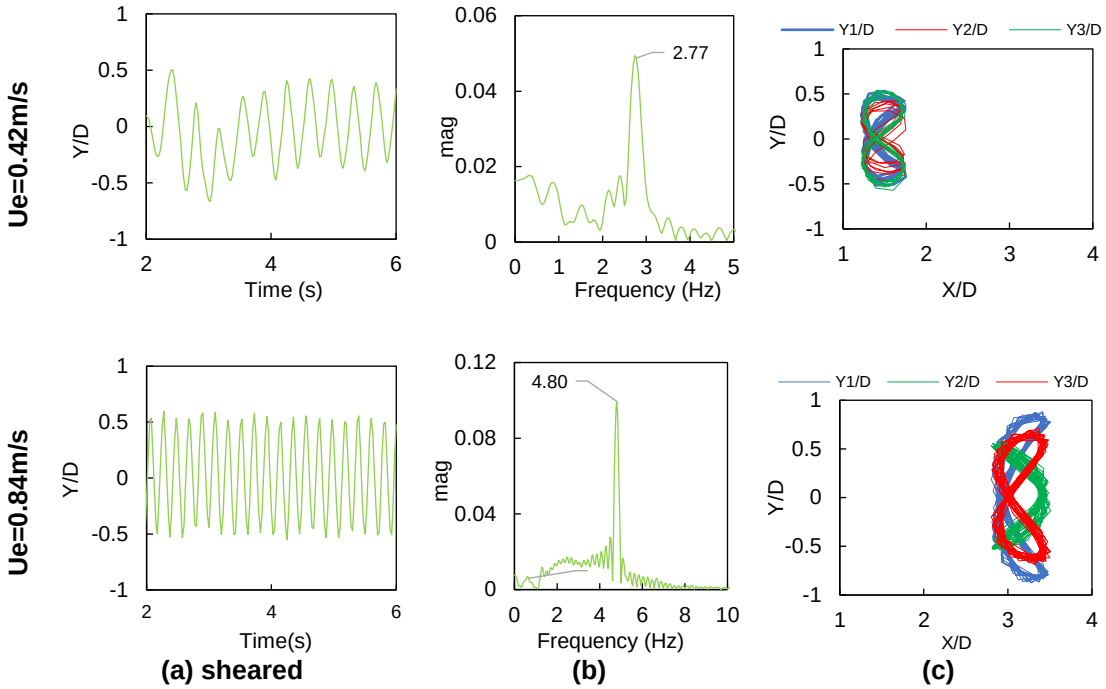

Figure 3-18 Comparison of (a) time histories, (b) vibrating frequencies and (c) orbital trajectories, and of a vertical riser with an elastic modulus of 102.5GPa and aspect ratio of 482 subjected to sheared flow with maximum velocities of 0.42m/s (First row) and 0.84m/s (second row).

3.4.4 Effect of elastic modulus on the dynamic response of a riser

The previous studies in section 3.4.3 and 3.4.2 discussed the effect of aspect ratio, orientation, current velocity, and the flow profile on the riser's VIV response. In this section, the effect of the elastic modulus on the VIV response of a riser is investigated. The elastic modulus of the riser is reduced from E= 102.5 GPa to 1.025 GPa. The study is limited to a horizontal riser with an aspect ratio of 300 and 482 and uniform velocities of 0.42m/s and 0.84 m/s. Four cases are considered, corresponding to cases 13-16 in Table 3-3. A modal analysis was performed for the two-aspect ratio using the ANSYS MODAL module in ANSYS 2019 R2. The natural frequency and mode shape of the first six modes of the riser are presented in Table 3-7 and Figure 3-19 .

Table 3-7 Natural frequency of a horizontal riser with E= 1.025GPa

Mode	Frequency (Hz)	
	L/D=300	L/D=482
1	0.25	0.10
2	0.68	0.26
3	1.34	0.52
4	2.21	0.86
5	3.30	1.28
6	4.60	1.79

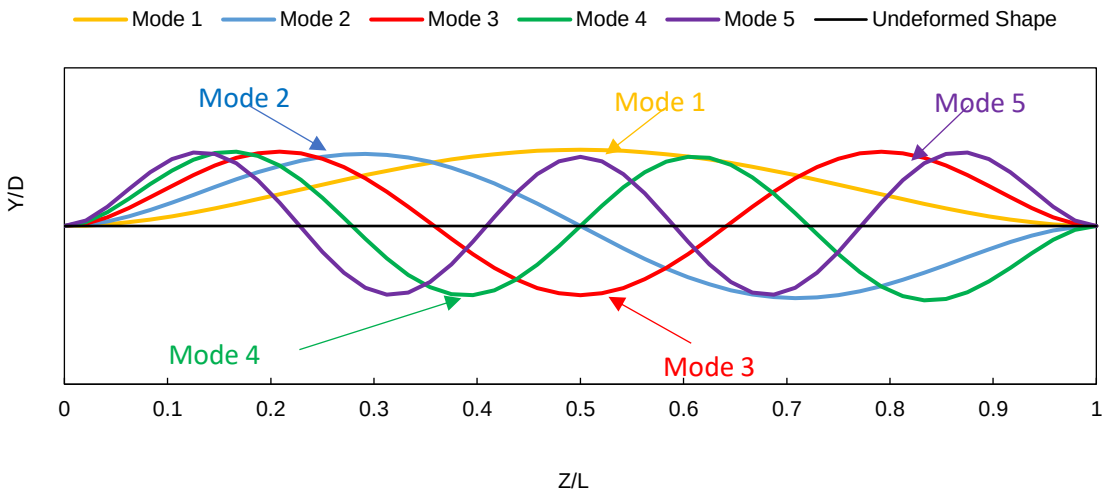

Figure 3-19 Mode shape of riser with an elastic modulus of 1.025GPa

3.4.4.1 Inline displacement

The maximum IL displacement of a horizontal riser with an elastic modulus E=1.025GPa and aspect ratios of 300 and 482 exposed to uniform velocities of 0.42m/s and 0.84m/s are presented in Figure 3-20 (a) and (b). The solid line shows the results for 0.42ms/ while the dashed line shows those at 0.84m/s. It can be seen that the maximum IL displacement occurs in the middle of the riser irrespective of the aspect ratio and velocity magnitude. For L/D =300, it can be observed in Figure 3-20 (a) that the maximum IL displacement increases from 9.37 to 14.18 when the velocity increases from 0.42m/s to 0.84m/s.

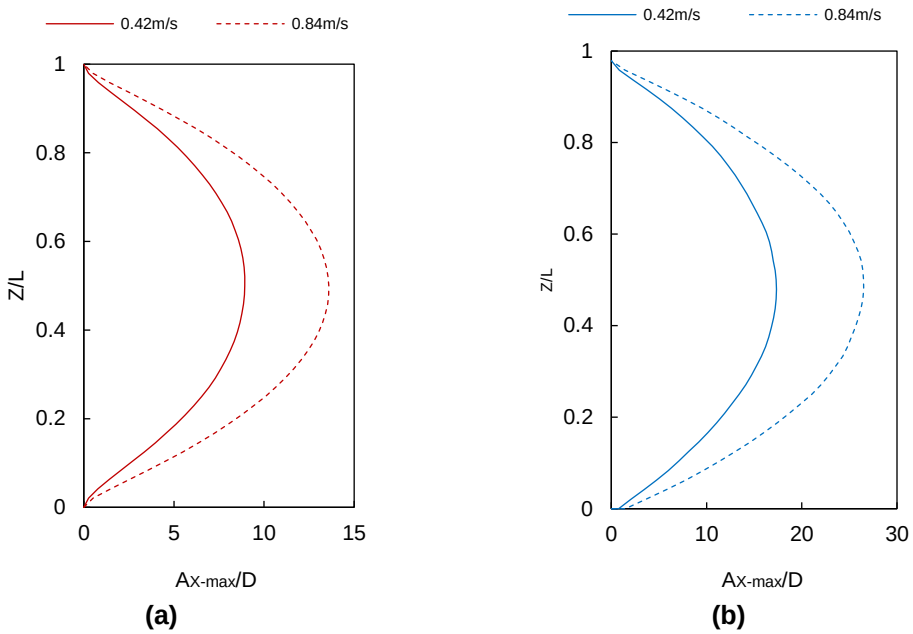

Figure 3-20 Comparison of maximum IL displacement of a horizontal riser with E= 1.025GPa and varying L/D (a) 300 and (b) 482 subjected to different uniform velocity of 0.42m/s (solid line) and 0.84m/s(dash line).

In contrast, for the riser with E=102.5GPa, studied previously in Section 3.4.1.1, the maximum IL displacement increases from 1.79 to 2.47 when the velocity increases from 0.42m/s to 0.84m/s see, Figure 3-7(a). Likewise, for L/D =482, the IL displacement increases from 19.08 to 27.92 when the velocity increases from 0.42m/s to 0.84m/s as shown in Figure 3-20 (b). However, when E =102.5GPa, the maximum IL displacement increases from 3.89 to 6.03. see Figure 3-13 (a).

Therefore, results show that, as the elastic modulus decreases from 102.5GPa to 1.025GPa, the maximum riser deflection amplitude increases for all velocities considered here. Likewise, as the velocity increases, the maximum riser deflection amplitude increases. This is because the drag force acting on the riser is proportional to the square of the current velocity (Huang, Chen and Chen, 2011).

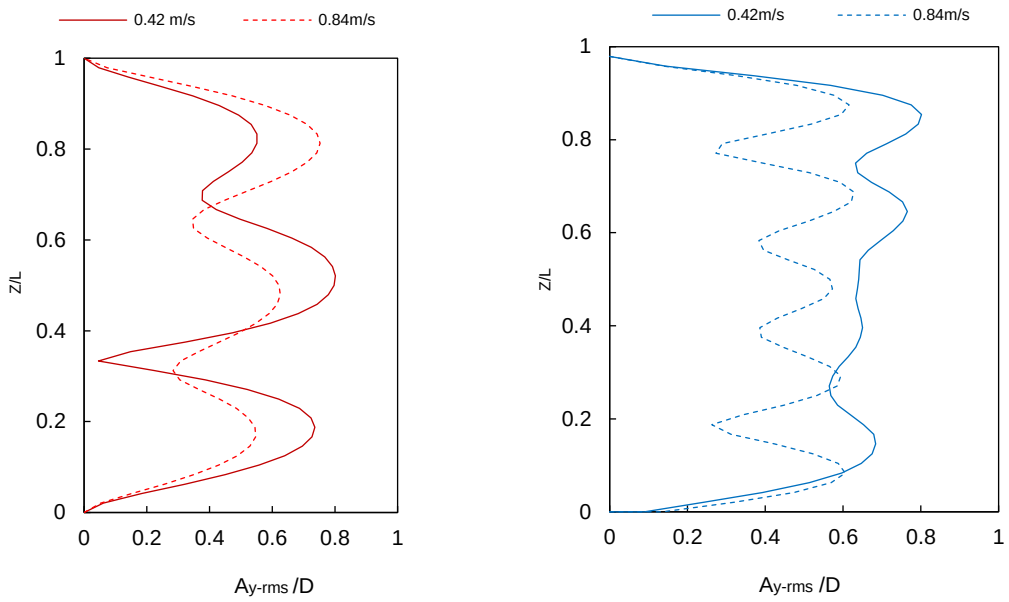

Figure 3-21 Comparison of CF RMS displacement of a horizontal riser with E= 1.025GPa and varying L/D= (a) 300 and (b) 482, subjected to different uniform velocity of 0.42m/s (solid line) and 0.84m/s(dash line).

3.4.4.2 Crossflow displacement

The effect of elastic modulus, aspect ratio and velocities on the vibrating mode and CF RMS displacements are discussed in this section. Figure 3-21 Figure 3-20 (a) and (b) showed the RMS of CF displacement of the horizontal riser with the elastic modulus E = 1.025 GPa under different velocities (0.42 and 0.84m/s) and aspect ratios (300 and 482). The effect of elastic modulus on the dynamic response of the rise is examined by comparing the present result (cases 13, 14, 15 and 16) with that of the horizontal riser with E =1.025GPa (cases 1,2,7 and 8).

For L/D=300, Figure 3-21 (a) showed that as the velocity increased from 0.42m/s (Case 13) to 0.84m/s (Case 14), the3rd mode remained the dominant vibration mode. However, the maximum CF displacement increased from 0.8D to 0.75D. Moreover, the dominant mode increased from Mode 1 when the E= 102.5GPa to Mode 3 when the elastic modulus is reduced to 1.025GPa for the two velocities considered. Thus, the mode shape is affected by the elastic modulus of the riser.

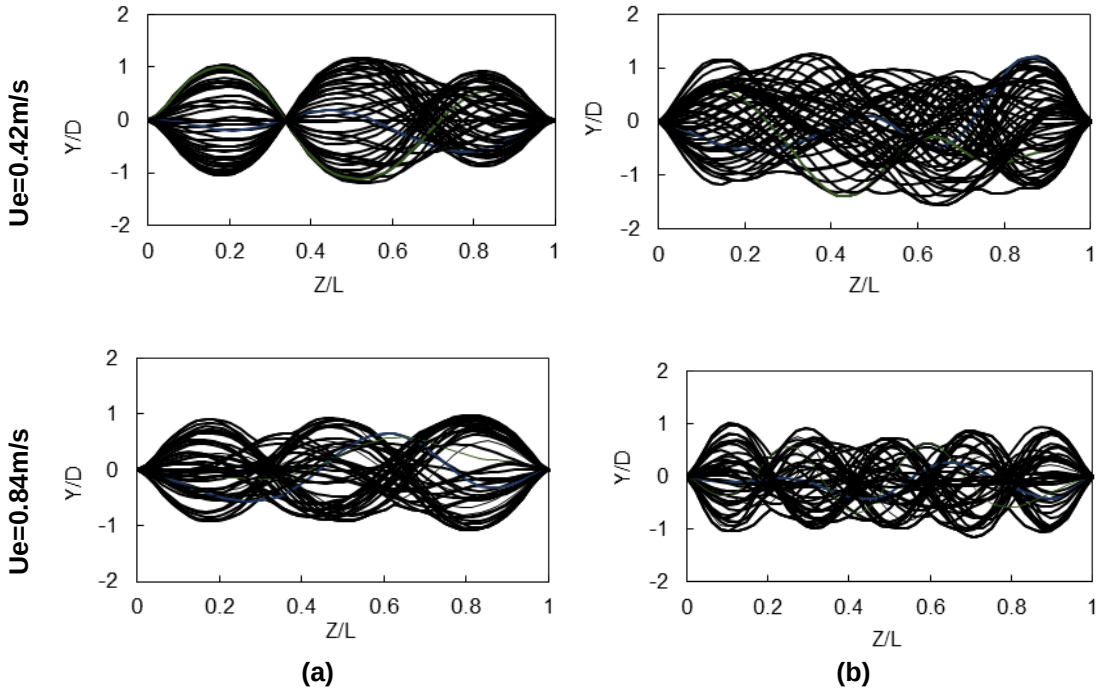

Figure 3-22 Comparison of instantaneous response envelopes of the horizontal riser with E 1.025 GPa and L/D= (a) 300 and (b) 482 under the uniform velocity of Ue=0.42m/s (first row) and 0.84m/s (second row)

For L/D=482, it can be seen from Figure 3-21Figure 3-20 (b) that as the velocity increased from 0.42m/s (case 15) to 0.84m/s(case 16), the mode increased from the 4th mode to the 5th mode of vibration. Therefore, under these conditions, the maximum CF displacement decreases from 0.8D to 0.63D. Moreover, at Ue=0.42m/s, the dominant mode increased from Mode 2 when the elastic modulus was E=102.5GPa to Mode 5 when the elastic modulus was reduced to 1.025GPa. Likewise, at Ue=0.84m/s, the dominant mode increases from Mode 3 to Mode 5 when the elastic modulus is reduced from E= 102.5GPa to 1.025GPa

Generally, the order of the mode shape increases with the increase of current velocity, aspect ratio and decrease of elastic modulus. Figure 3-22 shows the envelope of instantaneous CF displacement of the horizontal riser with an aspect ratio of 300 and 482 and subjected to uniform velocities of 0.42 and 0.84m/s. For L/D=300, a multimodal response combining Modes 2 and 3 is observed, with Mode 3 being the dominant mode, see Figure 3-22 (a). When the aspect ratio of the riser is increased to 482, it can be seen from Figure 3-22 (b) that under the

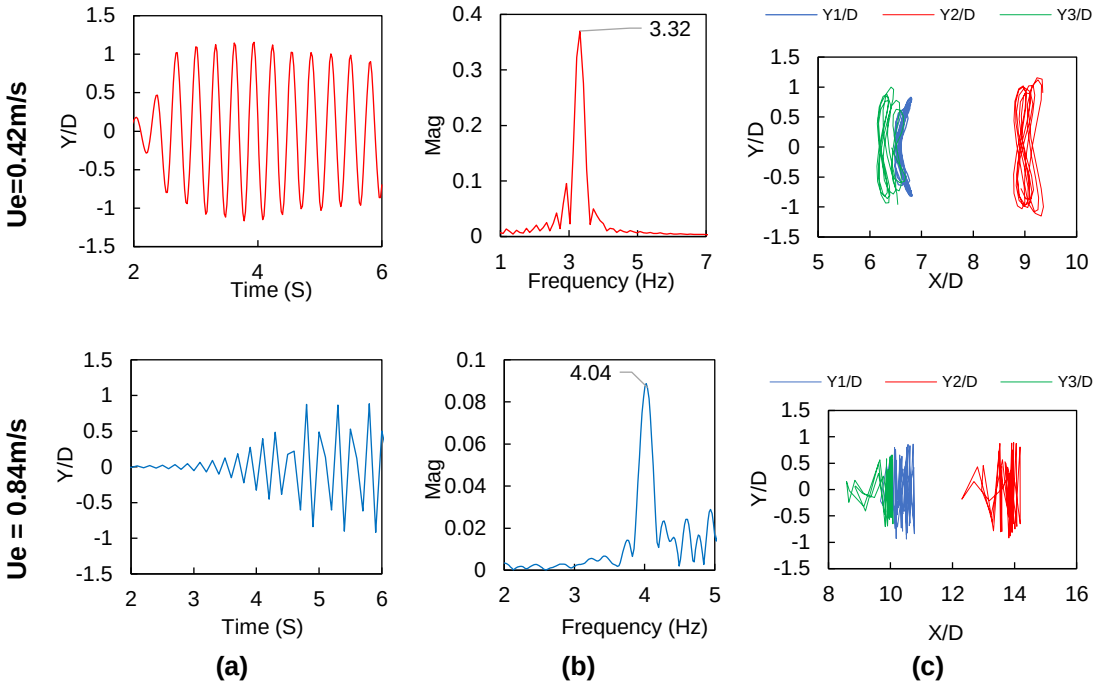

Figure 3-23 Comparison of (a) time histories, (b) oscillation frequencies and (c) orbital trajectories, and of a Horizontal riser with E= 1.025Gpa and L/D= 300 under uniform velocity of Ue=0.42m/s (first row) and 0.84m/s(second row).

uniform velocity Ue=0.42m/s and 0.84m/s, a multimodal response comprising several modes is observed, with modes 4 and 5 being the dominant modes respectively.

3.4.4.3 Vibrating frequencies and orbital trajectories of a riser.

The time histories, orbital trajectories, and response frequencies of the midpoint of a horizontal riser with elastic modulus E=1.025GPa and varying aspect ratios (300 and 482) and velocities (0.42 and 0.84m/s) are shown in Figure 3-23 and Figure 3-24 .The first column represents the time histories of CF displacement at varying external velocities, the second column represents the response frequency of the time history in the first column, and the third column represents the orbital trajectory.At Ue=0.42m/s, it can be seen that the oscillations of the midsection of the riser are periodic. However, as the velocity increases to 0.84m/s, the vibrations become non-periodic with varying amplitudes, as shown in Figure 3-23 (a). The frequency spectra of the CF vibration are presented in Figure 3-23 (b) and Figure 3-24 (b).

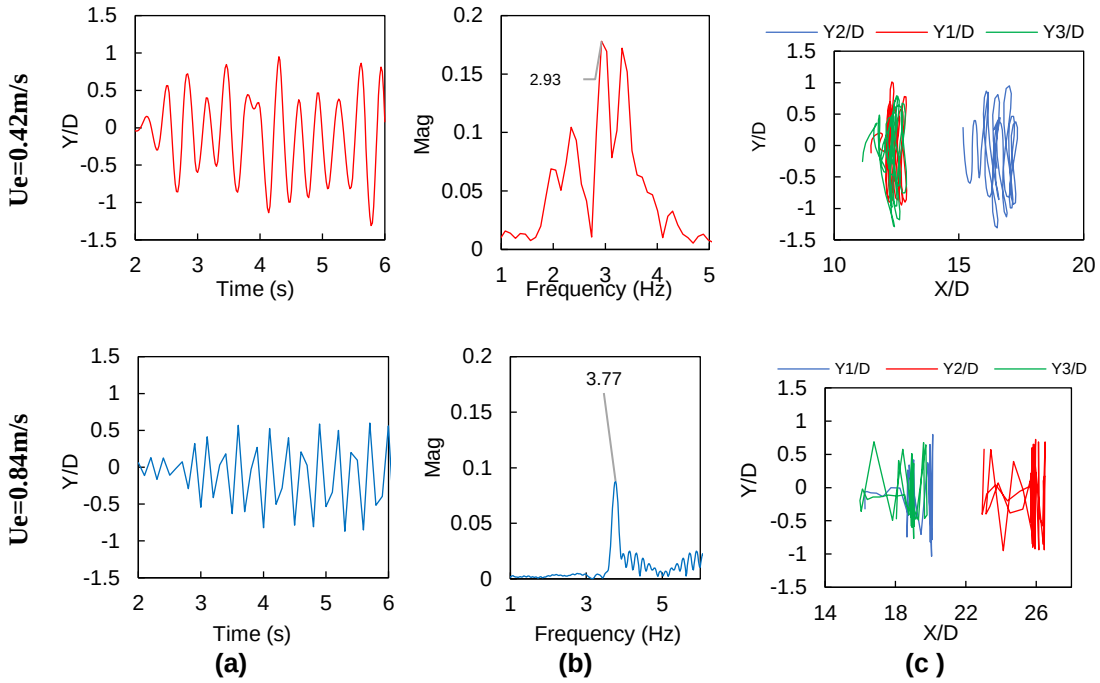

Figure 3-24 Comparison of (a) time histories, (b) oscillation frequencies and (c) orbital trajectories, and of a Horizontal riser with E= 1.025Gpa and L/D = 482 under the uniform velocity of Ue=0.42m/s (first row) and 0.84m/s(second row).

For L/D=300, it can be seen that as Ue increases from 0.42m/s to 0.84m/s, the dominant frequency in CF oscillation increases from 3.32Hz to 4.04 Hz, respectively. Similarly, for L/D=482, when the velocity increases from 0.42m/s to 0.84m/s, the CF oscillation frequencies increase from 2.93 Hz to 3.77Hz, respectively. In addition, it can be seen that at Ue=0.42m/s, the dominant frequencies are accompanied by weaker frequencies. This can be because the IL and CF responses of the riser affect each other.

The orbital trajectories at three different positions (z/L=0.25, 0.5 and 0.75) along the span of the horizontal riser with an E= 1.025GPa and aspect ratios of 300 and 482 are shown in Figure 3-23 (c) and Figure 3-24 (c), respectively. For L/D=300, it can be seen from Figure 3-23 (c) that at Ue=0.42m/s, a crescent shape is present. However, when the speed is increased to 0.84m/s, the orbital trajectory becomes chaotic. it can also be observed that the orbital trajectories shape at the mid-section is larger than that at the top and bottom points. As the length of the riser is increased to L/D=482, it can be seen from Figure 3-24 (c) that the crescent

shape disappears, and chaotic trajectories are observed at Ue=0.42m/s and Ue=0.84m/s. This contrasts with the riser with an elastic modulus E=102.5GPa, where a regular figure 8 shape is observed. This shows that the elastic modulus affects the orbital trajectory of the riser.

3.5 Conclusion

The effect of different aspect ratios (300 and 481.5), velocity flow profile (uniform and sheared), velocity magnitude (0.42m/s and 0.84m/s), elastic modulus (102.5 GPa and 1.025GPa), and orientation (horizontal and vertical) of a riser on the VIV responses of this riser, were studied numerically. The ANSYS system coupling, which connects ANSYS Fluent and Mechanical solvers, was used to solve the fluid-structure interaction problem. The VIV characteristics such as the IL displacement, CF displacement, vibrating mode, oscillating frequencies, and orbital trajectories were numerically examined. The following conclusions can be drawn from this study:

(1) The maximum IL displacement increases with an increase in velocity, irrespective of the velocity profile, aspect ratio, and orientation.

(2) The maximum IL displacement of the riser occurs at the mid-section of the riser when the velocity profile is uniform. However, the maximum displacement occurs at a point lower than the mid-section for a linearly sheared velocity profile. In addition, the maximum amplitude when the velocity profile is uniform is greater than that of the linearly sheared profile.

(3) Similarly, when the aspect ratio is low (L/D=300), the first vibration mode is dominant, irrespective of the velocity profile and magnitude. However, the vibration mode increases when the elastic modulus is reduced from 102.5GPa to 1.025GPa. Thus, at a low aspect ratio (L/D=300), only the elastic modulus affects the vibration mode of the riser.

(4) When the aspect ratio increases to 482, the vibration mode increases and becomes multimodal under the elastic modulus E=102.5GPa. As the velocity increases to 0.84m/s, the vibration mode increases. In addition, as the elastic modulus is reduced to 1.025GPa, the vibration mode also increases. Thus, increasing the velocity and aspect ratio increases the

vibration mode, while reducing the elastic modulus increase the vibration mode. In general, at a higher aspect ratio, the vibration mode of the riser is affected by the velocity profile and magnitude, as well as the riser configuration and elastic modulus.

(5) The VIV displacements of a riser with a small aspect ratio (L/D =300) and current velocities of 0.42 and 0.84m/s are periodic and have only one dominant frequency. However, as the aspect ratio increases, the VIV displacements become non-periodic, and smaller frequencies accompany the dominant vibration peak. Hence, it indicates the presence of a multimodal vibration.

(6) The orbital trajectory of the low aspect ratio riser (L/D=300) takes the shape of a ‘figure 8’, indicating the occurrence of a dual resonance. However, as the aspect ratio increases, the orbital trajectories become chaotic. In addition, the orbital trajectories for a uniform flow always take a more regular shape than a linearly sheared flow. The orbital trajectory generally becomes irregular with the increase in aspect ratio, velocity profile and reduction of elastic modulus.

Chapter 4

4 VIV OF A FLEXIBLE RISER TRANSPORTING SINGLE-PHASE FLUID

ABSTRACT

A series of 3D numerical simulations were conducted to investigate the dynamic response of a riser transporting single-phase fluid subjected to combined internal flow-induced vibration (FIV) and external vortex-induced vibration (VIV). The riser has an aspect ratio of 482. The maximum IL displacement, the Root Mean Square (RMS) of crossflow (CF) displacement, orbital trajectory, and vibrating frequency of the riser under two external velocity magnitudes (0.42 and 0.84m/s), four internal velocities (1,2,5,10m/s), two elastic moduli (102.5 and 1.025GPa) and two riser orientation (horizontal and vertical) are examined and compared. The results showed that the maximum IL displacement slightly increases as the internal flow velocity increases. Moreover, the results demonstrated that the magnitude of internal flow velocity affects the dominant vibration mode and frequency. Similarly, as the elastic modulus is reduced from 102.5 to 1.025GPa, the vibration becomes multimodal, with high mode dominating the vibration.

4.1 Introduction

The search for hydrocarbon has pushed drilling activities into ultra-deep-water zones in the oil and gas industry. As a result, drilling moves deeper into oceans; subsea risers are subjected to increasing external pressures due to subsea currents and waves. The stability and integrity of risers are thus essential for the safe transportation of oil and gas from the well at the seabed onto platforms.

When external flow past a bluff body such as a pipe, vortices are shed behind the body at a specific frequency called the vortex shedding frequency, the vortices induce an oscillatory motion onto the pipe. This phenomenon is referred to as vortex-induced vibration (VIV). When the vortex shedding frequency is close to the natural frequency of the pipe, resonance or VIV lock-in will occur, causing significant vibration that can lead to fatigue damage to the riser. Therefore,

knowledge of VIV is required to prevent offshore assets from failing (Williamson and Govardhan 2004).

Researchers such as Williamson and Govardhan (2008), Bearman (2011) and Derakhshandeh and Alam (2019) have conducted comprehensive reviews on VIV of elastically mounted rigid cylinders. However, such studies do not illustrate the actual VIV situation of a riser in a deep offshore environment. Real risers are indeed flexible and have a large length to diameter ratio.

Various studies have also been performed on the dynamic response of flexible risers subjected to uniform and sheared flows. To understand the characteristic of VIV, experimental and numerical methods are mainly considered. There are several ways to establish the VIV of a flexible riser; the methods can be classified into experimental, computational fluid dynamics (CFD) and semi-empirical models.

In recent times, Lehn (2003), Trim et al. (2005), Chaplin et al. (2005b), Song et al. (2011), and Huera-Huarte et al. (2014) explored the dynamic response of flexible riser using the experimental method However due to the costs involved when conducting full-scale tests, their experimental study was mostly limited to small-scale model testing, and only a few field tests were performed. As a result, many studies have been performed based on numerical methods such as computational fluid dynamics (CFD), wake oscillator and semi-empirical models to predict the dynamic response of the riser. Authors such as Menter et al. (2006), Huang et al. (2011) and Wang and Xiao (2016) considered CFD to predict the VIV response of a pipe. However, one downside of CFD is that numerical simulations usually require high computing power, thus making three-dimensional models rather expensive in time and CPU for large aspect ratio risers. High power computing is thus usually required. Therefore, analytical methods have been developed to study the VIV of a riser using mathematical formulations; see, for instance, studies by Facchinetti et al. (2004), Srinil (2011), Zanganeh and Srinil (2016) and Gao et al. (2019a, 2019b, 2019c).

Risers are usually used to transport fluids from the seabed to the platform. Therefore, the effects of the internal flow on the dynamic response of the riser

cannot be ignored. Both numerical and experimental investigations of the effects of internal flow have been carried out in recent years as the aspect ratio of the riser continues to increase. However, experimental studies on the VIV response of risers transporting single-phase fluids are limited. Guo et al. (2008) experimentally studied the dynamic response of a flexible riser conveying single-phase fluid exposed to uniform external flow. Their results showed that an increase in internal flow velocity increases the response amplitude and decreases vibration frequency.

Several empirical studies have also focused on the VIV response of flexible risers carrying single-phase flow. Keber and Wiercigroch (2008) mathematically analysed the dynamic behaviour of a fluid-conveying pipe subjected to VIV. They compared the VIV responses of the riser with and without internal flow. They showed that the internal flow enhanced the impact of structural nonlinearity on the VIV dynamics of a flexible pipe. Dai and Wang (2012) used multiple scales methods to study the effects of the internal fluid velocity on the dynamic response of a riser. They established that the internal fluid velocity affects the riser's oscillation amplitude. Dai et al. (2013, 2014) analytically investigated the dynamic response of a pipe subjected to uniform and pulsating internal and constant external flows. They found that the pipe motion changes from periodic to chaotic when the internal flow velocity increases. He et al. (2017) used a theoretical model to examine the effects of top-end lateral excitation and internal fluid flows on the VIV amplitude of a pipe. They concluded that the top-end excitation affects the vibration amplitude of such systems. Wang et al. (2018a) developed a three-dimensional nonlinear model to examine the VIV of flexible pipes conveying an internal fluid flow. They used van der Pol wake oscillators to model the unsteady hydrodynamic forces associated with the wake dynamics. They showed that the natural frequencies of the pipe were affected by the internal flow velocities. However, at higher external velocities, they established that the internal fluid flow had little effect on the VIV responses of the pipe. Jiang et al. (2019) used the wake oscillator and nonlinear equations to study the dynamic response of a riser transporting a single-phase flow and subjected to an external sheared flow. They found that the vibration modes of the riser are significantly affected by the external

flow velocity and slightly affected by the internal flow velocity. Meng et al. (2011) developed a mathematical model to analyse the dynamic response of a pipe conveying multiphase flow and subjected to an external flow. The results show that the magnitude of external and internal flow velocity significantly affects the vibration amplitude of the riser. Meng et al. (2017) developed a mathematical model to analyse the dynamic responses of a pipe conveying a single-phase fluid and simultaneously exposed to different internal and external flow velocities. Their result showed that increasing the internal flow velocity can increase the vibration mode of the riser.

Yang et al. (2018) developed a model to examine the effects of internal and external flow velocity on the dynamic behaviour of a flexible fluid-conveying pipe. They established that a critical internal velocity changes a riser's vibration mode at various external flow velocities. Duan et al. (2018a) used a mathematical model to examine the dynamic response of a riser subjected to internal and external flows. Their results showed that the vibration mode increases as the internal flow velocity increases. However, the dominating frequency does not change significantly. Duan et al. (2021a) predict the dynamic response of a fluid conveying riser exposed to uniform external flow using a semi-empirical time model and a Finite Element Method (FEM) model to describe the fluid flow and structural response. The results showed that the vibration mode increased significantly when the external fluid increased but remained constant while the internal flow velocity increased. In addition, Duan et al. (2021b) then studied the effect of internal flow velocity and density on the dynamics response of a flexible riser transporting single-phase flow. They observed that the CF vibration amplitude and mode increase as internal flow density increases. Kaewunruen et al. (2005) investigated nonlinear free vibrations of a fluid-conveying pipe. Their results showed that the internal fluid velocity significantly impacted the vibration behaviours of the riser. Zhang et al. (2015) analytically examined the combined effects of internal fluid flow and external currents on the vibration of a deep-water top-tensioned riser. Their results showed that increasing the internal flow velocity does not significantly influence the riser's vibration. Li, Deng and Wan (2020) used the VIV FOAM STJU code based on the strip method to investigate the

dynamic response of a flexible riser simultaneously exposed to varying internal and external flow velocities. They showed that external and internal flows affect the VIV response. Chen and Kim (2010b) used ANSYS MFX (coupling of ANSYS Mechanical and CFX solvers) to study the effect of tension and internal flow velocities on the VIV response of a single and a tandem riser. They showed that internal flow at different velocities affects the riser's vibration mode and amplitude. Chen et al. (2012) and Chen and Kim (2012a, 2012b) also used ANSYS MFX to numerically investigate the VIV response of a vertical riser exposed to the internal flow and linearly sheared external flow. They showed that the introduction of internal flow affects the vibration amplitude and mode.

Although CFD has been considered for some time, information/studies on the combined effects of the two sources of vibrations due to internal and external flows on a pipe/riser using this numerical method are still limited. In this study, a three-dimensional (3D) numerical model is developed using ANSYS 2019R1 solver to simulate the dynamic response of a flexible riser under internal single-phase flow and external VIV. The system coupling within the commercial ANSYS 2019 R2 platform has been used to link CFD and computational structural dynamics (CSD). The system coupling enables the exchange of information between CFD and CSD during a fluid-structure interaction (FSI) simulation. The chapter is organised as follows. First, the problem description, such as the geometry and physical properties of the riser, are defined in section 4.2. Next, the numerical method utilised to perform the simulation is elaborated in section. 4.3.Then, section 4.4 examines the IL displacement, CF displacement, vibration mode, vibrating frequencies, and orbital trajectory of the riser under different internal flow conditions and constant external velocity. Finally, the conclusion and recommendation for further study are provided in Section 4.5.

4.2 Problem description

Numerical simulations of a flexible riser conveying a single-phase flow subjected to varying external and internal flow velocities have been performed. In addition, the effects of elastic modulus on the dynamic response of the riser have also been investigated. Figure 4-1 shows the schematic diagram of a riser with both ends fixed and exposed to external and internal flow. The riser geometry considered has been adopted from studies by Lehn (2003). The riser has a 20 mm outer diameter, a thickness of 0.45 mm and a length of 9.63 m (equal to 482D). The geometrical and material properties of the riser are presented in Table 4-1 . The riser is subjected to two different external uniform velocities of 0.42 and 0.84 m/s and five internal flow velocities of 1, 2, 5, and 10 m/s. In addition, two different elastic moduli (102.5GPa and 1.025GPa) are also considered. In total, 30 cases have been investigated with varying internal/external velocities and riser elastic modulus, as summarised in Table 4-2, with Ue_1 and Ue_2 representing external velocities of 0.42 and 0.84 m/s, respectively.

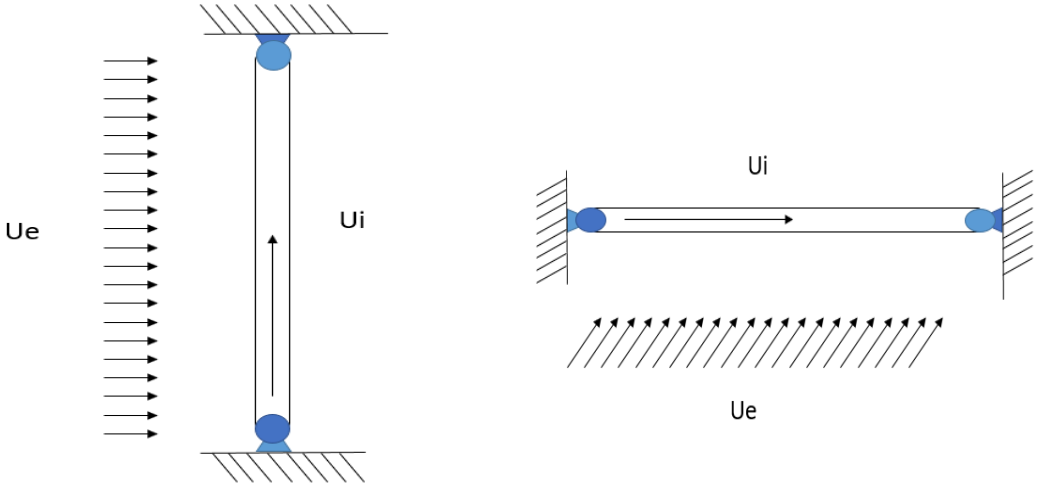

Figure 4-1 schematic of riser conveying fluid under FIV VIV (a) Vertical (b) Horizontal

Table 4-1 properties of riser for FIV and VIV analysis

Length, L	9.63	m
Outer Diameter, D	0.02	m
Thickness, t	0.45	mm
Aspect ratio, L/D	481.5	
Density of riser, ρ_s	7850	kg/m^3
Elastic modulus, E	102.5; 1.025	GPa
Fluid Property		
Density of external fluid, ρ_e	1000	kg/m^3
Density of internal fluid, ρ_i	1000	kg/m^3
Viscosity of external fluid, μ_e	0.001	Pa. s(Ns/m^2)
Viscosity of internal fluid, μ_i	0.001	Pa. s(Ns/m^2)
External Velocity, U_e	0.42; 0.84	m/s
Internal flow velocity, U_i	1- 10	m/s

Table 4-2 Cases considered in the study of the flexible riser transporting single phase flow

Case Number	Orientation	Elastic modulus (GPa)	U_e(m/s)	U_i(m/s)
1	Horizontal	102.5	0.42	0
2	Horizontal	102.5	0.42	1
3	Horizontal	102.5	0.42	2
4	Horizontal	102.5	0.42	5
5	Horizontal	102.5	0.42	10
6	Vertical	102.5	0.42	0
7	Vertical	102.5	0.42	1
8	Vertical	102.5	0.42	2
9	Vertical	102.5	0.42	5
10	Vertical	102.5	0.42	10
11	Horizontal	102.5	0.84	0
12	Horizontal	102.5	0.84	1
13	Horizontal	102.5	0.84	2
14	Horizontal	102.5	0.84	5
15	Horizontal	102.5	0.84	10
16	Vertical	102.5	0.84	0
17	Vertical	102.5	0.84	1
18	Vertical	102.5	0.84	2
19	Vertical	102.5	0.84	5
20	Vertical	102.5	0.84	10

21	Horizontal	1.025	0.42	0
22	Horizontal	1.025	0.42	1
23	Horizontal	1.025	0.42	2
24	Horizontal	1.025	0.42	5
25	Horizontal	1.025	0.84	10
26	Horizontal	1.025	0.84	0
27	Horizontal	1.025	0.84	1
28	Horizontal	1.025	0.84	2
29	Horizontal	1.025	0.84	5
30	Horizontal	1.025	0.84	10

4.3 Numerical method

ANSYS FLUENT and ANSYS MECHANICAL are used to simulate the flow field and the dynamic response of the riser, while ANSYS system coupling served as the coupling platform for data transfer during the two-way FSI process. Figure 4-2 shows how the two solvers are connected via the ANSYS system coupling module in ANSYS 2019R2 software (workbench). The VIV simulations of the flexible riser were carried out on the Cranfield HPC system.

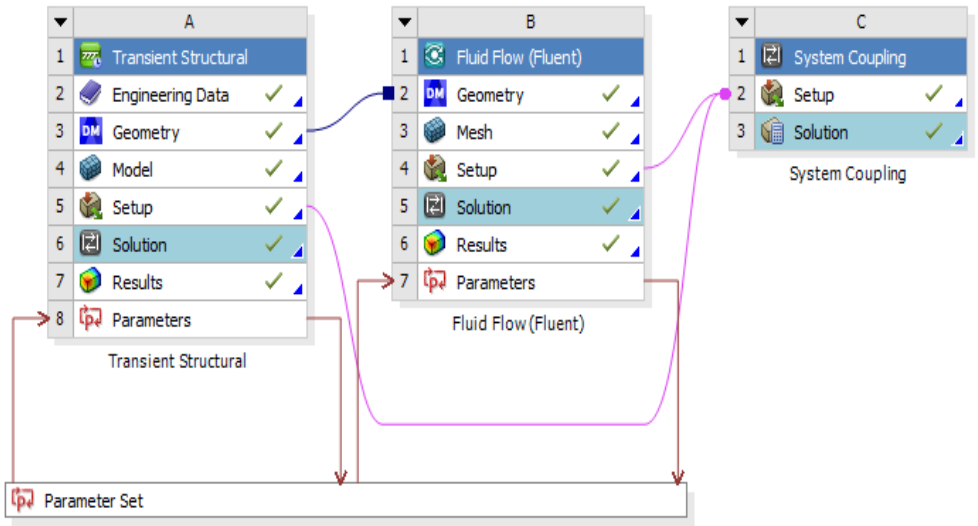

Figure 4-2 Flow chart of system coupling set up in ANSYS Workbench

4.3.1 Fluid domain

The fluid domain was created using the ANSYS design modeller, while the computational structured mesh was created using ANSYS meshing. The schematic of the rectangular fluid domain is presented in Figure 4-3. The domain dimensions are normalised with the outer diameter D of the riser. The fluid domain has a length of 40D, a width of 20D and a height of 482D. The riser is 10D and 30D far from the inlet and outlet boundaries. Velocity inlet and pressure outlet boundary conditions are applied at the inlet and outlet sections of the domain. A symmetry-type boundary condition is considered at the two-transverse and two spanwise boundaries. A symmetry condition implies that the velocity component perpendicular to the boundary is zero ($\partial u/\partial y = 0; v = 0$). A no-slip boundary condition is applied on the riser surface; the fluid velocity is thus identical to the vibration velocity of the riser. The riser surface also serves as a fluid-structure interaction surface, where the fluid force and the structural response data are exchanged between the flow field solver and the structural dynamic response solver.

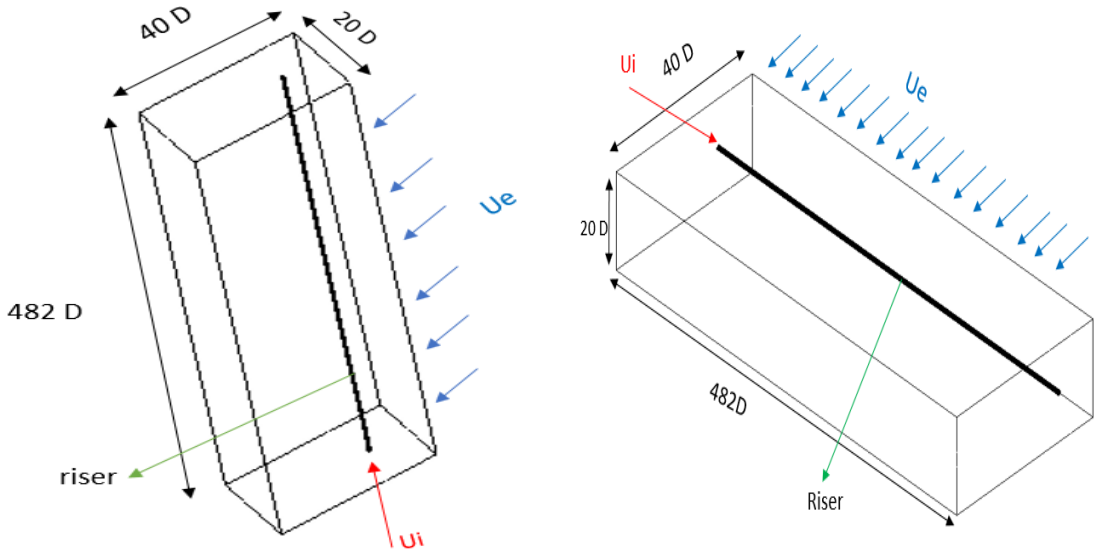

(a) **(b)**

Figure 4-3 computational domain of (a) vertical riser and (b) horizontal riser conveying single-phase fluid

The fluid flow surrounding and inside the riser is assumed to be incompressible and viscous. The following equations for mass and momentum are used to describe the fluid flow:

$$\frac{\partial \bar{u}_i}{\partial x_i} = 0 \tag{4-1}$$

$$\frac{\partial(\rho\bar{u}_i)}{\partial t} + \frac{\partial\left(\rho\bar{u}_i\bar{u}_j\right)}{\partial x_j} = -\frac{\partial \bar{p}}{\partial x_i} + + \frac{\partial}{\partial x_j}\left(2\mu\overline{S_{ij}} - \rho\,\overline{u'_i\,u'_j}\right) \tag{4-2}$$

Where μ is the dynamic viscosity, ρ is the density, and p is the pressure.

Also, $\bar{S}_{ij}$ is the mean rate of the strain tensor described in Equation **(4-3**).

$$\bar{S}_{ij} = \frac{1}{2}\left(\frac{\partial \bar{u}_i}{\partial x_j} + \frac{\partial \bar{u}_j}{\partial x_i}\right) \tag{4-3}$$

with $-\overline{\rho u'_i\,u'_j}$ in Equation **(4-2**) referred to as the Reynolds stress, described as

$$-\overline{\rho u'_i\,u'_j} = 2\mu_t\bar{S}_{ij} - \frac{2}{3}k_t\rho\delta_{ij} \tag{4-4}$$

where μ_t is the turbulent viscosity, δ_{ij} is the Kronecker function and $k_t = \frac{1}{2}\overline{u'_i u'_i}$ is the turbulent energy computing from the fluctuating velocity field.

For turbulence closure, the (SST) k-ω turbulence model is used to compute the Reynolds stresses in this paper. The k-ω turbulence model (Wilcox, 1993) is a two-equation model where one equation solves the the turbulent kinetic energy *k*, and the other one solves the specific dissipation ω. The Shear Stress Transport (SST) variant of the k-ω model was developed by Menter (1994).(Fluent, 2015; Loyseau and Verdin, 2016; Loyseau et al., 2018).

The fluid flow governing equations are solved using the pressure-based segregated algorithm. The Coupled algorithm was selected as the pressure-

velocity coupling. Also, a first-order upwind scheme was used to solve both *k* and ω equations, and a second-order upwind scheme was used to discretise the pressure and momentum equations. In addition, a Least Squares Cell-Based scheme was used for the gradient in spatial discretisation. Finally, a first-order implicit transient formulation was selected to solve the transient formulation. A convergence criterion of 10^{-3} and a time-step of 0.005s was considered for all simulations.

4.3.2 Solid domain

The solid structure of the riser was created and discretised using the ANSYS design modeller and ANSYS meshing, respectively. The riser is fully immersed in the fluid domain, as shown in Figure 4-3. The riser's top and bottom ends are fixed, while the inner and outer surface forms a fluid-solid interface where hydrodynamic forces obtained from the flow solver are applied, enabling data transfer between the flow and the structure solvers.

The flexible pipe is modelled as a beam governed by the Euler-Bernoulli beam theory. The axial tension was ignored in this study. The motion of an empty flexible pipeline with both ends fixed and no pretension in the IL and CF directions are described in Equations (4-5) and (4-6).

$$m\frac{\partial^2 x}{\partial t^2} + c\frac{\partial x}{\partial t} + \frac{\partial^2}{\partial z^2}\left[EI\ \frac{\partial^2 x}{\partial z^2}\right] = F_x \tag{4-5}$$

$$m\frac{\partial^2 y}{\partial t^2} + c\frac{\partial y}{\partial t} + \frac{\partial^2}{\partial z^2}\left[EI\ \frac{\partial^2 y}{\partial z^2}\right] = F_y \tag{4-6}$$

where m, c, *E,* and I are the mass per unit length, structural damping, Elastic modulus and moment of inertia, respectively. Also, x,y, and z are the cartesian coordinate. In addition, F_x and F_y are the hydrodynamic forces in the IL and CF directions, respectively.

Since the cylinder is fixed at both ends, the boundary conditions at the two ends are defined as:

$$y(0,t) = 0, y(l,t) = 0;\ \frac{\partial y(0,t)}{\partial z} = 0, \frac{\partial y(L,t)}{\partial z} = 0 \tag{4-7}$$

For a flexible pipe conveying fluid, the dynamical behaviour of the riser caused by both external and internal flows is considered. Therefore, the governing equation takes into account the influence of the internal flow mass; therefore, the governing equation equations become:

$$2m_i U_i \frac{\partial^2 x}{\partial z \partial t} + (m_s + m_i)\frac{\partial^2 x}{\partial t^2} + c\frac{\partial x}{\partial t} + EI \frac{\partial^4 x}{\partial z^4} = f_z(z,t) \tag{4-8}$$

$$2m_i U_i \frac{\partial^2 y}{\partial z \partial t} + (m_s + m_i)\frac{\partial^2 y}{\partial t^2} + c\frac{\partial y}{\partial t} + EI \frac{\partial^4 y}{\partial z^4} = f_y(z,t) \tag{4-9}$$

where m_s is the mass per unit length of the riser, m_i is the mass per unit length of the internal flow, and *c* is the structural damping coefficient. *E* and *I* are the elastic modulus and moment of inertia, respectively.

ANSYS Mechanical 2019R2, based on the finite element method (FEM), is used to solve the vibration response of the flexible pipe transporting the single-phase fluid. The riser was discretised into many elements. For each element, the governing equation was written as Equations (4-10) and (4-11).

$$m\ddot{X} + c\dot{X} + kx = F_x \tag{4-10}$$

$$m\ddot{Y} + c\dot{Y} + kY = F_y \tag{4-11}$$

Where m is the mass, c is the damping and k is the stiffness element. Also, fx and fy are the hydrodynamic forces in the IL and CF direction, respectively.

The structural equation of the whole pipe combining all the elements then becomes equations (4-12) and (4-13)

$$[M]\{\ddot{X}\} + [C]\{\dot{X}\} + [K]\{X\} = \{F_X\} \tag{4-12}$$

$$[M]\{\ddot{Y}\} + [C]\{\dot{Y}\} + [K]\{Y\} = \{F_Y\} \quad (4\text{-}13)$$

where *[M]*, *[C]*, *[K]* are the mass, damping and stiffness matrixes of the riser; $\{X\}$, $\{\dot{X}\}$ and $\{\ddot{X}\}$ are the displacement, velocity and acceleration vector, respectively. Also, $\{F_X\}$ and $\{F_y\}$ are hydrodynamic force vectors in the IL and CF directions.

4.3.3 Fluid-structure interaction

A fluid surface interface was created between the external flow and the riser's outer surface, allowing data to be exchanged between the fluid and solid solvers. In addition, as the riser transports a fluid, an additional fluid-structure interface is formed between the internal fluid and the inner surface of the riser to cater to the internal flow-induced vibration. Therefore, unlike the two-way FSI simulation of an empty riser, two FSI interfaces were created when simulating the dynamic response of the riser under the combined influence of external and internal flows. Note that the data exchanged between the two solvers could be either one way or two ways. In the one-way coupling method, only the fluid forces obtained from the fluid solver were transferred to the structural solver. However, the fluid force and the structural displacement obtained from the fluid and structural solvers were exchanged during the numerical simulation for the two-way coupling method. In this study, two FSI was performed using the ANSYS system coupling, which is based on a partitioned method, where the two solvers solve their equations separately. At each computational time step, the drag and lift forces acting on the riser were obtained from the fluid solver and transferred to the structural solver as external forces during the coupling process. The structural solver then computed the dynamic response of the riser. As the riser deformed, the mesh around the fluid domain deformed too. Therefore, a dynamic mesh was used to model the movement of the mesh. This process was repeated until the fluid/solid solution was converged. Smoothing and dynamic meshing strategies were used in this study to update and compute the position of the mesh during oscillations to avoid the negative volume error. As the cylinder vibrates, the mesh moves according to the Laplace Equation (4-14).

$$\nabla.(\gamma\nabla\vec{u}) = 0 \tag{4-14}$$

Where $\vec{u}$ represents the velocity of mesh displacement, and γ represents the diffusion coefficient.

4.3.4 Mesh

A 3D FSI calculation can be computationally intensive, depending on the mesh size in the fluid and solid domains. Therefore, a mesh sensitivity study was performed using three mesh sizes to determine the optimum mesh size and ensure that the numerical results are independent the mesh density. The computational domain was divided into multiple blocks, as shown in Figure 4-4(a). The multi-block concept controls the mesh size so that a fine mesh could be created near the riser to capture flow separation while a coarse mesh was created far away from it, as shown in Figure 4-4 (b) and (c). The minimum distance of the first cell next to the riser was established as 0.0001D to obtain a y^+ value less than 1, ensuring compliance with the turbulence model requirements selected for this work. The y^+ value is a non-dimensional distance at the wall, the function of the wall shear stress, fluid density and viscosity.

$$y^+ = \frac{yu_\tau}{\nu} \tag{4-19}$$

where y is the distance at the wall of the first cell, ν is the kinematic viscosity of the fluid, and u_τ is the friction velocity defined as:

$$u_\tau = \sqrt{\frac{\tau_w}{\rho}} \tag{4-20}$$

with ρ the density of the fluid, and τ_w the wall shear stress.

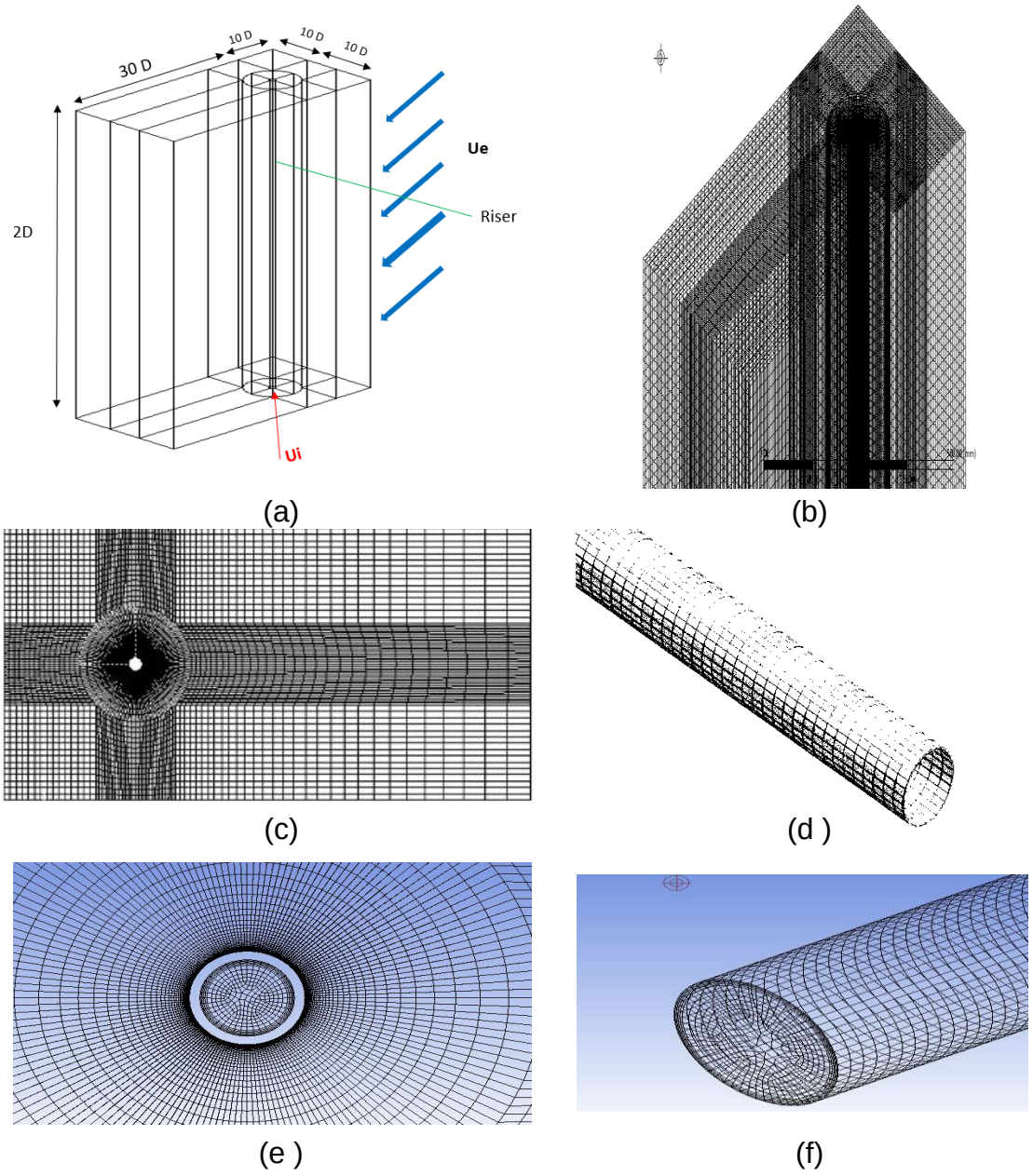

Figure 4-4 (a) computational fluid domain divided into block, (b) 3D fluid domain mesh (c) Top view of fluid domain mesh (d) snapshot of solid domain mesh (e) Top view of fluid and liquid mesh (f) inner liquid mesh

Figure 4-4 (d) shows a snapshot of the solid mesh of the riser. The riser circumferential edges are divided into 60 equal divisions. The span of the riser was discretised into 500 elements. The solid meshing strategy is adopted from the work of Wang and Xiao (2016). Likewise, the computational domain of the inner liquid is divided into equal division in the circumference and an inflation layer is applied at the liquid mesh.as shown in Figure 4-4 (e) and (f).

A mesh sensitivity study was performed on a fluid conveying horizontal pipe subjected to Ue-0.84m/s and Ui=1m/s. The maximum IL displacement and drag coefficient of the three different mesh sizes are tabulated in Table 4-3, where Nz represents the number of elements along the span, and Nc represents the number of cells along the circumference of the riser. It can be seen in Table 4-3, that the difference in drag coefficient Cd results between Mesh 1 and Mesh 2 is not large, but the difference between Mesh 2 and Mesh 3 is even lower. Mesh 2 is therefore selected for the numerical simulations in the present study.

Table 4-3 Mesh dependency study of fluid conveying horizontal pipe with L/D=482 subjected to Ue=0.84 m/s and Ui=1m/s

	CFD Mesh			FEA Mesh				
	Nc	Nz	Total	Nc	Nz	Total	Cd	IL
Mehs1	160	30	677,000	30	500	15,000	1.30	4.99
Mesh 2	160	50	775,338	30	500	15,000	1.59	5.33
Mesh 3	160	100	1,357,000	60	1,000	60,000	1.54	5.42

4.3.5 Time step study

The maximum IL displacement of three different time step sizes using the mesh 2 are tabulated in Table 4-4. The study shows that the difference between the IL displacement value of time steps 1 and 2 is significant. However, for times step 2 and 3 the difference is small. Therefore, a time step of 0.005s selected for the numerical simulations in the present study.

Table 4-4 Time dependency study of a fluid conveying horizontal pipe with L/D=482 subjected to Ue=0.84 m/s and Ui=1m/s

Time step	Time	IL
1	0.020	5.296
2	0.005	5.334
3	0.002	5.331

The FSI simulations of a fluid conveying pipeline were carried out on Cranfield university High performance computer (HPC), DELTA. The HPC is made up of two Intel E5 2620 v4 (Broadwell) CPU, a user is allowed up to 128 cores in multiple of 16 cores and a total of 250GB of shared memory. In this research, for the 3D simulation of the flexible riser, it takes 69 hours with 32 cores to obtain 5 seconds of simulation. In addition, the simulation takes 50GB of space for each 5 seconds. One of the major challenges faced during simulation is the inability to restart the simulation at a given time when the simulation fails while running on the HPC. This has caused much delay in the simulation.

4.3.6 Validation

The numerical simulation of an empty horizontal riser with an aspect ratio of 482 and under uniform velocity of 0.42 was used for validation study. The present horizontal riser with aspect ratio of 482, exhibits the second mode of vibration in the CF direction when exposed to uniform flow of 0.42m/s, which is in agreement to the experimental study of Lehn (2003) and the numerical study of Wang and Xiao (2016). Similarly, for a vertical riser under similar condition, a multimodal mode is observed comprising mode 1 and mode 2, with mode 1 being dominant for vertical riser. Therefore, the present simulation for vertical riser under predict the dominant vibration mode at Ue=0.42m/s. The discrepancies can be attributed to the tension applied in the riser in the experimental study of Lehn (2003) which is omitted in the present study. Tension is neglected in this study because it affects the stability of the simulation. The horizontal riser is tensioned due to its weight compared to the vertical riser.

4.4 Results and discussion

A two-way FSI numerical simulations are performed to examine the dynamic response of the riser under FIV and external VIV. The effects of external flow velocities Ue (0.42 and 0.84m/s), internal flow velocities Ui (1, 2, 5 and 10m/s) are investigated. Ui=0 in this study refers to an empty riser without any fluid flowing into it. In addition, the effects of elastic modulus (102.5 and 1.025 GPa) and orientation (horizontal and vertical) are also investigated. In summary, 30 cases combining external and internal flows are performed; see Table 4-2 for details.

4.4.1 Modal analysis

The natural frequencies (f_n) and mode shape of the riser are obtained by performing modal analysis using the ANSYS modal 2019 R2. The modal analysis is performed for the two different orientations. It was found that the natural frequency of the horizontal and vertical are similar. Table 3-6 and Figure 3-6 present the riser's natural frequency and mode shape, respectively.

Table 4-5 Natural frequency (f_n) of the riser with an elastic modulus E= 102.5GPa

Mode	Frequency (Hz)
1	0.96
2	2.64
3	5.18

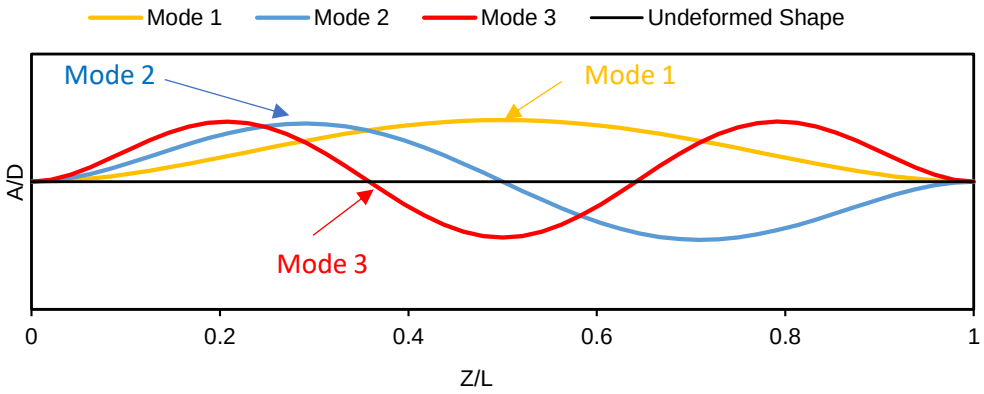

Figure 4-5 Vibration mode shape of a riser with E=102.5GPa

4.4.2 FIV and VIV of a riser; Ue =0.42m/s and varying Ui

In this section, the results of the riser positioned either horizontally (Cases 1-5) or vertically (Cases 5-10) and subjected to Ue_1= 0.42m/s and Ui= 1, 2, 5, 10m/s are examined. The dynamic characteristics of the riser, such as the IL and CF displacements, orbital trajectories, instantaneous CF displacement and vibrating frequency are presented.

4.4.2.1 Inline displacement

Figure 4-6 shows the variation of maximum IL displacement of a horizontal and vertical risers under a constant Ue= 0.42m/s and varying Ui. As can be seen, injecting an internal flow reduces the maximum IL displacement when compared to that of an empty riser (Ui=0). Subsequently, as the fluid is injected and its velocity increases, the displacement increases as well. This trend is observed for both horizontal and vertical risers.

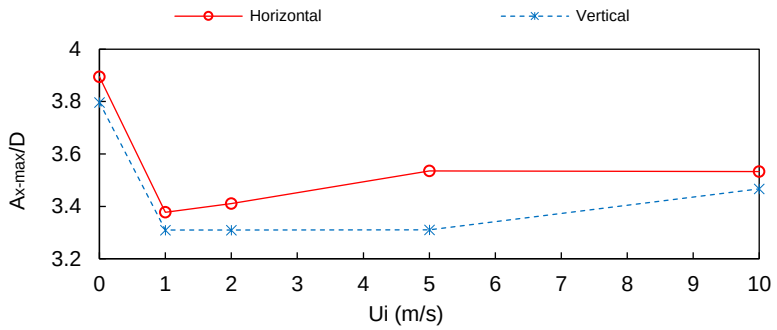

Figure 4-6 Comparison of Maximum IL displacement of the horizontal and vertical risers for Ue_1=0.42m/s and different Ui

It can also be noted from Figure 4-7 (a) and (b) that the maximum IL displacement is located around the midpoint of the risers at all internal flow velocities and for both riser orientations. This makes the maximum displacement of the riser symmetrical around its elevation.

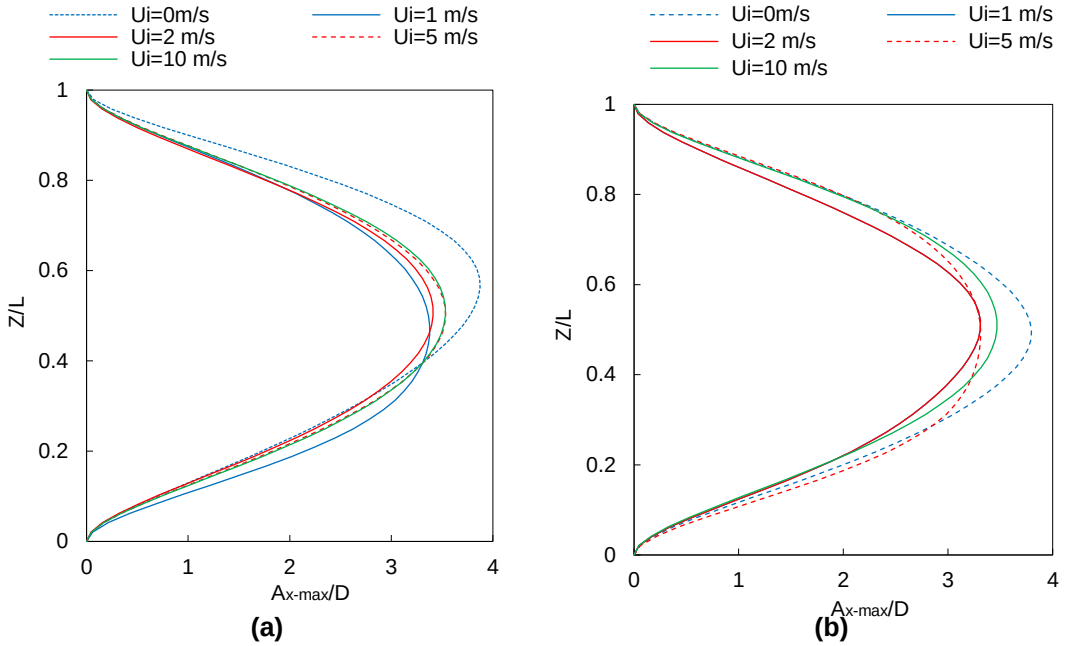

Figure 4-7 Comparison of maximum IL displacement of a riser under Ue_1=0.42m/s and varying Ui: (a) Horizontal (b) Vertical riser

4.4.2.2 Crossflow displacement and dominating mode

Figure 4-8 and Figure 4-9 show the effect of increasing Ui on the CF RMS displacement of the horizontal and vertical risers subjected Ue= 0.42m/s and varying Ui. It can be seen in Figure 4-8 (a) and Figure 4-9 (a) that, without internal fluid, the second and first modes are the dominant ones for the horizontal and vertical riser configurations, respectively. Figure 4-10 shows the instantaneous response envelope of the vertical and horizontal risers over a period of 2s. Without internal flow velocity, a single mode (Mode 2) is dominant when the riser is horizontal. However, for the vertical riser, the dynamic response is multimodal; this comprises the first and second modes, with the first mode being the dominant one. To investigate the impact of the internal flow velocity on the vibration mode, the CF RMS response of the riser under increasing internal flow velocity is shown in Figure 4-8 and Figure 4-9, and the instantaneous response envelope is shown in Figure 4-10. For the horizontal riser, it can be seen from Figure 4-8 (b-e) that when the internal flow velocity increases, the first mode becomes the dominant one for all the five velocities considered. This shows that introducing an internal

flow reduced the mode order compared to empty pipe, but the mode order does not change with increasing internal velocity. A further look into the instantaneous response envelope in Figure 4-10 shows that a single mode is present for all internal flow velocities except for Ui=1m/s. For this velocity, a multimodal response comprising Modes 1 and 2 is observed, with Mode 1 being the dominant one. For the vertical riser, Figure 4-9 (b-e) demonstrates that the vibration mode reduces with the increased internal flow velocity. When Ui=1 and 2m/s, a multimodal response combining Mode 2 and 3 is observed, with Mode 3 being the dominant one, see Figure 4-10 . The mode transition can be attributed to the change of the flexible riser stiffness with the increase of internal velocity (Duan et al., 2021). However, when Ui increases to 5m/s and 10m/s, the second mode becomes the dominant one.

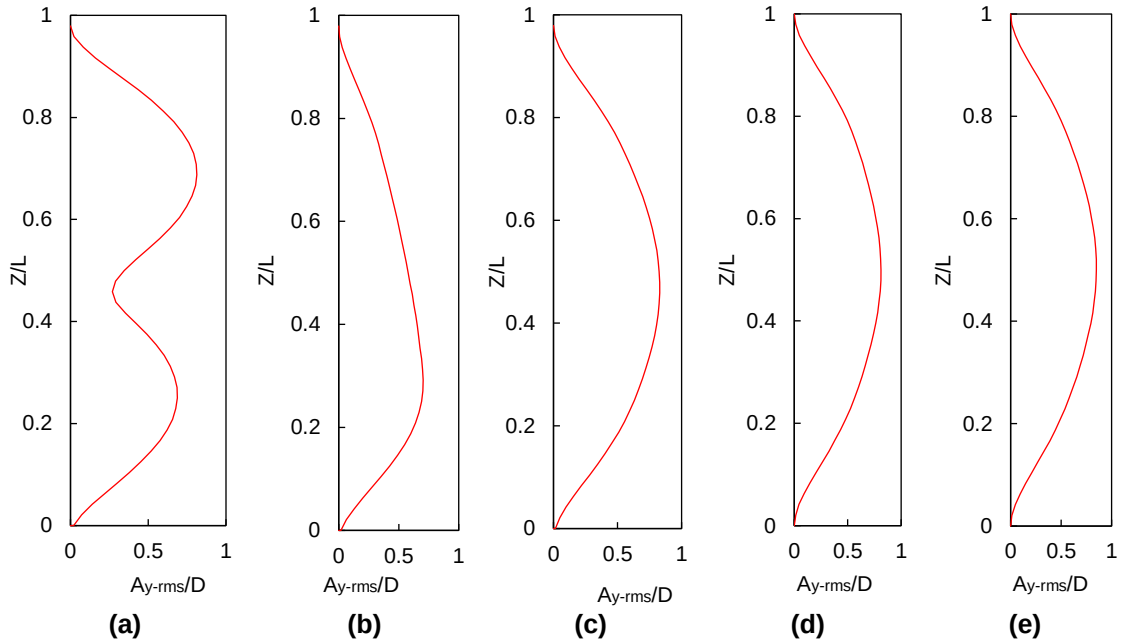

Figure 4-8 Comparison of CF RMS displacement of a horizontal pipe under constant Ue_1=0.42m/s and varying Ui: (a) 0m/s, (b) 1m/s, (c) 2m/s, (d) 5m/s, (e) 10m/s

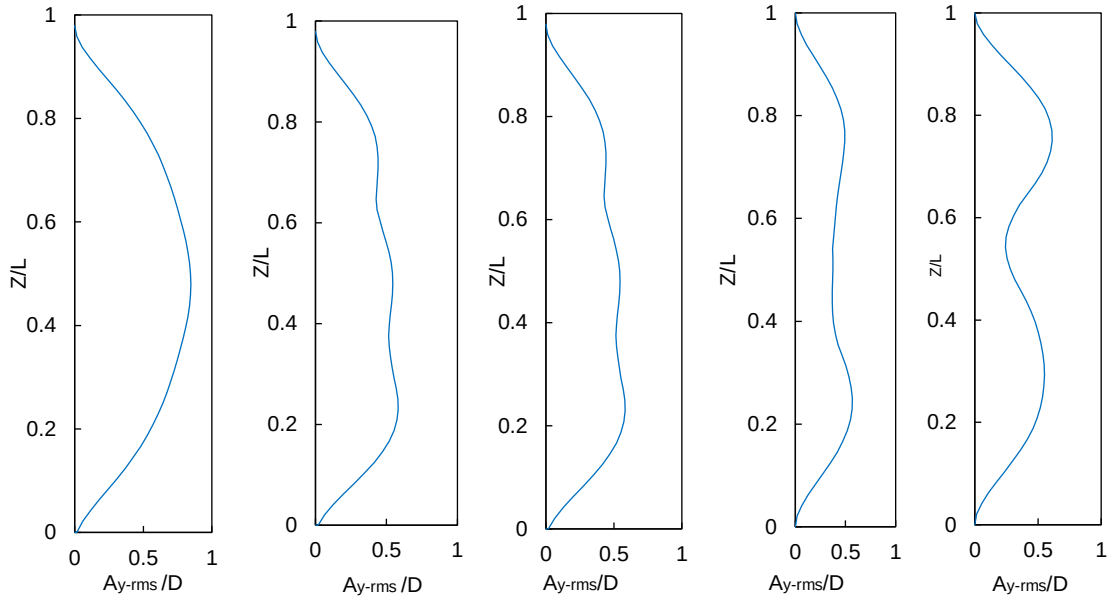

Figure 4-9 Comparison of CF RMS displacement of the vertical riser under constant Ue_1=0.42m/s and varying Ui: (a) 0m/s, (b) 1m/s, (c) 2m/s, (d) 5m/s, (e) 10m/s

One can conclude that the introduction of internal flow and the subsequent increase of internal flow velocity affect the vibration mode of a vertical riser. This is in contrast with that of the horizontal riser under the same conditions, where the dominant vibration mode remains unchanged even when the internal fluid velocity is increased. Furthermore, the maximum RMS values of CF displacement of the horizontal and vertical risers for different internal flow velocities are shown in Figure 4-11. It can be seen that the maximum value of CF RMS occurs when the riser is empty. With the introduction of internal flow, the maximum CF RMS displacements of the horizontal riser decrease slightly for Ui=1m/s, and slight changes occur as the internal flow velocity increases.

The maximum CF RMS displacements for the vertical riser show slight variations when the internal flow velocity increases. Those small changes observed are due to the presence of the internal flow and its variation of velocity. Those changes can thus be attributed to the energy provided by the flow causing the CF displacement to increase (Yang et al., 2018).

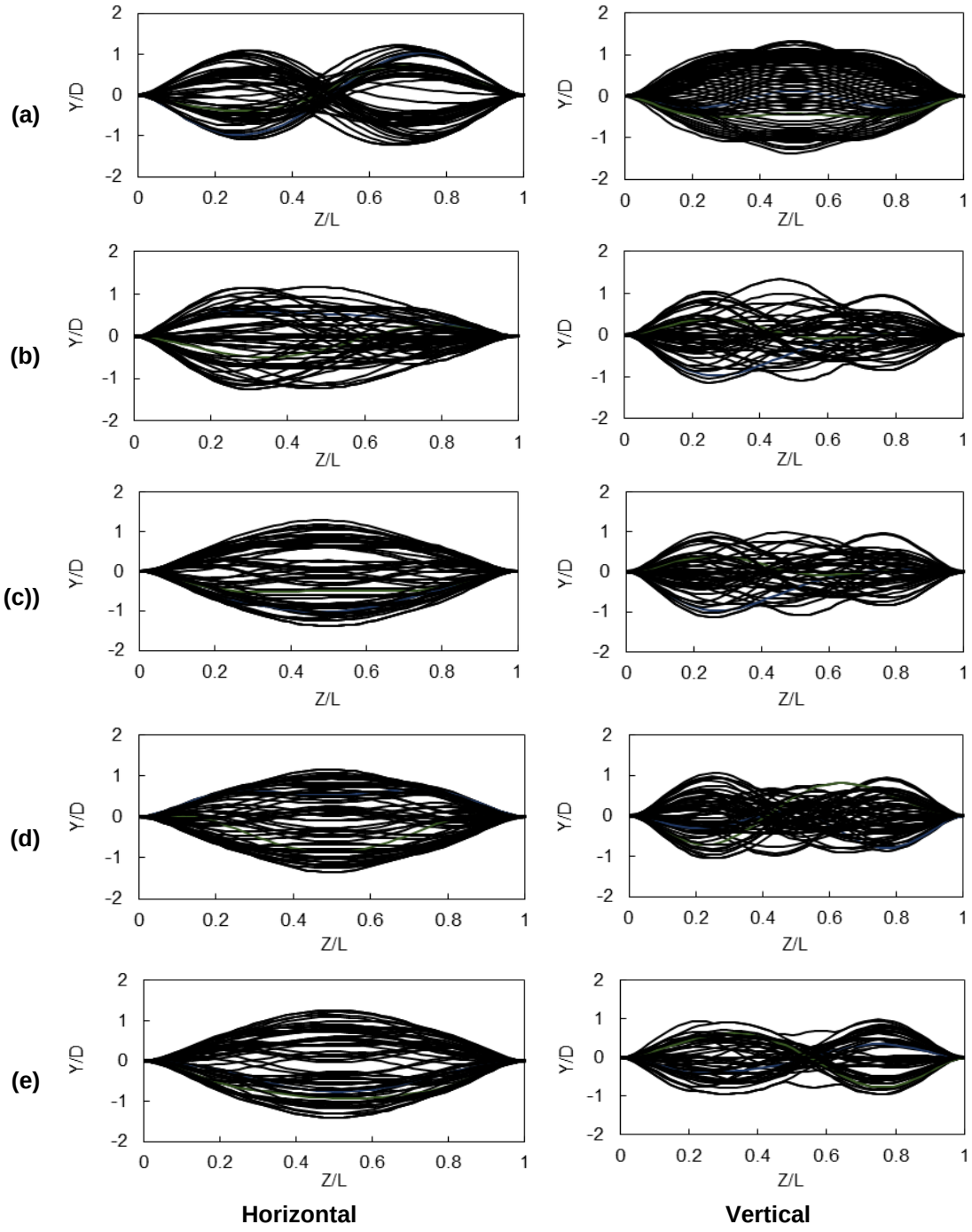

Figure 4-10 comparison of riser response envelopes of Horizontal (right) and Vertical (left) riser for constant external velocity of Ue_1=0.42m/s and varying Ui: (a) 0m/s, (b)1m/s, (c) 2m/s, (d) 5m/s, (e) 10m/s

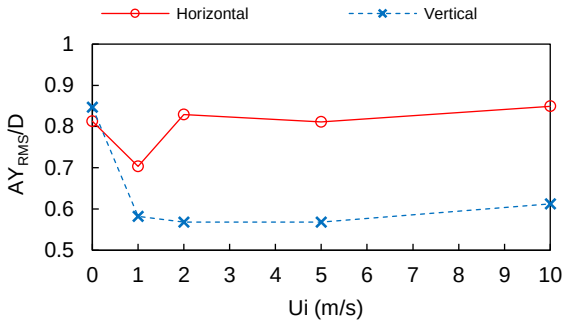

Figure 4-11 Comparison of RMS CF displacement of the horizontal and vertical risers for Ue=0.42m/s and different Ui

4.4.2.3 Vibrating frequencies and orbital trajectories

The time histories, orbital trajectories, and response frequencies of the midpoint of the horizontal and vertical risers subject to the external flow velocity Ue_1= 0.42 m/s and internal flow velocities Ui = 1, 2, 5 and 10m/s are shown in Figure 4-12 and Figure 4-13, respectively. For each figure, the first column shows the time histories of the dimensionless CF displacement at varying internal velocities, the second column shows response frequency of the time history of the first column. and the third column shows the orbital trajectory.

It can be observed that the oscillation of the midsection of the horizontal riser is non-periodic and becomes relatively stable after 2s, see Figure 4-12 (a-e). Compared to the oscillation of the horizontal riser, the oscillation of the vertical riser becomes more unstable as the internal flow velocity increases, see Figure 4-13(a-e).To assess the impact of the internal fluid velocity on the response frequencies, the frequency spectra of the CF time histories are plotted in Figure 4-12 and Figure 4-13. For the horizontal riser, it can be seen that one dominant frequency is excited for all five internal velocities considered, which means that the vibration is dominated by a single mode (Mode 1) see Figure 4-12 (a-e). However, for the vertical riser, two or more minor frequencies are excited around the dominant frequency, as shown in Figure 4-13, which indicates the existence of multimodal vibration and the occurrence of a chaotic trajectory. In addition, it

can also be observed that the horizontal riser frequency reduces from 3.48HZ to 3.09Hz when Ui increases from 1 to 2 m/s and maintained a frequency of 3.09Hz as the Ui increased from 2 to m/s.For the vertical riser, Figure 4-13 shows that introducing a single-phase fluid at a velocity of 1m/s reduced the dominant riser frequency from 3.32Hz to 2.21Hz. However, when the velocity increases from 2 to 5m/s the dominant frequency increased to 3.13Hz, then reduced to 2.93hz when Ui increased to 5 and 10m/s. Thus, as the internal flow velocity increases the dominant frequency increases. This trend agrees with the results from Guo et al. (2008).

Regarding the effects of internal fluid velocity on the orbital trajectory of a riser exposed to Ue=0.42m/s, it can be seen from Figure 4-12 that as the velocity increases, the orbital trajectories does not take a regular shaped trajectory. Figure 4-13 shows that a regular 8-shape trajectory is obtained for the vertical riser without internal fluid flow, which indicates the occurrence of dual resonance. However, with the introduction of internal flow and a subsequent increase in the internal fluid velocity, the riser orbital trajectory becomes chaotic and no longer follows any regular pattern.

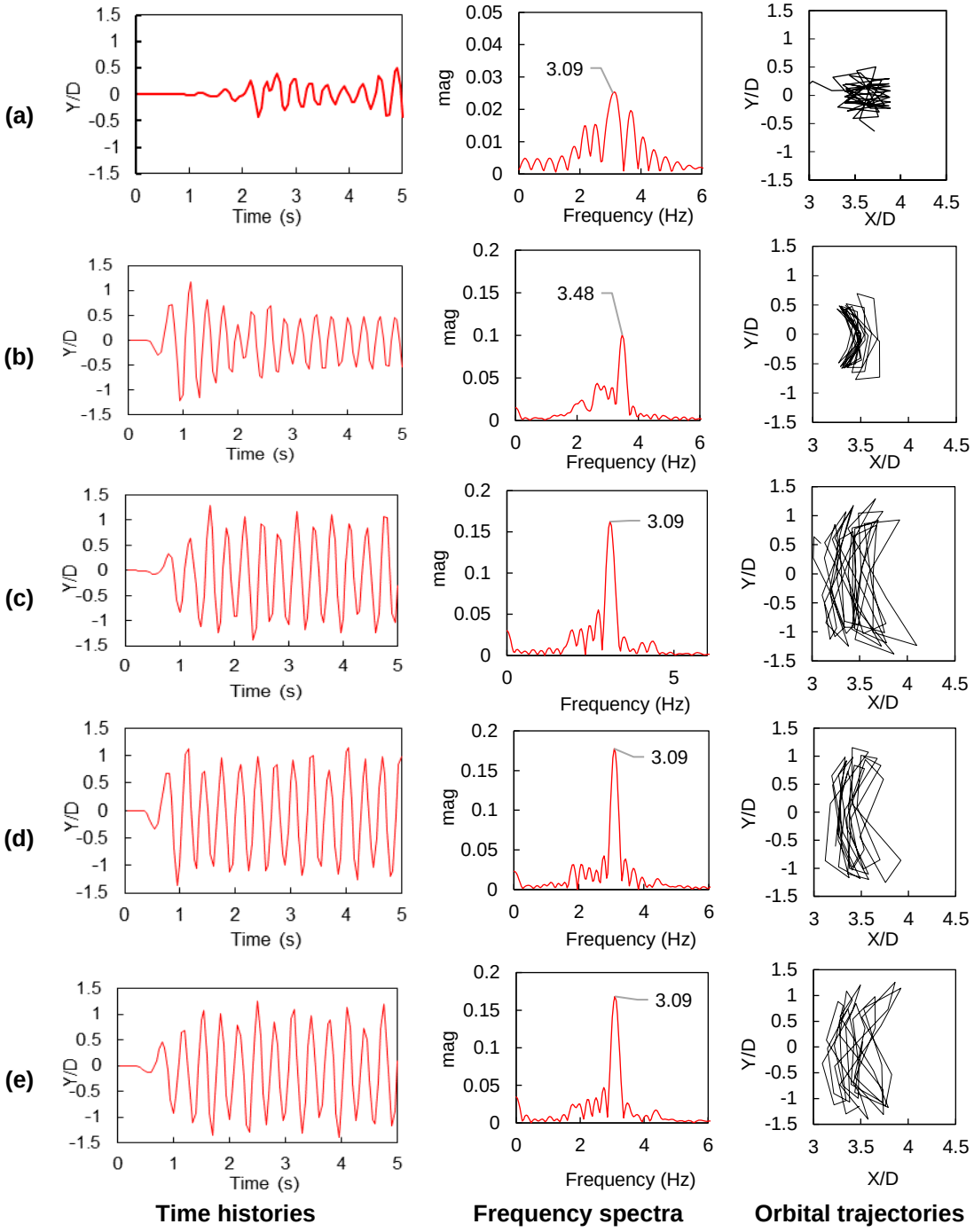

Figure 4-12 Comparison of time histories, orbital trajectories, and oscillation frequencies of the horizontal riser at Z/L=0.5, for constant Ue_1=0.42m/s and varying Ui: (a) 0m/s, (b)=1m/s, (c) 2m/s, (d) 5m/s, (e) 10m/s

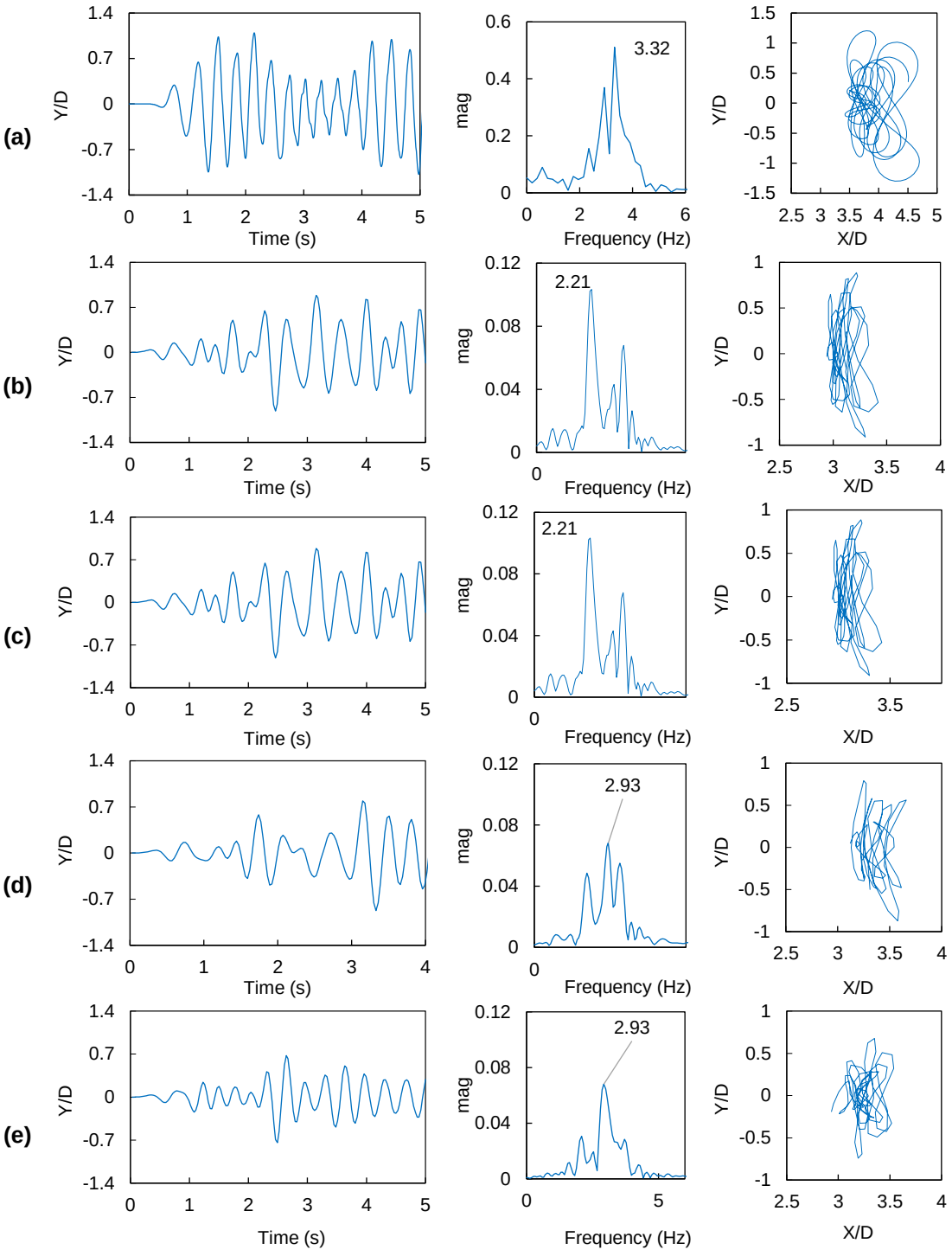

Figure 4-13 Comparison of time histories, orbital trajectories, and oscillation frequencies of a vertical riser at Z/L=0.5, for constant Ue_1=0.42m/s and varying Ui: (a) 0m/s, (b)=1m/s, (c) 2m/s, (d) 5m/s, (e) 10m/s

4.4.3 FIV and VIV of a riser; Ue =0.84m/s and varying Ui

In this section, the dynamic response of a horizontal (Cases 11-15) and vertical (Cases 15-20) fluid conveying riser subjected to Ue=0.84m/s and Ui=1, 2, 5 and 10m/s are now examined, with the riser having similar properties as described in sections. 4.4.2.

4.4.3.1 Inline displacement

The maximum IL displacement variation with increasing internal flow velocities is shown in Figure 4-14. As stated previously, a 0 value of the internal flow velocity describes an empty pipe. The graph shows that the maximum IL displacement does not change significantly when the internal flow velocity increases. This trend is similar to what is obtained in the analytical studies from Duan et al. (2021a). In general, the external flow velocity has more impact on the IL displacement than the internal flow.

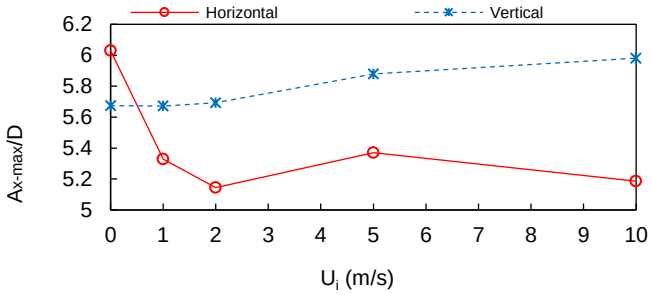

Figure 4-14 Comparison of Maximum IL displacement of Horizontal and vertical risers under different internal flow velocities and constant Ue=0.84m/s

Compared to the riser exposed to Ue=0.42m/s, when the Ue increases to 0.84m/s, the maximum IL displacement of the riser under all five internal flow velocities considered increases to almost twice that of Ue=0.42m/s, as shown in Figure 4-15 . This can be explained by the drag force from the fluid acting on the riser that is proportional to the square of the current velocity (Huang, Chen and Chen, 2011). Similar to the maximum IL deflection at Ue=0.42m/s, the largest deflection when Ue=0.84m/s occurs around the midpoint of the riser, regardless of the riser's orientation and internal flow velocity. Thus, the riser displacement is symmetrical about the elevation.

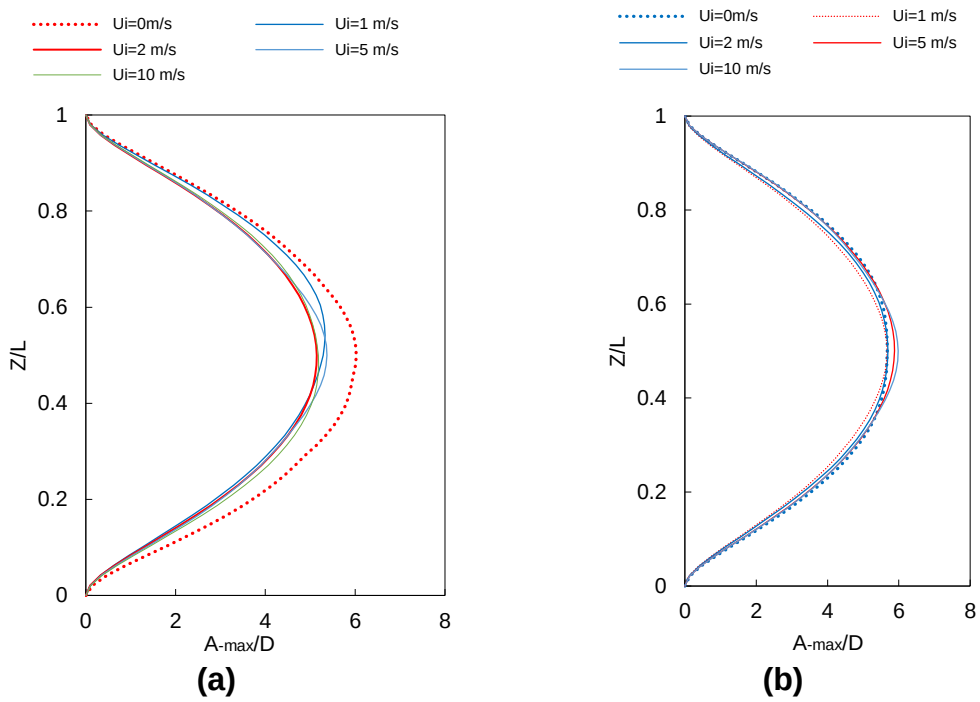

Figure 4-15 Maximum IL response of a riser when Ue_2 =0.84m/s with different flow velocities and different orientations (a) Horizontal (b) Vertical

4.4.3.2 Crossflow displacement and dominating mode

Figure 4-16 and Figure 4-17 show variation of the RMS CF vibration of horizontal and vertical risers under a constant Ue =0.84m/s and the same internal flow velocities Ui = 1,2,5 and10 m/s. It can be seen from Figure 4-16 (a) and Figure 4-17 (a) that when the riser is empty (Ui=0), the second and third modes of vibration are the dominant ones in horizontal and vertical configurations, respectively. Compared to Ue=0.42m/s, the vibration mode of the horizontal and vertical empty risers increase from modes 2 and 1 to modes 2 and 3 when Ue increases from 0.42m/s to 0.84m/s. In addition, the response envelope in Figure 4-18 (a) shows that when the riser is empty, the horizontal and vertical risers are dominated by a single vibration mode. Subsequently, when internal fluid is injected into the horizontal riser, the vibration mode increases with the internal flow velocity. The mode first increases to a weak mode 3 at Ui=1m/s, then decreases to mode 2 at Ui=2m/s, see Figure 4-16(b-c).

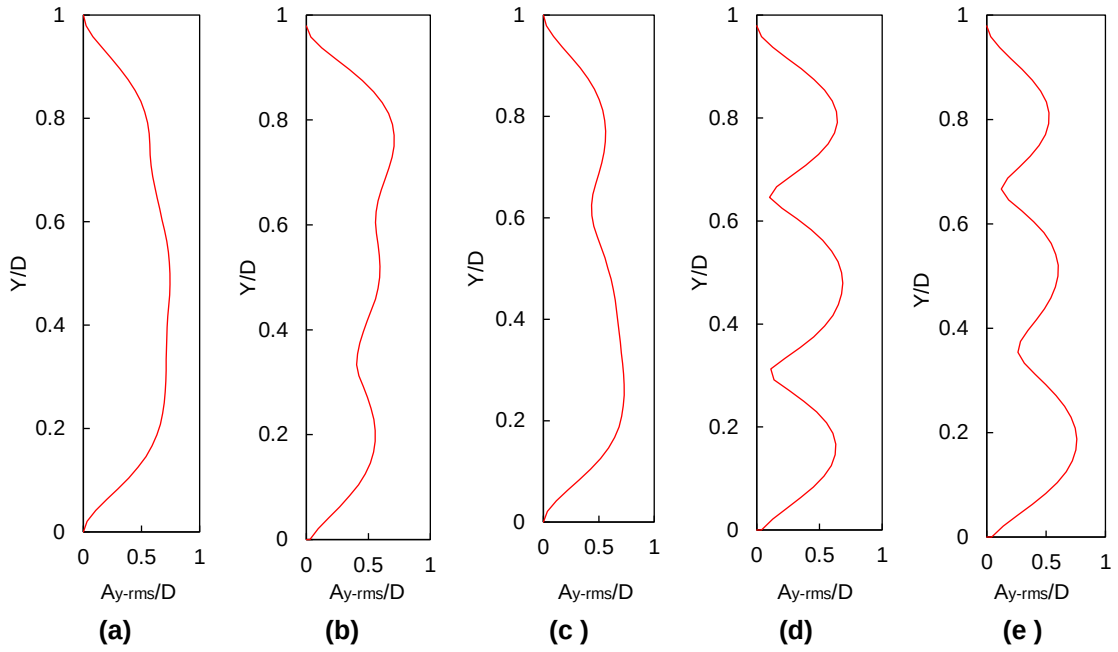

Figure 4-16 Comparison of CF RMS displacement of the horizontal under constant Ue_1=0.42 and varying Ui: (a) 0, (b) 1m/s, (c) 2m/s, (d) 5m/s, (e) 10m/s

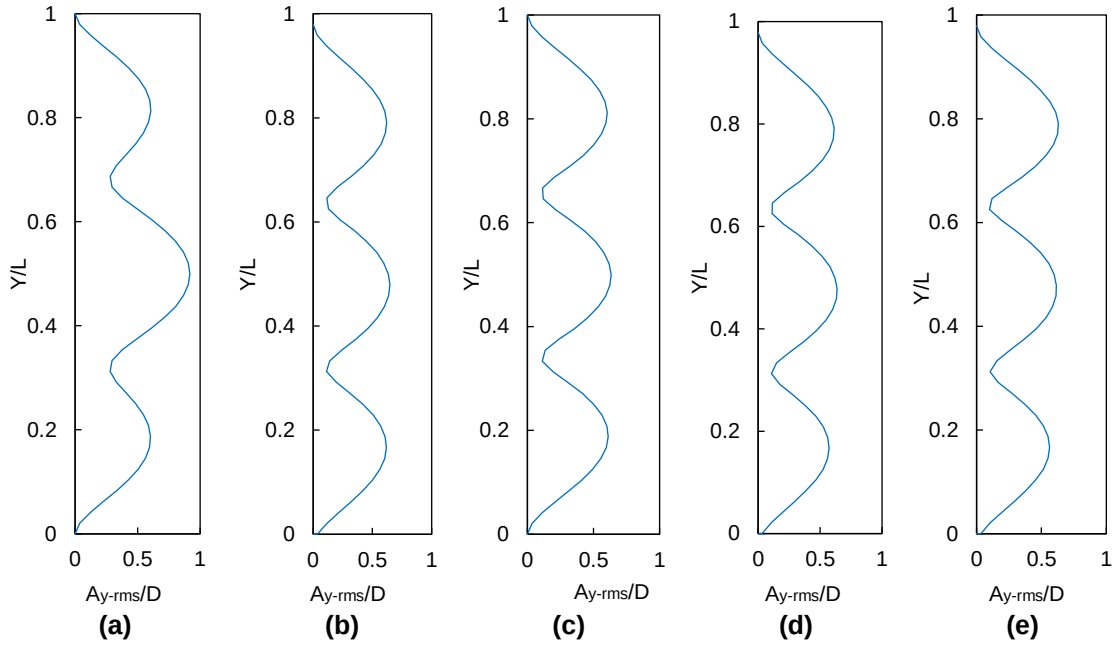

Figure 4-17 Comparison of CF RMS displacement of the vertical riser under constant Ue_1=0.42 and varying Ui: (a) 0, (b) 1m/s, (c) 2m/s, (d) 5m/s, (e) 10m/s

As the velocity increases to Ui=5m/s and 10m/s, mode 3 becomes the dominant mode see Figure 4-16 (d) and (e). Therefore, it can be seen that the velocity of the internal flow significantly influences the mode shape of the horizontal riser at Ue=0.84m/s.

For the vertical riser configuration, mode 3 is the dominant one, irrespective of the internal fluid velocity, as shown in Figure 4-17 (b-e). The results thus show that for a vertical riser under Ue= 0.84m/s, increasing the internal flow velocity has little impact on the vibration mode. The CF response envelope of the horizontal and vertical risers is presented in Figure 4-18 . A multimodal vibration which combines modes two and three occurs at Ui=1m/s and 2m/s for the horizontal riser. With the velocity increase, the mode shape transitioned to a single mode (mode 3) at Ui=5m/s and 10m/s. However, a single mode (Mode 3) is dominant for the vertical riser, irrespective of the internal flow velocity. This trend of increased mode with increasing internal fluid velocity agrees with the results from (Yang et al., 2018) and (Duan et al., 2021). Generally, the velocity of the internal fluid has much more influence on the horizontal riser than on the vertical riser. In addition, it can be seen that the internal flow determines the vibration mode when the velocity ratio of the internal flow against the external current is comparably high. As a general rule, the higher the velocity ratios of internal flow against the external current, the larger the internal flow affects the vibration response.

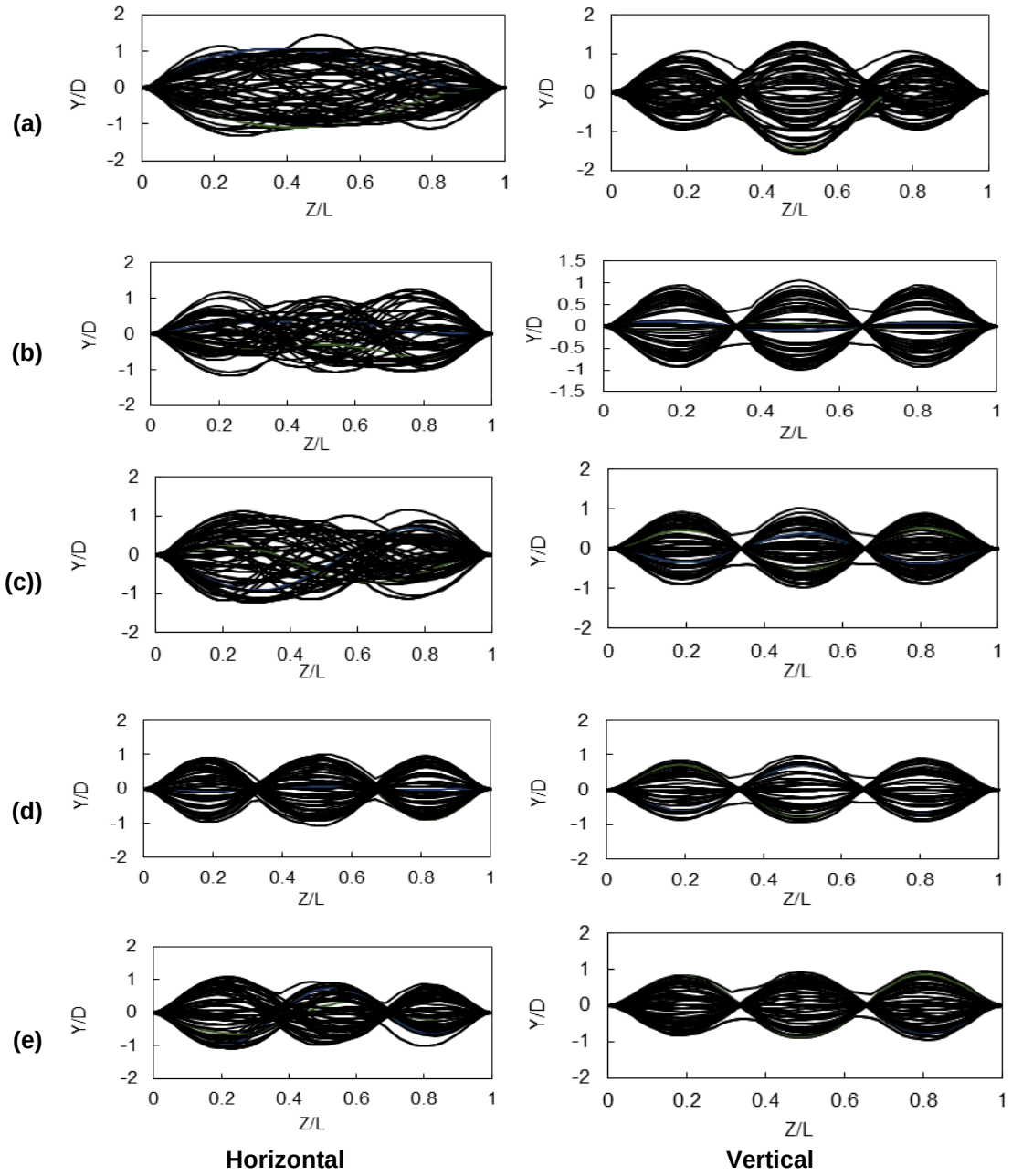

Figure 4-18 Comparison of response envelopes of the horizontal (right) and vertical (left) risers under constant Ue=0.84m/s and varying Ui: (a) 0m/s, (b) 1m/s, (c) 2m/s, (d) 5m/s, (e) 10m/s

Figure 4-19 shows the variation of RMS CF displacement of the riser under Ue= 0.84 m/s and Ui = 1, 2, 5, and 10m/s. The solid and dash lines represent the horizontal and vertical riser configurations, respectively. It can be seen that for the introduction of internal fluid, the CF dimensionless RMS displacements of the riser decreased slightly. As the internal velocity increases, the maximum dimensionless RMS displacements of the riser show slight variations for both horizontal and vertical risers.

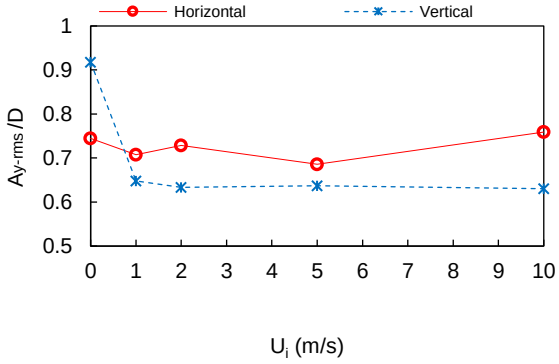

Figure 4-19 Comparison of RMS CF displacement of Horizontal and vertical risers under different internal flow velocities and constant Ue=0.84m/s

4.4.3.3 Vibrating frequencies and Orbital trajectories

Section 4.4.2 examined the impact of internal fluid velocity on the vibrating frequencies of a horizontal pipe exposed to Ue=0.42m/s. In this section, Ue is increased from 0.42m/s to 0.84m/s while the internal velocities, Ui = 1, 2, 5 and 10m/s are maintained. The impacts of the internal fluid velocities on the dynamic response, vibration frequencies and orbital trajectories of the midpoint of the horizontal and vertical risers for Ue= 0.84m/s are presented in Figure 4-20 and Figure 4-21 , respectively. The first column shows the time histories of the dimensionless CF displacement at varying internal velocities, the second column shows the response frequency of the time history of the first column and the third column shows the orbital trajectories. It can be observed from the graphs that the oscillation of the midsection of the horizontal riser is non-periodic.

For horizontal riser, it can be observed from Figure 4-20 that introducing a single-phase fluid at a velocity of 1m/s increased the dominant riser frequency from 6.09Hz to 7.07 Hz. However, as the internal flow velocity increases, the dominant frequency slightly decreases to 7.03Hz. This trend agrees with the results from Guo et al. (2008). For vertical riser, it can also be observed from Figure 4-21 that introducing a single-phase fluid at a velocity of 1m/s decreased the dominant riser frequency from 6.64Hz to 5.99Hz. Similarly, the dominant frequency decreases to 5.92Hz as the internal velocity increases. The results show that increasing the internal flow velocities slightly affects the frequency of both the horizontal and vertical risers. This trend agrees with the results from Duan et al. (2021a).

Moreover, Figure 4-21 shows that the dominant frequency of the horizontal riser is accompanied by a smaller frequency when Ue=1 and 2 m/s. The presence of smaller frequencies indicates the occurrence of a multimodal vibration for the horizontal riser. As the Ui increases, the smaller frequencies disappear, and the vibration becomes dominated by a single frequency.

Similarly, from the FFT diagram of the vertical risers in Figure 4-20 , it can be observed that a single dominant frequency is recorded for all the internal flow velocities. In general, the external velocity impacts the dominant mode and frequency more than the internal flow velocity.

The orbital trajectories of the horizontal riser midpoint are plotted in Figure 4-20 . It can be seen that the orbital shapes appear to be unstable and irregular for all the internal flow velocities considered. For the vertical riser, it can be seen that a regular 8-shape trajectory is observed when the riser is empty. When internal fluid is introduced, the orbits trajectory shows a crescent shape, with the lobes facing the right directions. As the internal flow velocity increases, the crescent shape remains unchanged, as shown in Figure 4-21 . The 8-shape shows that the frequency of the IL vibration is almost twice that of the CF.

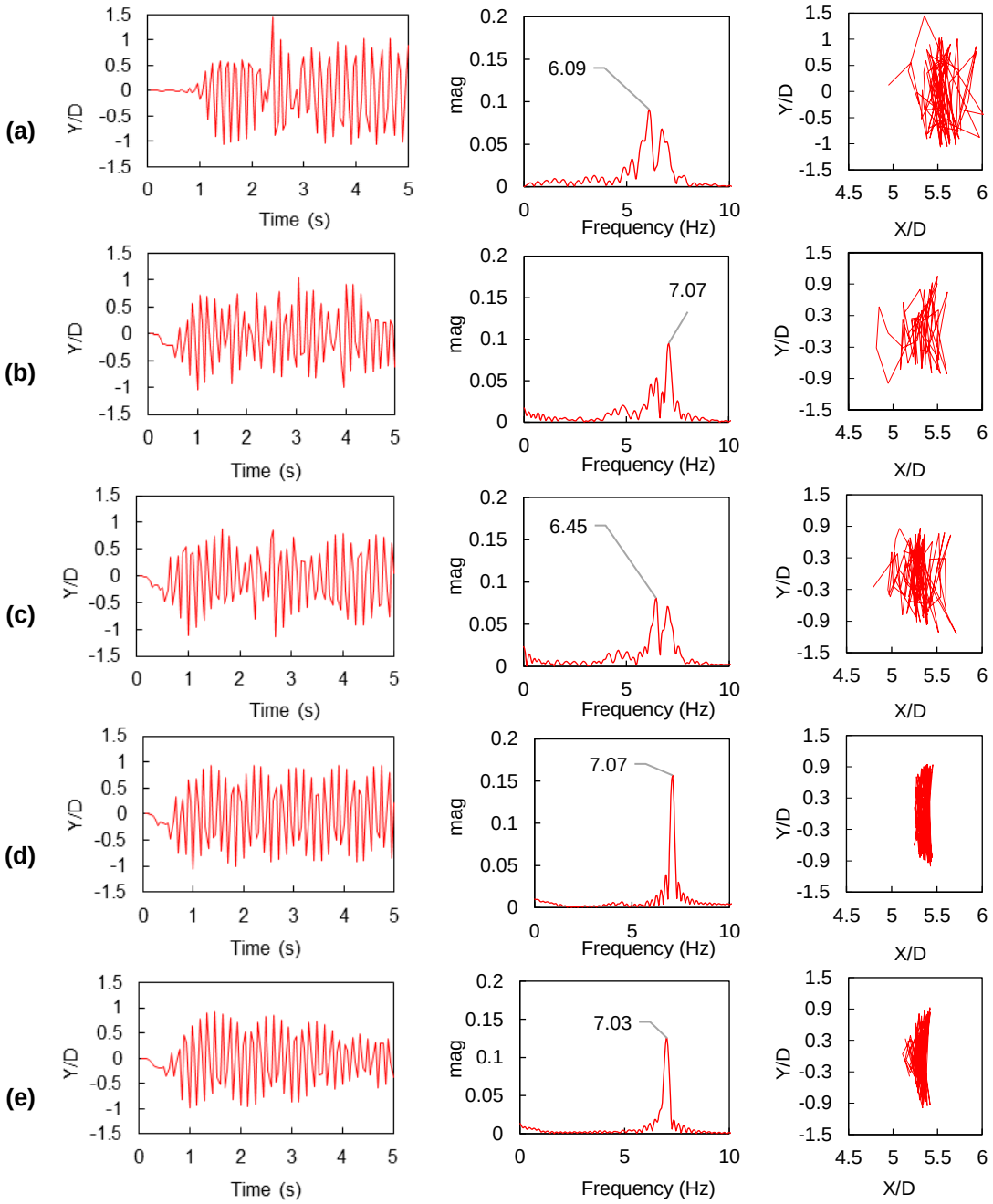

Figure 4-20 Comparison of time histories, orbital trajectories, and oscillation frequencies of a horizontal riser at Z/L=0.5, for constant Ue=0.84m/s and varying Ui: (a) 0m/s, (b) 1m/s, (c) 2m/s, (d) 5m/s, (e) 10m/s

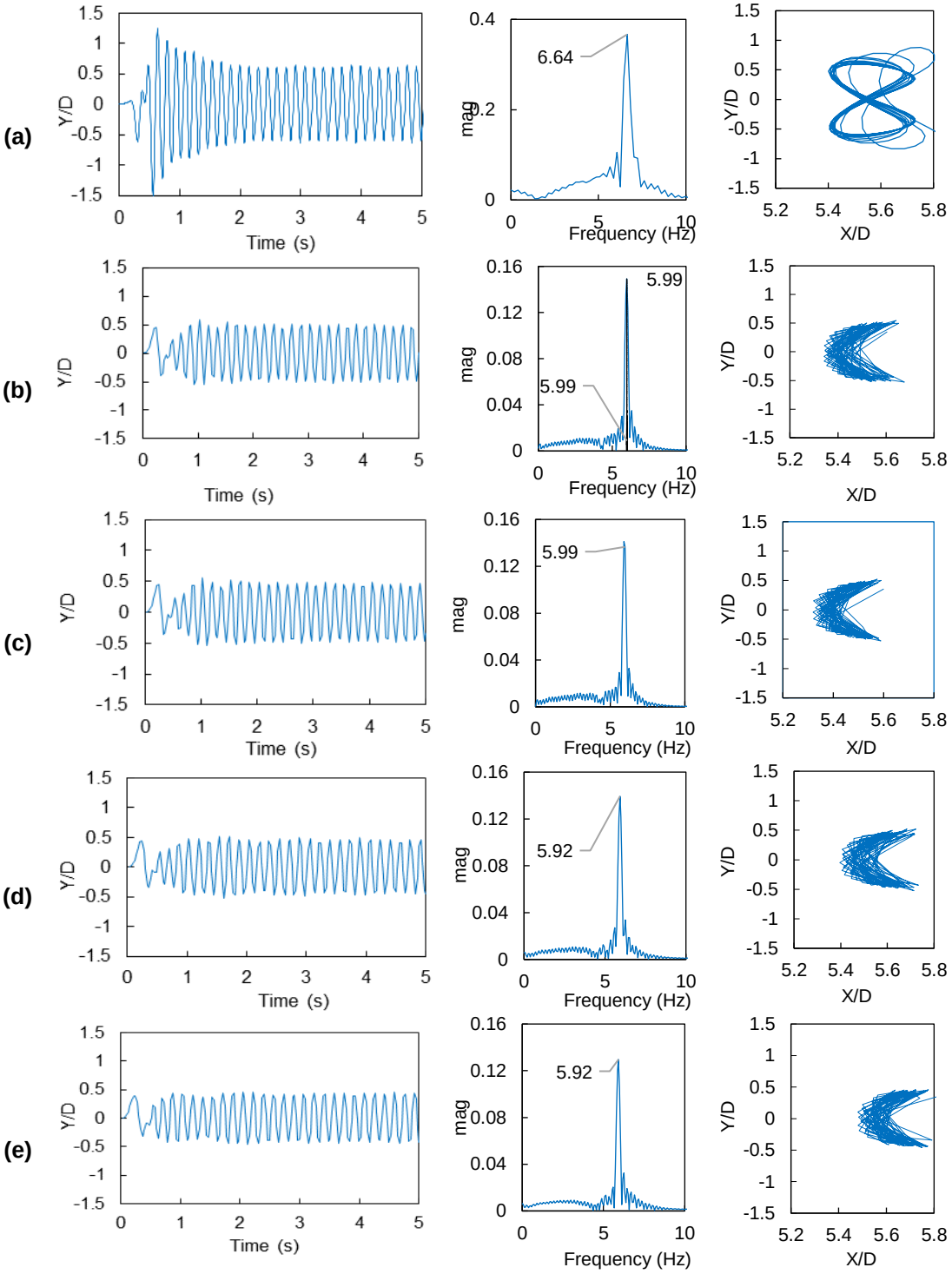

Figure 4-21 Comparison of time histories, orbital trajectories, and oscillation frequencies of a vertical riser at Z/L=0.5, for constant Ue=0.84m/s and varying Ui: (a) 0m/s, (b) 1m/s, (c) 2m/s, (d) 5m/s, (e) 10m/s

4.4.4 Effect of elastic modulus on the dynamic response of a riser transporting single-phase fluid

The effect of elastic modulus is examined to understand further the dynamic responses of a horizontal riser transporting fluid. The riser property is similar to that in sections 4.4.2 and 4.4.3, except for the elastic modulus, which is reduced from 102.5GPa to 1.025GPa. The dynamic characteristics such as the vibration mode, IL displacement, CF displacement and vibration frequencies are compared to those in sections 4.4.2 and 4.4.3. Two external velocities of 0.42m/s (Cases 21-25) and 0.84m/s (Cases 26-30) and five internal flow velocities of 1, 2,5 and 10 m/s are considered. The natural frequency and mode shape of the riser are obtained by performing modal analysis using the ANSYS MODAL module in ANSYS 2019 R2 software. The natural frequencies and the mode shape of the riser are presented in Table 4-6 and Figure 4-22

Table 4-6 Natural frequency of a horizontal riser with an elastic modulus of 1.025GPa

Mode	Frequency (Hz)
1	0.10
2	0.26
3	0.52
4	0.86
5	1.28
6	1.79

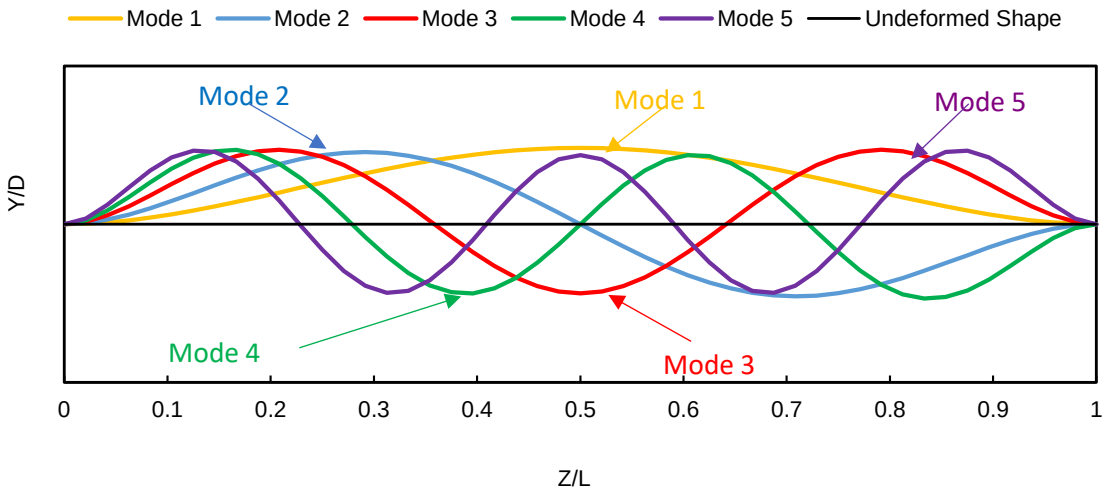

Figure 4-22 Mode shape of the horizontal riser with E= 1.025GPa

4.4.4.1 Inline displacement

Figure 4-23 (a) and (b) show the comparison between the maximum IL displacement with increasing internal flow velocity (Ui=1, 2, 5 and10m/s) for Ue=0.42m/s and Ue=0.84m/s respectively. It can be seen from Figure 4-23 (a) that the maximum values are present near the midpoint of the riser for all internal flow velocities considered. In addition, Figure 4-24 shows that the maximum IL displacement increases when Ue increases from 0.42m/s to 0.84m/s for all internal flow velocities considered. Similarly, as Ui increases, the maximum IL displacement shows slight fluctuations for all internal flow velocities considered. Compared to the horizontal riser with E=102.5GPa, the maximum IL displacement of the horizontal riser at all velocities increased when the elastic modulus reduced to E=1.025GPa. Thus, the reduction of elastic modulus increased the Maximum IL displacement of the riser.

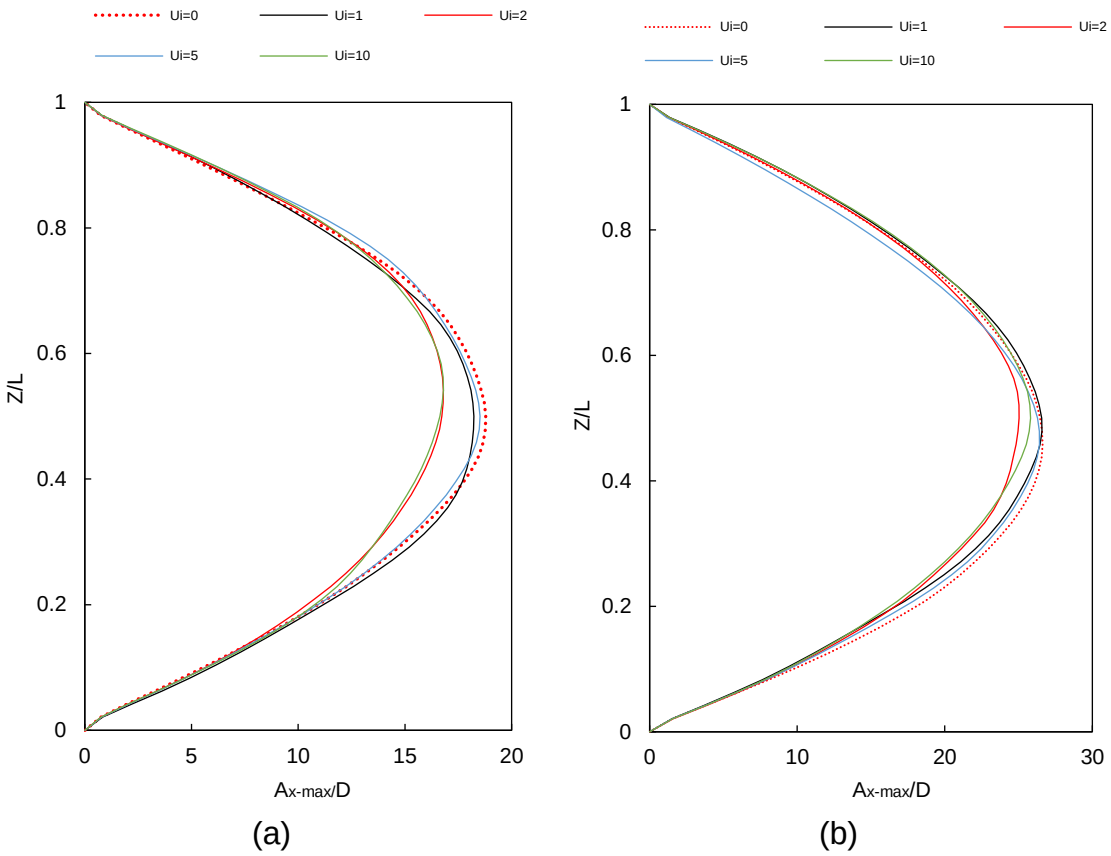

Figure 4-23 Comparison of IL response of a horizontal riser with E=1.025 GPa and varying Ui (1m/s, 2m/s, 5m/s, 10m/s) and Ue a) 0.42m/s b) 0.84m/s

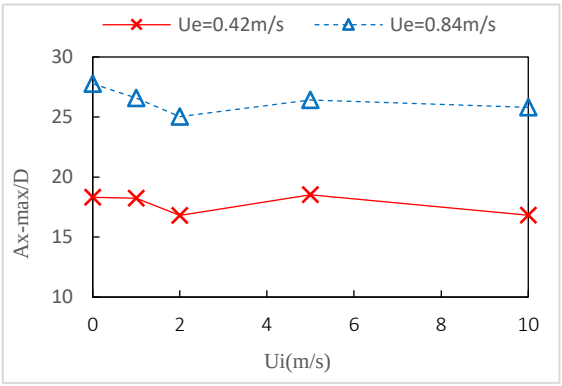

Figure 4-24 Comparison of (a) Maximum IL displacement of flexible riser with E= 1.025GPa and Ui = 1m/s, 2m/s, 5m/s, 10m/s and Ue=0.42m/s and 0.84 m/s.

4.4.4.2 Crossflow displacements and dominating modes

Figure 4-26 compares the CF RMS displacement of a horizontal pipe with E= 1.025 GPa, subjected to Ue = 0.42 and 0.84m/s and varying Ui=1,2,5 and 10 m/s. It can be seen in Figure 4-26 (a) that without internal flow, modes 3 and 5 are the dominant modes when Ue is 0.42m/s and 0.84m/s, respectively.

To investigate the impact of internal flow velocities on the vibration mode, the CF RMS response of the riser under increasing internal flow velocity is shown in Figure 4-26 (b-e).

For Ue=0.42m/s, introducing an internal flow with Ui=1m/s changes the mode shape from mode 3 for the empty riser to a multimodal response. The multimodal response is shown in detail in Figure 4-27 . As the internal fluid flow increases, a combination of modes 3 and 4 is observed, with mode 4 becoming the dominant mode at Ui=10m/s.

When Ue increases to 0.84m/s, the vibration mode also increases from mode 5 for an empty riser to a multimodal one when the internal flow is injected at Ui=1m/s, as shown in Figure 4-27 As the internal flow velocity increases, the dominant mode reaches mode 7 for Ui=10m/s. The results thus show that increasing the external flow velocity increases the riser's vibration mode order.

Compared to the horizontal with E=102.5Gpa, the vibration mode of the horizontal riser at all internal flow velocities increased when the elastic modulus reduced to E=1.025GPa. Thus, the reduction of elastic modulus increased the vibration mode of the riser. Figure 4-25 shows the maximum CF RMS displacement of the riser under varying external and internal flow velocities. The graph shows that the internal flow velocities slightly affect the maximum CF RMS displacement.

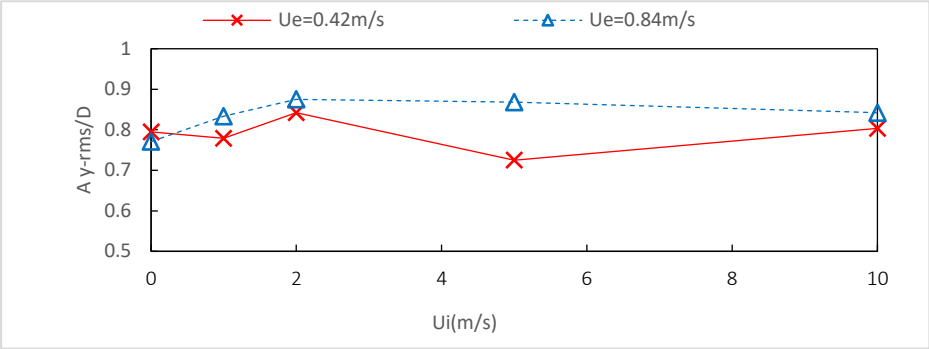

Figure 4-25 Comparison of CF RMS displacement of flexible riser with E= 1025GPa and varying internal (1m/s, 2m/s, 5m/s, 10m/s) and external fluid velocity (Ue=0.42m/s and Ue_2=0.84 m/s)

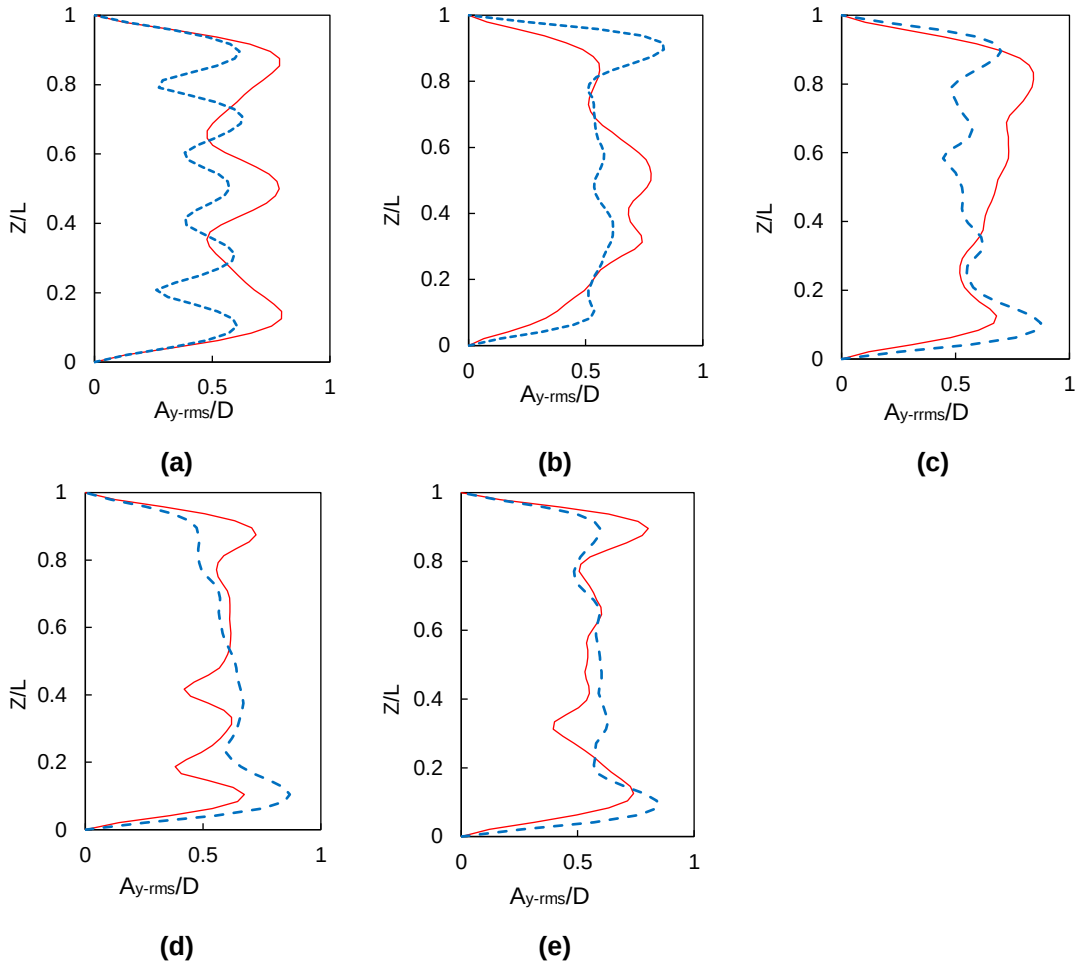

Figure 4-26 Comparison of CF RMS displacement of Horizontal riser with Ue= 0.42m/s (Red solid line) and 0.84m/s(blue dash line), E=1.025Gpa and varying Ui: (a) 0, (b)=1m/s, (c) 2m/s, (d) 5m/s, (e) 10m/s

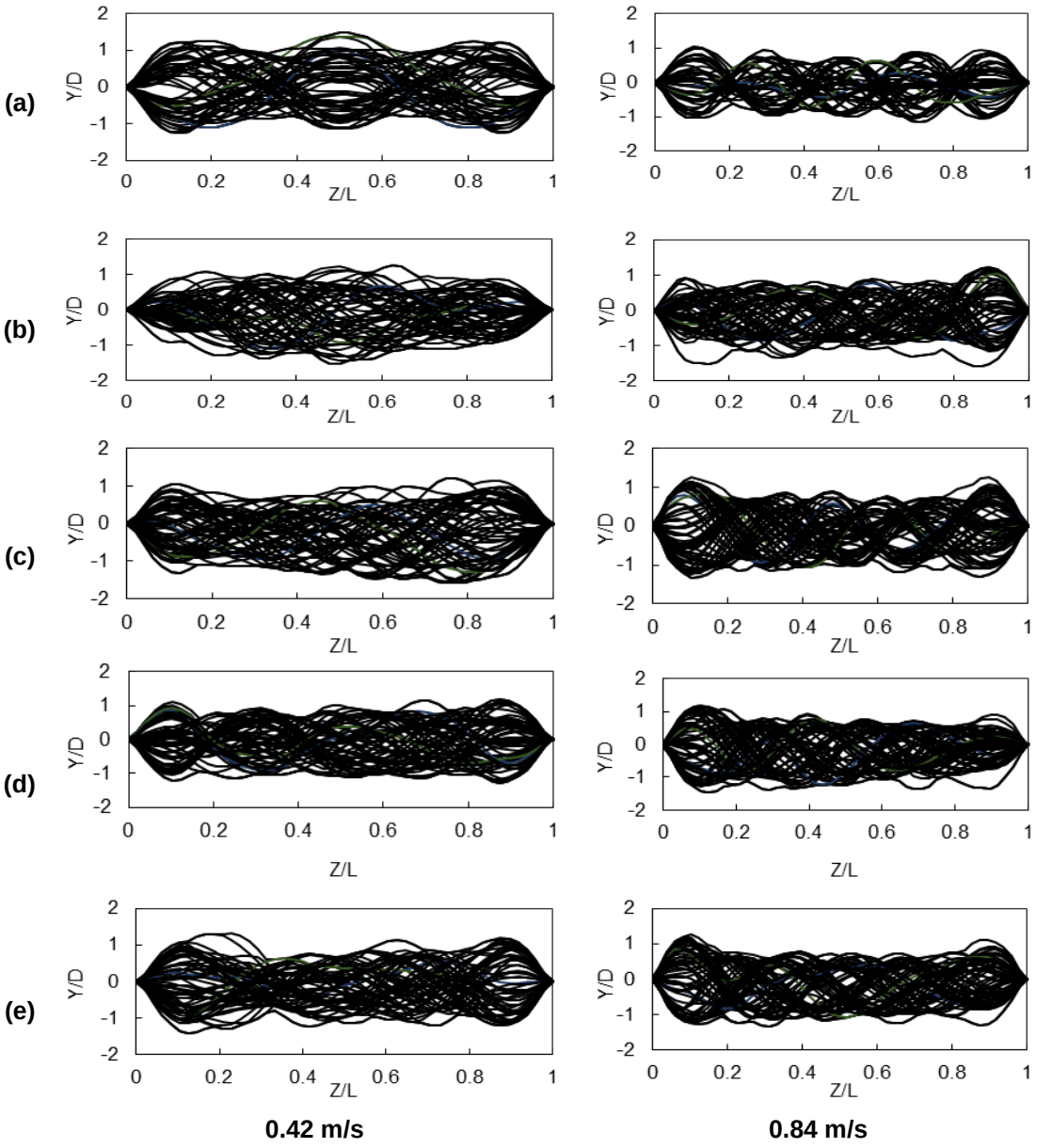

Figure 4-27 Comparison of riser response envelopes of the horizontal riser for external velocity Ue=0.42m/s (left) and Ue=0.84m/s (right), E=1.025 GPa and varying Ui: (a) 0, (b)=1m/s, (c) 2m/s, (d) 5m/s, (e) 10m/s

4.4.4.3 Vibrating frequencies and orbital trajectories

Sections 4.4.2.3 and 4.4.3.3 examined the impact of external/internal fluid velocities on the vibrating frequencies of a horizontal pipe with E=102.5Pa. In this section, the elastic modulus is reduced from 102.5Gpa to 1.025Gpa. The effect of elastic modulus reduction is examined while the internal and external velocities are maintained. The time histories, orbital trajectories, and response frequencies of the midpoint of the horizontal riser with E=1.025GPa, subject to Ue= 0.42 m/s and 0.84m/s and Ui = 1, 2, 5 and 10m/s are shown in Figure 4-28 and Figure 4-29 , respectively. The first column shows the time histories of the dimensionless CF displacement at varying internal velocities, the second column shows the orbital trajectories, and the third column shows the response frequency of the time history of the first column. It can be observed from the graphs that the oscillation of the midsection of the horizontal riser is non-periodic.

When Ue=0.42m/s, it can be observed from Figure 4-28 that the frequency increases from 3.09Hz to 3.44Hz as the internal flow velocity of 1m/s is injected into the pipe. However, the dominant frequency reduces as the Ui increases.

In addition, when Ue=0.84m/s, it can also be observed from Figure 4-29 that introducing a single-phase fluid at a velocity of 1m/s increased the dominant riser frequency from 5.94Hz to 6.2Hz. Similarly, when the velocity increases from 2m/s to 10m/s, the dominant frequency increases as the internal velocity increases.

The trajectories of a riser with an elastic modulus of 1.025Gpa under varying external and internal fluid velocities are shown in Figure 4-28 and Figure 4-29 . For different internal flow velocities considered, the riser's orbital movement is chaotic and does not necessarily take any regular shapes. Such irregular shapes were also described in the work of (Huang, Chen and Chen, 2007), where the riser has a large mode shape.

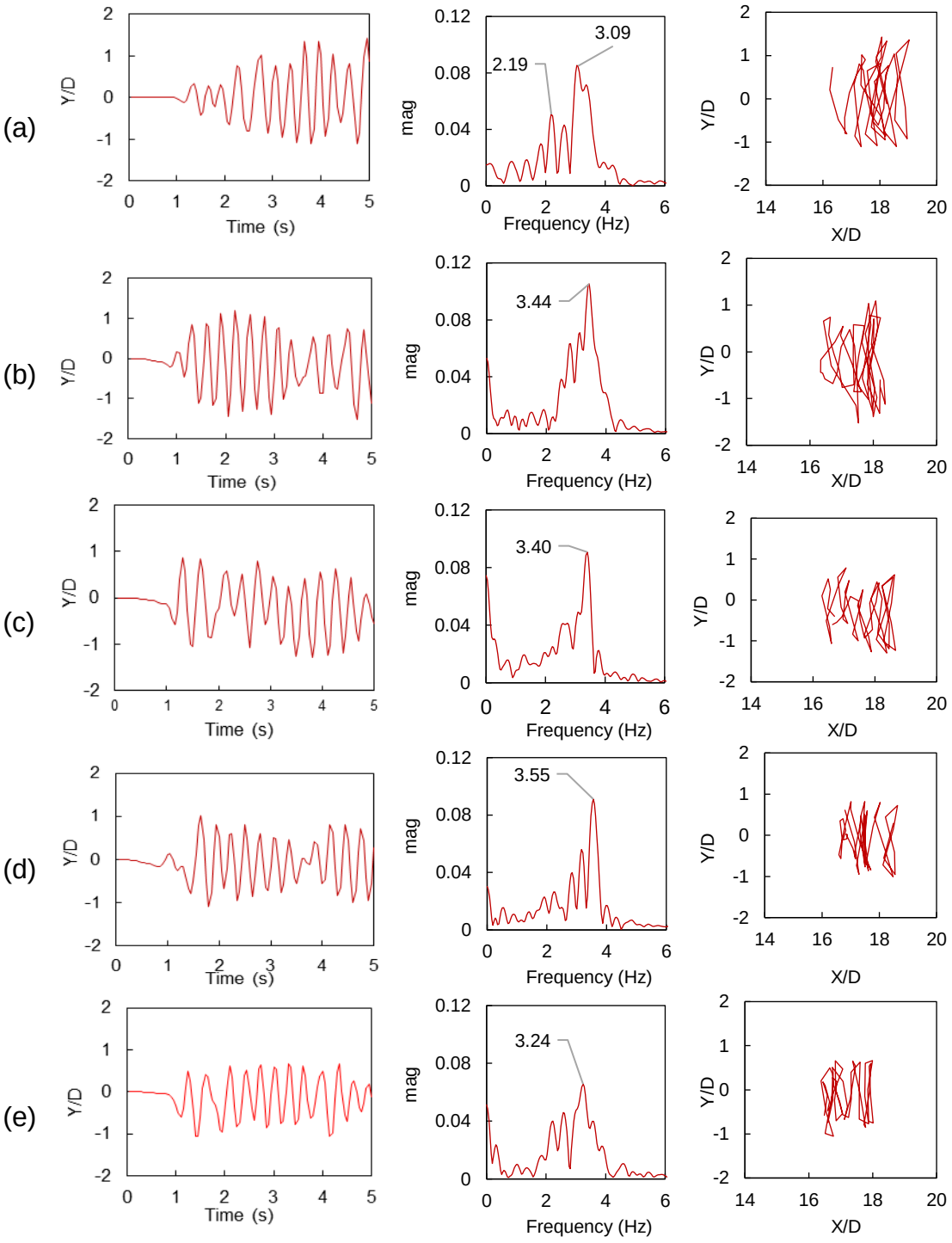

Figure 4-28 Comparison of time histories(first column), orbital trajectories(second column), and oscillation frequencies(third column) of a horizontal riser at Z/L=0.5, for constant Ue=0.42m/s and varying Ui: (a) 0m/s, (b)=1m/s, (c) 2m/s, (d) 5m/s, (e) 10m/s

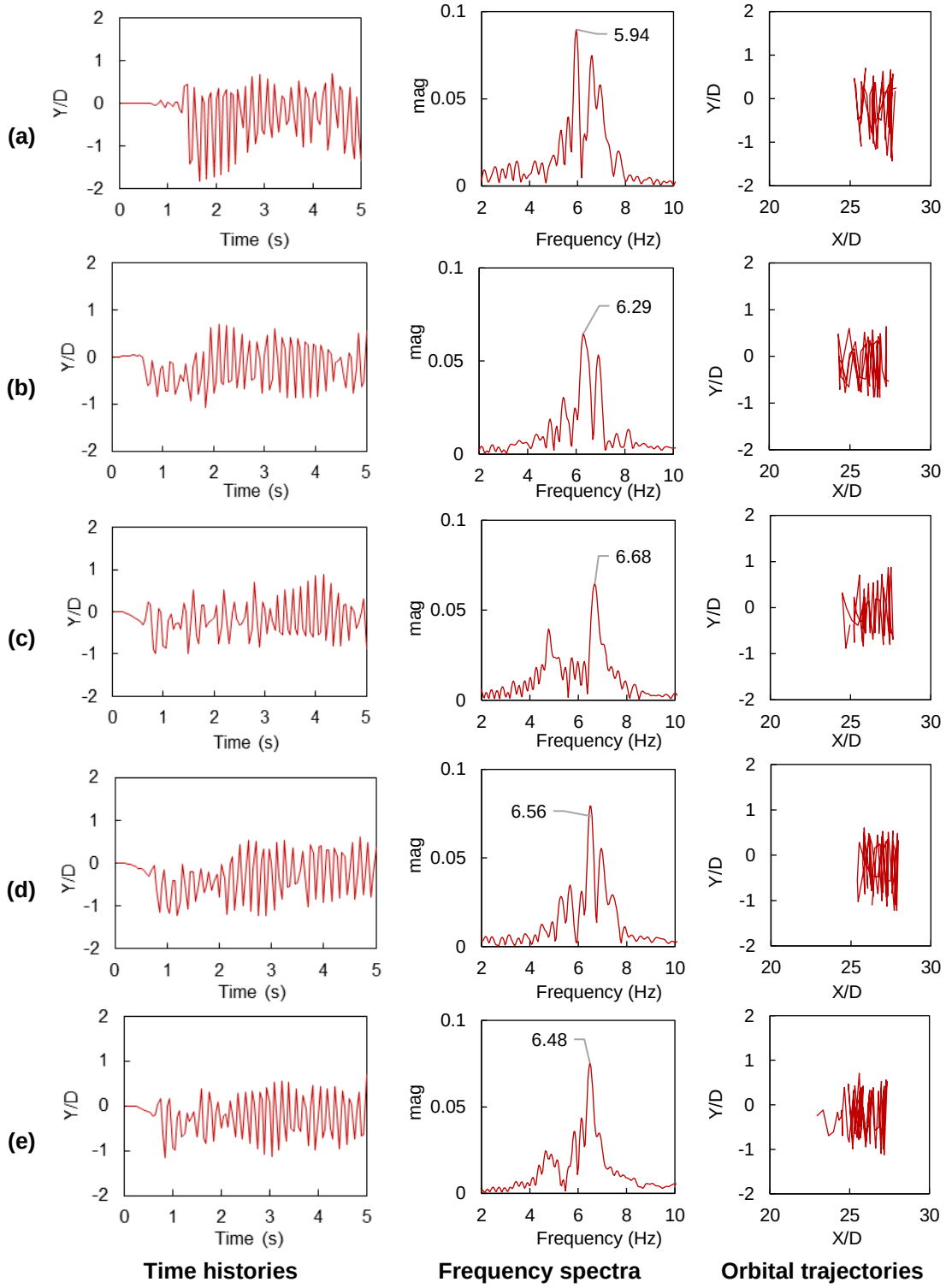

Figure 4-29 Comparison of time histories, orbital trajectories, and oscillation frequencies of a horizontal pipe at Z/L=0.5, for constant Ue2=0.84m/s and varying Ui: (a) 0m/s, (b)=1m/s, (c) 2m/s, (d) 5m/s, (e) 10m/s

4.5 Conclusion

ANSYS system coupling, an FSI module in the ANSYS workbench, was used to investigate the effect of external and internal flow on the VIV response of a horizontal riser transporting single-phase internal fluid flow. In addition, the effect of elastic modulus on the dynamic response of the riser was evaluated by reducing the elastic modulus from E=102.5GPa to E=1.025GPa. Various 3D numerical simulations were carried out to examine the effect of the riser's elastic modulus and the external and internal fluid flow velocity on the VIV response of the riser. By analysing the simulation results obtained from this study, the following conclusions can be drawn:

(1) The maximum IL displacement shows slight changes with the increased internal flow velocity at a particular external flow velocity. However, the maximum IL velocity increases with an increase in external flow velocity and reduction of the riser's elastic modulus. Therefore, it can be concluded that for a particular external flow velocity and elastic modulus, the variation of the internal flow velocities has little effect on the vibration amplitude of the riser.

(2) At lower external flow velocity (0.42m/s), the dominant vibrating mode in the CF direction for the horizontal riser shows slight changes when the internal flow velocities increase. However, for the vertical riser, the results show dominant vibrating mode decreases with the increase of the internal flow velocities.

(3) At higher external flow velocity, i.e., Ue=0.84m/s, the vibration mode increases with the increase of the internal flow velocity for the horizontal riser. However, the third vibration remains the dominant mode for the vertical riser, irrespective of the internal flow velocity. Therefore, it can be concluded that internal flow velocities have more effect on the dynamic response of the vertical riser at lower external flow velocity. In contrast, the internal flow velocities affect the horizontal riser at higher external flow velocities.

(4) As the elastic modulus of the riser is reduced from E=102.5GPa to E=1.025GPa, the vibration mode becomes more sensitive to the internal flow velocity. As the internal flow velocity increases, the vibration mode increases and becomes multimodal.

(5) The orbital trajectories of the riser at low external velocities (0.42m/s) take the crescent shape at lower internal flow velocities. However, as the internal flow velocities increase, the orbital trajectories become chaotic and do not take any regular shape. As the external velocity increases to 0.84m/s, the horizontal riser trajectory shape remains chaotic irrespective of the magnitude of the internal flow velocity. In contrast, the vertical riser maintains a crescent shape under all internal flow velocities. Therefore, it can be seen that the riser configuration and external and internal flow velocities significantly affect the orbital trajectory of the system.

(6) The vibration frequency of the riser is slightly affected by the magnitude of the internal flow velocity under the two external velocities considered. However, compared to an empty riser, the results show that the presence of internal flow velocity increased the vibration frequency when an internal flow is injected.

Chapter 5

5 VIV OF A FLEXIBLE PIPE TRANSPORTING MULTIPHASE FLUID

ABSTRACT

3D numerical simulation was conducted to examine the effects of internal air-water volume fractions on the dynamic response of a riser transporting a two-phase flow. The influence of gas fraction on a pipe with no external flow, on a jumper pipe with no external flow and on a fluid conveying pipe exposed to external flow is investigated. The numerical results show that a variation of the air volume fraction slightly affects the dynamic characteristics of the riser.

5.1 Introduction

Subsea risers and pipelines are essential to safely transport hydrocarbon from the wellhead to the platform. Most subsea equipment such as jumpers, pipelines and risers transport internal fluid in multiphase form. When a multiphase fluid flows through the pipe/jumper, fluid forces acting on the pipe fluctuate due to the non-uniform distribution of the gas and liquid phases, thereby inducing oscillation on the pipe, referred to as multiphase flow-induced vibration (MFIV). When the induced vibration frequency coincides with the pipe/jumper's natural frequency, a resonance occurs, resulting in high vibration amplitude and fatigue failure of the structure.

The vibration caused by MFIV affects the integrity and stability of subsea structures. Therefore, it is pertinent for engineers to understand the mechanism of MFIV and how to prevent it (Miwa et al., 2015). MFIV is a fluid fluid-structure interaction (FSI) problem where the vibration of the pipe affects the multiphase flow regime and vice versa. One of the leading causes of high fluid force fluctuation is the rate of the fluid and the type of flow pattern formed by the multiphase fluid.

There are different types of flow patterns depending on the orientation of the pipe and the flow rate of multiphase flows, usually two-phase flows. These are churn

flow, bubbly flow, stratified flow, slug flow, and annular flow (Triplett et al., 1999). Slug flow occurs when liquid "slugs" and gas "bubbles" alternate in a pipe, thereby causing a significant fluctuation of fluid force acting on the pipe, and eventually causing the structure to fail due to MFIV.

Miwa et al. (2015) conducted an extensive review on the FIV of a riser transporting two-phase fluids. The FIV of a riser transporting multiphase flow has been extensively studied experimentally in the past few decades. In the experimental work of Riverin and Pettigrew (2007), the vibration of a pipe transporting slug flow was analysed. The authors observed that the fluctuation of the two-phase flow caused resonance on the pipe. Zhang and Xu (2010) measured the vibration of a pipe injected with a bubbly flow using an accelerometer. They found out that the wall vibration of the pipe increased when a bubbly flow was injected. The effects of a two-phase bubbly flow on the FIV of a pipe were investigated experimentally by Charreton et al. (2015) and established that the flow pattern and the volumetric fraction of the bubbly flow affect FIV. Miwa et al. (2016) developed a numerical model based on an experiment they conducted to examine the FIV of an elbow pipe conveying two-phase fluid. Vieiro et al. (2015) performed a two-way numerical simulation by coupling a multiphase solver and a structural to examine the effect of slug flow on the FIV of a flexible lazy wave riser. Their two-way FSI models could predict the shape of the pipe and the slug formation. Al-Hashimy et al. (2016) studied the effect of slug flow on the vibration response of a pipe experimentally. They observed that the increased superficial velocities increase the vibration amplitude and decrease the vibration frequency. Ortiz-Vidal et al. (2017) used an experimental method to examine the FIV of a pipe carrying a two-phase flow. They found that the flow parameters such as mixture velocity and void fraction affect the dynamic response of the pipe. Wang et al. (2018) employed the experimental and numerical method to investigate the effect of slug flow velocity on the FIV of horizontal pipes transporting slug flow. They found out that the vibration response of the pipe is affected by the slug velocity. Mohmmed et al. (2019) ran experiments to compute slug-induced stress and frequencies in a horizontal pipe and then developed an empirical model to predict such stress.

Bordalo and Morooka (2018) used a slug model to examine the FIV of a pipeline conveying multiphase flow. Zhu et al. (2018a, 2018b), Zhu et al. (2019a), Zhu et al. (2021a), and Zhu et al. (2021b) experimentally investigated the effect of the gas-liquid ratio on the FIV of a flexible riser with different aspect ratios. The authors established that the riser's response increases as the gas-liquid ratio increases. Ma et al. (2020, 2021) used a similar experimental set-up to examine the response of an inclined riser with an increased aspect ratio of 360.

Due to the cost associated with experimental studies, analytical models were also developed to predict the FIV of a pipe and jumper system. Patel and Seyed (1989) studied the dynamic response of a flexible pipe transporting slug flow using mathematical models. They established that internal flow affects the dynamic behaviour of flexible pipes. Seyed and Patel (1992) further developed the mathematical model to include the effects of internal flow and pressure on a flexible pipe conveying fluid. Alternatively, the flexible pipe can be modelled using the Euler-Bernoulli beam model (Liang et al., 2018) and the Timoshenko beam model (Li et al. 2011) to investigate the dynamic response of pipe conveying a single-phase fluid with different boundary conditions. Similarly, Gu et al. (2013) and Gu et al. (2016) used the generalised integral transform technique (GITT) to evaluate the effect of flow velocity and aspect ratio on the FIV of a pipe conveying a single-phase fluid. They compared their results with those of the Euler–Bernoulli beam model.

Researchers such as An and Su (2015), Ma et al. (2017), and Li et al. (2020) used GITT to examine the effects of the gas fraction, flow rate and aspect ratio on the dynamic response of pipes conveying two-phase flows. They observed that the vibration amplitude increases with an increasing gas volume fraction and water flow rate. Ortega et al. (2012) developed a model to predict the FIV of flexible risers transporting slug flows. Chatjigeorgiou (2017) used the frequency domain method to numerically examine the effect of slug flow on the FIV response of a riser. The result showed that slug-flow increases the vibration but does not change the vibration mode. Wang (2009) used the Galerkin method to investigate the dynamic response of a pipe transporting a pulsating single-phase

fluid. They found out that at a high mean fluid velocity, the pipe might experience chaotic motion. The dynamic response of a long catenary riser was analytically examined by Ma and Srinil (2020). The authors examined the effects of slug flow on the dynamic response of the riser. The improved computing capacity of high-performance computers has made it possible to perform a numerical simulation to evaluate the vibration characteristics of a pipe transporting a multiphase flow.

The MFIV is calculated by coupling a Computational Fluid Dynamics (CFD) flow solver with a finite element method (FEM) structural solver. Li et al. (2016) used ANSYS R15 to examine the effect of a gas fraction on the MFIV of a pipe transporting a multiphase flow. Jia (2012, 2013) used CFD to investigate the dynamic responses of pipelines, jumpers, and risers transporting a slug flow. Onuoha et al. (2018) explored the effects of severe slug flow on the dynamic response of a riser by coupling CFD solvers and a structural solver based on a modified Euler-Bernoulli beam theory.

At the wellhead, curve-shaped pipes called jumpers are used to connect the wellhead and the subsea manifold and pipeline. The jumpers are subjected to high internal pressure and external current. Therefore, the dynamics of curved pipes, such as the riser, can be more complex than the straight pipe. Cooper et al. (2009) examined the effect of slug flow on the fatigue life of a flowline system conveying multiphase fluids. They established that slugging conditions affect the design life of a piping system. Urthaler et al. (2011) used the finite element method to assess the fatigue life of a jumper subjected to internal FIV. They observed that the jumper was prone to fatigue damage due to vibration. Pontaza and Menon (2011) conducted 3-D numerical simulations to investigate the FIV of a jumper carrying internal multiphase flow. They found that the internal FIV predominantly occurs within the jumper configuration plane. Chica et al. (2012) performed a two-way numerical simulation to analyse the FIV of a jumper transporting two-phase flow using STAR CCM+ and Abaqus as the fluid and structural solver. They found that the slug flow can induce a significant level of vibration. Jia (2012, 2013) performed a two-way simulation using ANSYS to examine the dynamic response of a horizontal and jumper pipe carrying pulsating

multiphase flow. They analysed the effects of different pipe boundaries and slug flow properties on the dynamic response of a horizontal pipe carrying multiphase flow. Elyyan et al. (2015) used ANSYS to perform both one and two-way FSI simulations of a jumper transporting pulsating multiphase fluids. They found that the frequency of the slug flow affects the jumper's dynamic response. Also, their results showed that the one-way FSI overestimated the vibration amplitude. Jujuly et al. (2017) used ANSYS FLUENT to study the dynamic response of an M-shape riser transporting hydrate flow. Kim and Srinil (2018) performed a one-way numerical simulation to explore the FIV of a jumper transporting pulsating multiphase flows using ANSYS FLUENT and ANSYS Mechanical as as the fluid and structural solvers, respectively.

Furthermore, the combined effect of MFIV and VIV on the dynamic behaviour of a horizontal pipe transporting multiphase flows, has recently received considerable attention. To explain a bit more VIV, when an external fluid flows past a bluff body such as a pipe, vortices are shed behind the body at a specific frequency called the vortex shedding frequency, the vortices induce an oscillatory motion onto the pipe. This phenomenon is referred to as VIV. When the vortex shedding frequency is closed to the natural frequency of the pipeline, the vortex shedding frequency 'lock-in' to the system's natural frequency, thereby causing significant amplitude vibration and subsequent failure of the structure.

Most studies have been devoted to either VIV, based on external flows surrounding risers or MFIV in pipes due to multiphase flows, but not for both phenomena acting simultaneously. Therefore, a complete understanding of how these two sources of vibration (MFIV and VIV) affect the structural integrity of risers is required.

As risers usually transport multiphase fluids from the seabed to the platform, the effects of the composition and characteristics of internal multiphase flows on the VIV have received considerable attention. Both numerical and experimental investigations of the effects of multiphase internal flows have been carried out in recent years. However, few experimental studies have been published on the combined effect of MVIV and VIV on the response of risers transporting

multiphase fluids. For instance, Zhu et al. (2019b) conducted experiments to examine the effect of the gas-liquid ratio on the dynamic response of curved flexible risers subjected to external VIV and internal MFIV. They observed that the magnitude of internal and external flow affects the pipe's vibration response. Due to the high cost of the experimental setup, several empirical models have been developed to predict the complex FSI problems involving MFIV and VIV. Blanco and Casanova (2010) examined the dynamic response of a riser transporting slug flow using the wake oscillator model and a finite difference method to solve the fluid and structural equations. Their results showed that the fatigue life of a pipe is significantly affected by the combined effect of an external uniform flow and an internal slug flow. Montoya-Hernández et al. (2014) developed a numerical algorithm to investigate the effects of a three-phase flow on the dynamic response of flexible risers. They established that the VIV of a riser was affected by the internal fluid flow rate. Bossio V. et al. (2014) developed a model that considered the pipe stiffness, tension and added mass when examining the VIV of a flexible pipe transporting slug flow. Knudsen et al. (2016) numerically assessed the combined effect of external current and internal slug flow on the dynamic response of a riser. They found out that the presence of internal slug flow affects the response of the pipe. Safrendyo and Srinil (2018) investigated the effect of internal slug flow on the dynamic response of a steel catenary riser (SCR) exposed to an external uniform current. Xie et al. (2019) considered mathematical models to investigate the VIV response of a pipe carrying different internal fluid densities. They found out that the internal fluid density would increase or decrease the displacement of the riser. Yang et al. (2019) used the wake oscillator model to examine the VIV of a flexible riser conveying a two-phase flow. Their results showed that an increase in the gas fraction increases the natural frequencies. Ortega, Rivera and Larsen (2013, 2018) investigated the dynamic response of the pipe under the combined influence of an internal slug flow and regular external waves. Lou and Liang (2020) analysed the vibration of a riser transporting multiphase flows using the finite difference method and the virtual work principle to solve the flow field and nonlinear vibration. They established that the natural frequencies of the riser

increase with an increase in gas intake, and the amplitude envelope of the riser decreases with an increase in gas intake. Liang and Lou (2020) further investigated the effects of multiphase internal flow with hydrate phase transition on the VIV response of the pipe. Chang et al. (2021) analytically studied the VIV response of a marine riser subjected to two-phase internal flow with different gas volume fractions. The results showed that the volume fraction of the gas phase significantly influenced the dynamic response characteristics of the marine riser. More recently, Meng et al. (2020) developed a mathematical code using MATLAB to study the VIV response of a horizontal riser transporting a two-phase fluid exposed to uniform external flow. The result showed that the slug flow triggers a new vibration mode. However, few research studies used the CFD and FEM methods to examine the dynamic response of a pipe conveying two-phase flows under the combined influence of external VIV and internal MFIV. A more detailed numerical investigation based on CFD and FEM methods is being here performed to address this research gap.

In this study, a series of numerical simulations are conducted to investigate the multiphase flow-induced vibration of a horizontal pipe and an M-shape jumper transporting a multiphase flow. In addition, the combined effect of internal MFIV and external VIV on horizontal pipe transporting multiphase flow is investigated. The system coupling module in ANSYS 2019 R2 software links the ANSYS FLUENT fluid solver and ANSYS MECHANICAL structural solver to perform FSI simulations. The system coupling provides an interface between the fluid and the structural solver to exchange information during simulations.

The paper is organised as follows. First, the CFD and FEM models used to evaluate the dynamic response of a flexible pipe/jumper transporting two-phase flows are described in section 5.2. Then, in section 5.3, the problem is explained in detail. Next, section 5.4 examines the vibrating displacement, vibrating frequencies, and orbital trajectories of the pipe/jumper under different internal and external flow conditions. Finally, the conclusions and recommendations for further study are summarised in Section 5.5.

5.2 Problem description

Three cases are considered in this study. For case 1, the MFIV of a horizontal riser transporting multiphase flow with different air gas intake ratios are investigated. In case 2, the MFIV of an M-jumper carrying a pulsating two-phase flow are analysed. Finally, the combined effects of external VIV and internal MFIV of a flexible horizontal riser transporting a multiphase flow with different air gas intake ratios are investigated in case 3.

For cases 1 and 2, no external flow is applied to the horizontal pipe and jumper, while in case 3, the effects of external flow (VIV) and the internal multiphase flow (MFIV) are assessed.

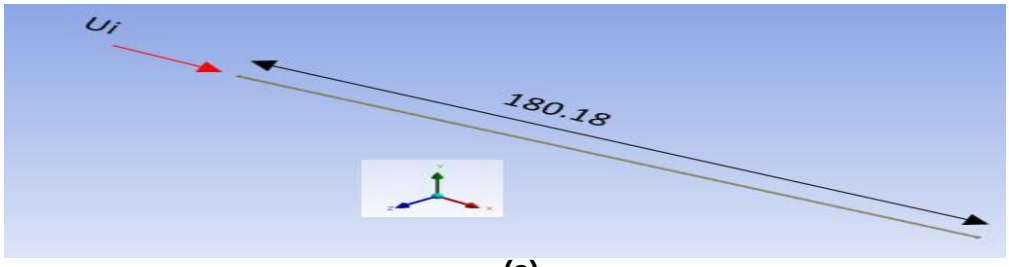

(a)

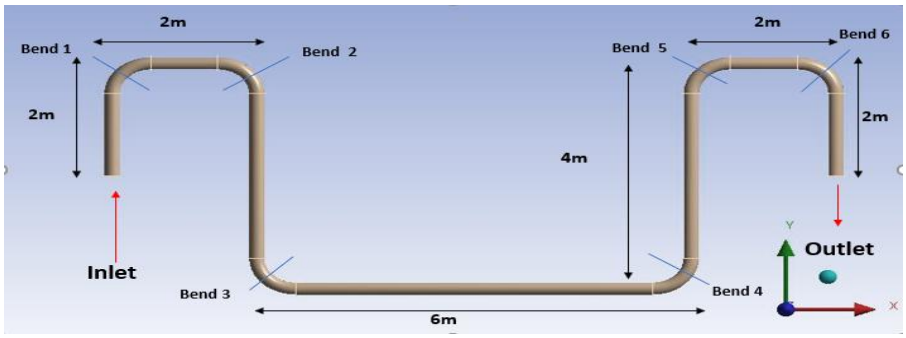

(b)

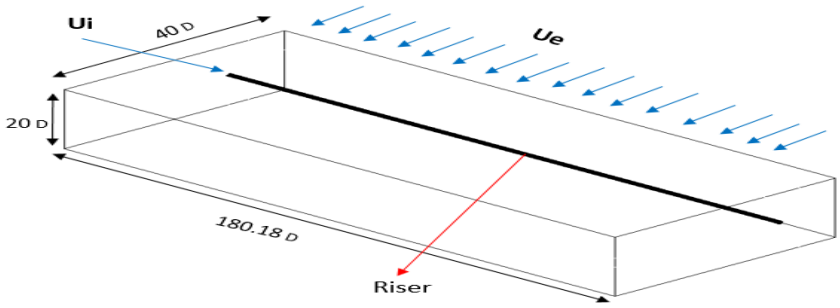

(c)

Figure 5-1 Schematic of (a) horizontal pipe under MFIV, (b) Jumper pipe under MFIV (c) Flexible pipe under MFIV and VIV.

Figure 5-1(a) shows the geometry of the horizontal riser transporting a multiphase flow with both ends fixed. The geometry and physical properties of the pipe are similar to that of Li et al. (2016). The two-phase fluid is a mixture of liquid (water) and gas (air) flowing with gas (U_g) and liquid (U_l) velocities of 1m/s. The properties of the multiphase fluid are presented in Table 5-1. The riser is assumed to be filled with air initially.

Figure 5-1(b). depicts the geometry of the jumper with both ends fixed. The jumper has an outer diameter (D) of 270 mm and a thickness (t) of 30 mm see Table 5-2. The riser geometry considered has been adopted from studies of Kim and Srinil (2018). The fluid flowing into the jumper is similar to that of a horizontal riser. However, a pulse-type air-water intake is injected into the jumper at 5Hz, see Figure 5-2. The pulsating two-phase fluid has a gas (Ug) and liquid (U_L) velocity of 3 m/s. Note that compared to the horizontal riser, higher inlet velocities were considered for the jumper analysis, to enable comparison with the numerical results of Kim and Srinil (2018).

Furthermore, the fluid and structural properties of the riser in case 3 (MFIV and VIV) are similar to that of case 1(MFIV), except that the riser is fully immersed in water and exposed to external current as shown in Figure 5-1 (c). The external fluid has a density of 1000kg/m^3, viscosity of 0. 001Pa.s and a velocity of 0.84m/s, see Table 5-1.

Table 5-1 fluid and structural properties of the horizontal riser conveying two phase flow

Property	Value	SI units
Length(L)	6	m
Outer Diameter (D_o)	33.3	mm
Thickness (t)	3	mm
Aspect ratio (L/D)	180.18	
Elastic Modulus (E)	207	GPa
Density of riser (ρ_s)	7850	Kg/m^3
Density of external flow (ρ_e)	1000	Kg/m^3

Density of gas-phase internal flow (ρ_g)	1.225	Kg/m^3
Density of liquid phase internal flow (ρ_L)	1000	Kg/m^3
Viscosity of external flow (μ_e)	0.001	Ns/m^2
Viscosity of gas-phase internal flow (μ_g)	1.789×10^{-5}	Ns/m^2
Viscosity of Liquid-phase internal flow (μ_L)	0.001	Ns/m^2
External flow Velocity (U_e)	0.84	m/s
Internal flow velocity liquid (U_{Li})	1	m/s
Internal flow velocity gas (U_{gi})	1	m/s

Table 5-2 Geometrical and material properties of the jumper

Property	Value	SI Units
Outer Diameter (D_o)	270	mm
Thickness (t)	30	mm
Density of jumper ($\rho_{s)}$	7850	Kg/m^3
Modulus of Elasticity (E)	207	Gpa
Density of gas-phase internal flow (ρ_g)	1.225	Kg/m^3
Density of liquid phase internal flow (ρ_L)	1000	Kg/m^3
Viscosity of gas-phase internal flow (μ_g)	1.789×10^{-5}	Ns/m^2
Viscosity of liquid-phase internal flow (μ_L)	0.001	Ns/m^2
Internal flow velocity gas (U_L)	3	m/s
Internal flow velocity Liquid (U_g)	3	m/s

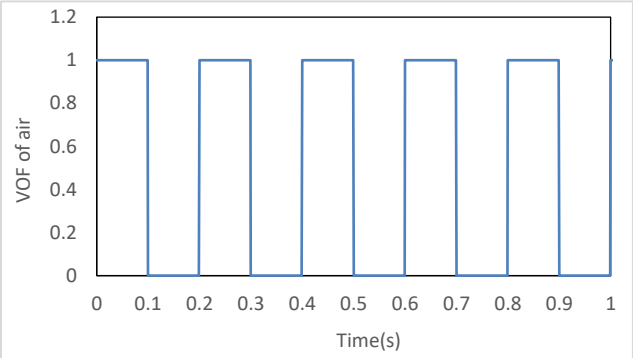

Figure 5-2 Time history of pulsating gas intake

5.3 Numerical method

5.3.1 Fluid equation

ANSYS Fluent 2019R2 was used to simulate the external fluid flow and internal multiphase fluid flow using the volume of fluid (VOF) multiphase model; see Gourma and Verdin (2016, 2020) and Livinus and Verdin (2021) for previous related studies. The VOF model assumes that the two-phase fluids are immiscible. Thus, a single set of momentum equations is solved. The Reynolds Average Navier Stokes (RANS) k-ω SST turbulence model was selected. Such a combination of the multiphase flow method and turbulence models has proved efficient in recent studies of fluid flow past circular cylinders (Ibnu Syihab et al., 2021). The continuity equations for liquid and gas volume fractions α_L and α_g, respectively, can be written as:

$$\frac{\partial}{\partial t}(\alpha_i) + \nabla.(\alpha_i \vec{u}) = 0 \tag{5-1}$$

where the subscript *i* denotes either the liquid (L) or the gas (g) phase. Then, the volume fraction is solved only for the secondary phase, and the volume fraction for the primary phase is obtained using the following constraint.

The phase volume fraction has a value of 0 or 1 when a control volume is entirely filled with either liquid or gas and a value between 0 and 1 if an interface is present in the control volume. For the VOF model, the volume fractions of the two phases sum to unity. When using this model, a single set of momentum equations is solved, and the resulting velocity $\vec{u}$ is shared among the phases. The momentum equation is dependent on the volume fractions of all phases through the properties density $\rho = \alpha_g \rho_g + \alpha_L \rho_L$ and the dynamic viscosity $\mu = \alpha_g \mu_g + \alpha_L \mu_L$.

$$\rho = \alpha_g \rho_g + (1 - \alpha_g)\rho_L \tag{5-2}$$

$$\mu = \alpha_g \mu_g + (1 - \alpha_g)\mu_L \tag{5-3}$$

The momentum balance in conservative form is:

$$\frac{\partial}{\partial t}(\rho\,\vec{u}) + \nabla.(\rho\,\vec{u}\,\vec{u}) = -\nabla p + \nabla.\tau + + \rho.\vec{g} + \rho.\vec{F} \tag{5-4}$$

where τ is the deviatoric stress tensor, given by:

$$\tau = (\mu\,(\nabla\,\vec{u} + \nabla\,\vec{u}^{T})) \tag{5-5}$$

where p the pressure. The last term on the right-hand side of Equation (5-4) represents the interfacial surface tension F between phases which can be expressed as:

$$F = \sigma_{ij}\,\frac{k_i\,.\nabla\alpha_i}{\frac{1}{2}(\rho_i + \rho_j)} \tag{5-6}$$

with σij representing the surface tension coefficient, and k_i the curvature at the interface where the surface tension is calculated.

For Case 3, which involves external flow around the pipeline, the ANSYS FLUENT flow solver was used to solve the governing equations describing the flow field around the riser. This flow field was considered transient and incompressible. The following equations of mass and momentum were solved when running the flow simulations.

$$\frac{\partial \overline{u}_i}{\partial x_i} = 0 \tag{5-7}$$

$$\frac{\partial(\rho\overline{u}_i)}{\partial t} + \frac{\partial(\rho\overline{u}_i\overline{u}_j)}{\partial x_j} = -\frac{\partial \overline{p}}{\partial x_i} + + \frac{\partial}{\partial x_j}\left(2\mu\overline{S_{ij}} - \rho\,\overline{u'_i\,u'_j}\right) \tag{5-8}$$

where $\bar{S}_{ij}$ is the mean rate of the strain tensor described in in equation **(5-9).**

$$\bar{S}_{ij} = \frac{1}{2}\left(\frac{\partial \bar{u}_i}{\partial x_j} + \frac{\partial \bar{u}_j}{\partial x_i}\right) \quad (5\text{-}9)$$

with $-\overline{\rho u'_\iota u'_J}$ is referred to as the Reynolds stress, described as

$$-\overline{\rho u'_\iota u'_J} = 2\mu_t \bar{S}_{ij} - \frac{2}{3} k_t \rho \delta_{ij} \quad (5\text{-}10)$$

where μ_t is the turbulent viscosity, δ_{ij} is the Kronecker function, and $k_t = \frac{1}{2}\overline{u'_i u'_i}$ is the turbulent kinetic energy,

As mentioned previously, the (SST) k-ω turbulence model was used to compute the Reynolds stresses in this study. The k-ω two-equation formulation from Wilcox (1988, 1991, 1993) is commonly used, where one equation solves the transport of the turbulent kinetic energy k, and the other one solves the specific dissipation rate ω. The Shear Stress Transport (SST), developed by Menter, (1994), is a variant of the k-ω model. This model switches automatically from a k-ω definition near the walls to the k-ε definition in the bulk flow, which makes this model efficient in the sublayer near the walls, and far away from the walls (Loyseau, Verdin and Brown, 2018).

The fluid flow governing equations are solved using the pressure-based segregated algorithm. The SIMPLE algorithm was selected as the pressure-velocity coupling for Cases 1 and 2, while the COUPLED algorithm was considered for Case 3. The PRESTO! scheme was chosen to calculate the face pressure, while a second-order upwind scheme was used to discretise the momentum equations. A first-order upwind scheme was selected for both k and ω equations. In addition, a Least Squares Cell-Based scheme was used for the gradient in spatial discretisation. Also, the Geo-Reconstruct scheme was used at the gas-liquid interface. Finally, a first-order implicit transient formulation was selected. A convergence criterion of 10^{-3} and a time-step of 0.002s was considered for all simulations.

5.3.2 Structural equation

The flexible pipe is modelled as a beam governed by the Euler-Bernoulli beam theory. The motion of the flexible pipeline with both ends fixed and no pretension in the IL and CF directions are described in Equations (5-11) and (5-12).

$$m\frac{\partial^2 x}{\partial t^2} + c\frac{\partial x}{\partial t} + \frac{\partial^2}{\partial z^2}\left[EI\ \frac{\partial^2 x}{\partial z^2}\right] = F_x \tag{5-11}$$

$$m\frac{\partial^2 y}{\partial t^2} + c\frac{\partial y}{\partial t} + \frac{\partial^2}{\partial z^2}\left[EI\ \frac{\partial^2 y}{\partial z^2}\right] = F_y \tag{5-12}$$

where m, c, E and I are the mass per unit length, structural damping, Elastic modulus and moment of inertia, respectively. Also, x,y, and z are the cartesian coordinates. In addition, F_x and F_y are the hydrodynamic forces in the IL and CF directions. Since the cylinder is fixed at both ends, the boundary conditions at the two ends are defined as:

$$y(0,t) = 0, y(l,t) = 0;\ \frac{\partial y(0,t)}{\partial z} = 0, \frac{\partial y(L,t)}{\partial z} = 0 \tag{5-13}$$

For a flexible pipe conveying fluid, the governing equation takes into account the influence of the internal flow mass; therefore, the governing equation equations become:

$$2m_i u_i\ \frac{\partial^2 x}{\partial z \partial t} + (m_s + m_i)\frac{\partial^2 x}{\partial t^2} + c\frac{\partial x}{\partial t} + \ EI\ \ \frac{\partial^4 x}{\partial z^4} = f_x(z,t) \tag{5-14}$$

$$2m_i u_i\ \frac{\partial^2 y}{\partial z \partial t} + (m_s + m_i)\frac{\partial^2 y}{\partial t^2} + c\frac{\partial y}{\partial t} + \ EI\ \ \frac{\partial^4 y}{\partial z^4} = f_y(z,t) \tag{5-15}$$

where m_s is the mass per unit length of the riser, m_i is the mass per unit length of the internal flow, and *c* is the structural damping coefficient.

ANSYS Mechanical 2019R2, based on the finite element method (FEM), is used to solve the vibration response of the flexible pipe transporting a multiphase flow.

The riser was discretised into many elements. For each element, the governing equation was written as Equations (5-16) and (5-17).

$$m\ddot{X} + c\dot{X} + kx = F_x \tag{5-16}$$

$$m\ddot{Y} + c\dot{Y} + kY = F_y \tag{5-17}$$

where m, c , and k are the mass, the damping and the stiffness of the element. Also, F_x and F_y are the hydrodynamic forces in the IL and CF direction, respectively.

The structural equation of the whole pipe combining all the elements then becomes equations (**5-18**) and (**5-19**).

$$[M]\{\ddot{X}\} + [C]\{\dot{X}\} + [K]\{X\} = \{F_X\} \tag{5-18}$$

$$[M]\{\ddot{Y}\} + [C]\{\dot{Y}\} + [K]\{Y\} = \{F_Y\} \tag{5-19}$$

where $[M]$, $[C]$, and $[K]$ are the mass, damping and stiffness matrixes of the riser.

5.3.3 Fluid domain

The horizontal pipe and jumper were created using the ANSYS design modeller, while the computational structured mesh was created using ANSYS meshing. For Cases 1 and 2, the inlet and outlet boundaries of the horizontal pipe and jumper were set as velocity inlet and pressure outlet, while the pipe body was set as a no-slip wall. For Case 3, the external fluid domain has a length of 40D, width of 20D and height of 180.18D. The pipe is located 10D and 30D, far from the inlet and outlet boundaries. The inlet boundary was assumed to be a velocity inlet, while a pressure outlet was considered at the outlet section of the domain. Symmetry (free slip) boundary conditions were applied to the two-transverse and two spanwise boundaries. A symmetric condition implies that the velocity component perpendicular to the boundary is zero ($\partial u/\partial y = 0; v = 0$). A no-slip

boundary condition was applied on the inner and external cylinder surface, which means that the fluid velocity is the same as the vibration velocity of the riser. The inner and outer surface of the riser also serves as a fluid-structure interaction surface, where fluid force and structural response data are transferred in-between the flow field solver (FLUENT) and the structural dynamic response solver (ANSYS MECHANICAL).

5.3.4 Solid domain

ANSYS Design modeler and Mechanical were used to create the solid geometry and discretise it. The two ends of the pipe and jumper are fixed for all the cases considered. For Cases 1 and 2, the inner surface of the pipe/jumper served as a fluid-solid interface, while for Case 3, the inner and outer surfaces of the pipe served as the fluid-solid interface. The hydrodynamic forces obtained from the flow solver were applied at the interface, enabling data transfer from the fluid and structure solvers. The circumferential edge of the pipe and jumper were divided into 60 equal divisions, thereby producing a total mesh of 60,000 elements.

5.3.5 Fluid structure interaction

The ANSYS system coupling provides a platform for data transfer between the two solvers (ANSYS Fluent and ANSYS Mechanical). Two fluid surface interfaces were created for the external VIV, and the internal FIV. Data exchange during FSI can be either one way or two ways. Only the fluid forces obtained from the fluid solver were transferred to the structural solver in the one-way coupling method. However, for the two-way coupling method, the fluid force and the structural displacement obtained from the fluid and structural solvers were transferred between the two solvers. The ANSYS system coupling is based on a partitioned method where the two solvers solve their various equations separately.

At each computational time step, the hydrodynamic forces (drag and lift forces) acting on the pipe are obtained from the flow equation, which are then substituted into the structural equation to calculate the displacement of the pipe. The new position of the pipe is communicated to the fluid solver via the ANSYS system coupling before the next step. This process continues until convergence is reached. A time step of 0.002s was used to perform all simulations, see section

5.4.2 for time step study. The movement of the mesh during the cylinder oscillation is enabled by the dynamic mesh method in FLUENT.

In this study, the smoothing and dynamic meshing features are used to update the mesh during oscillations to avoid any negative volume error. As the cylinder vibrates, the mesh moves according to the diffusion Equation (5-20)

$$\nabla.(\gamma \nabla u) = 0 \tag{5-20}$$

where u represents the velocity of mesh displacement, and γ represents the diffusion coefficient.

5.4 Results and discussion

5.4.1 Mesh sensitivity study

A mesh sensitivity study was performed using three mesh sizes to determine the optimum mesh size and ensure that the numerical results are independent of the mesh density. The mesh dependency study of a pipe transporting a two-phase flow containing 30% air (case 1) is presented in Table 5-3. The maximum displacement in the Y direction is used to compare the results of the different mesh sizes. Nz in this table represents the mesh divisions along the span, and Nc represents the mesh divisions along the circumference of the pipe. It can be seen from Table 5-3. that the difference between Mesh-1 and Mesh-2 is significant, while the results are similar between Mesh 2 and Mesh 3. Therefore Mesh 2 is adopted in the numerical simulations in the present study. Furthermore, similar mesh strategy adopted for the horizontal pipe was used for the jumper (case 2) layer is added at the circumference.

Table 5-3 Mesh independency study of a pipe transporting two phase flow (30% air and 70% water) with Ui=1 and undergoing only FIV

	CFD Mesh		FEA Mesh			
	Nc	Number of mesh	Nc	Nz	Number of mesh	Y/D
Mesh 1	40	275,000	60	1000	60,000	0.000495
Mesh 2	50	377,000	60	1000	60,000	0.000561
Mesh 3	60	451,000	60	1000	60,000	0.000565

For case 3, where the pipe is submerged in fluid, the computational domain is divided into multiple blocks, as shown in Figure 5-3 (a).The multi-block concept controls the mesh size so that a finer mesh is created near the pipe while a coarse mesh is created far away from the pipe, as shown in Figure 5-3 (b). The minimum distance between the first mesh next to the pipe is 0.001D to obtain a y+ value less than 1 and comply with the requirements of the turbulence model selected here.

Table 5-4 Mesh independency study of an empty pipe exposed to Ue =0.84m/s and undergoing only VIV

Mesh	Nz	Nc	Total	Cd	IL
Mesh 1	40	160	442,800	2.00	0.30
Mesh 2	50	160	616,000	2.16	0.38
Mesh 3	60	160	739, 200	2.30	0.37

Figure 5-3 (c). shows a snapshot of the solid mesh of the riser. The riser circumferential edges are divided into 60 equal divisions while the span of the riser was discretised into 500 elements. Figure 5-3 (d) shows the computational domain of the external fluid and inner liquid, while Figure 5-3 (e) shows a snapshot of the inner liquid. The maximum IL displacement and drag coefficient of the three different mesh sizes are tabulated in Table 5-4. It can be seen from this Table 5-4. that Mesh-1 and Mesh-2 based results show significant differences, while the results are similar between Mesh 2 and Mesh 3. Therefore Mesh 2 is adopted in the numerical simulations in the present study.

5.4.2 Time step study

A time step dependency study was conducted for FIV and VIV separately. For FIV, the maximum IL displacements of three different time step sizes using Mesh 2 are tabulated in Table 5-5.The study shows that the difference between the IL displacement of time steps 1 and 2 is significant. However, for times step 2 and 3 the difference is small. Therefore, a time step of 0.002s was selected for the simulations.

Table 5-5 Time dependency study of a pipe transporting two phase flow (30% air and 70% water) with Ui=1 and undergoing FIV

Time step	Time	IL
1	0.02	0.000551
2	0.005	0.000561
3	0.002	0.000563

Furthermore, for case 3, a time independency study was conducted for an empty pipe using three different time size. see, Table 5-5. The result shows that at no significant difference between the three different time size, therefore, 0.0002s was selected for the simulations.

Table 5-6 Time dependency study of an empty pipe exposed to Ue =0.84m/s and undergoing only VIV

Time step	Time	IL
1	0.02	0.369
2	0.005	0.379
3	0.002	0.383

The FSI simulations were carried out on Cranfield university High performance computer (HPC), DELTA. The HPC is made up of two Intel E5 2620 v4 (Broadwell) CPU, a user is allowed up to 128 cores in multiple of 16 cores and a total of 250GB of shared memory. In this research, for the MFIV and VIV simulation, it takes 24 and 50 hours respectively with 32 cores to obtain 5 seconds of simulation. In addition, the simulation takes 20GB of space for both simulations. One of the major challenges faced during simulation is the inability to restart the simulation at a given time when the simulation fails while running on the HPC. This has caused much delay in the simulation.

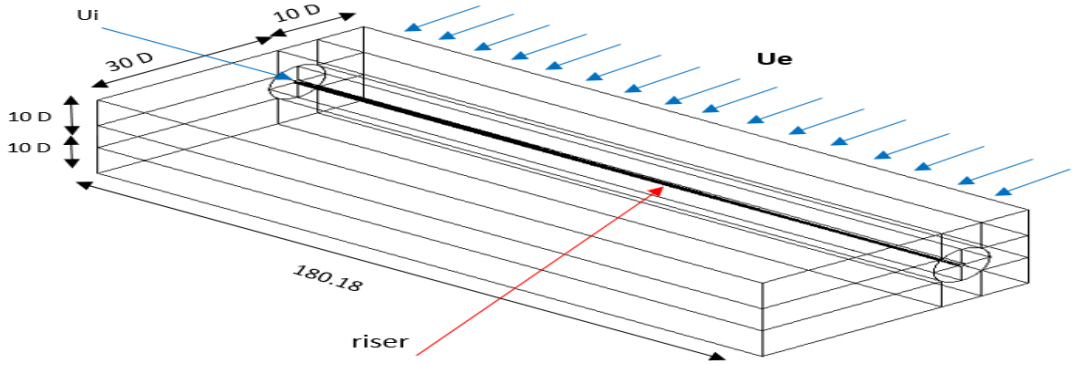

(a)

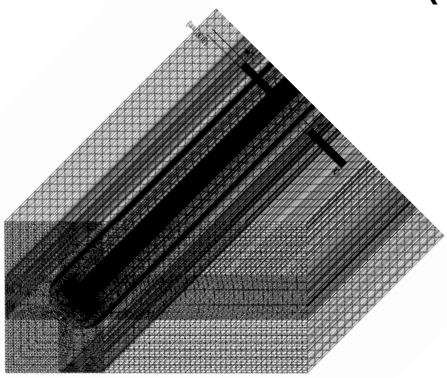

(b)

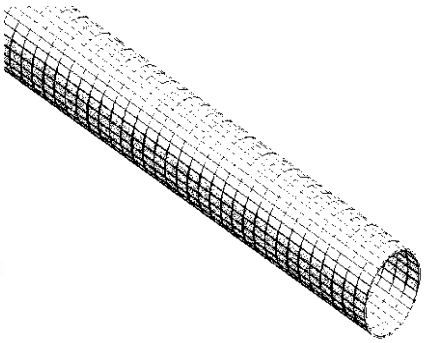

(c)

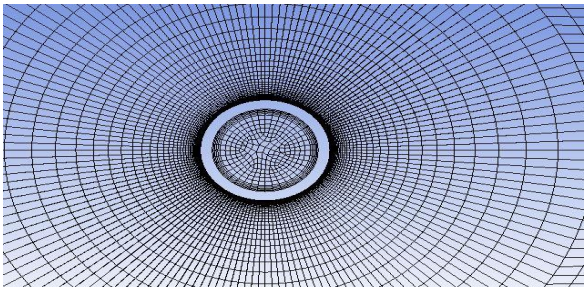

(d)

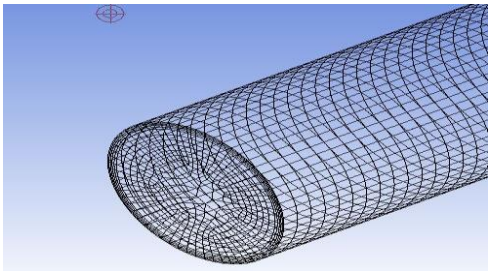

(e)

Figure 5-3 snapshot of (a) computational domain (b) fluid domain meh (c) solid domain mesh (d) Top view of fluid and liquid mesh (e) inner liquid mesh

5.4.3 MFIV of a horizontal pipe transporting two-phase fluid with varying gas-liquid ratio

3D two-way FSI numerical simulations are performed to examine the multiphase flow-induced vibration (MFIV) of a horizontal pipe conveying a two-phase flow with no external current. Five simulations involving varying air-water ratios were performed, as shown in Table 5-7. The simulation time was set to 10s, with a fixed time step of 0.002s.

Table 5-7 Cases considered for MFIV of a horizontal pipe transporting two-phase fluid with no external force acting on the pipe

Case	Air percentage (%)	U_g (m/s)	U_L(m/s)
1	30	1	1
2	40	1	1
3	50	1	1
4	60	1	1
5	70	1	1

5.4.3.1 Modal analysis

The natural frequency and mode shape of the pipe are obtained by performing modal analysis using ANSYS Modal 2019R2 software. The first three natural frequencies and mode shape of the pipe are presented in Table 5-8 and Figure 5-4.

Table 5-8 Natural Frequency of the pipe with an elastic modulus E= 207 GPa

Mode	Frequency (Hz)
1	5.37
2	14.82
3	29.03

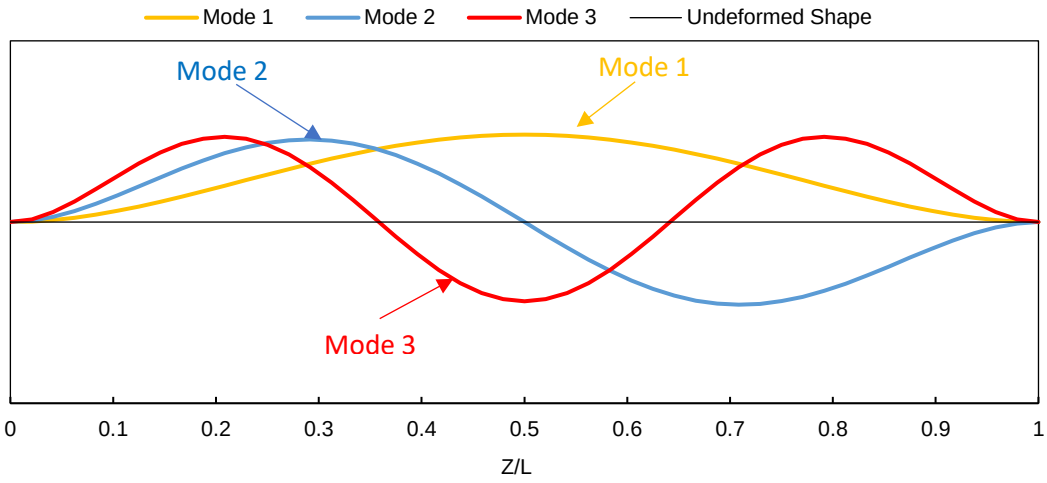

Figure 5-4 Vibration mode shape of a pipe with E=207GPa for L/D= 180

5.4.3.2 Dynamic response at the mid-point of the pipe

Figure 5-5 shows the time histories of the midpoint of the pipe with different gas intake ratios in the X and Y directions. It can be seen from Figure 5-5 (a) that the vibration of the midpoint of the pipe in the X direction is irregular and non-periodic. As the percentage of air intake increases, the vibration of the pipe remains irregular irrespective of the gas intake ratios. However, in the Y direction, it can be seen in Figure 5-5 (b) that the pipe undergoes a damped vibration that decays with time for all gas intake ratios considered. A primary reason for this may be the damping from the internal fluid flow. Figure 5-5 (b) also shows that the percentage gas fraction has little effect on the damped vibration motion of the pipe in the Y direction. This trend is similar to that of Onuoha et al. (2018) and Li et al. (2020). Moreover, it can be observed that the vibrations in the X direction are small in the order of 10^{-2} and 10^{-3}.

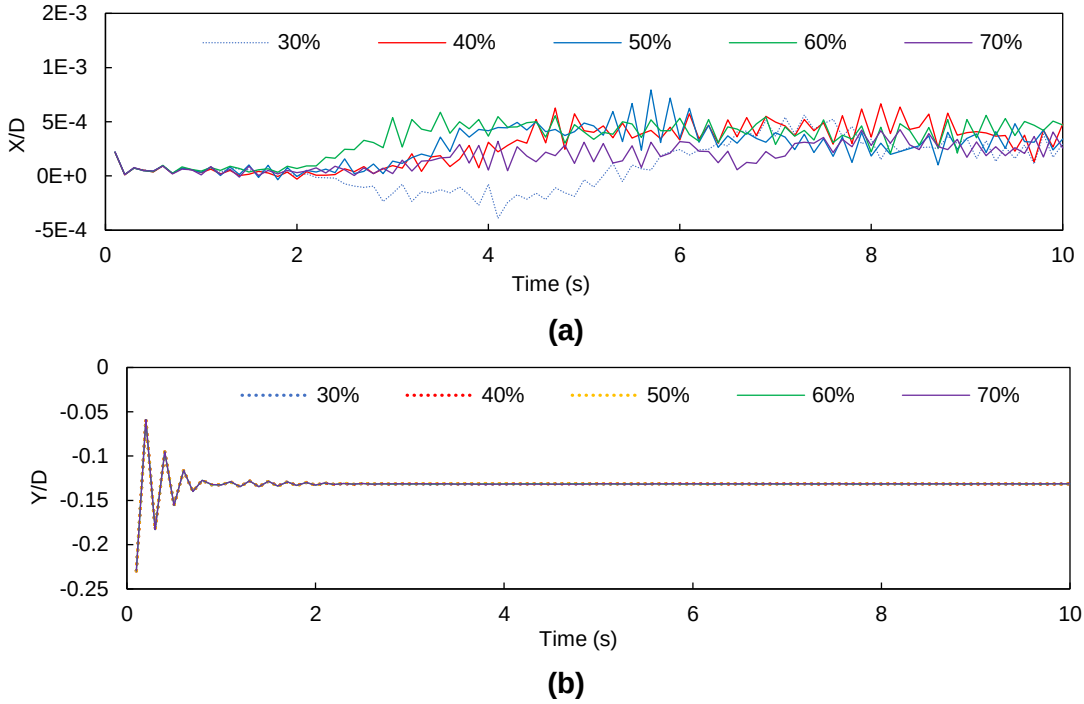

Figure 5-5 Time histories of displacement of horizontal pipe transporting two-phase flow in a) X direction (b) Y direction

5.4.3.3 Vibration Frequencies

The vibration frequencies of the midpoint of the pipe in the X direction under different air intake ratios are shown in Figure 5-6. They are obtained by performing a Fast Fourier Transform (FFT) of the displacement time histories of the midpoint of the pipe. The frequency spectra show that the dominant frequency is accompanied by many smaller frequencies, thus, indicating the presence of multimodal vibration, with the first mode of vibration being dominant. In addition, the response frequency shows a slight variation with the change in gas intake ratio. Moreover, the vibration frequencies in the X direction are close to the first natural frequency (5.37Hz), thus indicating that the first mode is the dominant mode under all the air-intake ratio.

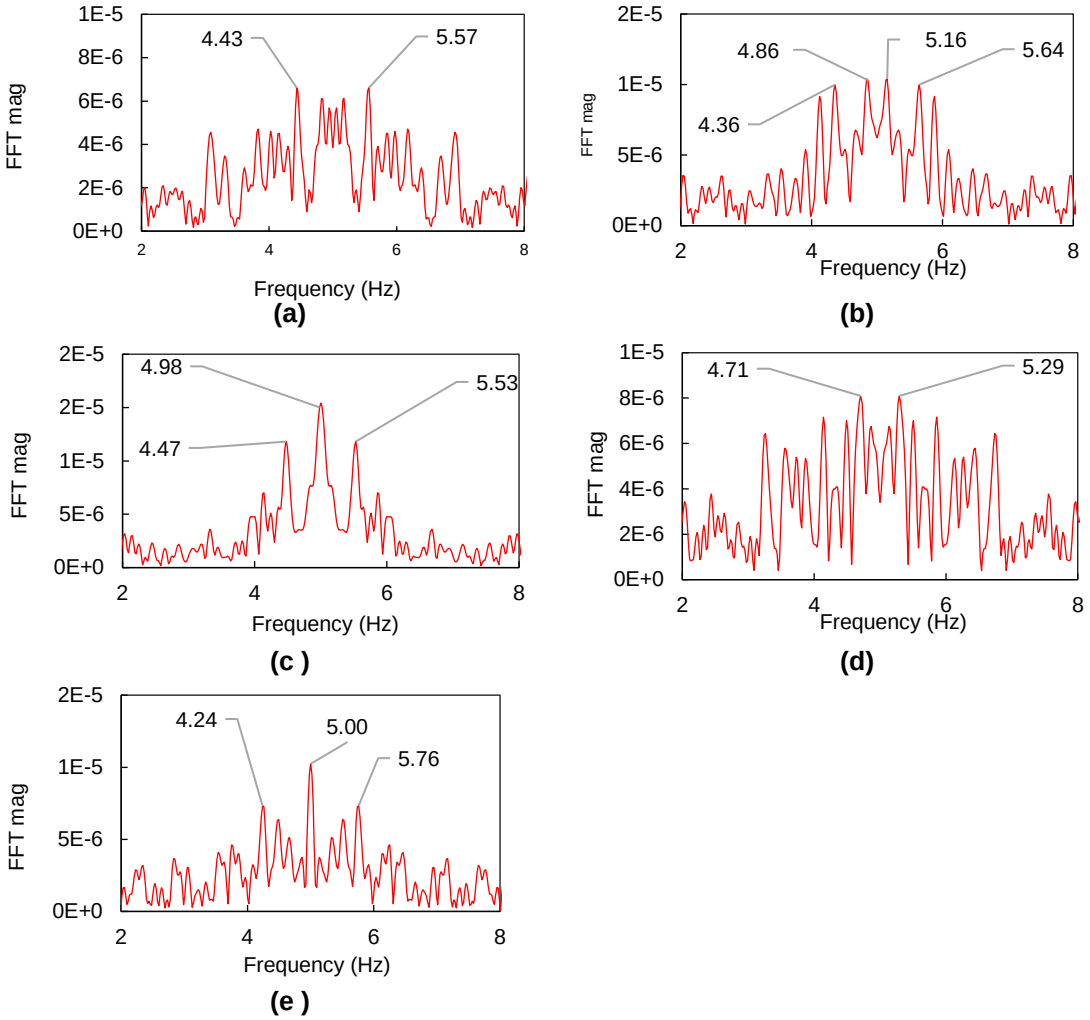

Figure 5-6. Comparison of Frequency spectra of midsection of a horizontal pipe transporting fluid two phase fluid with air intake ratio of (a) 30%; (b) 40 %; (c)50 %.(d) 60% and (e) 70 %.

5.4.4 MFIV of a jumper transporting pulse type two-phase fluid.

Section 5.4.3 described the MFIV of a horizontal pipe with different air intake ratios. The dynamic response of a jumper transporting pulsating air-water flow is now investigated. Unlike the horizontal pipe, a one-way FSI numerical simulation is performed to examine the MFIV of the M-shape jumper transporting a pulsating air-water flow. A one-way coupling was considered based on the assumption that the deformation of the pipe will be small and, therefore, will have little effect on the fluid flow (Elyyan et al., 2015).

5.4.4.1 Modal analysis

The modal analysis was performed for an empty jumper to obtain the natural frequencies of the jumper. The natural frequency of the jumper is essential in determining the occurrence of resonance. When the jumper's vibration frequency is close to the natural frequency, resonance may occur, leading to a large deflection and eventually, to a failure of the jumper system. The six natural frequencies of the jumper are presented in Table 5-9.

Table 5-9 Natural frequency of jumper with an elastic modulus (E)=200GPa

Mode	Frequency (Hz)
1	3.6037
2	8.6164
3	9.9818
4	10.535
5	13.695
6	15.007

Table 5-10 Dominant vibrating frequency of jumper at six different bend

	Frequency (Hz)		
Bend	X Direction	Y Direction	Z direction
1	13.67	13.67	3.52
2	13.67	13.67	3.52
3	8.59	13.67	3.52

4	8.59	13.67	3.52
5	13.67	13.67	3.52
6	13.67	13.67	3.52

5.4.4.2 Dynamic response and vibrating frequencies at the different points along the jumper

Figure 5-7 presents the displacement time histories of the jumper transporting a two-phase fluid at six locations. It can be seen from Figure 5-7 (a)–(e) that the pipe experienced a damped vibration that decays over time in the X and Y directions. However, in the Z direction, the vibration grows with time until it reaches a steady harmonic. The FFT of the displacement time histories is performed to determine the dominant frequency at the six bends (Bends 1-6) along the jumper. Figure 5-8 shows the frequency spectra and dominant frequency at six different locations along the span of the jumper. As can be seen from Figure 5-8 , the dominant frequency is accompanied by a smaller frequency, thus, indicating the presence of multimodal vibration.

Table 5-10 summaries the dominant vibration frequencies at the six different bends along the jumper in the X, Y and Z directions. In the X direction, a dominant frequency of 13.67Hz is recorded at the upper bends comprising Bend 1, Bend 2, Bend 5 and Bend 6. While at the lower bend, namely Bend 3 and Bend 4, a dominant mode of 8.59Hz is recorded, see Figure 5-8 . In the Y direction, a dominant frequency of 13.67Hz is recorded for all bends. Finally, a dominant frequency of 3.522Hz is recorded in the Z direction for all six bends. As mentioned previously, resonance occurs when the dominant vibrating frequency of the jumper is close to the natural frequency of the jumper. The dominant vibrating frequencies, namely 3.52Hz, 8.59Hz and 13.67Hz, are close to the first (3.5Hz), second (8.62Hz), and fifth (13.69Hz) natural frequencies, see Table 5-9. Hence, resonance will likely occur on the jumper transporting a pulsating fluid as it vibrates close to its natural frequency.

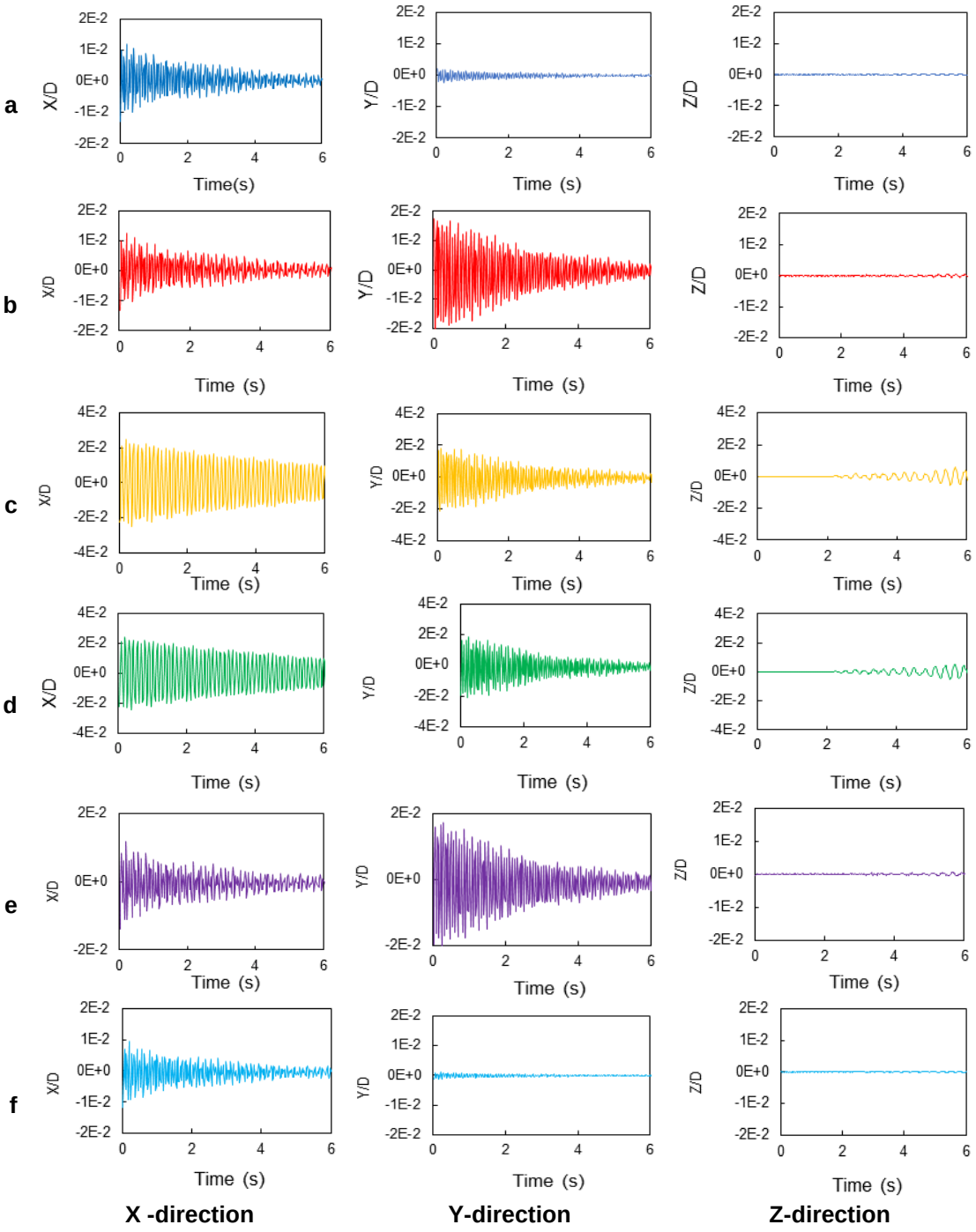

Figure 5-7 Time histories of vibration at the different bends along the jumper (a) bend 1 (b) bend 2 (c) bend 3 (d) bend 4 (e) bend 5 (f) bend 6

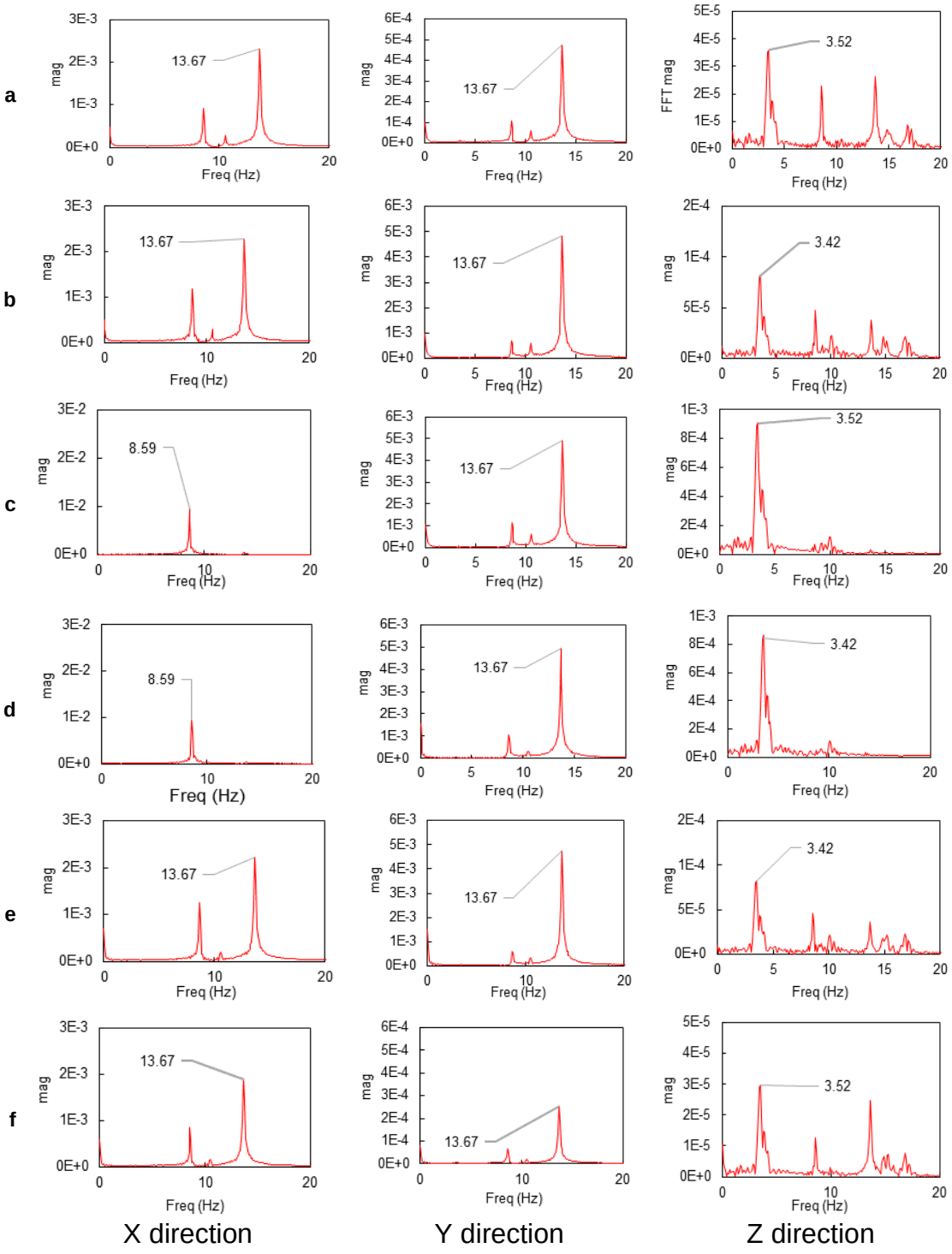

Figure 5-8 vibration frequency at the different bends along the jumper (a) bend 1 (b) bend 2 (c) bend 3 (d) bend 4 (e) bend 5 (f) bend 6

5.4.4.3 Summary

The ANSYS System coupling FSI module has been utilised to perform one-way FSI numerical simulations of a jumper pipe transporting a pulsating two-phase flow. In addition, the dynamic response of the jumper at different locations and directions has been investigated. The following conclusions can be drawn:

1. A damped vibration is observed in the X and Y directions, with the maximum vibration occurring at the lower section (Bends 3 and 4). In the Z direction, the vibration amplitude increases with time, and the maximum vibration occurs at the lower bends.
2. The vibration amplitude at different jumper bends decreases as the fluid moves down the jumper. This can be due to the fluid momentum reduction and the pressure drop along the jumper.
3. The dominant vibration frequencies vary along the jumper. In the X direction, a dominant frequency of 8.59Hz is recorded at Bends 3 and 4, while a dominant frequency of 13.67Hz is recorded at the other bends. However, in the Y and Z directions, frequencies of 13.67 and 3.142Hz are dominant in all bends, respectively.
4. In most cases, the dominant vibrating frequencies were accompanied by smaller frequencies, which signifies the presence of multimodal vibration.

5.4.5 MFIV and VIV of a horizontal pipe transporting two-phase fluid; with varying gas-liquid ratio.

Section 5.4.3 described the effect of air volume fraction on the flow-induced vibration on a horizontal pipe transporting a two-phase fluid without external flow. In contrast, section 5.4.4 describes the dynamic response at six locations along the span of an M-shaped jumper, transporting only a pulsating fluid without any external flow.

Similar to the case of a horizontal pipe with no external flow, this section examines the effect of air intake ratios on the dynamic response of the fluid conveying pipe exposed to an external flow velocity U_e = 0.84m/s. Again, as with the case of the horizontal pipe without external fluid velocity, the internal two-phase fluid has a liquid velocity (U_L) of 1 m/s and gas velocity (Ug) of 1 m/s. Different scenarios were considered for the pipe, keeping U_e=0.84 m/s constant: a flexible pipe without fluid passing through (Case 1), a flexible pipe transporting water only (Case 2), and a flexible pipe transporting a two-phase flow. For the latter case, the effect of the gas-liquid fraction on the combined MFIV and VIV of the pipe was evaluated based on four different two-phase inlet conditions. Three different systems consisting of 30% air (Case 3), 40% air (Case 4), and 50% air (Case 5) were simulated. A fluid flow comprising pulsating liquid and gas intakes with a frequency of 5 Hz was finally investigated (Case 6). A summary of all simulated cases is provided in Table 5-11.

Table 5-11 Cases of the pipe subjected to combined MFIV and VIV

Case Number	Air fraction (%)	U_g(m/s)	U_L(m/s)	U_e(m/s)
Case 1	Empty	0	0	0.84
Case 2	water	1	1	0.84
Case 3	30%	1	1	0.84
Case 4	40%	1	1	0.84
Case5	50%	1	1	0.84
Case 6	100 % (PULSE)	1	1	0.84

5.4.5.1 Inline and crossflow displacement

Before examining in detail, the effects of the different two-phase flow conditions on the IL and CF response, pipes without internal fluid (Case 1) and with a single-phase fluid (Case 2) were investigated. The results obtained from these initial simulations are then compared to subsequent simulations of pipes transporting a two-phase flow. Figure 5-9 (a) and (b) shows the Maximum IL displacement of Cases 1 and 2, while the RMS CF displacements of Cases 1 and 2 are shown in Figure 5-10 (a) and (b).

It can be seen from Figure 5-10 (a) and (b) that in the CF direction, the first mode is the dominant mode in both cases. Also, Figure 5-11 (a) and (b) shows the instantaneous nondimensional deflections (envelope) of the flexible riser for Cases 1 and 2. It can be observed that the vibration is dominated by a single mode (Mode 1).

After investigating the dynamic response of the pipe with no fluid (case 1) and a single-phase fluid (case 2), the effect of the two-phase flow (cases 3-6) are investigated. The maximum IL displacement and RMS CF displacements for various gas-liquid ratios are plotted in Figure 5-9 (c-f) and Figure 5-10 (c-f).It can be seen that the first mode of vibration is the dominant mode for all air intake scenarios considered. Thus, increasing the gas-liquid ratio has little effect on the dominant vibration mode of the pipe. In addition, the response envelope in Figure 5-11 shows that the pipe CF displacement is dominated by a single mode (Mode 1), irrespective of the inlet flow type.

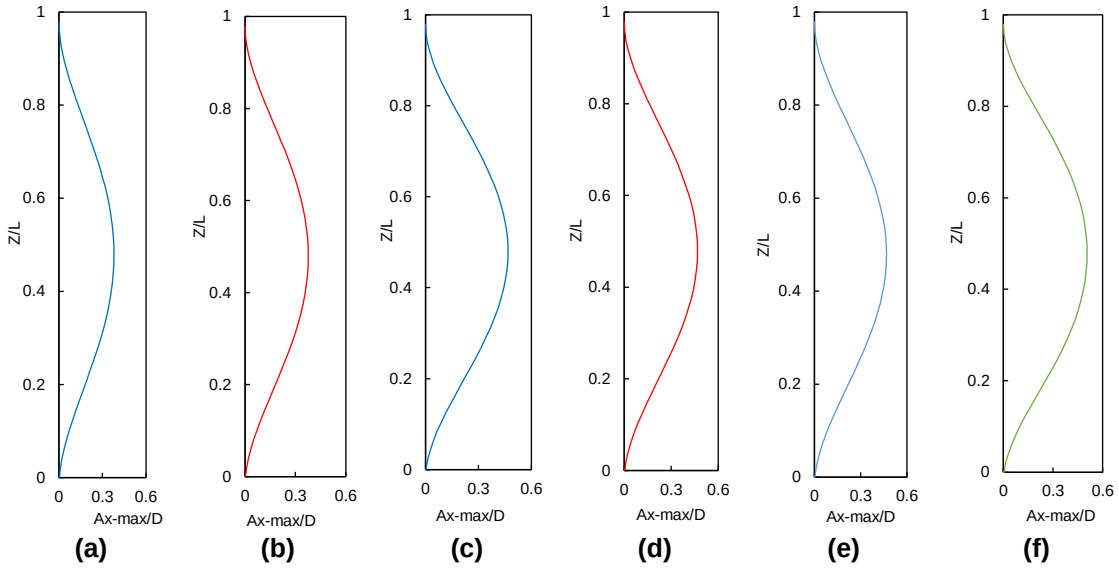

Figure 5-9 Maximum IL displacement of pipe transporting (a) empty (b) single phase fluid (c) (30% air (d) 40% air (e) 50% air (f) pulse intake fluid

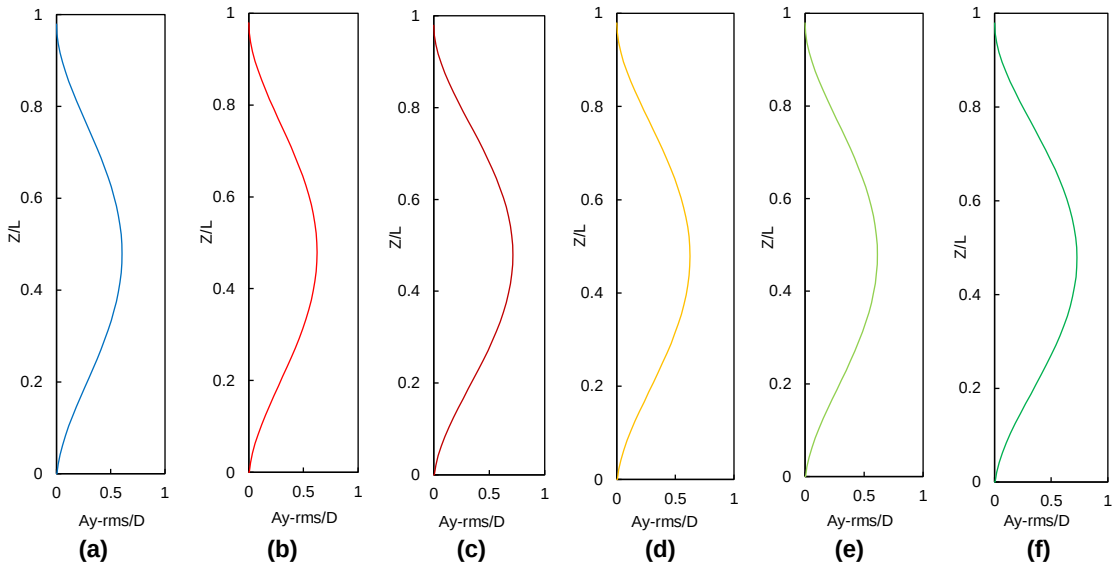

Figure 5-10 RMS of CF displacement of pipe transporting (a) empty (b) single phase fluid (c) (30% air (d) 40% air (e) 50% air (f) pulse intake fluid

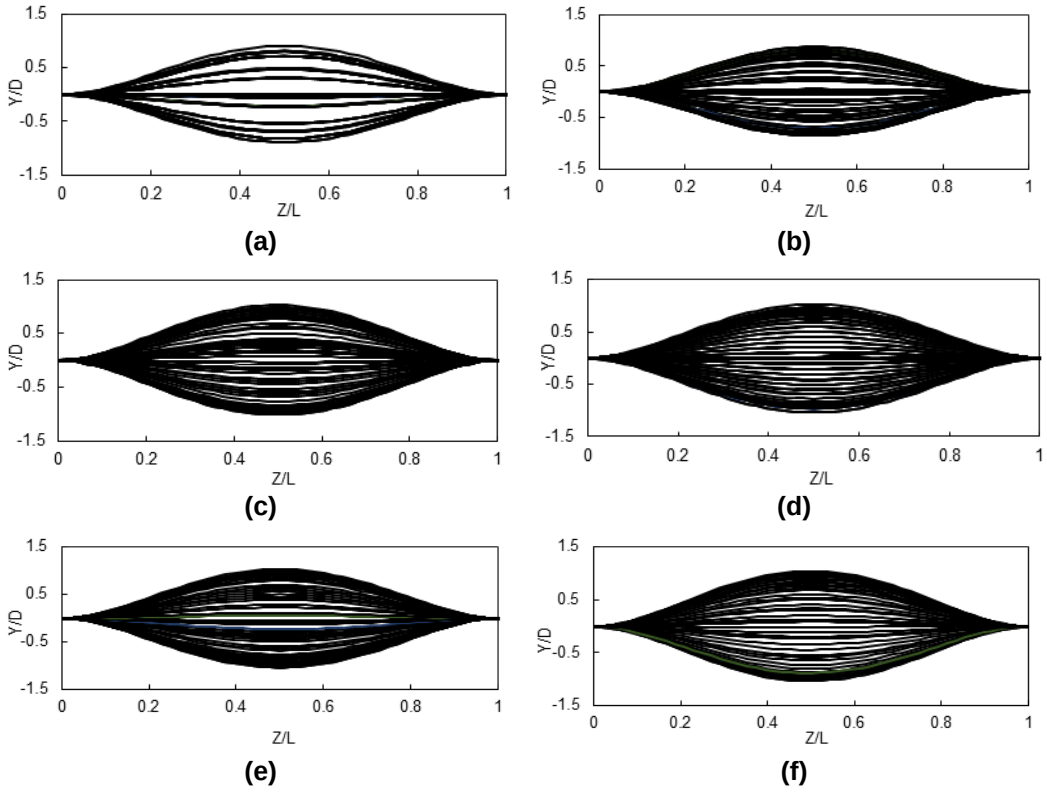

Figure 5-11 response envelope of a horizontal pipe transporting fluid (a) empty fluid (b) water, (c) 30% air (d) 40 % air (e)50 % air and (f) pulse intake air-gas

Figure 5-12. depict the variation of the maximum CF RMS displacement of the pipe under an external uniform current velocity U_e= 0.84m/s and varying air ratio intake (30%, 40%, 50% and pulsating type multiphase flow).The graph shows that the maximum CF RMS decreases with the increase in gas intake ratio, which is similar to the results obtained by Liang and Lou (2020). However, it can be noted that the CF displacement increases when a pulse-type gas intake is considered. The results thus show that the type of two-phase flow condition affects the amplitude of vibrations of the pipe but has little effect on the mode shape. Likewise, Figure 5-12 shows the variation of maximum IL displacement with air intake ratio. The graph shows that the maximum IL displacement is slightly affected by the type of flow in the pipe.

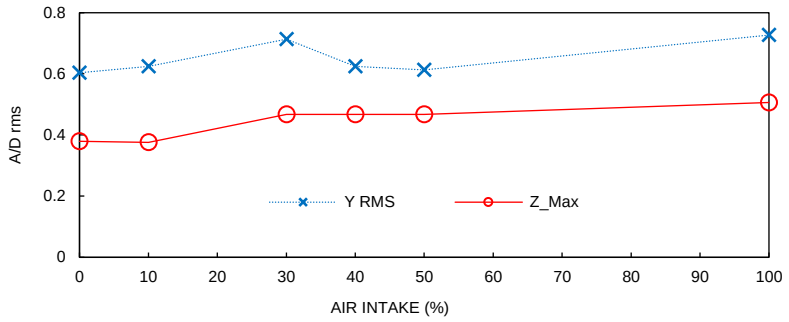

Figure 5-12 Variation of IL and CF with varying gas intake ratio.

5.4.5.2 Vibration frequency and orbital trajectories

Figure 5-13 shows the displacement time histories, frequency spectra, and orbital trajectories of a horizontal pipe subjected to a uniform flow U_e=0.84m/s and different internal flow conditions. The first column represents the time histories of dimensionless CF displacement at varying gas intake ratios, the second column represents the response frequency of the time history in the first column, and the third column represents the orbital trajectories. It can be observed that the oscillation of the midsection of the pipe is periodic regardless of the flow condition, as shown in Figure 5-13 (a-e). The impacts of the air intake ratio on the vibrating frequencies of the horizontal pipe at U_e= 0.84m/s are presented in Figure 5-13 (a-e). When no fluid is injected into the pipe (case 1), the midpoint of the pipe vibrates at a frequency of 4.45Hz. However, when a single-phase flow (Case 2) of velocity Ui=1 m/s is injected into the pipe, the CF frequency decreases slightly to 4.4Hz.

Subsequently, when a two-phase flow comprising a 30% air intake ratio (Cases 3) is injected, the vibration frequency increases to 4.64 Hz. As the gas intake increases, the frequency remains the same except for the 50% air intake (Case 5), which shows a frequency of 2.73Hz. Thus, changing the gas intake ratio affects the pipe's vibration frequency. Similarly, the vibration frequency for the pulse-type intake (Case 6) remains at 4.64Hz.

Compared to the natural frequency, the dominant vibration frequencies for all the cases considered are lower than the first natural frequency of the pipe obtained from the modal analysis, see Table 5-8 and Table 5-12.

The orbital trajectories of the midsection of the pipes (a) with no internal fluid, with single-phase fluid (b), and different two-phase flow conditions(c-e) are shown in Figure 5-13 (a-e). The 'figure-eight' trajectory shape is observed clearly for all flow conditions considered, which indicates the occurrence of dual resonance where the IL and CF vibration frequencies have a ratio of two (Dahl et al., 2010). This trend is similar to that of Guo et al. (2008).

Table 5-12 vibrating frequency of pipe transporting different internal fluid

S/No	case	CF Frequency (Hz)
1	Empty pipe	4.45
2	Single-phase	4.45
3	30%	4.64
4	40%	4.64
5	50%	2.44
7	Pulse	4.64

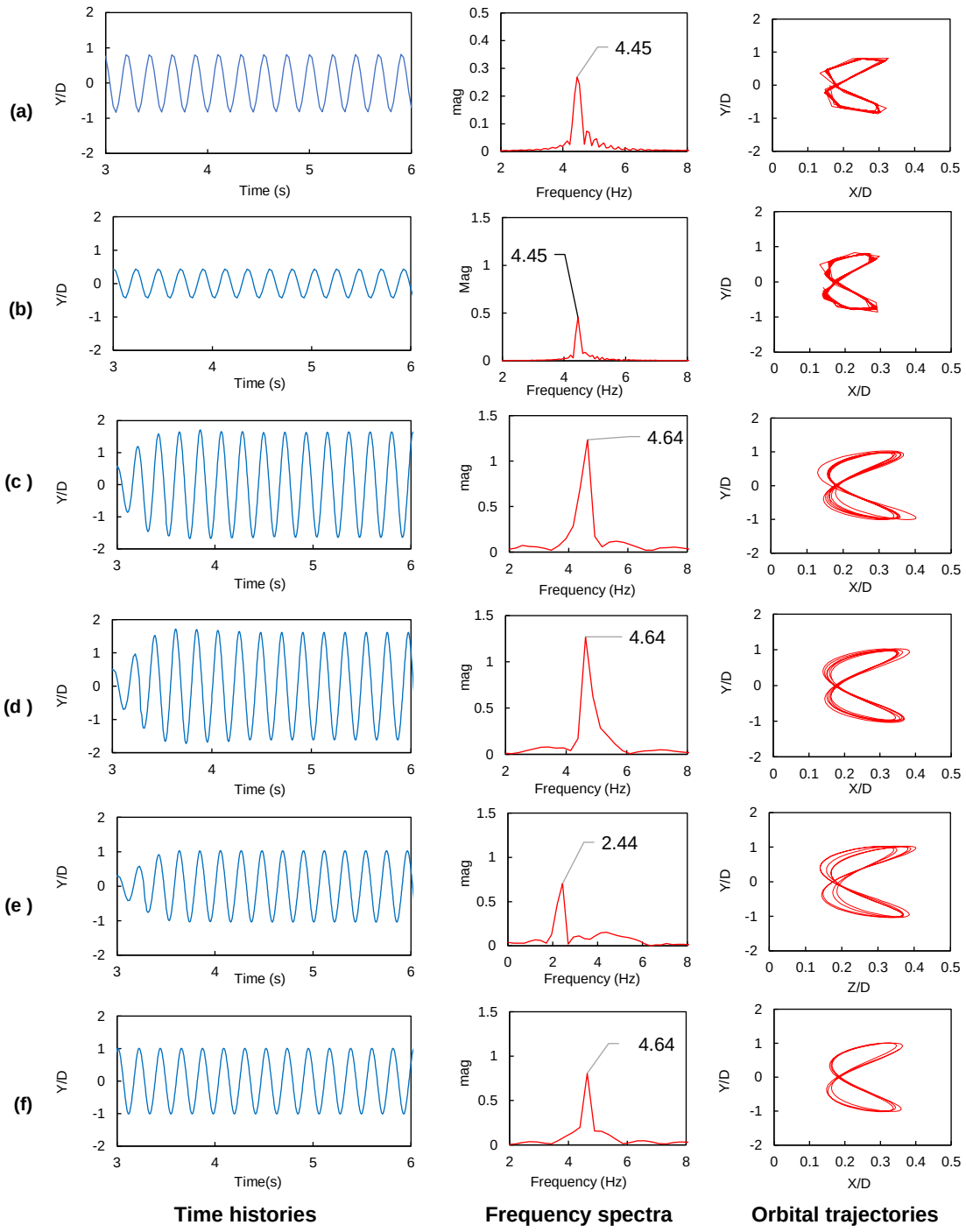

Figure 5-13 Comparison of Time history(First column), Frequency spectra (second column) and orbital trajectories(third column) of a horizontal pipe transporting fluid (a) without fluid (b) water (c) 30% air; (d) 40 % air; (e)50 % air; (f) pulse intake

5.4.5.3 Summary

The dynamic response of a horizontal pipe transporting a two-phase internal flow and exposed to external flow are examined. The effects of the internal two-phase flow air intake ratio on the IL displacement, CF displacement, vibration frequencies and orbital trajectories of the pipe are investigated. The ANSYS System coupling, an FSI module in the ANSYS Workbench interface, was used to connect the ANSYS Fluent fluid solver and the ANSYS Mechanical structural solver.

A two-way FSI simulation was conducted when the pipe was under a constant uniform external flow velocity of 0.84m/s and with varying air gas intake ratios of 30%, 40 %, 50% and a pulse-type air injection intake. The combined effects of the two-phase internal and external flows on the vibration response of the pipe were performed. The following conclusion can be drawn.

1. The vibration of the midsection of the pipe showed that the pipe vibrates periodically when the pipe is empty, carrying single-phase fluid and two-phase fluid with varying air gas intake ratios.
2. The orbital trajectories of the pipe under different internal flow conditions follow the 'figure 8' shape trajectory irrespective of the internal flow conditions. Thus, changing the internal flow conditions has little effect on the orbital trajectory of the pipe.
3. The maximum IL displacement of the pipe increased slightly as the gas intake increased. Similarly, the maximum RMS CF displacement increased with increasing air gas intake ratio. Thus, it can be seen that the air gas intake ratio affects the vibration amplitude but has little effect on the vibration mode.

5.5 Conclusion

A Series of 3D FSI numerical simulations are conducted to investigate the dynamic response of a pipe and jumper transporting two-phase fluid with no external flow and a pipeline transporting two-phase flow subjected to external flow. First, the effect of air-water volume fraction (30%, 40%, 50%, 60% and 70% air ratio) on the dynamic response of the fluid conveying pipe is examined. Secondly, the dynamic response at different locations along the span of an M-shaped jumper transporting pulsating two-phase fluid is examined. Finally, the combined effect of MFIV and external VIV on the dynamic response of a pipe transporting two-phase fluid with varying air-water ratios (30%, 40%, 50 and pulse-type) and exposed to an external flow velocity of 0.84m/s are investigated. The vibration characteristics such as the IL displacement, crossflow displacement, vibration frequencies and orbital trajectories of the pipe under different flow conditions are investigated. The ANSYS System coupling, an FSI module in the ANSYS Workbench interface, was used to connect the ANSYS FLUENT fluid solver and the ANSYS MECHANICAL structural solver. As a result, the following conclusion can be drawn.

1. For a fluid conveying pipe with no external flow acting on it, the air-liquid volumetric fraction has little effect on the vibration motion of the pipe in the X and Y direction.
2. For a jumper pipe transporting pulsating flow with no external flow acting on it, the dominant vibration frequencies vary along the jumper. Likewise, the vibration amplitude at different jumper bends decreases as the fluid moves down the jumper.
3. For a pipe subjected to the combined influence of MFIV and VIV, the vibration of the midsection of the pipe showed that the pipe vibrates periodically irrespective of the air gas intake ratios.
4. Also, the orbital trajectories of the pipes follow the 'figure 8' shape trajectory irrespective of the internal flow conditions. Thus, changing the internal flow conditions has little effect on the orbital trajectory of the pipe.

5. The maximum IL displacement of the pipe increased slightly as the gas intake increased. Similarly, the maximum RMS CF displacement increased with increasing air gas intake ratio. Thus, it can be seen that the air gas intake ratio affects the vibration amplitude but has little effect on the vibration mode.

6 OVERALL CONCLUSION

Subsea pipelines and risers transport hydrocarbon from the wellhead to the platform for export. In most cases, the transported hydrocarbon is a mixture of oil, gas and water. As located offshore, the subsea pipeline is exposed to harsh environments, making the pipe's dynamic response complex. Therefore, it is essential to maintain the integrity of these structures for the safe transportation of hydrocarbon. This study simulates the fluid-structure interaction between the fluid flow around and inside the pipe and the pipe structure. A two-way numerical simulation was performed using the ANSYS 2019 R2 software, where the ANSYS Fluent CFD solver was coupled to the ANSYS Mechanical software via the ANSYS System coupling module.

The first objective of the thesis was to conduct a comprehensive literature review where the previous and latest developments in the field were summarised and analysed. The various methods used to evaluate the dynamic response of the riser were evaluated and relevant information used in this PhD research project were highlighted.

The second objective was to examine the dynamic response of a rigid and flexible riser exposed to different external flows. The study was divided into two parts. The first part numerically investigated the VIV of an elastically mounted rigid cylinder. The effect of mass and damping ratio on the vibration amplitude of the cylinder was evaluated. The ANSYS Fluent flow solver was used to solve the Navier-Stokes equations that describe the fluid flow around the cylinder. Next, the vibration of the cylinder was calculated using a User Defined Function (UDF) to describe the vibration of the cylinder as a mass spring damper system. The results showed good agreement with previous numerical and experimental results from the literature. In addition, the effect of the mass damping ratio on the vibration amplitude of the riser over a wide range of reduced velocities was examined. The results showed that when the mass ratio increased, the maximum amplitude and the synchronisation range were reduced. Also, as the damping ratio increased, the vibration amplitude increased.

The second part of the second objective of this work focused on the VIV response of a flexible pipe fixed at both ends. The effect of the fluid properties, such as the velocity magnitude and profile, were examined. In addition, the effects of structural properties such as the orientation, aspect ratio and elastic modulus on the VIV characteristics of the riser were investigated. A two-way FSI simulation was carried out. The results showed that the IL displacement and CF dominant vibration mode increased with increased flow velocity and aspect ratio. Similarly, the vibration mode increased with the reduction of elastic modulus.

The third objective of this PhD work was to numerically investigate the effect of a single-phase internal flow on the vibration characteristics of pipes exposed to different external flow velocities. The results showed that for a horizontal riser, the vibration mode increased as the internal flow velocity magnitude increased at higher external velocity (0.84m/s). In contrast, the vibration mode remained the same at lower external velocity (0.42m/s) despite an increased internal flow velocity magnitude. For a vertical riser, as the internal flow velocity magnitude increased, the vibration became multimodal, with the second and third modes being the dominant modes under external velocities of 0.42m/s and 0.84m/s. The IL velocity increased as the internal flow velocity magnitude increased for all the external velocities considered. The vibrating frequencies of the riser showed slight changes with the increase of internal fluid velocity.

The fourth objective was to investigate the effects of multiphase FIV and external VIV on pipelines transporting a two-phase flow. The study was divided into three parts. The first part analysed the multiphase flow-induced vibration of pipelines under different air-water gas fractions. The velocity of the mixture was maintained while the air-water gas fraction was varied. The results showed that the riser exhibit a damped vibration in the Y direction. Also, the vibration in the X direction was small in the magnitude of 10^{-2}. The second part of the study focused on the multiphase flow-induced vibration of jumper pipes. Here the velocity of the jumper was increased to 3m/s, and a pulsating two-phase flow with a frequency of 5 Hz was injected to obtain a slug flow condition. The results showed that the vibration at different bends along the jumper was multimodal, caused by the two-phase

interaction. The last part of the study focused on the effects of the gas fraction on the dynamic response of the riser subjected to both MFIV and VIV. A 3D numerical model was developed to perform a two-way FSI simulation to investigate the effect of the gas fraction on the displacement and vibrating frequencies of a flexible riser transporting a multiphase flow and exposed to an external flow. The external and internal velocities were maintained at 0.84m/s and 1m/s, while the air fraction was 30%, 40%, 50% and a pulse-type air injection was considered. The results revealed that the vibration of the midsection of the riser was periodical and followed a ‘figure 8’ shape trajectory, irrespective of the air fraction. In addition, the variation of the air fraction had a slight impact on the pipeline's displacements and CF vibrating frequencies.

Future research

In this work, a 3D numerical method has been utilised to investigate the combined effect of FIV, MFIV and VIV of a flexible riser with different aspect ratios, elastic modulus, and velocity magnitude. The results obtained in this study can be used further analysed the effects of other flow and solid parameters. The study of FSI of the long flexible riser requires high computing time and resources. However, with recent advances in computational power, the following studies can be further investigated.

- The effect of tension was neglected in this study. Therefore, further analysis can be performed to examine the structural response of a tensioned pipe/riser under the combined effect of MFIV and VIV.
- The effect of three-phase multiphase flow on the dynamic response of a riser exposed to high external velocity can be further studied.
- Numerical study of the dynamic response of a jumper under the combined effect of MFIV and VIV can be studied.
- The fatigue damage caused by the combined impact of MFIV, and VIV can be further studied.
- The VIV of single pipe were analysed in this study, the scope can be expanded to consider the effect of pipe placed at the downstream of a

stationary or flexible pipeline. The wake induced vibration can be analysed.

- This study focusses on the fluid structure interaction of pipeline and its environment. The same methodology can be extended to study rotary equipment such as wind turbine. Thereby contributing to achieve renewable energy source.

REFERENCES

Al-Hashimy, Z.I., Al-Kayiem, H.H. and Time, R.W. (2016) 'Experimental investigation on the vibration induced by slug flow in horizontal pipe', *ARPN Journal of Engineering and Applied Sciences*, 11(20), pp. 12134–12139.

An, C. and Su, J. (2015) 'Dynamic behavior of pipes conveying gas-liquid two-phase flow', *Nuclear Engineering and Design*, 292 Elsevier B.V., pp. 204–212.

Bao, Y., Zhu, H.B., Huan, P., Wang, R., Zhou, D., Han, Z.L., Palacios, R., Graham, M. and Sherwin, S. (2019) 'Numerical prediction of vortex-induced vibration of flexible riser with thick strip method', *Journal of Fluids and Structures*, 89 Elsevier Inc., pp. 166–173.

Bearman, P.W. (2011) 'Circular cylinder wakes and vortex-induced vibrations', *Journal of Fluids and Structures*, 27(5–6) Elsevier, pp. 648–658. Available at: 10.1016/j.jfluidstructs.2011.03.021 (Accessed: 27 October 2019).

Blanco, A. and Casanova, E. (2010) 'A preliminary study on the interaction between slug flow and vortex induced vibration in fatigue life of submarines pipelines', *Proceedings of the International Conference on Offshore Mechanics and Arctic Engineering - OMAE*., Vol.5, pp. 545–550.

Bordalo, S.N. and Morooka, C.K. (2018) 'Slug flow induced oscillations on subsea petroleum pipelines', *Journal of Petroleum Science and Engineering*, 165 Elsevier, pp. 535–549.

Bossio V., B.M., Blanco A., A.J. and Casanova M., E.L. (2014) 'Numerical modeling of the dynamical interaction between slug flow and vortex induced vibration in horizontal submarine pipelines', *Journal of Offshore Mechanics and Arctic Engineering*, 136(4) American Society of Mechanical Engineers, pp. 1–5. Available at: 10.1115/1.4028027 (Accessed: 25 April 2018).

Bourguet, R., Karniadakis, G.E. and Triantafyllou, M.S. (2011a) *Vortex-induced vibrations of a long flexible cylinder in shear flow*. Cambridge University Press. Available at: 10.1017/jfm.2011.90 (Accessed: 3 December 2020).

Bourguet, R., Karniadakis, G.E. and Triantafyllou, M.S. (2011b) ‘Lock-in of the vortex-induced vibrations of a long tensioned beam in shear flow’, *Journal of Fluids and Structures*, 27(5–6), pp. 838–847. Available at: 10.1016/J.JFLUIDSTRUCTS.2011.03.008 (Accessed: 16 May 2022).

Bourguet, R., Karniadakis, G.E. and Triantafyllou, M.S. (2013a) ‘Distributed lock-in drives broadband vortex-induced vibrations of a long flexible cylinder in shear flow’, *Journal of Fluid Mechanics*, 717 Cambridge University Press, pp. 361–375. Available at: 10.1017/jfm.2012.576 (Accessed: 8 August 2021).

Bourguet, R., Karniadakis, G.E. and Triantafyllou, M.S. (2013b) ‘Multi-frequency vortex-induced vibrations of a long tensioned beam in linear and exponential shear flows’, *Journal of Fluids and Structures*, 41, pp. 33–42.

Bourguet, R., Modarres-Sadeghi, Y., Karniadakis, G.E. and Triantafyllou, M.S. (2011) *Wake-body resonance of long flexible structures is dominated by counterclockwise orbits*. De. Available at: 10.1103/PhysRevLett.107.134502 (Accessed: 2 March 2020).

Chang, T.J. and Lua, K.B. (2020) ‘Simulation on Vortex Induced Vibration of Circular Cylinder’, *Journal of Physics: Conference Series*, 1509(1) IOP Publishing, p. 012024. Available at: 10.1088/1742-6596/1509/1/012024 (Accessed: 28 August 2021).

Chang, X., Fan, J., Yang, W. and Li, Y. (2021) ‘In-Line and Cross-Flow Coupling Vibration Response Characteristics of a Marine Viscoelastic Riser Subjected to Two-Phase Internal Flow’, *Shock and Vibration*, 2021 Hindawi Limited

Chaplin, J.R., Bearman, P.W., Cheng, Y., Fontaine, E., Graham, J.M.R., Herfjord, K., Huera-Huarte, F.J., Isherwood, M., Lambrakos, K., Larsen, C.M., Meneghini, J.R., Moe, G., Pattenden, R.J., Triantafyllou, M.S. and Willden, R.H.J. (2005a) ‘Blind predictions of laboratory measurements of vortex-induced vibrations of a tension riser’, *Journal of Fluids and Structures*, 21(1 SPEC. ISS.), pp. 25–40.

Chaplin, J.R., Bearman, P.W., Huera-Huarte, F.J. and Pattenden, R.J. (2005b) ‘Laboratory measurements of vortex-induced vibrations of a vertical tension riser

in a stepped current', *Journal of Fluids and Structures*, 21(1 SPEC. ISS.) Academic Press, pp. 3–24.

Charreton, C., Béguin, C., Ross, A., Étienne, S. and Pettigrew, M.J. (2015) 'Two-phase damping for internal flow: Physical mechanism and effect of excitation parameters', *Journal of Fluids and Structures*, 56 Academic Press, pp. 56–74.

Chatjigeorgiou, I.K. (2017) 'Hydroelastic response of marine risers subjected to internal slug-flow', *Applied Ocean Research*, 62 Elsevier B.V., pp. 1–17. Available at: 10.1016/j.apor.2016.11.008 (Accessed: 17 July 2021).

Chen, H. (2006) 'CFD Simulation of Riser VIV', *Texas A&M University*.

Chen, Z. shou, Kim, W. joan and Xiong, C. bo (2012) 'Effect of upward internal flow on dynamics of riser model subject to shear current', *China Ocean Engineering*, 26(1), pp. 95–108.

Chen, Z.S. and Kim, W.J. (2010a) 'Numerical investigation of vortex shedding and vortex-induced vibration for flexible riser models', *International Journal of Naval Architecture and Ocean Engineering*, 2(2) Elsevier BV, pp. 112–118. Available at: 10.3744/JNAOE.2010.2.2.112 (Accessed: 25 June 2020).

Chen, Z.S. and Kim, W.J. (2010b) Numerical Study of Vortex-Induced Vibration for Flexible Riser and Pipe Models *Proceedings of the Twentieth(2010) International Offshore and Polar Engineering Conference*. OnePetro, Available at: 10.3744/JNAOE.2010.2.2.112 (Accessed: 30 July 2021).

Chen, Z.S. and Kim, W.J. (2012a) 'Effect of bidirectional internal flow on fluid-structure interaction dynamics of conveying marine riser model subject to shear current', *International Journal of Naval Architecture and Ocean Engineering*, 4(1) Society of Naval Architects of Korea. Production and hosting by ELSEVIER B.V., pp. 57–70.

Chen, Z.S. and Kim, W.J. (2012b) 'Dynamic effect of internal flow on curved pipe', *Proceedings of the International Offshore and Polar Engineering Conference*, , pp. 403–409. Available at: www.isope.org (Accessed: 22 July 2021).

Chica, L., Pascali, R., Jukes, P., Ozturk, B., Gamino, M. and Smith, K. (2012) 'Detailed FSI analysis methodology for subsea piping components', *Proceedings of the International Conference on Offshore Mechanics and Arctic Engineering - OMAE*, 5, pp. 829–839.

Constantinides, Y., Holmes, S. and Oakley, O.H. (2007) 'CFD high L/D riser modeling study', *Proceedings of the International Conference on Offshore Mechanics and Arctic Engineering - OMAE*., Vol.3, pp. 715–722.

Constantinides, Y. and Oakley, O.H. (2008a) 'Numerical prediction of VIV and comparison with field experiments', *Proceedings of the International Conference on Offshore Mechanics and Arctic Engineering - OMAE*, 5, pp. 577–583.

Constantinides, Y. and Oakley, O.H. (2008b) 'Assessment of empirical VIV analysis tools and benchmark with experiments', *Proceedings of the International Conference on Offshore Mechanics and Arctic Engineering - OMAE*, 5 American Society of Mechanical Engineers Digital Collection, pp. 585–591. Available at: 10.1115/OMAE2008-57216 (Accessed: 6 September 2020).

Cooper, P., Burnett, C. and Nash, I. (2009) 'Fatigue design of flowline systems with slug flow', *Proceedings of the International Conference on Offshore Mechanics and Arctic Engineering - OMAE*, 3 ASME, pp. 207–212. Available at: 10.1115/OMAE2009-79308 (Accessed: 24 April 2018).

Dai, H. and Wang, L. (2012) *Vortex-induced vibration of pipes conveying fluid using the method of multiple scales*. Elsevier Ltd.

Dai, H.L., Wang, L., Qian, Q. and Ni, Q. (2013) 'Vortex-induced vibrations of pipes conveying fluid in the subcritical and supercritical regimes', *Journal of Fluids and Structures*, 39 Academic Press, pp. 322–334.

Dai, H.L., Wang, L., Qian, Q. and Ni, Q. (2014) *Vortex-induced vibrations of pipes conveying pulsating fluid*.

Deng, D., Zhao, W. and Wan, D. (2020) *Vortex-induced vibration prediction of a flexible cylinder by three-dimeansional strip model*. Elsevier Ltd.

Derakhshandeh, J.F. and Alam, M.M. (2019) ‘A review of bluff body wakes’, *Ocean Engineering*, 182 Elsevier Ltd, pp. 475–488.

Doan, V.P. and Nishi, Y. (2015) ‘Modeling of fluid–structure interaction for simulating vortex-induced vibration of flexible riser: finite difference method combined with wake oscillator model’, *Journal of Marine Science and Technology (Japan)*, 20(2) Springer Japan, pp. 309–321.

Dong, S., Karniadakis, G.E., Ekmekci, A. and Rockwell, D. (2006) ‘A combined direct numerical simulation-particle image velocimetry study of the turbulent near wake’, *Journal of Fluid Mechanics*, 569, pp. 185–207. Available at: 10.1017/S0022112006002606 (Accessed: 4 March 2020).

Duan, J., Chen, K., You, Y. and Li, J. (2018) ‘Numerical investigation of vortex-induced vibration of a riser with internal flow’, *Applied Ocean Research*, 72 Elsevier Ltd, pp. 110–121.

Duan, J., Wang, X. and Chen, K. (2021) ‘Numerical investigation on effect of internal flow on vortex-induced vibration dynamics of a full-scale mining riser’, *Modern Physics Letters B*, 35(15), pp. 1–17.

Duan, J., Zhou, J., You, Y. and Wang, X. (2021) ‘Time-domain analysis of vortex-induced vibration of a flexible mining riser transporting flow with various velocities and densities’, *Ocean Engineering*, 220 Pergamon, p. 108427.

Duan, M., Fu, B. and Wan, D. (2016) *The effect of top tension on VIV model analysis of a vertical flexible riser*.

Duan, M., Zou, L. and Wan, D. (2017) ‘Numerical simulations of vortex-induced vibrations of a flexible riser with different aspect ratios in uniform and shear currents’, *Journal of Hydrodynamics*, 29(6) Publishing House for Journal of Hydrodynamics, pp. 1010–1022.

Duan, M., Zou, L. and Wan, D. (2018) ‘Numerical analysis of multi-modal vibrations of a vertical riser in step currents’, *Ocean Engineering*, 152(October 2017) Elsevier Ltd, pp. 428–442.

Elyyan, M.A., Perng, Y.Y. and Najafi, A. (2015) *Fluid-structure interaction modeling of subsea jumper pipe*.

Evangelinos, C., Lucor, D. and Karniadakis, G.E. (2000) 'Dns-Derived Force Distribution on Flexible Cylinders Subject To Vortex-Induced Vibration', *Journal of Fluids and Structures*, 14(3) Academic Press, pp. 429–440.

Facchinetti, M.L., De Langre, E. and Biolley, F. (2004) 'Coupling of structure and wake oscillators in vortex-induced vibrations', *Journal of Fluids and Structures*, 19(2) Academic Press, pp. 123–140. Available at: 10.1016/j.jfluidstructs.2003.12.004 (Accessed: 25 April 2018).

Fluent, A. (2015) *Workshop 08b Vortex shedding Introduction to ANSYS Fluent Learning*.

Fu, B., Duan, M. and Wan, D. (2016) 'Effect of mass ratio on the vortex-induced vibrations of a top tensioned riser', *Proceedings of the Second Conference of Global Chinese Scholars on Hydrodynamics (CCSH'2016), Vols 1 & 2*, , pp. 431–435.

Fu, B., Zou, L. and Wan, D. (2017) 'Numerical study on the effect of current profiles on vortex-induced vibrations in a top-tension riser', *Journal of Marine Science and Application*, 16(4), pp. 473–479.

Gabbai, R.D. and Benaroya, H. (2005) 'An overview of modeling and experiments of vortex-induced vibration of circular cylinders', *Journal of Sound and Vibration*, 282(3–5) Academic Press, pp. 575–616.

Gao, X., Xie, W. de, Xu, W. hai, Bai, Y. chuan and Zhu, H. tao (2018) 'A Novel Wake Oscillator Model for Vortex-Induced Vibrations Prediction of A Cylinder Considering the Influence of Reynolds Number', *China Ocean Engineering*, 32(2), pp. 132–143. Available at: 10.1007/s13344-018-0015-z (Accessed: 6 August 2021).

Gao, Y., Yang, B., Zou, L., Zong, Z. and Zhang, Z. (2019a) *Vortex-Induced Vibrations of A Long Flexible Cylinder in Linear and Exponential Shear Flows*.

Gao, Y., Zhang, Z., Zou, L., Zong, Z. and Yang, B. (2019b) ‘Effect of boundary condition and aspect ratio on vortex-induced vibration response of a circular cylinder’, *Ocean Engineering*, 188(July) Elsevier Ltd, p. 106244.

Gao, Y., Zou, L., Zong, Z., Takagi, S. and Kang, Y. (2019c) ‘Numerical prediction of vortex-induced vibrations of a long flexible cylinder in uniform and linear shear flows using a wake oscillator model’, *Ocean Engineering*, 171(August 2018) Elsevier Ltd, pp. 157–171.

Ge, F., Long, X., Wang, L. and Hong, Y. (2009) ‘Flow-induced vibrations of long circular cylinders modeled by coupled nonlinear oscillators’, *Science in China, Series G: Physics, Mechanics and Astronomy*, 52(7), pp. 1086–1093.

Gedikli, E.D. and Dahl, J.M. (2017) ‘Mode excitation hysteresis of a flexible cylinder undergoing vortex-induced vibrations’, *Journal of Fluids and Structures*, 69 Academic Press, pp. 308–322.

Gourma, M. and Verdin, P. (2020) ‘Nature and magnitude of operating forces in a horizontal bend conveying gas-liquid slug flows’, *Journal of Petroleum Science and Engineering*, 190 Elsevier, p. 107062.

Gourma, M. and Verdin, P. (2016) ‘Two-phase slug flows in helical pipes: Slug frequency alterations and helicity fluctuations’, *International Journal of Multiphase Flow*, 86 Pergamon, pp. 10–20.

Govardhan, R. and Williamson, C.H.K. (2000) ‘Modes of vortex formation and frequency response of a freely vibrating cylinder’, *Journal of Fluid Mechanics*, 420 Cranfield University, pp. 85–130.

Govardhan, R. and Williamson, C.H.K. (2002) ‘Resonance forever: Existence of a critical mass and an infinite regime of resonance in vortex-induced vibration’, *Journal of Fluid Mechanics*, 473(473) Cambridge University Press, pp. 147–166. Available at: 10.1017/S0022112002002318 (Accessed: 29 July 2021).

Govardhan, R. and Williamson, C.H.K. (2004) ‘Critical mass in vortex-induced vibration of a cylinder’, *European Journal of Mechanics - B/Fluids*, 23(1) Elsevier Masson, pp. 17–27.

Gsell, S., Bourguet, R. and Braza, M. (2019) ‘One- versus two-degree-of-freedom vortex-induced vibrations of a circular cylinder at Re=3900’, *Journal of Fluids and Structures*, 85 Academic Press, pp. 165–180.

Gu, J., An, C., Duan, M., Levi, C. and Su, J. (2013) ‘Integral transform solutions of dynamic response of a clamped-clamped pipe conveying fluid’, *Nuclear Engineering and Design*, 254 North-Holland, pp. 237–245.

Gu, J., Ma, T. and Duan, M. (2016) ‘Effect of aspect ratio on the dynamic response of a fluid-conveying pipe using the Timoshenko beam model’, *Ocean Engineering*, 114 Pergamon, pp. 185–191.

Guilmineau, E. and Queutey, P. (2004) ‘Numerical simulation of vortex-induced vibration of a circular cylinder with low mass-damping in a turbulent flow’, *Journal of Fluids and Structures*, 19(4) Academic Press, pp. 449–466.

Guo, H.Y., Lou, M., Hong, N. and Huh, T. (2008) ‘Effect of internal flow on vortex-induced vibration of risers’, *Journal of Fluids and Structures*, 24(4) OnePetro, pp. 496–504. Available at: 10.1016/j.jfluidstructs.2007.10.002 (Accessed: 18 June 2020).

Han, X., Lin, W., Zhang, X., Tang, Y. and Zhao, C. (2016) *Two degree of freedom flow-induced vibration of cylindrical structures in marine environments: frequency ratio effects*. Springer Japan.

He, F., Dai, H., Huang, Z. and Wang, L. (2017) ‘Nonlinear dynamics of a fluid-conveying pipe under the combined action of cross-flow and top-end excitations’, *Applied Ocean Research*, 62 Elsevier B.V., pp. 199–209.

Holmes, S., Constantinides, Y. and Oakley, O.H. (2006) ‘Simulation of riser VIV using fully three dimensional CFD simulations’, *Proceedings of the International Conference on Offshore Mechanics and Arctic Engineering - OMAE*, 2006 American Society of Mechanical Engineers Digital Collection, pp. 1–8.

Hover, F.S., Miller, S.N. and Triantafyllou, M.S. (1997) ‘Vortex-induced vibration of marine cables: Experiments using force feedback’, *Journal of Fluids and Structures*, 11(3) Academic Press, pp. 307–326.

Huang, K., Chen, H.-C. and Chen, C.R. (2011) ‘Numerical scheme for riser motion calculation during 3-D VIV simulation’, *Journal of Fluids and Structures*, 27(7) Academic Press, pp. 947–961.

Huang, K., Chen, H. and Chen, C.R. (2007) ‘Time-domain simulation of riser VIV in sheared current’, *Proceedings of the International Conference on Offshore Mechanics and Arctic Engineering - OMAE*. American Society of Mechanical Engineers Digital Collection, Vol.3, pp. 911–920.

Huang, K., Chen, H. and Chen, C.R. (2012) ‘Vertical riser VIV simulation in sheared current’, *International Journal of Offshore and Polar Engineering*, 22(2), pp. 142–149. Available at: http://onepetro.org/ISOPEIOPEC/proceedings-pdf/ISOPE09/All-ISOPE09/ISOPE-I-09-112/1789467/isope-i-09-112.pdf (Accessed: 18 July 2021).

Huera-Huarte, F.J., Bangash, Z.A. and González, L.M. (2014) *Towing tank experiments on the vortex-induced vibrations of low mass ratio long flexible cylinders*. Academic Press.

Huera-Huarte, F.J. and Bearman, P.W. (2009a) *Wake structures and vortex-induced vibrations of a long flexible cylinder-Part 1: Dynamic response*.

Huera-Huarte, F.J. and Bearman, P.W. (2009b) *Wake structures and vortex-induced vibrations of a long flexible cylinder-Part 2: Drag coefficients and vortex modes*.

Ibnu Syihab, A.B.M., Verdin, P.G., Wright, R.M., Piper, A.T. and Rivas Casado, M. (2021) ‘Computational fluid dynamics simulations of water flow on a studded upstream eel pass’, *River Research and Applications*, 37(9) John Wiley and Sons Ltd, pp. 1279–1293.

Jaiman, R.K., Shakib, F., Oakley, O.H. and Constantinides, Y. (2009) ‘Fully coupled fluid-structure interaction for offshore applications’, *Proceedings of the International Conference on Offshore Mechanics and Arctic Engineering - OMAE*, 5, pp. 757–765.

Jeon, D. and Gharib, M. (2001) ‘On circular cylinders undergoing two-degree-of-

freedom forced motions', *Journal of Fluids and Structures*, 15(3–4) Elsevier, pp. 533–541.

Jia, D. (2012) 'Slug Flow Induced Vibration in a Pipeline Span, a Jumper and a Riser Section', *Proceedings of Offshore Technology Conference (OTC)*. Houston, Texas.

Jia, D. (2013) 'Effect of Boundary Conditions, Flow Rate, Slug Length, and Slug Frequency on Slug Flow Induced Vibration in a Pipeline Span', *Proceedings of Offshore Technology Conference (OTC)*. Houston, Texas, pp. 1–14.

Jiang, H., Cheng, L., Draper, S., An, H. and Tong, F. (2016) 'Three-dimensional direct numerical simulation of wake transitions of a circular cylinder', *Journal of Fluid Mechanics*, 801 Cambridge University Press, pp. 353–391. Available at: 10.1017/jfm.2016.446 (Accessed: 21 August 2021).

Jiang, T., Dai, H. and Wang, L. (2020) 'Three-dimensional dynamics of fluid-conveying pipe simultaneously subjected to external axial flow', *Ocean Engineering*, 217 Pergamon, p. 107970.

Jiang, T., Liu, Z., Dai, H., Wang, L. and He, F. (2019) 'Nonplanar multi-modal vibrations of fluid-conveying risers under shear cross flows', *Applied Ocean Research*, 88 Elsevier Ltd, pp. 187–209.

Jujuly, M.M., Rahman, M.A., Maynard, A. and Addy, M. (2017) 'Hydrate induced vibration in an offshore pipeline', *Proceedings - SPE Annual Technical Conference and Exhibition*

Kaewunruen, S., Chiravatchradej, J. and Chucheepsakul, S. (2005) 'Nonlinear free vibrations of marine risers/pipes transporting fluid', *Ocean Engineering*, 32(3–4) Elsevier BV, pp. 417–440.

Keber, M. and Wiercigroch, M. (2008) 'Dynamics of a vertical riser with weak structural nonlinearity excited by wakes', *Journal of Sound and Vibration*, 315(3) Academic Press, pp. 685–699.

Khalak, A. and Williamson, C.H.K. (1996) 'Dynamics of a hydroelastic cylinder

with very low mass and damping', *Journal of Fluids and Structures*, 10(5) Academic Press, pp. 455–472.

Khalak, A. and Williamson, C.H.K. (1997a) 'Fluid forces and dynamics of a hydroelastic structure with very low mass and damping', *Journal of Fluids and Structures*, 11(8) Academic Press, pp. 973–982.

Khalak, A. and Williamson, C.H.K. (1997b) 'Investigation of relative effects of mass and damping in vortex-induced vibration of a circular cylinder', *Journal of Wind Engineering and Industrial Aerodynamics*, 69–71 Elsevier, pp. 341–350.

Khalak, A. and Williamson, C.H.K. (1999) 'Motions, forces and mode transitions in vortex-induced vibrations at low mass-damping', *Journal of Fluids and Structures*, 13(7–8), pp. 813–851. Available at: 10.1006/jfls.1999.0236 (Accessed: 30 August 2020).

Khan, N.B. and Ibrahim, Z. (2019) 'Numerical investigation of vortex-induced vibration of an elastically mounted circular cylinder with One-degree of freedom at high Reynolds number using different turbulent models', *Proceedings of the Institution of Mechanical Engineers Part M: Journal of Engineering for the Maritime Environment*, 233(2) SAGE Publications Ltd, pp. 443–453. Available at: 10.1177/1475090217751992 (Accessed: 7 March 2020).

Kim, J. and Srinil, N. (2018) '3-D numerical simulations of subsea jumper transporting intermittent slug flows', *Proceedings of the International Conference on Offshore Mechanics and Arctic Engineering - OMAE*. American Society of Mechanical Engineers (ASME), Vol.2. Available at: 10.1115/OMAE2018-77299 (Accessed: 25 August 2020).

Knudsen, T.H., Sævik, S., Thorsen, M.J., Huse Knudsen, T., Sævik, S. and Thorsen, M.J. (2016) 'Numerical analysis of combined VIV and slug flow in time domain', *Proceedings of the International Conference on Offshore Mechanics and Arctic Engineering - OMAE*. Busan, South Korea: Proceedings of the ASME 2016 35th International Conference on Ocean, Offshore and Arctic Engineering OMAE2016, Vol.2, p. V002T08A043. Available at: 10.1115/OMAE2016-54891 (Accessed: 6 August 2021).

Lee, A.H., Campbell, R.L. and Hambric, S.A. (2014) ‘Coupled delayed-detached-eddy simulation and structural vibration of a self-oscillating cylinder due to vortex-shedding’, *Journal of Fluids and Structures*, 48, pp. 216–234.

Lee, L. and Allen, D.W. (2010) *Vibration frequency and lock-in bandwidth of tensioned, flexible cylinders experiencing vortex shedding*.

Lehn, E. (2003) ‘VIV suppression tests on high L/D flexible cylinders’, *VIV suppression tests on high L/D flexible cylinders. Norwegian Marine Technology Research Institute, Trondheim, Norway.*

Li, B.H., Gao, H.S., Zhai, H.B., Liu, Y.S. and Yue, Z.F. (2011) ‘Free vibration analysis of multi-span pipe conveying fluid with dynamic stiffness method’, *Nuclear Engineering and Design*, 241(3) North-Holland, pp. 666–671.

Li, F., An, C., Duan, M. and Su, J. (2020) ‘Combined damping model for dynamicas and stability of a pipe conveying two-phase flow’, *Ocean Engineering*, 195 Elsevier Ltd

Li, F., Cao, J., Duan, M., An, C. and Su, J. (2016) *Two-phase flow induced vibration of subsea span pipeline*.

Li, M., Deng, D. and Wan, D. (2020) Viv of flexible riser conveying internal fluid subjected to uniform current *Proceedings of the International Offshore and Polar Engineering Conference*. OnePetro, Available at: www.isope.org (Accessed: 3 August 2021).

Liang, W. and Lou, M. (2020) ‘Numerical simulation of vortex-induced vibration of a marine riser with a multiphase internal flow considering hydrate phase transition’, *Ocean Engineering*, 216 Pergamon, p. 107758.

Liang, X., Zha, X., Jiang, X., Wang, L., Leng, J. and Cao, Z. (2018) ‘Semi-analytical solution for dynamic behavior of a fluid-conveying pipe with different boundary conditions’, *Ocean Engineering*, 163 Pergamon, pp. 183–190.

Lin, K. and Wang, J. (2019) ‘Numerical simulation of vortex-induced vibration of long flexible risers using a SDVM-FEM coupled method’, *Ocean Engineering*, 172

Elsevier Ltd, pp. 468–486.

Livinus, A. and Verdin, P.G. (2021) ‘CFD study of the characteristics of a single elongated gas bubble in liquid in a moderately inclined pipe’, *Upstream Oil and Gas Technology*, 7 Elsevier, p. 100037.

Lou, M. and Liang, W. (2020) ‘Effect of multiphase internal flows considering hydrate phase transitions on the streamwise oscillation of marine risers’, *Ocean Engineering*, 197 Pergamon, p. 106905.

Loyseau, X.F. and Verdin, P.G. (2016) ‘Statistical model of transient particle dispersion and deposition in vertical pipes’, *Journal of Aerosol Science*, 101 Pergamon, pp. 43–64.

Loyseau, X.F., Verdin, P.G. and Brown, L.D. (2018) ‘Scale-up and turbulence modelling in pipes’, *Journal of Petroleum Science and Engineering*, 162 Elsevier, pp. 1–11.

Lucor, D., Imas, L. and Karniadakis, G.E. (2001) ‘Vortex dislocations and force distribution of long flexible cylinders subjected to sheared flows’, *Journal of Fluids and Structures*, 15(3–4), pp. 641–650.

Ma, B. and Srinil, N. (2020) ‘Planar dynamics of inclined curved flexible riser carrying slug liquid–gas flows’, *Journal of Fluids and Structures*, 94 Academic Press, p. 102911.

Ma, B., Srinil, N., Zhu, H. and Gao, Y. (2020) ‘Experiment on the effect of superficial Gas-liquid velocities on slug flow-induced vibration in an inclined sagged riser’, *Proceedings of the International Conference on Offshore Mechanics and Arctic Engineering - OMAE*., Vol.8, pp. 1–7.

Ma, B., Srinil, N., Zhu, H. and Gao, Y. (2021) *Experimental Measurement of Large-Amplitude Intermittent Vibrations of an Inclined Bendable Riser Transporting Unsteady Multiphase Flows*., *Applied Ocean Research* Available at: 10.1016/j.apor.2021.102731 (Accessed: 16 July 2021).

Ma, T., Gu, J. and Duan, M. (2017) ‘Dynamic response of pipes conveying two-

phase flow based on Timoshenko beam model', *Marine Systems and Ocean Technology*, 12(3), pp. 196–209.

Mathelin, L. and De Langre, E. (2005) 'Vortex-induced vibrations and waves under shear flow with a wake oscillator model', *European Journal of Mechanics, B/Fluids*, 24(4) Elsevier Masson, pp. 478–490.

Matin Nikoo, H., Bi, K. and Hao, H. (2019) 'Three-dimensional vortex-induced vibration of a circular cylinder at subcritical Reynolds numbers with low-Re correction', *Marine Structures*, 66 Elsevier, pp. 288–306.

Meneghini, J.R., Saltara, F., Fregonesi, R.D.A., Yamamoto, C.T., Casaprima, E. and Ferrari, J.A. (2004) 'Numerical simulations of VIV on long flexible cylinders immersed in complex flow fields', *European Journal of Mechanics, B/Fluids*, 23(1), pp. 51–63.

Meng, D., Guo, H.Y. and Xu, S.P. (2011) 'Non-linear dynamic model of a fluid-conveying pipe undergoing overall motions', *Applied Mathematical Modelling*, 35(2) Elsevier, pp. 781–796.

Meng, S., Chen, Y. and Che, C. (2020) 'Slug flow's intermittent feature affects VIV responses of flexible marine risers', *Ocean Engineering*, 205 Elsevier Ltd

Meng, S., Zhang, X., Che, C. and Zhang, W. (2017) 'Cross-flow vortex-induced vibration of a flexible riser transporting an internal flow from subcritical to supercritical', *Ocean Engineering*, 139(May) Elsevier Ltd, pp. 74–84. Available at: 10.1016/j.oceaneng.2017.04.039 (Accessed: 25 August 2020).

Menter, F., Yakubov, S., Sharkey, P. and Kuntz, M. (2006) 'Overview of fluid-structure coupling in ANSYS-CFX', *Proceedings of the International Conference on Offshore Mechanics and Arctic Engineering - OMAE*, 2006 American Society of Mechanical Engineers Digital Collection, pp. 1–7.

Menter, F.R. (1994) *Two-equation eddy-viscosity turbulence models for engineering applications*. Available at: 10.2514/3.12149 (Accessed: 30 December 2018).

Miwa, S., Hibiki, T. and Mori, M. (2016) ‘Analysis of Flow-Induced Vibration Due to Stratified Wavy Two-Phase Flow’, *Journal of Fluids Engineering, Transactions of the ASME*, 138(9), pp. 1–9.

Miwa, S., Mori, M. and Hibiki, T. (2015) *Two-phase flow induced vibration in piping systems*. Elsevier Ltd. Available at: 10.1016/j.pnucene.2014.10.003 (Accessed: 25 August 2020).

Mohmmed, A.O., Al-Kayiem, H.H., Nasif, M.S. and Time, R.W. (2019) ‘Effect of slug flow frequency on the mechanical stress behavior of pipelines’, *International Journal of Pressure Vessels and Piping*, 172 Elsevier, pp. 1–9.

Montoya-Hernández, D.J., Vázquez-Hernández, A.O., Cuamatzi, R. and Hernandez, M.A. (2014) ‘Natural frequency analysis of a marine riser considering multiphase internal flow behavior’, *Ocean Engineering*, 92 Pergamon, pp. 103–113.

Newman, D.J. and Karniadakis, G.E. (1997) ‘A direct numerical simulation study of flow past a freely vibrating cable’, *Journal of Fluid Mechanics*, 344, pp. 95–136.

Nguyen, V.T. and Nguyen, H.H. (2016) ‘Detached eddy simulations of flow induced vibrations of circular cylinders at high Reynolds numbers’, *Journal of Fluids and Structures*, 63 Academic Press, pp. 103–119. Available at: 10.1016/j.jfluidstructs.2016.02.004 (Accessed: 10 March 2020).

Onuoha, M.D.U., Li, Q. and Duan, M. (2018) ‘On the interaction between severe slug buildup and dynamic response of a submerged top-tensioned riser’, *Ocean Engineering*, 164(December 2017) Elsevier Ltd, pp. 683–697. Available at: 10.1016/j.oceaneng.2018.07.005 (Accessed: 25 July 2020).

Ortega, A., Rivera, A. and Larsen, C.M. (2013) ‘Flexible riser response induced by combined slug flow and wave loads’, *Proceedings of the International Conference on Offshore Mechanics and Arctic Engineering - OMAE*, 4 B American Society of Mechanical Engineers Digital Collection Available at: 10.1115/OMAE2013-10891 (Accessed: 27 July 2021).

Ortega, A., Rivera, A. and Larsen, C.M. (2018) ‘Slug Flow and Waves Induced

Motions in Flexible Riser', *Journal of Offshore Mechanics and Arctic Engineering*, 140(1) American Society of Mechanical Engineers (ASME) Available at: 10.1115/1.4037842 (Accessed: 25 August 2020).

Ortega, A., Rivera, A., Nydal, O.J. and Larsen, C.M. (2012) 'On the dynamic response of flexible risers caused by internal slug flow', *Proceedings of the International Conference on Offshore Mechanics and Arctic Engineering - OMAE*. American Society of Mechanical Engineers, Vol.5, pp. 647–656. Available at: 10.1115/OMAE2012-83316 (Accessed: 25 August 2020).

Ortiz-Vidal, L.E., Mureithi, N.W. and Rodriguez, O.M.H. (2017) *Vibration response of a pipe subjected to two-phase flow: Analytical formulations and experiments*. Elsevier B.V.

Pan, Z.Y., Cui, W.C. and Miao, Q.M. (2007) 'Numerical simulation of vortex-induced vibration of a circular cylinder at low mass-damping using RANS code', *Journal of Fluids and Structures*, 23(1) Academic Press, pp. 23–37.

Patel, M.H. and Seyed, F.B. (1989) 'Internal flow-induced behaviour of flexible risers', *Engineering Structures*, 11(4), pp. 266–280.

Placzek, A., Sigrist, J.-F.F. and Hamdouni, A. (2009) 'Numerical simulation of an oscillating cylinder in a cross-flow at low Reynolds number: Forced and free oscillations', *Computers and Fluids*, 38(1), pp. 80–100.

Pontaza, J.P. (2014) 'Fluid-structure interaction and applications to screening pipeline span VIV and subsea piping FIV', *Proceedings of the Annual Offshore Technology Conference*., Vol.5, pp. 3623–3634.

Pontaza, J.P. and Menon, R.G. (2011) 'Flow-induced vibrations of subsea jumpers due to internal multi-phase flow', *Proceedings of the International Conference on Offshore Mechanics and Arctic Engineering - OMAE*. American Society of Mechanical Engineers Digital Collection, Vol.7, pp. 585–595. Available at: 10.1115/OMAE2011-50062 (Accessed: 17 July 2021).

Qu, L., Norberg, C., Davidson, L., Peng, S.H. and Wang, F. (2013) 'Quantitative numerical analysis of flow past a circular cylinder at reynolds number between 50

and 200', *Journal of Fluids and Structures*, 39, pp. 347–370.

Riverin, J.L. and Pettigrew, M.J. (2007) *Vibration excitation forces due to two-phase flow in piping elements*. Available at: 10.1115/1.2388994 (Accessed: 25 August 2020).

Safrendyo, S. and Srinil, N. (2018) 'Slug flow-induced oscillation in subsea catenary riser experiencing VIV', *Proceedings of the International Conference on Offshore Mechanics and Arctic Engineering - OMAE*, 2 American Society of Mechanical Engineers Digital Collection Available at: 10.1115/OMAE2018-77298 (Accessed: 29 July 2021).

Saltara, F., Neto, A.D.A. and Lopez, J.I.H. (2011) '3D CFD simulation of vortex-induced vibration of cylinder', *International Journal of Offshore and Polar Engineering*, 21(3), pp. 192–197.

Sarpkaya, T. (2004) 'A critical review of the intrinsic nature of vortex-induced vibrations', *Journal of Fluids and Structures*, 19(4) Academic Press, pp. 389–447.

Seyed-Aghazadeh, B., Edraki, M. and Modarres-Sadeghi, Y. (2019) 'Effects of boundary conditions on vortex-induced vibration of a fully submerged flexible cylinder', *Experiments in Fluids*, 60(3) Springer Berlin Heidelberg, pp. 1–14.

Seyed, F.B. and Patel, M.H. (1992) 'Mathematics of flexible risers including pressure and internal flow effects', *Marine Structures*, 5(2–3) Elsevier, pp. 121–150.

Song, J.N., Lu, L., Teng, B., Park, H. Il, Tang, G.Q. and Wu, H. (2011) 'Laboratory tests of vortex-induced vibrations of a long flexible riser pipe subjected to uniform flow', *Ocean Engineering*, 38(11–12) Elsevier, pp. 1308–1322. Available at: 10.1016/j.oceaneng.2011.05.020 (Accessed: 25 August 2020).

Song, L., Fu, S., Cao, J., Ma, L. and Wu, J. (2016a) 'An investigation into the hydrodynamics of a flexible riser undergoing vortex-induced vibration', *Journal of Fluids and Structures*, 63 Elsevier, pp. 325–350. Available at: 10.1016/j.jfluidstructs.2016.03.006 (Accessed: 25 August 2020).

Song, L., Fu, S., Dai, S., Zhang, M. and Chen, Y. (2016b) 'Distribution of drag force coefficient along a flexible riser undergoing VIV in sheared flow', *Ocean Engineering*, 126, pp. 1–11.

Srinil, N. (2011) *Analysis and prediction of vortex-induced vibrations of variable-tension vertical risers in linearly sheared currents*. Elsevier. Available at: 10.1016/j.oceaneng.2009.08.010 (Accessed: 29 July 2021).

Stabile, G., Matthies, H.G. and Borri, C. (2018) 'A novel reduced order model for vortex induced vibrations of long flexible cylinders', *Ocean Engineering*, 156, pp. 191–207.

Sun, L., Zong, Z., Dong, J., Dong, G.H. and Liu, C.F. (2012) 'Stripwise discrete vortex method for VIV analysis of flexible risers', *Journal of Fluids and Structures*, 35 Academic Press, pp. 21–49.

Trim, A.D., Braaten, H., Lie, H. and Tognarelli, M.A. (2005) 'Experimental investigation of vortex-induced vibration of long marine risers', *Journal of Fluids and Structures*, 21(3 SPEC. ISS.) Academic Press, pp. 335–361.

Urthaler, Y., Breaux, L.E., McNeill, S.I., Luther, E.M., Austin, J., Tognarelli, M.A., Breaux, L.E., McNeill, S.I., Austin, J., Tognarelli, M.A., Urthaler, Y., Breaux, L.E., McNeill, S.I., Luther, E.M., Austin, J. and Tognarelli, M.A. (2011) 'A methodology for assessment of internal flow-induced vibration (FIV) in subsea piping systems', *Proceedings of the International Conference on Offshore Mechanics and Arctic Engineering - OMAE*, 1, pp. 567–577.

Vandiver, J.K., Jaiswal, V. and Jhingran, V. (2009) 'Insights on vortex-induced, traveling waves on long risers', *Journal of Fluids and Structures*, 25(4) Elsevier, pp. 641–653. Available at: 10.1016/j.jfluidstructs.2008.11.005 (Accessed: 25 August 2020).

Vandiver, J.K., Swithenbank, S., Jaiswal, V. and Marcollo, H. (2006) 'The Effectiveness of Helical Strakes in the Suppression of High-Mode-Number VIV', *Offshore Technology Conference*., pp. 1–9.

Vieiro, J., Ita, E.I. and Nydal, O.J. (2015) 'Two-Way fluid-Structure interaction in

a flexible pipe conveying gas-Liquid slug flow', *Proceedings of Offshore Technology Conference (OTC)*. Offshore Technology Conference, pp. 1035–1044.

Violette, R., de Langre, E. and Szydlowski, J. (2007) 'Computation of vortex-induced vibrations of long structures using a wake oscillator model: Comparison with DNS and experiments', *Computers and Structures*, 85(11–14), pp. 1134–1141.

Wang, C., Ge, S., Jaworski, J.W., Liu, L. and Jia, Z. (2019a) 'Effects of different design parameters on the vortex induced vibration of FRP composite risers using grey relational analysis', *Journal of Marine Science and Engineering*, 7(7)

Wang, C., Ge, S., Sun, M., Jia, Z. and Han, B. (2019b) 'Comparative Study of Vortex-Induced Vibration of FRP Composite Risers with Large Length to Diameter Ratio Under Different Environmental Situations', *Applied Sciences 2019, Vol. 9, Page 517*, 9(3) Multidisciplinary Digital Publishing Institute, p. 517. Available at: 10.3390/APP9030517 (Accessed: 5 August 2021).

Wang, C., Sun, M., Shankar, K., Xing, S. and Zhang, L. (2018a) 'CFD simulation of vortex induced vibration for frp composite riser with different modeling methods', *Applied Sciences (Switzerland)*, 8(5), pp. 1–18.

Wang, E. and Xiao, Q. (2016) 'Numerical simulation of vortex-induced vibration of a vertical riser in uniform and linearly sheared currents', *Ocean Engineering*, 121 Elsevier Ltd, pp. 492–515. Available at: 10.1016/j.oceaneng.2016.06.002 (Accessed: 25 June 2020).

Wang, J., Fan, D. and Lin, K. (2020) 'A review on flow-induced vibration of offshore circular cylinders', *Journal of Hydrodynamics*, 32(3) Springer, pp. 415–440. Available at: 10.1007/S42241-020-0032-2 (Accessed: 3 December 2020).

Wang, J., Lin, K., Zhou, J., Xu, L. and Sheng, L. (2017a) 'Three Dimensional Numerical Simulation of Vortex Induced Vibration for a 800-m-long Marine Riser', *Proceedings of the International Offshore and Polar Engineering Conference*, OnePetro, pp. 1251–1256. Available at:

http://onepetro.org/ISOPEIOPEC/proceedings-pdf/ISOPE17/All-ISOPE17/ISOPE-I-17-656/1257257/isope-i-17-656.pdf (Accessed: 4 August 2021).

Wang, J., Lin, K., Zhou, J., Xu, L. and Sheng, L. (2012) Three dimensional numerical simulation of vortex induced vibration for an 500-m-long drilling riser *Proceedings of the International Offshore and Polar Engineering Conference*. OnePetro, Available at: http://onepetro.org/ISOPEIOPEC/proceedings-pdf/ISOPE12/All-ISOPE12/ISOPE-I-12-354/1610986/isope-i-12-354.pdf (Accessed: 21 November 2021).

Wang, J., Zhan, L., Jiang, S., Xu, L., Sheng, L., Tian, Z. and Shi, J. (2013) 'Numerical simulation of VIV for a marine riser in uniform and linearly sheared currents', *Proceedings of the International Offshore and Polar Engineering Conference*, , pp. 501–507. Available at: www.isope.org (Accessed: 4 August 2021).

Wang, L. (2009) 'A further study on the non-linear dynamics of simply supported pipes conveying pulsating fluid', *International Journal of Non-Linear Mechanics*, 44(1) Pergamon, pp. 115–121.

Wang, L., Jiang, T.L., Dai, H.L. and Ni, Q. (2018b) 'Three-dimensional vortex-induced vibrations of supported pipes conveying fluid based on wake oscillator models', *Journal of Sound and Vibration*, 422 Academic Press, pp. 590–612.

Wang, L., Yang, Y., Li, Y. and Wang, Y. (2018c) 'Dynamic behaviours of horizontal gas-liquid pipes subjected to hydrodynamic slug flow: Modelling and experiments', *International Journal of Pressure Vessels and Piping*, 161 Elsevier Ltd, pp. 50–57.

Wang, X.K., Wang, C., Li, Y.L. and Tan, S.K. (2017b) 'Flow patterns of a low mass-damping cylinder undergoing vortex-induced vibration: Transition from initial branch and upper branch', *Applied Ocean Research*, 62 Elsevier, pp. 89–99.

Wilcox, D.C. (1993) *Turbulence modeling for CFD*.

Wilcox, D.C. (1988) ‘Reassessment of the scale-determining equation for advanced turbulence models’, *AIAA Journal*, 26(11), pp. 1299–1310.

Wilcox, D.C. (1991) ‘A half century historical review of the k-omega model’, *29th Aerospace Sciences Meeting*

Willden, R.H.J. and Graham, J.M.R. (2006) *Three distinct response regimes for the transverse Vortex-Induced Vibrations of circular cylinders at low Reynolds numbers*.

Willden, R.H.J. and Graham, J.M.R. (2004) ‘Multi-modal Vortex-Induced Vibrations of a vertical riser pipe subject to a uniform current profile’, *European Journal of Mechanics, B/Fluids*., Vol.23, pp. 209–218.

Williamson, C.H.K. and Govardhan, R. (2004) *Vortex-induced vibrations*. Annual Reviews 4139 El Camino Way, PO Box 10139, Palo Alto, CA 94303-0139, USA. Available at: 10.1146/annurev.fluid.36.050802.122128 (Accessed: 27 October 2019).

Williamson, C.H.K. and Govardhan, R. (2008) ‘A brief review of recent results in vortex-induced vibrations’, *Journal of Wind Engineering and Industrial Aerodynamics*, 96(6–7), pp. 713–735.

Wu, X., Ge, F. and Hong, Y. (2012) ‘A review of recent studies on vortex-induced vibrations of long slender cylinders’, *Journal of Fluids and Structures*, 28 Academic Press, pp. 292–308. Available at: 10.1016/j.jfluidstructs.2011.11.010 (Accessed: 27 April 2020).

Xie, F.F., Deng, J. and Zheng, Y. (2011) ‘Multi-mode of vortex-induced vibration of a flexible circular cylinder’, *Journal of Hydrodynamics*, 23(4) No longer published by Elsevier, pp. 483–490.

Xie, W., Gao, X., Wang, E., Xu, W. and Bai, Y. (2019) ‘An investigation of the nonlinear dynamic response of a flexible pipe undergoing vortex-induced vibrations and conveying internal fluid with variable-density’, *Ocean Engineering*, 183(June 2018) Elsevier Ltd, pp. 453–468.

Xu, J., He, M. and Bose, N. (2009) *Vortex modes and vortex-induced vibration of a long, flexible riser*.

Xu, W., Qin, W. and Gao, X. (2018) 'Experimental study on streamwise vortex-induced vibration of a flexible, slender cylinder', *Applied Sciences (Switzerland)*, 8(2)

Xu, W.H., Zeng, X.H. and Wu, Y.X. (2008) 'High aspect ratio (L/D) riser VIV prediction using wake oscillator model', *Ocean Engineering*, 35(17–18), pp. 1769–1774.

Yamamoto, C.T., Meneghini, J.R., Saltara, F., Fregonesi, R.A. and Ferrari, J.A. (2004) 'Numerical simulations of vortex-induced vibration on flexible cylinders', *Journal of Fluids and Structures*, 19(4) Academic Press, pp. 467–489.

Yang, W., Ai, Z., Zhang, X., Chang, X. and Gou, R. (2018) 'Nonlinear dynamics of three-dimensional vortex-induced vibration prediction model for a flexible fluid-conveying pipe', *International Journal of Mechanical Sciences*, 138–139(August 2017) Elsevier Ltd, pp. 99–109. Available at: 10.1016/j.ijmecsci.2018.02.005 (Accessed: 25 August 2020).

Yang, W., Chang, X. and Gou, R. (2019) 'Nonlinear vortex-induced vibration dynamics of a flexible pipe conveying two-phase flow', *Advances in Mechanical Engineering*, 11(10), pp. 1–9. Available at: 10.1177/1687814019881924 (Accessed: 22 November 2019).

Ye, H. and Wan, D. (2017) 'Benchmark computations for flows around a stationary cylinder with high Reynolds numbers by RANS-overset grid approach', *Applied Ocean Research*, 65, pp. 315–326. Available at: 10.1016/j.apor.2016.10.010 (Accessed: 30 August 2021).

Zanganeh, H. and Srinil, N. (2016) *Three-dimensional VIV prediction model for a long flexible cylinder with axial dynamics and mean drag magnifications*. Elsevier.

Zhang, L., Wu, H., Yu, Y., Zeng, X., Zhou, J., Xie, B., Shi, M. and Huang, S. (2015) 'Axial and Transverse Coupled Vibration Characteristics of Deep-water Riser with Internal Flow', *Procedia Engineering*, 126 Elsevier, pp. 260–264.

Zhang, M. and Xu, J. (2010) ‘Effect of internal bubbly flow on pipe vibrations’, *Science China Technological Sciences*, 53(2) Springer, pp. 423–428. Available at: 10.1007/s11431-009-0405-9 (Accessed: 27 July 2021).

Zhao, M. and Cheng, L. (2014) ‘Vortex-induced vibration of a circular cylinder of finite length’, *Physics of Fluids*, 26(1) American Institute of Physics Inc., p. 15111.

Zhao, M., Cheng, L., An, H. and Lu, L. (2014) *Three-dimensional numerical simulation of vortex-induced vibration of an elastically mounted rigid circular cylinder in steady current*. Elsevier. Available at: 10.1016/j.jfluidstructs.2014.05.016 (Accessed: 27 April 2020).

Zheng, H. and Wang, J. (2018) ‘Efficient three-dimensional high-resolution simulations of flow fields around cylinders’, *Journal of Ocean Engineering and Science*, 3, pp. 205–217. Available at: 10.1016/j.joes.2018.08.001 (Accessed: 4 August 2021).

Zhu, H., Gao, Y., Srinil, N. and Bao, Y. (2021) ‘Mode switching and standing-travelling waves in slug flow-induced vibration of catenary riser’, *Journal of Petroleum Science and Engineering*, 203 Elsevier, p. 108310.

Zhu, H., Gao, Y. and Zhao, H. (2018) ‘Experimental investigation on the flow-induced vibration of a free-hanging flexible riser by internal unstable hydrodynamic slug flow’, *Ocean Engineering*, 164 Elsevier Ltd, pp. 488–507.

Zhu, H., Gao, Y. and Zhao, H. (2019a) ‘Experimental investigation of slug flow-induced vibration of a flexible riser’, *Ocean Engineering*, 189 Elsevier Ltd, p. 106370. Available at: 10.1016/j.oceaneng.2019.106370 (Accessed: 25 August 2020).

Zhu, H., Gao, Y. and Zhao, H. (2019b) ‘Coupling vibration response of a curved flexible riser under the combination of internal slug flow and external shear current’, *Journal of Fluids and Structures*, 91 Academic Press, p. 102724. Available at: 10.1016/j.jfluidstructs.2019.102724 (Accessed: 25 August 2020).

Zhu, H., Hu, J. and Gao, Y. (2021) ‘Severe slug flow-induced nonlinear dynamic behavior of a flexible catenary riser’, *Physics of Fluids*, 33(7) AIP Publishing LLC

AIP Publishing, p. 071705. Available at: 10.1063/5.0054160 (Accessed: 4 August 2021).

Zhu, H., Lin, P. and Yao, J. (2016) ‘An experimental investigation of vortex-induced vibration of a curved flexible pipe in shear flows’, *Ocean Engineering*, 121 Elsevier Ltd, pp. 62–75.

Zhu, H. and Lin, P. zhi (2018) ‘Numerical Simulation of the Vortex-Induced Vibration of A Cuarved Flexible Riser in Shear Flow’, *China Ocean Engineering*, 32(3), pp. 301–311. Available at: 10.1007/s13344-018-0031-z (Accessed: 22 November 2019).

Zhu, H., Zhao, H. lei and Gao, Y. (2018) ‘Experimental Investigation of Vibration Response of A Free-Hanging Flexible Riser Induced by Internal Gas-Liquid Slug Flow’, *China Ocean Engineering*, 32(6) Springer Verlag, pp. 633–645.